SINDBIS VIRAL PERSISTENCE AND ANTIBODY-MEDIATED CLEARANCE FROM THE CENTRAL NERVOUS SYSTEM IN MICE

by
Voraphoj Nilaratanakul

A dissertation submitted to Johns Hopkins University in conformity with the requirements for the degree of Doctor of Philosophy

Baltimore, Maryland

October, 2016

Thesis Abstract

Growing evidence has indicated that typical RNA viruses can persist, which might be responsible for affinity maturation of antibody, life-long immunity, and post-viral autoimmune diseases.

Sindbis virus (SINV) has been known to persist in mouse CNS with 3 phases of clearance; 1st – rapid clearance of infectious virus within 7-8 days, 2nd – gradual clearance of SINV RNA during 7-60 days, and 3rd – sustained low-level SINV RNA after 60 days. My study characterized the nature of SINV persistence and tested the role of immunoglobulin classes in SINV clearance. We intracerebrally inoculated a low neurovirulent SINV TE strain into immunoglobulin-deficient mice, which are AID-/- (IgM only), sIgM-/- (no IgM), and double knockout (DKO, no antibody) mice, compared to wild-type (WT) mice.

In the 1st phase, RNA FISH and immunofluorescence (IF) showed an abundance of all viral components, which are genomic RNA, subgenomic RNA, dsRNA, nsP3, capsid, E2, 6K, and E1. Long-range RT-PCR showed intact genomic RNA. DKO mice cleared infectious virus from the spinal cord, but not from the brain. AID-/- and sIgM-/- mice completely cleared infectious virus from both brain and spinal cord similarly to WT mice.

In the 2nd phase, the viral components that persisted were mainly SINV subgenomic RNA and capsid protein. SINV genomic RNA was completely undetectable, and the subgenomic RNA had large deletions in the E2-E1 genes. Only DKO mice had

infectious virus reactivated in this phase. There was no difference in viral RNA clearance from both brains and spinal cords, detected by RT-qPCR, between 4 mouse groups.

In the 3rd phase, DKO mice sustained higher levels of viral RNA in both the brain and spinal cord than other groups. DKO mice also still had infectious virus in the brain.

Using SINV with fluorescent RNA aptamers, we demonstrated in live-cell imaging that antibody treatment cleared SINV RNA from differentiated neurons, except for a few cells without bound antibody.

In conclusion, SINV RNA persists primarily in a form of incomplete subgenomic RNA. Loss of the E2 gene prevents anti-E2 antibody binding, and may facilitate persistence by limiting antibody-mediated clearance.

Advisor: Professor Diane E. Griffin, MD, PhD

2nd reader: Dr. Patricia J. Gearhart, PhD

Thesis Committee:

Advisor: Dr. Diane E. Griffin

Thesis committee: Dr. J. Marie Hardwick

Dr. Patricia J. Gearhart

Dr. Isabelle Coppens

Acknowledgements

First, I would like to thank my advisor, Dr. Diane E. Griffin. Her calmness and support have made my days here at Johns Hopkins like I am in my second home. She is always available whenever I need her advice and her response to my email is lightning fast. This is very important to me, an international student who is not fluent in English. She also let me test my strange ideas for most of the times and contacted all kinds of people needed to help me with my project. After tiresome nights or weekends of house chores and continuous playing with my extremely active toddler son, I could relax and did what I was interested in during the day of weekdays in my lab.

I also want to acknowledge my thesis committee, Dr. J. Marie Hardwick, Dr. Isabelle Coppens, and Dr. Patricia J. Gearhart. They gave me critical suggestions every time we had a meeting. I feel sorry for them though, because they had to listen to my strong-accent sleep-induced monotonous speech, and read my writing full of grammatical errors.

I appreciate our lab manager, Debra Hauer, who has constructed all my fluorescent viruses. She has never backed down from more and more insertions I requested. We began with 1 copy of Spinach2 RNA and ended up with 28 copies of Broccoli RNA in viral genome. My colleagues also deserve my praise. Kirsten Kulcsar took care of me during the 2nd rotation of my first year and guided me when I started my thesis project. Kimberly Schultz helped me a lot about most of the *in vitro* protocols. Victoria Baxter provided me all kinds of knowledge about mice, and, together with Elizabeth Troisi and Jane Xie, helped me record the clinical score in my mouse

experiments. Nina Martin will take care of my invaluable mouse strains after I return to Thailand. Rupak Shivakoti and Ashley Nelson have been my wonderful lab mates. Though we work on the different viruses, I had some good conversations with Dr. E. Sreekumar and Rachy Abraham. Two rotation students, Angela Chen and Oanh Tran, helped me with the spinal cord specimens and TUNEL staining, respectively.

All my friends and faculties in both CMM (Cellular and Molecular Medicine) and MMI (Molecular Microbiology and Immunology) have always been kind to me, especially Hari Prasad who always found some topics to talk to me during my first year here. I give my special thanks to Leslie Lichter, Colleen Graham, and Gail O'Conner, who pushed me through all kinds of administrative problems; salary, insurance, tuition, etc.

I am grateful to both core and MMI microscope facilities, where I had taken more than 10000 images over the past 4 years. Dr. Seyed Ali Fatemi, and his lab members, Romy Sweda and Joel Marx, helped me with the brain slice culture. Hao Zhang provided me his FACS service for sorting my virus. Reference Pathology Lab also kindly handled my complicated requirements for my specimens.

Because I am a Thai doctor, who generally has very little experience on bench works and animal studies, the lab rotations in my first year took the main part in shaping me into a scientist. My 1st rotation with Dr. Lewis Romer and Fumin Chang guided me into working with general bench works and cell cultures. The 2nd rotation here in Dr. Griffin's lab helped me go through virus and animal studies. My 3rd rotation with Dr.

Zaver Bhujwalla, Mayur Gadiya, and Balaji Krishnamachary introduced me into the world of fluorescent imaging.

I received much support and many reagents from outside Johns Hopkins University; Spinach2 plasmid from Dr. Samie Jaffrey (Cornell University), AID+/- mice from Matthew Scharff (Albert Einstein College of Medicine), sIgM-/- mice from Dr. Nicole Baumgarth (University of California, Davis), and anti-PLP antibody from Dr. Bruce Trapp and Ansi Chang (Cleveland Clinic).

During training as a fellow in infectious diseases in Thailand, my advisor, Dr. Wanla Kulwichit, was a main force behind my achievement – scholarship and enrollment into Johns Hopkins University. My research about dengue virus persistence under his guidance was also the foundation of my research here at Johns Hopkins University. All faculty members of Infectious Disease Division at King Chulalongkorn Memorial Hospital are my role models to be a real doctor and I am very proud that they have accepted me to join them. Our administrators there, Panutda Khumniphat and Kesinee Arunyingmongkol, provided me all information I needed and took care of my businesses regarding my position in Thailand. I also thank Department of Medicine, Faculty of Medicine, Chulalongkorn University for permitting my study abroad almost immediately after my enrollment there.

I am deeply grateful to Her Royal Highness Princess Maha Chakri Sirindhorn and the committee of Anandamahidol Foundation for granting me the scholarship that has covered most of my tuition, fees, and expenses. I have been helped and guided through the processes that involved my scholarship by many people, including Dr. Mattana

Hanvanich, Dr. Weerapan Khovidhunkit, Komsorn Aukayapisud, Vichitra W.waratorn, Chutima Siangdee, and Manida Jatanilpan.

My Thai friends in US helped me settle here. When I had a pest nightmare on the first day in US, Natapong Jupatanakul, also a student in MMI department, sheltered me for a couple of weeks until I found a new room. Dr. Leilani Paitoonpong took me to see various places during my 1st year. At the beginning of my 2nd year, I changed my apartment to accommodate my wife and son. Our neighbors, Dr. Parichat Salee and her family, welcomed us and made our transition smooth.

I cannot be who I am without my family. My parents, Chiraphong and Matana Nilaratanakul, have never forced me to do anything I do not want to and unconditionally supported me in what I chose to do. My father envisioned the importance of English skill and instilled it in us, his five sons, when we were very young. He would read his Time magazine every night and taught us some vocabulary. My English skill is the worst in my family, but still enough to get me here. In elementary school, he always bought me some science magazines, which ignited my interest in science. After about four decades of his career as a businessman, he began to exploit his art talent seriously. Just before I started my first year here in US, he took some art classes and then created many marvelous art works. This has encouraged me, who has worked only as a clinician for almost a decade, to create my new path as a scientist.

My mother is very caring. When she saw I got all As on my exams, she was afraid that I was too tired or stressed and told me to get some Bs next time. Nowadays in her late sixties, she manages to exercise for an hour or more every day, a task, which I have

never accomplished. I feel like a little kid every time I am with my 4 elder brothers – Kitikorn, Praphon, Kamol, and Kongsith. I had played soccer with all of them since I could remember. We would gather our pocket money to buy toys or games. Quarreling among us is close to none.

Lastly, I want to thank my beloved wife and son, Dr. Pornsawan and Chawindhorn Cholsaktrakool. She sacrificed her job, her chance of training, and her family support in Thailand to follow me to US. She would stuff me with all kinds of delicious homemade Thai food, sweet, and cake, even though she had never cooked before. My parents and brothers can tell immediately whether I have been with my wife during the last month by looking at how thin or fat I have become. I am sincerely grateful to her parents, Sakdi and Suree, to let me marry their lovely daughter. They are also a great help for taking care of my son whenever we visit Thailand. My wife's younger sister, Pornphet, decided to come with us suddenly on the day that we departed from Thailand, because she worried that we would not survive in the US by ourselves. She stayed with us for a couple months until everything was settled.

My toddler son is very energetic and really wants to help us in cooking, baking, and all house chores, making simple daily tasks suddenly become fun and challenging (and exhausting too). Whenever he saw me work with my computer, he would jump to sit on my lap and seriously thought that he helped me edit my fluorescence images so that I could graduate and return to Thailand faster. He once managed to delete my 4-year worth of all experiment data from my hard drive and I had to recover them from the cloud. His favorite bedtime stories are my drawing about the battles between various types of white

blood cells and germs, especially when I put in some simplified molecular details. This forces me to study more, because I want my story to be both exciting and accurate.

Without support and inspiration form everyone, I would not be here today. Now it is time for me to take the 1st step in my new career path. I wish that one day I too can be the one who gives other people my support.

Table of Contents

List of Tables

List of Figures

Chapter 1

Introduction to Sindbis Viral Encephalomyelitis

Sindbis virus (SINV) was first isolated in 1952 from a group of mosquitoes, captured in the Egyptian village, after which the virus was named (1). In humans, SINV causes fever, rash, and arthritis; also known as Ockelbo disease in Sweden, Pogosta disease in Finland, and Karelian fever in Russia (2-4).

SINV is an alphavirus in Togaviridae family. New world alphaviruses (e.g. Western, Eastern, and Venezuelan equine encephalitis viruses) cause encephalitis. Old world alphaviruses (e.g. Chikungunya and Sindbis viruses) mainly cause rash and arthritis (5), but still have potential to induce encephalitis in some cases (6, 7).

Epidemiology

SINV infection is a mosquito-borne disease. SINV is usually circulated between birds and mosquitoes, but sometimes humans and domestic mammals can become incidental hosts from mosquito bites (5). Human cases have been reported from northern Europe, Africa, China, and Australia, with annual incidence from 2 to 6.6/100,000 and average seroprevalence of about 5% in middle-aged populations (8).

Virus structure

SINV is an enveloped virus, 70 nm in diameter. Its nucleocapsid core consists of 11.7 kb positive-sense single-stranded genomic RNA with 5' cap and 3' poly-A tail in an icosahedral capsid (240 monomers). Its envelope is derived from the host plasma membrane and includes 80 trimers of E1 and E2 glycoprotein heterodimers (8).

Life cycle (Figure 1.1)

- **Virus entry**

SINV utilizes various surface molecules in a wide-range of host cells (mammals, insects, birds) as a receptor for E2 glycoprotein attachment. Examples of these SINV receptors are laminin receptor, DC-SIGN, L-SIGN, heparan sulfate, and natural resistance-associated macrophage protein (NRAMP) (9). Upon binding, the virion is endocytosed. Exposure to low pH in the endosome triggers conformational change of envelope proteins and membrane fusion by E1 glycoprotein. The nucleocapsid core is released and disassembled, releasing its genomic RNA into cytoplasm (5).

- **Viral RNA replication (Figure 1.2)**

The 49S genomic RNA is translated into nonstructural polyproteins P123 and readthrough translated into P1234. Uncleaved P123 and nsP4 preferably replicate the minus strand in the early phase. Later, nsP2, which has proteolytic activity, cleaves the polyprotein into nsP1, nsP2, and nsP3. With the cleaved nsP1-4, the viral replication is shifted from minus to plus strands, which are 49S genomic and 26S subgenomic viral RNA (10, 11).

- **Functions of nonstructural proteins (nsP)**

nsP1 functions as a methyltransferase and guanyltransferase, essential for 5' capping of viral genomic and subgenomic RNAs. nsP1 also limits proteinase activity of nsP2. The N-terminal domain of nsP2 is an RNA helicase, while the C-terminal domain is a proteinase, responsible for the cleavage of the nonstructural polyproteins. The

functions of nsP3 are not well defined, but are involved in formation of the replication complex and its internalization that forms the type I cytopathic vacuoles (see below). nsP4 is the RNA polymerase (11).

- **Virus assembly and budding**

The 26S subgenomic RNA is translated into the structural polyproteins, capsid-E3-E2-6K-E1 and capsid-E3-E2-Transframe. Instead of 6K, the latter has transframe (TF), which is the result of C-terminal extension by ribosomal frameshifting (-1 open reading frame). Both 6K and TF mainly affect the efficacy of viral budding (12). The capsid cleaves itself from the polyprotein and encapsidates the viral genome, forming a nucleocapsid. The rest of polyproteins accumulate in the endoplasmic reticulum (ER) membrane and are cleaved into E1 and pE2 by signal peptidase. The envelope proteins are glycosylated in the Golgi apparatus and are matured upon transportation to the plasma membrane by cellular furin cleavage of pE2 into E2 and E3. The cytoplasmic tail of E2 interacts with a hydrophobic pocket in the capsid on the nucleocapsid, leading to assembly and budding of infectious virus (11).

Cytopathic vacuoles (CPV) (Figure 1.3)

Sindbis virus forms 2 types of cytopathic vacuoles (CPV), spherule-containing CPV-I and nucleocapsid-surrounded CPV-II; single-membrane vacuoles derived from late endosome and trans-Golgi network (TGN), respectively (13-15). One report claimed that there is another type of a spherule-containing vacuole, which has double membranes and is possibly derived from the mitochondrion (14).

Formation of alphavirus replication complexes and CPVs (Figure 1.4)

After clathrin-mediated endocytosis, the drop in pH induces fusion and the viral nucleocapsid is released. Viral RNA is translated into nonstructural proteins (nsP1-4), and the viral RNA-nsPs complex is transported to cell membrane where it forms a site of viral RNA synthesis (replication complex) (13, 16) in a 50-nm single membranous spherule, protruding outside of the cell (16, 17). Internalization of the spherules on the plasma membrane is mediated by actin-myosin (inhibited by blebbistatin) and PI3K (inhibited by wortmannin). These spherule-containing vesicles fuse with each other and with a late endolysosome (inhibited by nocodazole) to form an acidic large (600-2000 nm) cytopathic vacuole type I (CPV-I), which is transported by microtubules (inhibited by nocodazole) to the perinuclear area (17, 18). The spherules are inside and line the inner surface of CPV-I. The cytoplasm is connected to the inside of the spherule through a pore, 5-10 nm in inner and 19-20 in outer diameter (16, 17).

Interestingly, internalization of replication complexes in a spherule is not a universal phenomenon for alphaviruses. Internalization can be found in SINV and Semliki Forest virus (SFV), but not in Chikungunya virus (19, 20). This process requires PI3K activation, mediated by a hyperphosphorylated/acidic domain in the hypervariable c-terminal tail of nsP3, and can be inhibited by wortmannin, a PI3K inhibitor. A recombinant Chikungunya virus with the hypervariable c-terminal tail of nsP3 from SFV gains the ability to internalize its replication complex (19).

Sindbis viral encephalomyelitis in mice

SINV can cause encephalitis in mice. If the mice survive, there are 3 phases of SINV clearance; 1st – rapid infectious viral clearance (day 5-8), 2nd – gradual viral RNA clearance (week 2-8), and 3rd – sustained low level of viral RNA (after 8 weeks) (**Figure 1.5A**) (21).

In vivo imaging of mice infected with SINV-luciferase shows the steps of virus spread from first to last; the inoculated foot pad, the popliteal lymph node, the blood, the nasal mucosa, the brain, and the spinal cord (22).

Outcome determinants

The outcomes of mice with Sindbis encephalitis mainly depend on route of infection (23), strains of SINV, genetic background of mice, age of mice (**Table 1.1**) (24-26). Mature neurons are more resistant to apoptosis and the interferon response is primed, leading to better survival of adult mice than young mice with more immature neurons (27). For instance, compared to immature neurons (cAP7), interferon regulatory factor (IRF)-3 and IRF-7 are upregulated in differentiated rat olfactory neurons (dAP7). cAP7 cells express the short γ-isoform of IRF-7, but dAP7 cells express long active α-isoform. Nevertheless, RNA silencing of IRF-3 and IRF-7 does not improve the viral replication in dAP7 cells (28). Other neuronal cell lines, CSM14.1 (rat nigral cell) and NSC34 (mouse motor neuron), when differentiated, resist and survive SINV infections better than undifferentiated cells (29). Furthermore, adult mice express much higher levels of ISG12 (interferon stimulated gene). Newborn pups, infected with recombinant SINV-ISG12, have better outcomes than pups infected with control SINV (30).

BALB/c mice are resistant to fatal encephalitis from neuroadapted Sindbis virus (NSV). Their infected brains have a higher number of regulatory T-cell producing IL-10 and a lower number of Th17 than susceptible C57BL/6 mice. BALB/c mice that lack IL-10 will succumb to the fatal encephalitis (31). One genetic determinant for control of viral replication and outcome is mapped to chromosome 2, but the gene has not been identified (32).

Table 1.1 Summary of commonly used SINV strains (24-26)

Characteristics	AR339	NSV	TE
Sources	Mosquitoes in Sindbis village, Egypt, 1952 (1)	AR339 – 6 serial passages with intracerebral inoculation, alternately between newborns and weanling mice (33)	E2 from NSV E1 from SV1A (early passage of AR339) on TOTO1101 backbone (24)
Mutations	-	E2 – Q55H, R209G E1 – V72A, G313D	E2 – Q55H, R209G
Mortality in suckling mice	100%	100%	100%
Mortality in weanling mice	0%	100%	4%
Mortality in adult mice	0%	0% - BALB/c 100% - C57BL/6	0%
Encephalitis model	-	Immune-mediated pathology, prevention and treatment efficacy	Viral persistence and clearance

Innate immune responses.

Generally, the initial response to infection begins when pattern recognition receptors (PRR – e.g. toll-like receptors (TLR), protein kinase R (PKR), etc.) interact with viral pathogen-associated molecular patterns (PAMP – e.g. dsRNA), resulting in the production of IFN-α/β. IFN-α/β activates interferon-stimulated genes (ISG) to produce proteins, which have antiviral effects (34).

TLR3-/- and MyD88-/- (myeloid differentiation primary response) mice do not differ from WT C57BL/6 in term of infectious virus clearance, IFN-α production, and mortality from NSV infection. IRF7-/- mice fail to generate type-I IFN, are more susceptible to fatal encephalitis, and have higher titers of infectious virus than WT mice. Unc93b1$^{3d/3d}$ mice cannot transport TLR3, TLR7, and TLR9 from endoplasmic reticulum (ER) to their functional sites in the endosome. They die earlier and have higher amount of infectious virus, but still produce the same level of IFN-α as WT mice after NSV infection (35). TLR7 has not been studied in SINV encephalitis yet, but plays important role in a mouse model of Ross River virus (RRV)-induced myositis/arthritis. TLR7-/- mice have worse outcomes, higher RRV viral loads, and produce only low affinity antibody (36).

Mitochondrial antiviral-signaling protein (MAVS or IPS-1) is an intermediary protein for both MDA-5 and RIG-I, which can detect viral RNA in the cytosol. IPS-1-/- mice have worse outcomes and higher levels of both infectious virus and viral RNA. A mutation in nsP1 that attenuates viral neurovirulence leads to a better interaction with

MAVS (37). PKR, Mx-1, and RNase L have antiviral properties, but are not essential for SINV clearance from the CNS (38).

SINV Toto 1101 (low virulence, only 50% mortality in suckling mice) inoculation can kill all A129 mice, which lack the IFN-α/β receptor. Expression of ISG15 (interferon-stimulated gene 15), a ubiquitin homolog, can partially rescue mice that lack IFN-α/β receptor (39). ISG15-/- mice also have higher mortality rates than WT mice (40). The expression of zinc-finger antiviral protein (ZAP), another IFN-inducible factor, can destabilize viral RNA and rescue cells that lack type I interferon from SINV infection. ZAP-deficient mice are also very susceptible to SINV infection (41). STAT1 is needed for IFN-α, β, and γ responses. STAT1-deficient C57BL/6 mice, infected with the same strain of SINV, die even faster than A129 mice (23, 42). On the other hand, SINV TE inoculation does not kill IFN-β-deficient C57BL/6 mice. These mice have higher titer of infectious virus at the peak (day 3), but can clear the virus similarly to WT mice (43).

SINV nsP2 is thought to be involved in host transcription and translation shut-off, leading to the suppression of IFN-stimulated gene (ISG) induction (44).

Adaptive immune response

SINV-specific T and B cells, induced in the draining cervical lymph nodes, infiltrate foci of infection in the mouse CNS in this order; CD8 T-cells, CD4 T-cells, IgM-B-cells, and then IgG/A-B-cells (**Figure 1.5B**) (21). The main adaptive immune cells in the first phase of infectious viral clearance are CD8 T-cells, and IgM-producing plasmablasts, while CD4 T cells and IgG-producing plasmablasts are more prominent in the second phase of clearance of viral RNA .

T-cells

Both CD4 and CD8 T-cell depletion affects clearance of SINV. In μMT mice (no antibody production), depletion of both CD4 and CD8 T-cells results in similar levels of persistent virus as in severe combined immunodeficiency (SCID) mice in both the brain and the spinal cord. SINV-specific T-cell transfer reduces infectious virus from the brain and clears infectious virus from the spinal cord of persistently infected recombination activating gene-1 knockout (RAG-/-) mice (45).

IL-10 produced by regulatory T-cells (T_{reg}) is an important regulatory cytokine. Although IL-10 knock out mice clear SINV normally, they develop symptoms earlier and have worse outcomes, most likely due to the increase of pathogenic Th17 cells in the CNS (46).

Interferon-gamma (IFN-γ)

The main T-cell cytokine that helps clear SINV from the CNS is IFN-γ. In SCID mice, infection with recombinant SINV TEdsIFN-γ, in which infected cells produce IFN-γ reduces infectious virus in brains and clears virus from spinal cords similar to μMT mice, while SINV TEdsTNF-α infection increases the titer of infectious virus (45). IFN-γ deficient and IFN-γ-receptor 1 deficient mice clear infectious virus from brains similarly to WT mice, but have delayed clearance from spinal cords (43, 47).

In differentiated neuronal cells, CSM14.1 (rat nigral cell line), IFN-γ pretreatment limits SINV replication, while treatment at 24 hours post infection helps clear the virus and improves survival. IFN-γ treatment suppresses synthesis of viral RNA and proteins, and restores host protein synthesis (29). IFN-γ treatment also inhibits SINV replication in

differentiated NSC34, AP7, and mouse primary dorsal root ganglion neurons (29, 48). The antiviral and neuroprotective abilities of IFN-γ depend on JAK/STAT signaling (48).

B-cells

μMT mice that lack B cells and antibody can clear infectious SINV from spinal cords but not from brains (43).

In WT mice, prolonged up-regulation of CXCL9, CXCL10, CCL1, CCL2, and CCL5 chemokine production in the CNS recruits B-cells that express chemokine receptors – CXCR3, CXCR5, and CCR7. B-cell activating factor (BAFF) produced in the CNS may help in retention of these cells (49, 50). BrdU labeling indicates that infiltrating B-cell mainly originate from the early germinal center response in cervical lymph nodes and continue to proliferate in the CNS(50). At late time points, most B-cells in the brain are plasmablasts with few plasma cells and memory B-cells. An increase in IgA-secreting cells in CNS but not in the blood suggests on-going class-switching in the CNS without evidence of affinity maturation of antibody or extranodal germinal centers (50, 51).

Antibody

See details in Chapter 3.

Differential clearance of virus from CNS

Components of the immune response required for viral clearance are dependent on viral strains, the types of cells, and organs infected. For example, antibody is needed for mouse hepatitis virus (MHV) clearance from both brain and spinal cord, but not from liver (52). Mice immunized with vesicular stomatitis virus (VSV) can interact with cells

expressing VSV nucleoprotein and clear recombinant vaccinia virus in bystander cells in the brain, but not in testes or ovaries, by T-cell dependent IFN-γ production (53).

In SINV encephalomyelitis, viral clearance from brain is different from viral clearance from spinal cords. Antibody and IFN-γ are effective and synergistic in clearance of SINV from both brain and spinal cord. In brains, antibody can fully compensate for a lack of IFN-γ, but IFN-γ cannot compensate for the lack of antibody (**Figure 1.6**). In spinal cords, both can compensate for the lack of each other with only some delay in clearance (43, 47) **(Table 1.2**).

Table 1.2 Comparison between brain (B) and spinal cord (S) SINV clearance by antibody and IFN-γ (43, 47)

	Antibody+	Antibody-
IFN-γ+	B: normal S: normal	B: persistent (low level) S: short delayed
IFN-γ-	B: normal S: short delayed	B: persistent S: persistent (low level)

Unsolved questions

Though many previous studies have shown that Sindbis viral RNA can persist for a long period of time, very little is known about the nature of this persistence especially after the clearance of infectious virus. Where does the virus hide? How can the virus persist? We address these questions in Chapter 2 of this thesis.

Antibody is arguably the most powerful in viral clearance. It can protect mice even in some of the worst combinations between virus strains and hosts. Antibody-mediated non-cytolytic clearance does not require the Fc portion of the antibody, interferon, complement, or immune cells. How antibody clears intracellular viral RNA without killing the cells is still largely unknown. To bring some insight into this topic, we produced recombinant Sindbis virus that has fluorescent RNA aptamers in Chapter 4. This makes real-time observation of viral RNA replication and clearance in live cells possible. Most of anti-SINV antibodies tested for clearance in vitro and in vivo have been IgGs, but the fact that only IgM-secreting cells are present in mouse CNS during the clearance of infectious virus prompts us to compare the roles of IgG versus IgM in Chapter 3.

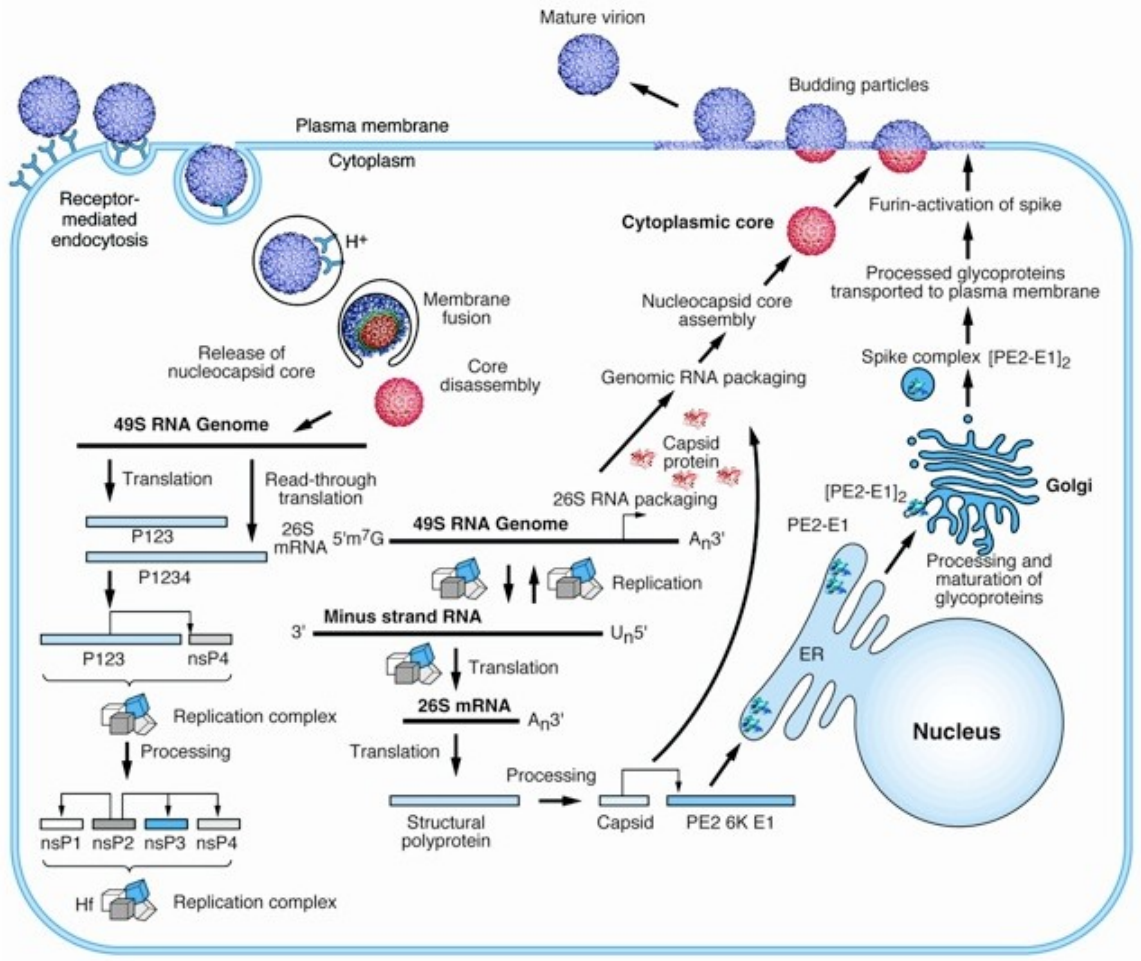

Figure 1.1 Sindbis virus life cycle (Richard J. Khun, Joyce Jose, http://bilbo.bio.purdue.edu/~viruswww/Kuhn_home/img/alpha_life.jpg)

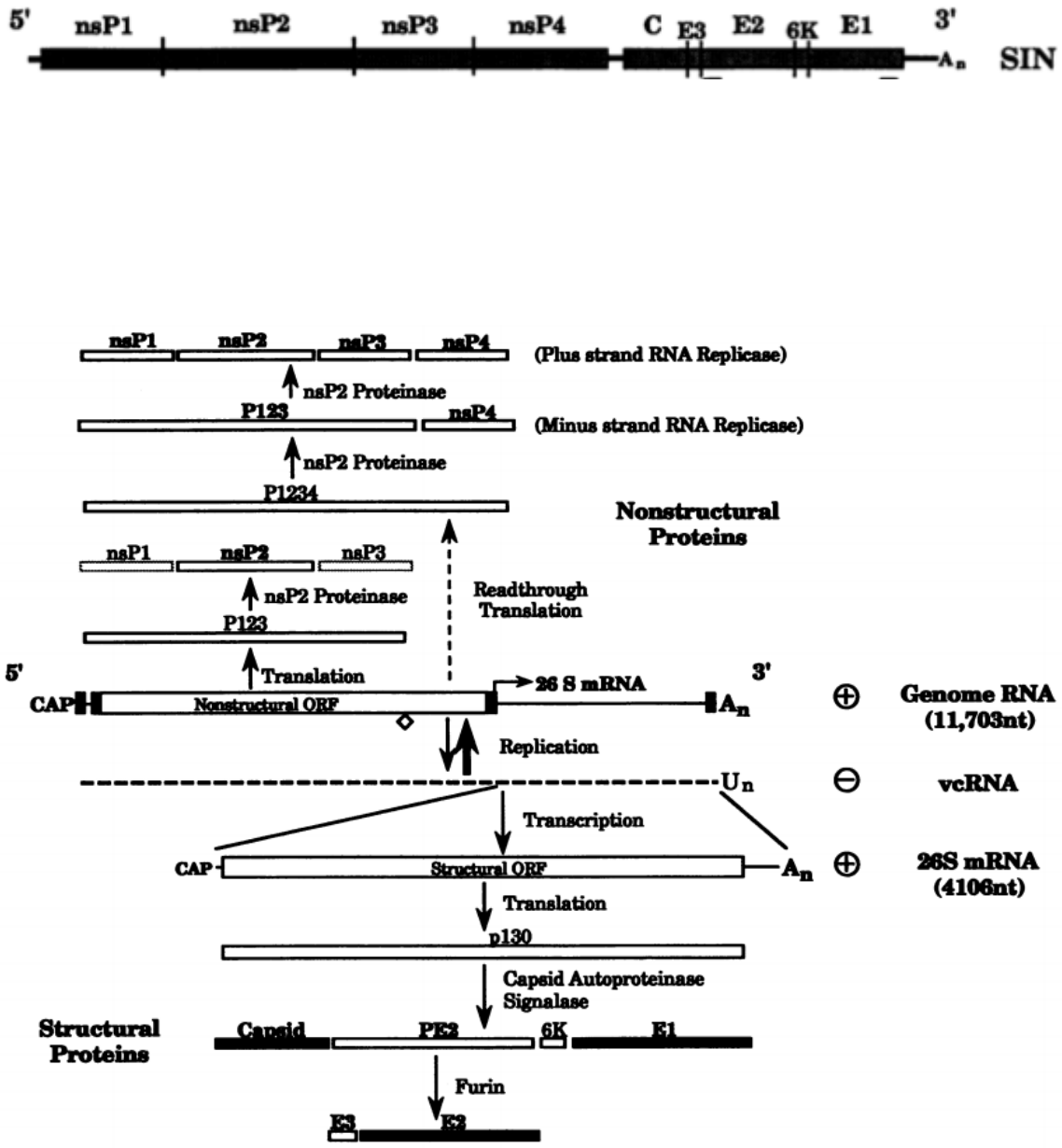

Figure 1.2 SINV genome and its replication strategy (11)

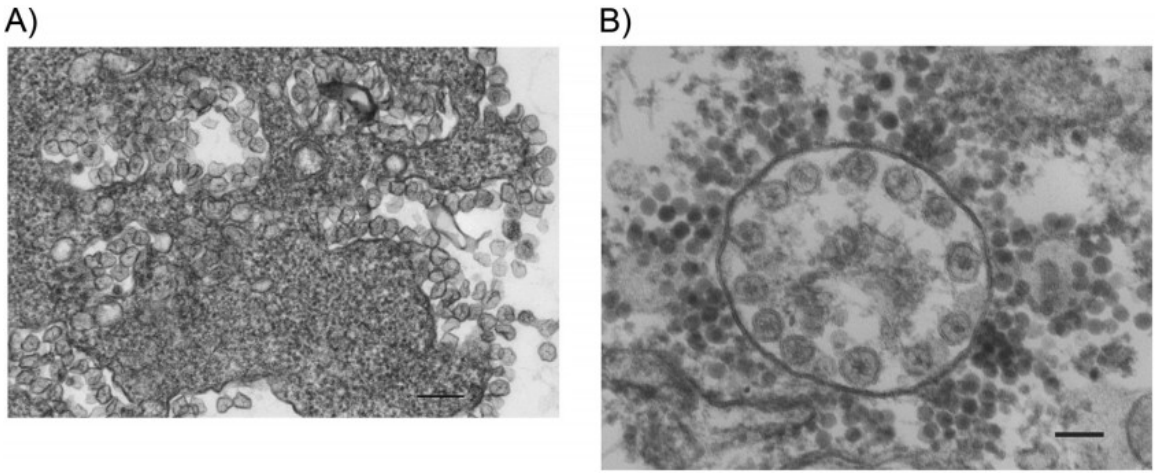

Figure 1.3 A – Replication complex-containing spherules on plasma membrane at early infection. B – CPV-I with spherules inside at late infection (20). C – CPV-II with envelope proteins inside and surrounded by nucleocapsid (15). (CPV – cytopathic vacuole)

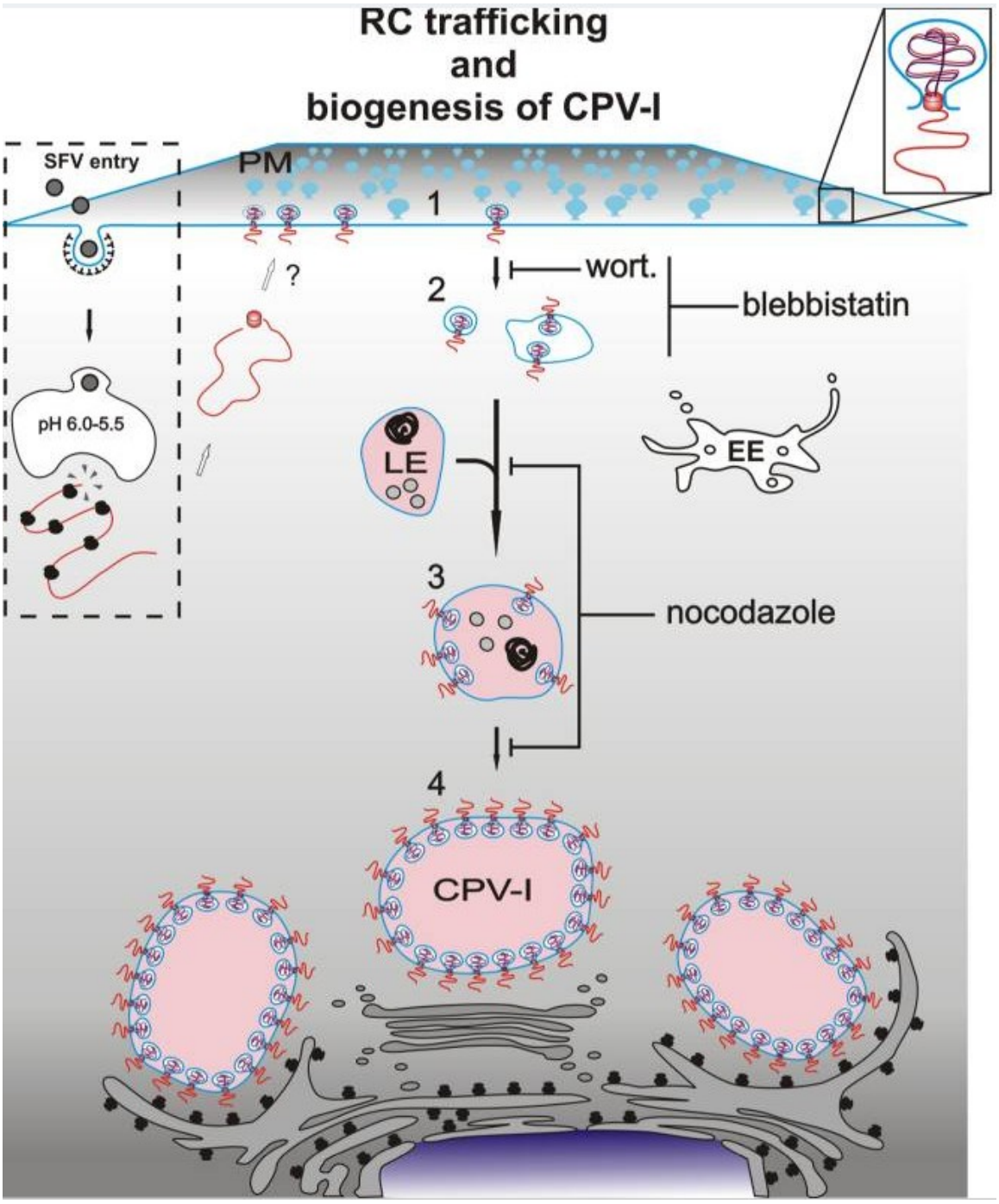

Figure 1.4 Formation of replication complex and CPV-I in alphavirus (18). RC – replication complex, PM – plasma membrane, SFV – Semliki Forest virus, LE – late endosome, wort – wortmannin, CPV-I – cytopathic vacuole type I, pink color – acidity.

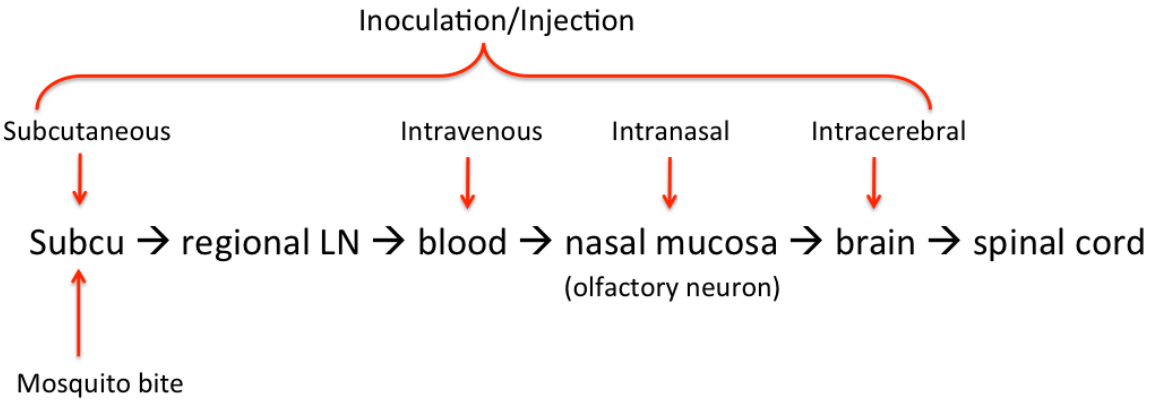

Figure 1.4 Spread of SINV from the periphery into the CNS (22). (Subcu – subcutaneous tissue, LN – lymph node)

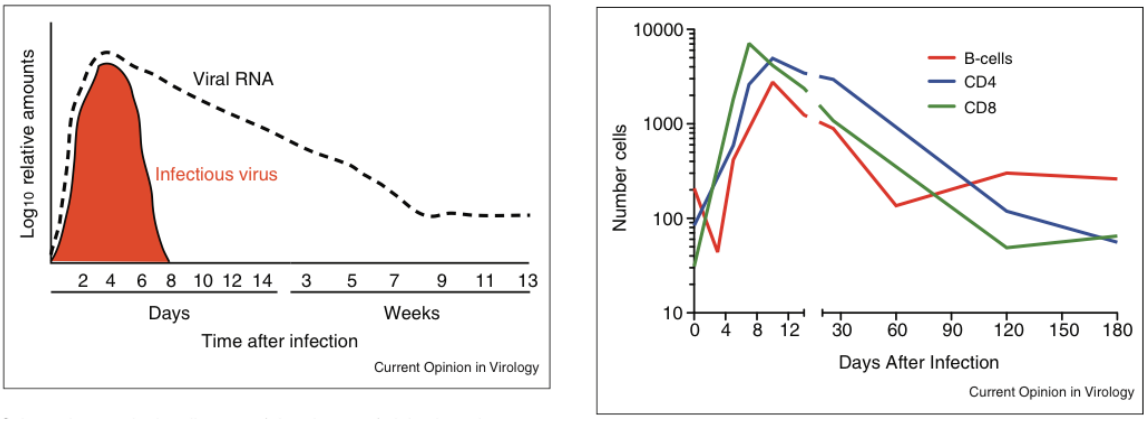

Figure 1.5 A – Clearance of Sindbis infectious virus and viral RNA, B – Immune cell infiltration into brains after SINV infection (21).

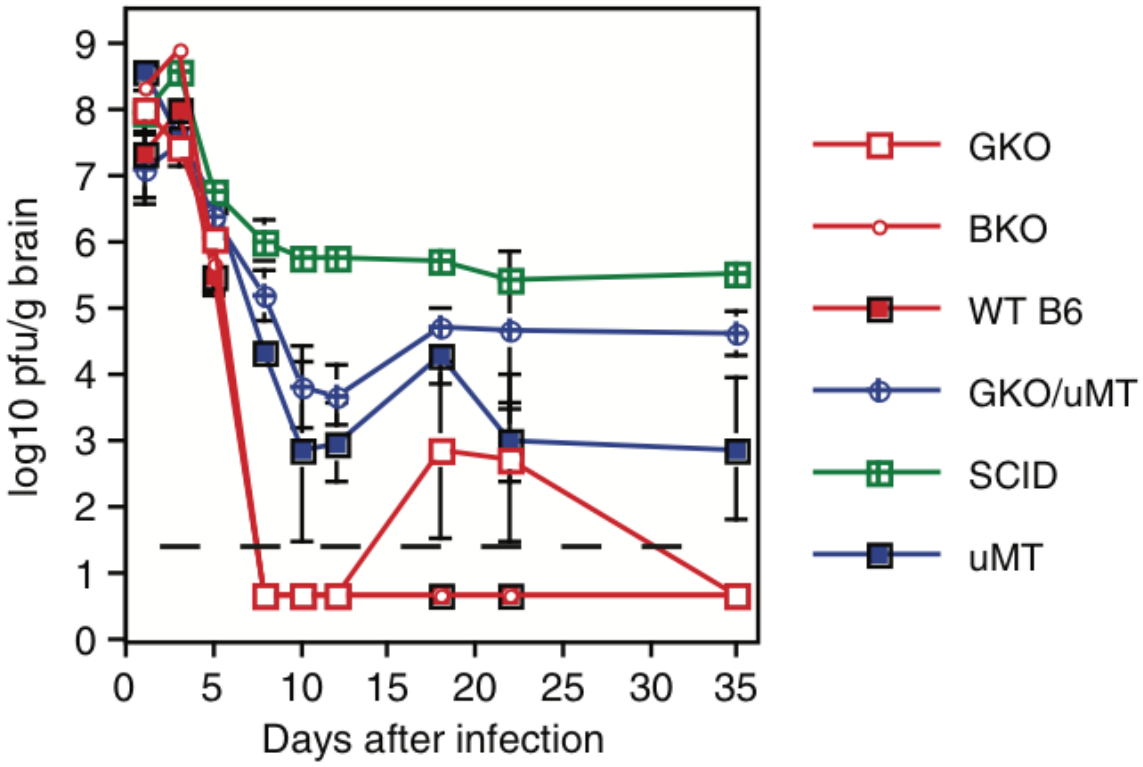

Figure 1.6 Clearance of infectious Sindbis virus from mouse brains (21, 43) (GKO – IFN-γ knock out, BKO – IFN-β knock out, WT B6 – wild type C57BL/6, SCID – severe combined immunodeficiency, μMT – B-cell deficient mice)

Chapter 2

Sindbis Viral Persistence in Central Nervous System

Introduction:

Viral persistence and/or latency are well known among DNA viruses, retroviruses, and RNA viruses that cause chronic infection like hepatitis C virus (54) and lymphocytic choriomeningitis virus (55). However, typical RNA viruses mostly cause acute infections. These include influenza, measles, rubella, mumps, dengue, rhinovirus, etc. Hosts usually recover and presumably eradicate the viruses completely from their bodies within 1 or 2 weeks. This assumption might be false, since there have been growing evidences of viral persistence by these RNA viruses.

Indirect evidence

Many RNA viral infections can cause life-long immunity. Some of them have been eradicated or a very low incidence in particular areas, making immunity boosting by re-infection unlikely. Viral persistence, if true, could be a source of endogenous boosting.

One of the well-known aspects of the immune response, the affinity maturation of antibody, is an antigen-driven process. For example, in SARS (severe acute respiratory syndrome) -associated coronavirus, it takes 3 months after acute viral infection to reach maximum affinity (56). By the time infectious virions have been cleared, 1-2 weeks after infection, low-affinity virus-specific antibody has just appeared. Thus, we may infer that, after the host's recovery and clearance of infectious virions, viral antigens at least still persist in hosts for months; otherwise, affinity maturation cannot happen.

Direct evidence

Most direct evidence of persistence relies on reverse transcription polymerase chain reaction (RT-PCR) detection of specific viral RNA. Following are some examples of persistence of RNA viruses that typically cause acute infections, followed by rapid clearance of infectious virions from hosts.

Humans

- West Nile viral RNA was found in 20% of urine samples up to 6 years after infection (57).
- Dengue viral RNA was found in 7% of bone marrow aspirations (58), 8% of lymphoid tissues (59), and 14% of kidneys (60) in Thai patients that had elective surgeries or procedures without clinical sign of infection. Paired sera for anti-dengue ELISA (enzyme-linked immunosorbent assay) before and after tissue collections confirmed no acute or recent infection in these patients. They most likely acquired dengue infection many years earlier because the dengue virus seroprevalence is 95% in Thai young adults (61).
- Rubella virus and antigen were found in 85% of peripheral blood lymphocytes from patients with rubella-associated arthritis up to 6 years after infection (62).
- Measles viral RNA was found in many sites, including blood, respiratory secretion, urine, and lymphoid tissues, up to 3 months in children after infection. It can also establish persistent infection in neurons and cause subacute sclerosing panencephalitis (SSPE) many years after acute infection (63).

Mammals

- Measles viral RNA was found in peripheral blood mononuclear cells (PBMC), nasal swabs, and lymph nodes of rhesus macaques up to 6 months after infection (64).
- Coxsackie viral RNA was found in mouse brains up to 3 months after infection, while chronic inflammation was observed in brains up to 9 months (65).
- Sindbis viral RNA was found in mouse brains up to 17 months after infection (66).

Persistence of Sindbis virus in a mouse encephalitis model

Neurons can host many kinds of viral persistence and latency. Non-fatal neurotropic Sindbis (TE strain) viral RNA persistence can be detected in mouse brains. Though infectious virus is cleared within the first week after infection, the clearance of viral RNA is much slower. After 8 weeks, the viral RNA level reaches its nadir and is maintained at a low level for the lifespan of the mouse (21). However, the distribution, cell types, and viral components of persistent virus after acute infection have not been elucidated.

Materials and Methods:

Sindbis virus TE strain preparation

BHK cells were cultured in a T150 flask at 37^{O}C 5% CO_2 in Dulbecco's Modified Eagle Medium (DMEM, Gibco) with 10% heat-inactivated fetal bovine serum (FBS), 1% PenStrep (PS, Gibco), and 2mM glutamine (Gibco). When cells were nearly confluent,

the media were replaced, after phosphate buffer saline (PBS) wash, with 5 ml of infection medium (DMEM, 1%FBS, 1%PS, 1%glutamine) containing recombinant TE virus (see details of *in vitro* transcription and transfection in Chapter 4) at a multiplicity of infection (MOI) of 2. After 1 hour of incubation at 37^{O}C 5% CO_2 with rocking every 20 minutes, 10 ml of DMEM with 1% FBS was added for another 3 hours of incubation. All medium was then replaced with 15 ml of fresh DMEM with 1%FBS. After overnight incubation at 37^{O}C 5% CO_2, the supernatant fluid was collected and centrifuged at 2000 rpm for 5 minutes (Sorvall) to eliminate cell debris. The supernatant fluid was aliquoted; the infectious virion number determined by plaque assay (see Chapter 3), and stored at -80^{O}C. The TE stock used for all experiments had a titer of 2.63 X 10^9 plaque forming units (pfu)/ml.

For purification, 1/3 volume of 40% polyethylene glycol (PEG8000, Sigma) with 2 M NaCl (Sigma) was added to virus-containing supernatant fluid. The mixture was incubated at 4^{O}C overnight on a rocker. The PEG precipitate was spun down at 10,000 rpm for 1 hour (Sorvall). Supernatant fluid was removed and the precipitate was resuspended in PBS. This concentrated virus was used directly for ELISA plate coating and gave a very low background. Thus, further sucrose gradient purification was not necessary for the experiments planned. The PEG-treated TE stock had a titer of 9 X10^9 pfu/ml.

Infected BHK cells could also be collected and used as infected cell lysate for ELISA plate coating. Using a cell scraper, cells were collected in cold PBS and centrifuged at 2000 rpm for 5 minutes (Sorvall). The cell pellet was resuspended in 1 ml of PBS with 0.05% Tween-20. Three freeze (-80^{O}C)-thaw (on ice) cycles were done to

lyse the cells. After centrifugation at 2000 rpm $4^{O}C$ for 20 minutes, the lysate (supernatant) was aliquoted and stored at $-80^{O}C$.

Mouse infection and tissue collection

C57BL/6 mice of both sexes, 4-6 weeks old, were inoculated with 20 μl of PBS, containing Sindbis virus TE strain from infected BHK cells either 10^3 pfu for intracerebral infection by an insulin syringe or 10^5 pfu for intranasal infection by a pipette under isoflurane anesthesia.

On planned dates after infection, the mice were euthanized under isoflurane anesthesia. Intracardiac perfusion with 15-20 ml of ice-cold PBS was followed by 40 ml of ice-cold 4% paraformaldehyde (PFA powder, Sigma) in PBS (final pH7.2). Each brain was sliced into 2-3 mm thickness with a razor and immersed in ice-cold 4% PFA overnight at $4^{O}C$. The PFA was then replaced with ice-cold PBS before the brain slices were sent to the Johns Hopkins Pathology Reference Laboratory. In the experiment 2 (below), the 4% PFA perfusion step was omitted, because the left brain hemisphere was used for plaque assay, which required live virus. For spinal cord, the whole spinal column was collected and processed in the same way plus a decalcification step.

Tissue handling and staining

Formalin-fixed paraffin-embedded (FFPE) mouse brains and spinal cords. The embedding, 5-μm sectioning, and mounting of the tissues on positively charged slides was done by Johns Hopkins Pathology Reference Laboratory. The tissues came from 3 independent experiments:

1. Previous study by Talibah Metcalf (50) – mice were intracerebrally inoculated and sacrificed for FFPE with collection of whole brains and spinal cords on days 7, 10, 14, 26, 120, and 180. For each time point, there were 3 infected mice and 2 mock-infected mice (injected with PBS only). Day 3 was added later to represent the peak of infection.
2. The current study (Chapter 3) – mice were intracerebrally inoculated and sacrificed for FFPE of right brain hemispheres on days 0, 1, 2, 3, 5, 7, 10, 14, 21, 30, 45, 60, 90, and 180. There were 3 mice per each time point.
3. The concurrent study by Victoria Baxter – mice were intranasally inoculated and sacrificed for FFPE of whole brains and spinal cords. Only day 3 and 7 were included in this study.

Slide rehydration. All slides were rehydrated before any staining. First, slides were baked at 58^{O}C to melt paraffin and then immersed in xylene substitute 2 times, 6 minutes each. The slides were serially submerged 2 times, 1 minute each, in an ethanol gradient from 100%, 95%, and then 70%. For RNA FISH, the slides were left in 70% ethanol at 4^{O}C for at least 1 hour. If no RNA FISH was involved, the slides were put under running dH_2O for 5 minutes. DEPC-treated H_2O (Quality Biological) was used for all steps of the RNA FISH protocol.

Antigen retrieval. For FISH and TUNEL, antigen retrieval was done by proteinase K digestion. The rehydrated slides (in either 70% ethanol or dH_2O) were immersed in PBS for 10 minutes. Then 50-150 µl of prewarmed 10 µg/ml proteinase K in PBS was put on each slide. A hydrophobic pen (PAP Pen) or coverslip could be used to lower the amount of the reagents needed. The slides were incubated in a slide box with

wet tissue paper on the bottom (humid chamber). They were then washed twice, 3 minutes each, in either PBS or RNA FISH washing buffer.

For IF and IHC, heat retrieval was applied. The rehydrated slides in dH_2O were boiled in 0.01 M sodium citrate pH 6.0 (2.94 g sodium citrate (Sigma) in dH_2O 1 liter, adjusted pH by HCl) with a 1000-watt microwave, 60% power, for 9 minutes. After letting the slides in the buffer cool at room temperature for 20 minutes with intermittent shaking, they were immersed in PBS for 10 minutes.

For protein detection, heat retrieval was the best, followed by proteinase K and no retrieval. In contrast, for RNA detection, proteinase K was the best, followed by no retrieval, and heat retrieval was the worst.

Endogenous peroxidase quenching. This step was done only when peroxidase was used in the detection process. After antigen retrieval, the slides were immersed in 3% H_2O_2 in methanol (7 ml 30% H_2O_2 and 63 ml methanol) for 10 minutes. The slides were washed 3 times, 3 minutes each, in PBS. Because this could decrease the amount of RNA detected, it was omitted in any experiments that involved RNA FISH. Without this step, the background was still acceptable.

Fluorescence in situ hybridization (FISH) of Sindbis viral RNA. The stocks of 25 μM Custom Stellaris RNA FISH probes (LGC Biosearch Technologies) in TE buffer (10 mM Tris-HCl, 1 mM EDTA, pH 8.0) were diluted in hybridization buffer (10% dextran and 10% deionized formamide in 2x saline-sodium citrate (SSC)). The dilutions were 1:100 for the probe against Sindbis viral genomic (nsP2, fluorescein) and 1:1000 for subgenomic (E1 or E2, Quasar570) RNAs.

After proteinase K digestion, the slides were washed twice, 3 minutes each, in washing buffer (10% deionized formamide in 2xSSC). Then 100 µl of hybridization buffer with RNA FISH probe(s) was applied on to each slide and covered by a coverslip. The slides were incubated at 37^{O}C overnight in a humid chamber.

Next day, each slide was washed at 37^{O}C twice, 30 minutes each, with 1 ml washing buffer. DAPI (Sigma) was sometime added to the 2^{nd} wash at 25 ng/ml.

Alternatively, the same probes could be biotinylated with 5'end biotinylation kit (Vector) and used the same protocol. However, after the 2^{nd} wash, the ABC Elite kit was applied as in the IHC protocol, followed by color development with DAB or TSA amplification as in the protocols below.

Immunofluorescence (IF) and immunohistochemistry (IHC). The non-specific binding of antibodies was blocked with 0.04% tritonX in PBS with 10% normal goat serum (NGS) at room temperature for 20 minutes. After brief rinsing of slides with PBS, 150 µl of 0.04% tritonX in PBS with 5% NGS containing diluted primary antibody(ies) was applied to each slide and incubated at 4^{O}C overnight in a humid chamber. A coverslip and/or a hydrophobic pen was applied to prevent the solution from running off the slide. The primary antibodies against viral components were mouse antibodies – dsRNA [J2] (Scicons), E1 [161], E2 [127]; rabbit antibodies – nsP3 [0857], capsid, 6K, poly-antigens (polyNSV). The cell marker antibodies were against mature neurons (NeuN – mouse [A60], Millipore MAB377 and rabbit [EPR12763], Abcam ab177487), immature neurons (DCX – mouse [E-6], Santa Cruz Biotechnology sc-271390), neural stem cells (Nestin – rat [7A3], Abcam ab81462), oligodendrocytes (Olig2 – rabbit

[EPR2673], Abcam ab109186 and PLP – rat [AA3], a gift from Ansi Chang and Bruce Trapp, Department of Neurosciences, Cleveland Clinic), astrocytes (GFAP – rabbit polyclonal, Abcam ab7260), microglia/macrophages (Iba1 – rabbit, Wako 019-19741), B-cell (B220 – rat [RA3-6B2], Abcam ab64100), and T-cells (CD3 epsilon – rabbit polyclonal, Abcam ab49943). All primary antibodies were diluted to 2.5 – 5 μg/ml for staining.

Next day, the slides were washed 3 times, 3 minutes each, with PBS. The species-matched secondary antibodies were diluted at 1:200 in 0.04% tritonX in PBS with 5% NGS. The secondary antibodies for IF were against mouse, rat, or rabbit IgG (H+L), conjugated with AF488 (Invitrogen), AF594 (Invitrogen), or CF633 (Biotium). Anti-mouse IgG-Dylight594 (gamma-chain specific, Abcam ab98738) and anti-mouse IgM-AF488 (mu-chain specific, Invitrogen A21042) were also used to detect classes of endogenous antibodies. DAPI (Sigma) was added at 25 ng/ml if desired. For IHC, secondary antibodies were biotinylated anti-mouse, rat, or rabbit (H+L, Vector) at 1:300 dilution. 150 μl of the diluted secondary antibodies was applied to the slides, incubated at room temperature for 30 minutes. Then the slides were washed 3 times, 3 minutes each with PBS. For IF, the slides were ready for mounting.

For IHC, 150 μl of avidin-HRP (horseradish peroxidase) complex mixture (ABC Elite Kit, Vector; 2 drops solution A and 2 drops solution B in 5 ml PBS) was applied to each slide at room temperature for 40 minutes. The slides were then washed 3 times, 3 minutes each in PBS.

For color development, the slides were incubated with150 µl of 3,3'-diaminobenzidine (DAB) substrate (Vector; 2 drops buffer, 4 drops DAB, and 2 drops H_2O_2 in 5 ml dH_2O) at room temperature for 8 minutes. The slides were then immersed in running dH_2O for 5 minutes.

Alternatively, TSA (protocol below) was applied instead of the DAB substrate.

Terminal deoxynucleotidyl transferase dUTP nick end labeling (TUNEL). Staining was carried out using the TACS 2 TdT Core Kit (Trevigen 4810-30-CK), according to the manufacturer's protocol. After proteinase K digestion and quenching steps, the slides were immersed in 1x TdT labeling buffer for 5 minutes. Then each slide was incubated with 50 µl of labeling reaction buffer (1 µl dNTP mix, 1 µl TdT enzyme, 1 µl Mn^{2+}, and 50 µl 1x TdT labeling buffer), covered by a coverslip, at $37^{O}C$ for 60 minutes in a humid chamber. The slides were then immersed in 1x TdT stop buffer for 5 minutes, and washed twice with PBS, 2 minutes each.

Each slide was incubated with 50 µl of Strep-HRP in PBS (1 µl Strep-HRP and 50 µl PBS) for 10 minutes at $37^{O}C$ in a humidity chamber. The slides were washed twice in PBS, 2 minutes each.

For color development with DAB, the above protocol for IHC was followed. For fluorescence, streptavidin-AF488 gave a poor signal. Thus, tyramide signal amplification was needed.

Tyramide signal amplification (TSA). According to the TSA Kit (Invitrogen) protocol, this method can be applied to any system that uses HRP for detection. HRP activates multiple tyramide-dyes. These many tyramide radicals then covalently bind to

nearby nucleophilic residues, resulting in the amplification of the signal. In this study, tyramide-AF488 was used according to the manufacturer's protocol. It successfully enhanced the signal in immunostaining, FISH, and TUNEL.

After rinsing off the HRP (the mixture of ABC Elite kit or Strep-HRP) with PBS, each slide was incubated with 100 µl of amplification buffer with 0.0015% H_2O_2 and tyramide (1:100 dilution from DMSO stock) at room temperature for 5 minutes. The slides were then washed 3 times, 3 minutes each, with PBS.

Combined RNA FISH and IF. The heat retrieval, quenching, and blocking steps were avoided. Primary antibody was added to the hybridization buffer and incubated together with the Stellaris probe(s) overnight as in FISH protocol. The secondary antibody step was added between the first and second washes: each slide was incubated with 100 µl of 1:200 secondary antibody(ies) in hybridization buffer at 37^{O}C for 30 minutes.

Combined TUNEL-TSA, RNA FISH, and IF. TUNEL-TSA did not affect the result of IF, and vice versa, when performed sequentially. However, RNA FISH first completely abolished the later TUNEL-TSA signal. On the other hand, TUNEL-TSA first partially decreased the later RNA FISH signal, but was acceptable.

After proteinase K digestion, without quenching or blocking, TUNEL-TSA was applied to each slide first, followed by combined RNA FISH/IF.

Imaging

DAB staining (brown) was captured in bright field with Nikon TE800. The fluorescence imaging was captured with various epifluorescence microscopes, which were Nikon TE800, Nikon TE2000, Nikon 90i, and Zeiss Axio Imager M2. The filter sets were DAPI (DAPI), FITC (AF488, fluorescein), Texas Red (AF594, Quasar570), and Cy5 (CF633). The imaging software was Spot Advance (Nikon TE800 and Nikon TE2000) and Volocity (Nikon 90i and Zeiss Axio Imager M2). Zeiss Axio Observer Z1 with LSM780FCS confocal microscope and Zen software was also used. The lasers used were 405 nm (DAPI), 488 nm (AF488, fluorescein), 561 nm (AF594, Quasar570), and 633 nm (CF633).

Neonatal mouse brain inoculation

For testing whether there were still a small number of infectious virions undetectable by plaque assay in the adult mouse brains at 14 days after infection with SINV TE, 26 CD1 and 36 C57BL/6 neonatal (day 0) mice were intracerebrally injected with 10 µl of pooled 10% brain homogenates (day 14 post TE). The pup whole brains were collected at either day 3 or day 7 after inoculation. The whole brains were homogenized in Lysing Matrix D (MP Biomedicals), filled with 1 ml ice-cold PBS, by FastPrep-24 (MP Biomedicals; speed 4 m/s, 40 seconds). The homogenates were tested for infectious virions by plaque assay (see Chapter 4).

Brain slice culture (Figure 2.1)

Mouse organotypic brain slice cultures were done to see whether persistent Sindbis virus could reactivate after the supply of immune cells and antibody from circulation had been eliminated. Three 5-week-old C57BL/6 mice, infected

intracerebrally with SINV TE as described above, were sacrificed on day 21 after infection (long after infectious virion had been cleared).

The process was adapted from organotypic hippocampal slice culture by Hyunjeong Kim, et al (67). After isoflurane euthanasia, intracardiac infusion of 15 ml ice-cold dissection medium (Hybernate A, 2% B27, 2mM glutamine, 1% PenStrep, all from Gibco), the brain was removed and immersed in a petri dish filled with ice-cold dissection medium. To prevent sticking to the razor blade, the brain was embedded in ice-cold precast 1.2% bacto agar on autoclaved Whatman filter paper. The agar-embedded brain was sliced, 300-μm thickness, with a McIlwain tissue chopper. Each slice was placed on a Transwell insert inside a 6-well plate filled with prewarmed slice culture medium (Neurobasal A, 2% B27, 2 mM glutamine, 1% PenStrep, all from Gibco). Two to three slices were put on each insert and each mouse had 2 inserts. The slices were cultured at 37^{O}C 5% CO_2. The supernatant fluids were collected and completely replaced with fresh culture medium everyday. The collected fluids were tested for SINV-specific IgG by ELISA. To assay for infectious virions, 50 μl of the supernatant fluid was added to BHK cells in a 96-well plate. The cells in each well were observed for cytopathic effect with an inverted microscope for 48 hours after infection.

Sindbis-specific enzyme-linked immunosorbent assay (ELISA)

Because mouse serum IgM strongly reacted with non-infected BHK lysate, using infected cell lysates for coating was not appropriate. TE-infected culture medium diluted in coating buffer gave much less background, but PEG-concentrated TE (see the preparation above) was better. Furthermore, PEG-treated TE coating was much more

efficient (200-1000 ELISA plates/T150 flask of BHK culture) than the traditional TE-infected cell lysate (1-5 ELISA plates/T150 flask).

Each well of the Maxisorp (Nunc) 96-well plate was coated with 10^6 pfu PEG-treated TE in 50 µl coating buffer (50 mM $NaHCO_3$ pH 9.6) at 4^OC overnight in plastic wrap. The plate was washed once with 200 µl/well of washing buffer (PBST-2% FBS; PBS, 0.05% Tween20, 2% FBS) and then blocked with 200 µl of blocking buffer (PBST-10% FBS) at 37^OC for 2 hours.

The plate was washed twice with washing buffer. The samples were diluted in 50 µl of blocking buffer at 1:100 for serum, 1:8 for 20% brain homogenate, and 1:2 for supernatant from brain slice culture. The plate was incubated with diluted samples, each in triplicate, at room temperature for 2 hours.

The plate was washed 4 times with washing buffer. Each well was then incubated with the desired secondary antibodies (HRP-conjugated anti-mouse IgG, IgG1, IgG2a, IgG2b, IgG3, IgM, or IgA; SouthernBiotech) diluted 1:1000 in 50 µl blocking buffer at room temperature for 1 hour.

The plate was washed 4 times with washing buffer and then incubated with 100 µl/well of TMB substrate (BD OptEIA TMB substrate Reagent Set, BD Biosciences) at room temperature up to 20 minutes. The reaction was stopped with 25 µl/well of H_2SO_4. The optical density (OD) was read at 450 nm with Multiskan MCC (Thermo Scientific).

Long-range reverse-transcription polymerase chain reaction (RT-PCR)

RT-PCR to detect Sindbis TE viral RNA was performed on 4 μg of brain RNA extract in 20-μl reaction, using LongRange 2Step RT-PCR Kit (Qiagen) according to the manufacturer's protocol. Long-range reverse transcription was done with a thermocycler (42^{O}C 2 hours, 85^{O}C 5 minutes) using either oligo-dT or Sindbis-specific oligo-dT (**Figure 2.15** GTAAAG-oligo-dT, included the last 6 complementary bases of SINV TE before poly-A). Then PCR was performed on 2 μl of the long-range cDNA in 50-μl reaction. The primer pairs were SV1400F-SV4100R (nsP1-nsP2), SV8996F-SV11384R (E2-E1), and SV8456F-SV11384R (E3-E1). The thermocycler setting was 3-minute hold at 95^{O}C; 40 cycles of 95^{O}C 30 seconds, 55^{O}C 30 seconds, and 68^{O}C 3 minutes; and then 2nd hold at 68^{O}C for 5 minutes. The PCR products were subjected to agarose gel electrophoresis. Pictures of the ethidium bromide-stained gels were captured with Gel Doc (Bio-Rad).

Immunoprecipitation of Sindbis virus replication complex

10 μg of anti-nsP3 (rabbit 0857) (68, 69) was incubated with 200 μg of protein (measured in brain homogenates by Pierce BCA Protein Assay Kit, Thermo Scientific) in 600 μl of RIPA buffer at 4^{O}C for 2 nights on a rocker. 20 μl of protein A plus agarose (Pierce) was equilibrated with RIPA buffer. After removing the buffer, the agarose was mixed with the anti-nsP3-brain complexes and rocked at 4^{O}C overnight. The agarose beads were washed 6 times with RIPA buffer, and then boiled (heat block, 95^{O}C) in 20 μl of SDS/βME lysis buffer. The whole supernatants were loaded onto a gel (see below).

SDS-PAGE and Western blot

Whole immunoprecipitate or 20 μg of protein in brain homogenate was loaded onto each lane of a precast gel (BioRad). Electrophoresis was run at 200 V in running buffer (25 mM Tris base, 0.2 M glycine, 0.1% SDS). The proteins on the gel were transferred to a nitrocellulose membrane at 100 V for 1 hour in transfer buffer (25 mM Tris base, 0.2 M glycine, 20% methanol). The membrane was blocked with 10 ml of 5% skim milk in TBST (20 mM Tris, 150 mM NaCl, 0.1% Tween20) at room temperature for 1 hour. Overnight incubation on a rocker at 4^{O}C was done with either rabbit anti-NeuN (1:5000, clone EPR12763, Abcam) or mouse anti-NeuN (1:500, clone A60, Millipore) in TBST with 5% bovine serum albumin (BSA, Sigma). After washing with TBST, either anti-rabbit-IgG-HRP or anti-mouse-IgG-HRP in TBST with 1% skim milk at room temperature for 1 hour. Substrate was added, and the chemiluminescence was detected by film.

Results:

Two patterns of viral distribution. There were two patterns of viral distribution in CNS, white and gray matter tropisms (**Figure 2.2**). After intranasal inoculation, it was always a gray matter pattern, while intracerebral injection could result in both white and gray matter infection (**Figure 2.3)**.

In gray matter tropism, infection began with a few infected cells scattered over the cerebral cortex, hippocampus, and basal ganglia on day 1. Later, the infection spread and formed multiple clusters of infected cells (**Figure 2.2, 2.3**).

In white matter tropism, infection began with diffuse involvement of white matter tracts, especially the corpus callosum and periventricular white matter as early as day 1.

Later, the infection spread to the adjacent pyramidal neurons in the CA1 layer of the hippocampus (**Figure 2.2, 2.3**).

The numbers of infected cells reached a peak on day 3 for both patterns, and then gradually declined. At late times, the patterns remained the same as at the early times. In white matter tropism, infection in the hippocampus was cleared first. In gray matter tropism, clearance began at the center of infected cluster, which represented the cells of early infection (**Figure 2.3**). Both FISH and IF detected infected cells up to 4 weeks after infection.

During late time points (day 7 and beyond) in both tropisms, the amount of viral RNA and proteins declined at the original sites of infection (**Figure 2.4**). SINV E1 protein appeared in autofluorescent brown-pigment macrophages (Iba+) that infiltrated the pia mater and blood vessels close to the infected sites. These macrophages also directly infiltrated infected areas, beginning on day 7-10, and were most abundant around 1 month after infection (**Figure 2.4-2.6**).

Two types of infected cells. Cell types that were infected mainly depended on the distribution patterns (**Figure 2.7**). For white matter tropism, the infected cells were mostly oligodendrocytes (Olig2+/-, PLP+). The infection decreased Olig2 expression (**Figure 2.8**), so more than one marker was needed to identify the cells. The spread of infection to hippocampus involved pyramidal neurons (typical cell shape in CA1 layer), which were positive for NeuN in the cytoplasm.

For gray matter tropism, the infected cells were neurons (NeuN+). However, the usual nuclear NeuN was relocalized to the cytoplasm in the infected cells. For neurons that contained no virus, NeuN was still in their nuclei (**Figure 2.7, 2.9**).

Suppression of NeuN. SDS-PAGE and Western blot of pooled infected-brain homogenates showed depletion of NeuN both 45 and 50 kD isoforms from day 7 until day 60, before recovering on day 90. NeuN could also be co-immunoprecipitated by anti-nsP3, the antibody for precipitation of SINV replication complex (**Figure 2.10**).

Persistent viral components. At peak of infection, day 3, all viral components could be found in abundance (**Figure 2.11**). However, from day 7 onward, the most prominent component was viral capsid, followed by viral subgenomic RNA (**Figure 2.12**). Genomic RNA was no longer detectable. Other components could be seen in a small number of cells. Unlike on day 3, the viral envelope proteins (E1 and E2) were seen only inside the cells, not on the plasma membrane at late time points. E1 could also be seen in macrophages (see above). Most viral components were seen only in the cell body at late time points. In contrast, viral components were found in dendrites and axons in the early phase.

Table 2.1 Viral components detected in brains

Viral components	D3	D7-26
Genomic RNA	+++	-
Subgenomic RNA	+++	++
dsRNA	++	+
nsP3	++	+
Capsid protein	+++	+++
6K	++	+
E1 protein	+++ (Perinuclear and cell membrane)	+ (Perinuclear)
E2 protein	+++ (Perinuclear and cell membrane)	+ (Perinuclear)

Persistent viral RNA only found in live cells. TUNEL, a test for cell death, was never positive in nuclei of cells that contained viral RNA, detected by FISH. Cells that had viral RNA always expressed some viral proteins (**Figure 2.13**), especially the capsid protein. Infected cells that contained viral proteins without RNA could be either positive or negative for TUNEL (**Figure 2.14**).

No infectious virus detected by newborn mouse brain inoculation. CD1 newborn mice intracerebrally injected with D14-infected brain homogenate had no infectious virus detected. The experiment was repeated with fresh D14-infected brain homogenates on C57BL/6 newborns. Again, none of them had any infectious virus in their brains either 3 or 7 days after infection.

Prolonged anti-SINV antibody production without viral reactivation *ex vivo*. ELISA could detect SINV-specific antibody in supernatant fluids from brain slice cultures of mice 3 weeks after infection for up to 3 weeks *ex vivo* (**Figure 2.15)**. No viral reactivation was found from slice cultures up to 4 weeks.

No complete genome detected in persistent SINV RNA. Both genomic and subgenomic SINV RNA could be detected by long-range RT-PCR in D3-infected brain RNA extract. However, in day 14 and 21 brain RNA, intact genomic RNA was not detectable, and multiple sizes of subgenomic RNA were found on agarose gel electrophoresis (**Figure 2.16**).

Table 2.2 Summary of persistent virus

Characteristics	Day 1-5	Day 7-30
Sindbis clearance	Infectious virions	Viral RNA
Distribution	White matter (oligo) or Gray matter (neuron)	
Viral components (RNA FISH and IF)	All	Subgenomic RNA, capsid No genomic RNA
Viral genomic RNA (RT-PCR)	Intact	Undetectable
Viral subgenomic RNA (RT-PCR)	Intact	Various sizes

Discussion:

The distributions and cell types during viral persistence are the same as in the early phase of infection and depend on the inoculation technique. Interestingly, Sindbis virus can infect neurons in gray matter, while sparing oligodendrocytes in white matter, and vice versa.

All intracerebrally inoculated brain tissues from previous study #1 (Talibah's) (50) and my early samples resulted in 100% white matter patterns. However, later on, the patterns shifted to approximate 1:1 ratio of white versus gray. This coincided with the change from 100- to 30-unit insulin syringes for intracerebral injection, since the tiny scale of the former was much harder to precisely deliver 20 µl of inoculum. Most of the

time, the volume was doubled when using 100-unit syringes. This suggests that the higher volume contributes to the higher chance of white matter tropism. The explanation is probably that the mouse brain left hemisphere, 90 μl (70), cannot contain the inoculum, which leaks into the cerebrospinal fluid (CSF) in the ventricular system and causes rapid widespread infection in periventricular white matter.

In the gray matter distribution, the infection begins with a few discrete infected cells, far apart from each other, in cerebral cortex of the right hemisphere. This suggests long distance transmission of virus from the inoculation site in the left hemisphere. The virus probably spread through the synapse of the long axon across the corpus callosum. After that, infected cells spread the virus to adjacent neurons and form an expanding cluster of infection. Sometimes, axon connections between foci can be observed.

Types of susceptible cells that Sindbis virus first encounters likely determine the tropisms. In intranasal inoculation, these very first susceptible cells will be in the olfactory neuroepithelium. If the intracerebral inoculum does not leak into the ventricles, the virus will infect the neurons that surround the injection site. However, if the inoculum does leak, the virus will infect oligodendrocytes in periventricular white matter instead. We can ensure the white matter tropism by increasing the volume of inoculation. This may be an alternative model for multiple sclerosis, after experimental autoimmune encephalomyelitis (EAE) and Theiler's murine encephalitis virus-Induced demyelinating disease (TMEV-IDD) (71).

The virus continues to target the same type of cells that it first infects. This ‘viral imprint’ might be due to an adaptation of the virus to particular host cells. In clinical

disease, some viruses also variously distribute in the nervous system, involving different cell types. For instance, cytomegalovirus (CMV) can cause polyradiculitis, focal brain lesions, encephalitis, or ventriculitis (72).

Some of autofluorescent-pigmented macrophages that appear at late time points contained SINV E1 protein. The viral protein was not freely distributed in cytoplasm. Thus, these macrophages most likely phagocytosed infected cells. So far, only E1 has been found in macrophages. It might be more resistant to proteases than other viral proteins. Finding these macrophages along the pia mater or blood vessels close to the infection sites suggests that resident cells of brain cannot clear all the viral proteins and need macrophages from the periphery for removal.

Sindbis virus infection also remarkably alters the cell marker expressions. It abolishes Olig2 in oligodendrocytes, and relocalizes NeuN from the nucleus to the cytoplasm in neurons. Other viruses and conditions can cause these phenomena too. EAE and TMEV-IDD deplete Olig2, a transcription factor involved in oligodendrocyte development, and inhibit remyelination (73, 74).

NeuN, also known as rbFOX3, is a splicing factor that controls alternative splicing of another splicing factor, rbFOX2 (75). The RNA binding site of NeuN is UGCAUG, which is found in TE both in the plus strand (7 sites - nsP1, nsP2, nsP3, 2 in nsP4, E2, E1) and minus strand (2 sites - nsP1, nsP4). Its use in viral replication might partially explain the neurotropism of SINV. There are 4 major isoforms, 2 in 50 kD and another 2 in 45 kD ranges. All retain their splicing activity. The cytoplasmic predominant isoform is one of the 45 kD isoforms (75). However, co-immunoprecipitation with anti-

nsP3 shows the 50 kD isoform(s) is the one that associates with viral replication complex. Thus, the SINV-induced cytoplasmic NeuN is likely due to the retention of nuclear isoform(s) in the cytoplasm rather than the accumulation of the cytoplasmic isoform.

Some exceptions for nuclear-localized NeuN include Dogiel type II neurons in guinea pig intestines, which express cytoplasmic NeuN (76). Some pathologic conditions can also alter the NeuN expression pattern. Cerebral ischemia can deplete NeuN immunoreactivity in intact neurons (77, 78). HIV encephalopathy can cause NeuN depletion and cytoplasmic relocalization in uninfected neurons affected by the secretion of Tat protein from HIV-infected microglia (79, 80).

The change of RNA binding protein localization from nucleus to cytoplasm by Sindbis virus has also been observed for HuR, an mRNA stabilizing protein (81). This phenomenon in mammalian cells is quite specific to alphaviruses, and occurs in Sindbis, Ross River, Western equine encephalitis, and Chikungunya, but not dengue or measles viruses (82). The high affinity binding sites between HuR and alphaviral RNAs are at a U-rich element (URE, just upstream of CSE) in Sindbis virus and 3' terminal conserved sequence element (CSE) in all alphaviruses. The cytoplasmic localization of HuR requires neither URE nor the presence of viral RNA. Instead, it requires viral replication and/or expression. Caspase-induced cleavage of HuR is another mechanism for cytoplasmic HuR localization found in stress, but not in SINV infection. SINV infection can also induce dephosphorylation of HuR localization, a mechanism not yet found in other conditions. This is likely the major mechanism for cytoplasmic localization of HuR, because Cdk1-induced phosphorylation of HuR is responsible for its nuclear accumulation (83). All major isoforms of NeuN are also phosphorylated (84). Thus, the

SINV-induced dephosphorylation might apply to SINV-induced cytoplasmic localization of NeuN too.

In addition to relocalization, SINV remarkably depleted all major isoforms of NeuN, shown in Western blot. Considering the small percentage of infected neurons, most uninfected neurons must be affected too, similar to HIV encephalopathy (79, 80). Unlike the cytoplasmic relocalization, depletion does not happen on post infection day 3, the peak of infectious virion and viral RNA titer, but later during clearance on day 7 to 60. Thus, inflammation rather than virus infection itself likely causes the depletion.

Contrary to what we had expected, detectable viral proteins (IF) persist longer than viral RNA (FISH), especially viral capsid in dying cells and E1 protein in macrophage phagosomes. FISH and IF are at least 100 times less sensitive than RT-qPCR. They can detect viral components only up to 1 month after infection, equal to 10^4 viral RNA copies/10^6 GAPDH RNA (see chapter 3), while RT-qPCR can easily detect 100 viral RNA copies for many months.

The persistent viral RNA most likely retains its function of protein translation, because it is found exclusively in live cells that express one (capsid) or more viral proteins. However, there are no data on the half-life of these proteins in infected cells. Thus, viral proteins may just outlive their encoding mRNA.

The persistent viral RNA is unlikely to be replication-competent, because genomic RNA is not detectable by FISH or long-range RT-PCR. Nevertheless, we can detect dsRNA up to 1 month after infection. Anti-dsRNA is a mouse antibody, making it impossible to distinguish the high background in mouse brains from the small amount of

dsRNA at later time points. Theoretically, dsRNA in viral replication complexes is a duplex of full genomic plus and minus strands. Therefore, there might be some intact viral genome left. In fact, in a mouse model of Coxsackie B viral encephalitis, the genomic plus/minus ratio declines over time and approaches 1:1 at late time points, which suggests that persistent RNA is double-stranded in nature (65). Unfortunately, neither methods for FISH nor long-range RT-PCR for dsRNA has yet been established.

How can the virus persist in the presence of high neutralizing antibodies at late time points? The absence of antibody on the surface of infected cells (**Figure 2.17**) suggests that anti-SINV antibody (found abundantly in brains with ELISA) cannot bind to the cell membrane of infected cells. The long-range RT-PCR also shows that there are some large deletions of E2-E1 gene by day 14. Thus, the lack of expression of envelope proteins may help the virus avoid antibody-mediated clearance, but renders the virus unable to be reactivated.

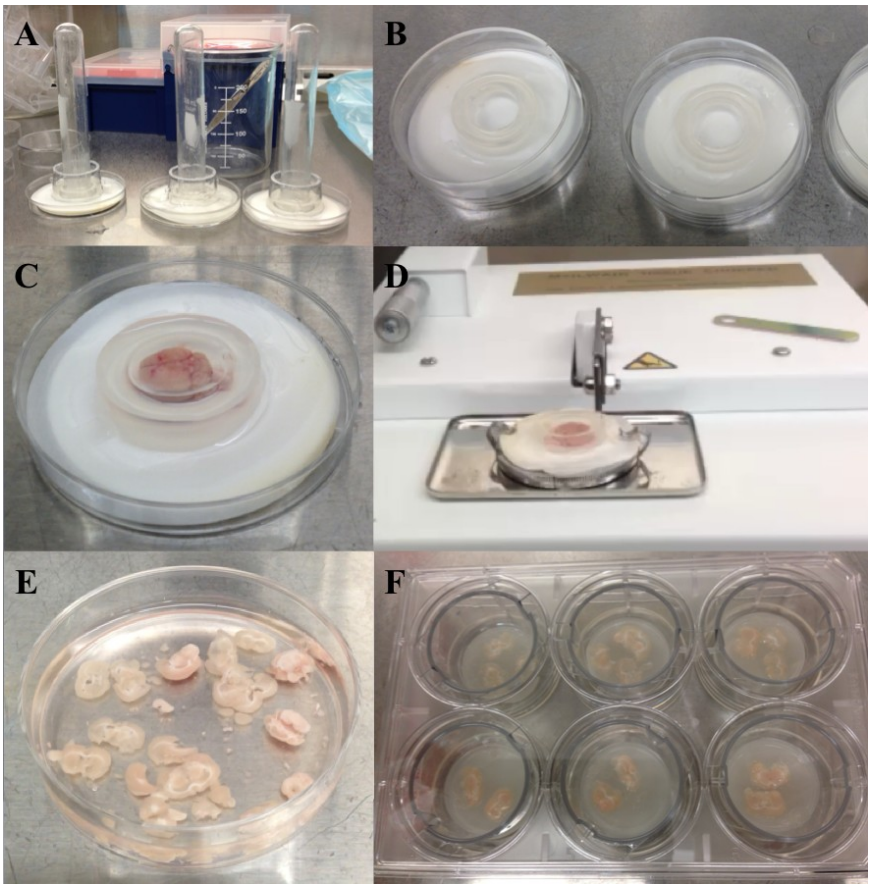

Figure 2.1 Brain slice culture procedure. The precast agar was prepared beforehand by pouring the liquefied (by microwave) 1.2% bacto agar into the mold made of clean filter paper, a Transwell insert (membrane removed), and a glass tube (A). The insert and the glass tube were removed after solidification of the agar (B). This precast agar was kept on ice inside a 60-mm dish. The brain was placed inside the center pit and more liquefied agar was added just to cover the brain (C). After the entire agar solidified, 300-μm thickness of the agar-embedded brain on filter paper was sliced by a McIlwain Tissue Chopper (D). The excess agar was removed by scalpel and the chopped brain was returned to the dissection medium. Each slice was separated by a spatula and scalpel (E). The slice was then placed on a 37^{O}C prewarmed Transwell insert with slice culture medium in a 6-well plate (F).

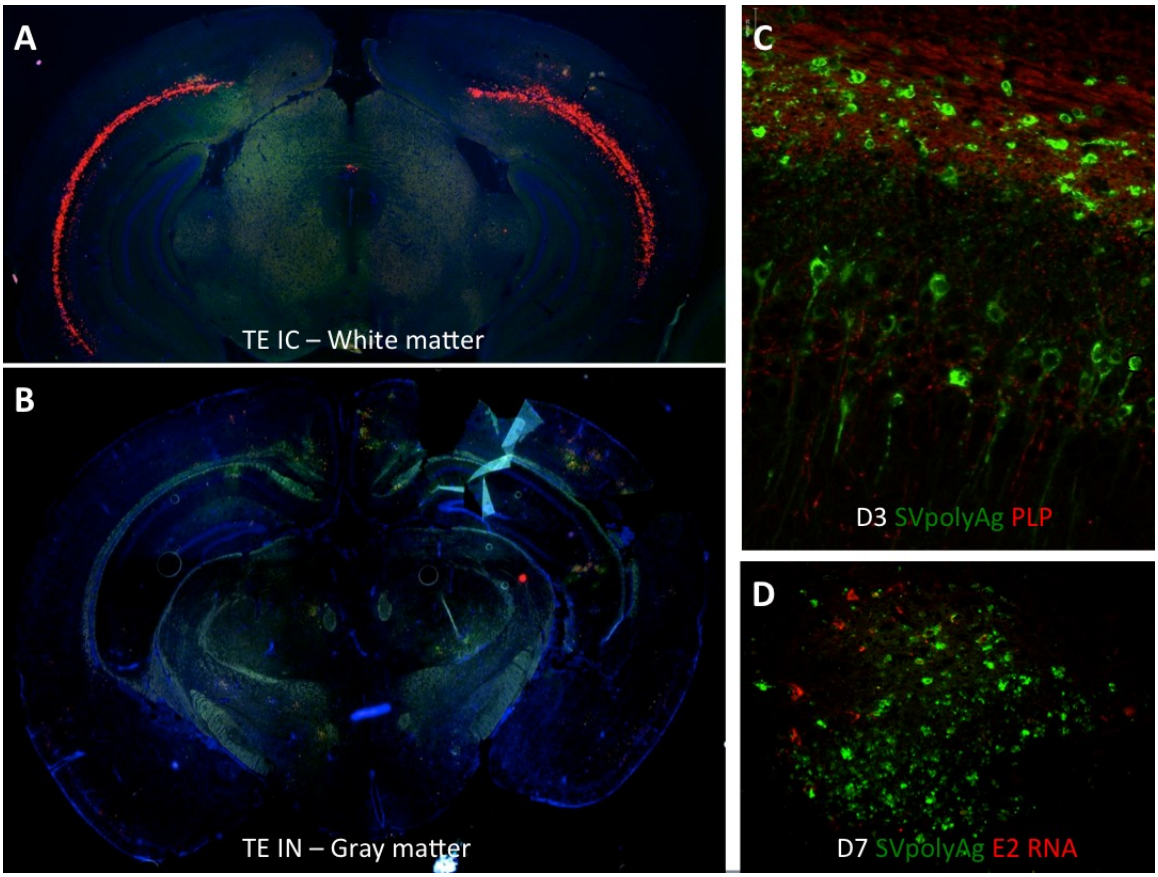

Figure 2.2 Mouse brains, 3 days post infection, show widespread white matter distribution (A) after intracerebral injection and multi-cluster gray matter distribution (B) after intranasal inoculation (red – SINV E1 RNA, green SVpolyAg). Higher magnification (C) of the white matter pattern shows the virus spreading to pyramidal neurons in the CA1 layer of the hippocampus (green – SVpolyAg, red – PLP). Higher magnification of an infected cluster in the gray matter pattern (D) (red – SINV E2 RNA, green – SVpolyAg)

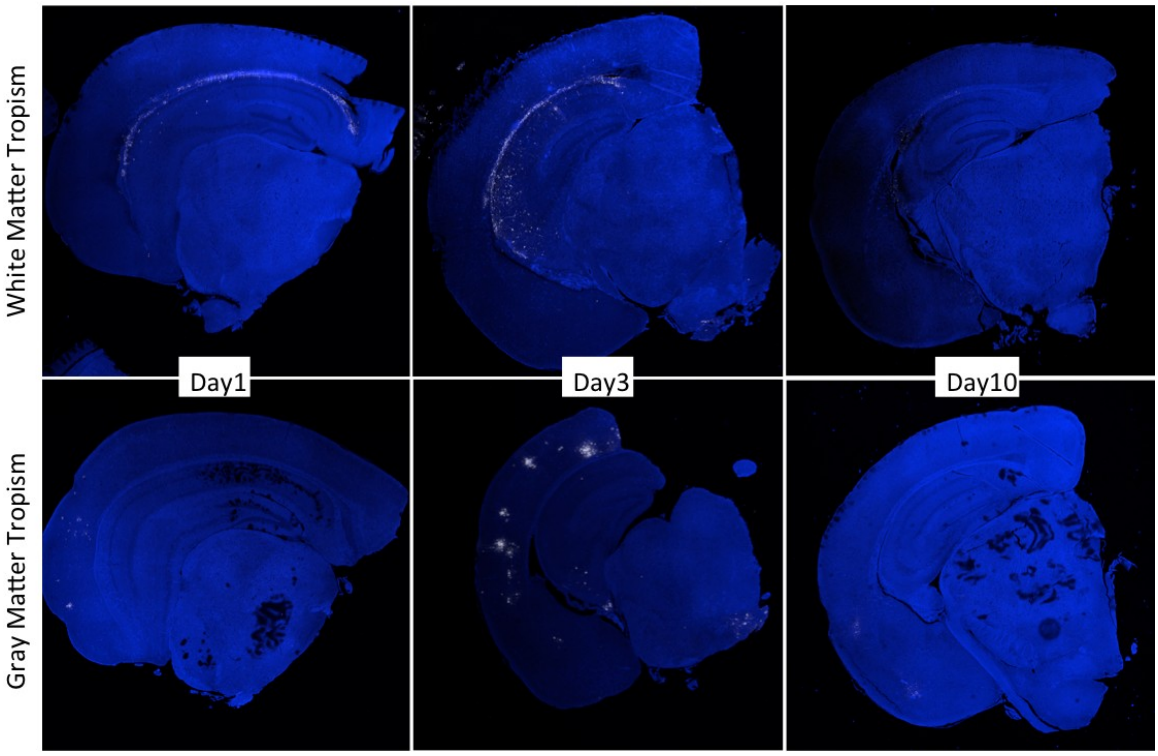

Figure 2.3 Right hemispheres of mice, intracerebrally injected with SINV TE from day1-10. These images demonstrate the progression of viral spreading and clearance in mouse brain (white – SvpolyAg, blue – Dapi). Though inoculated in the same way, the distribution patterns are opposite between the white matter pattern (upper row) and gray matter pattern (lower row).

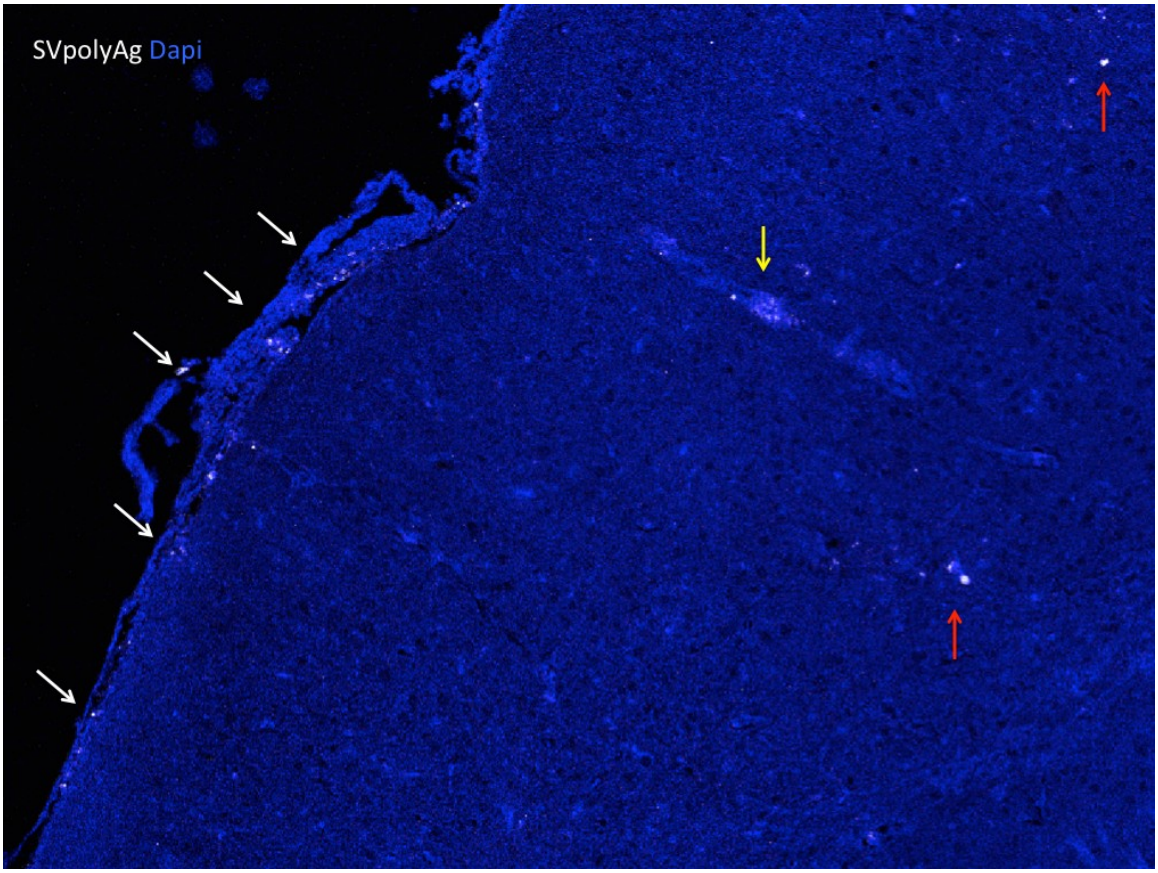

Figure 2.4 Image shows distribution of SINV protein (white) in a mouse brain, 3 weeks after infection. While the host clears most of the viral protein in the original infected areas (white arrows), the viral protein now can be seen in the wall of a blood vessel (yellow arrow) and along the thickened pia mater (white arrow).

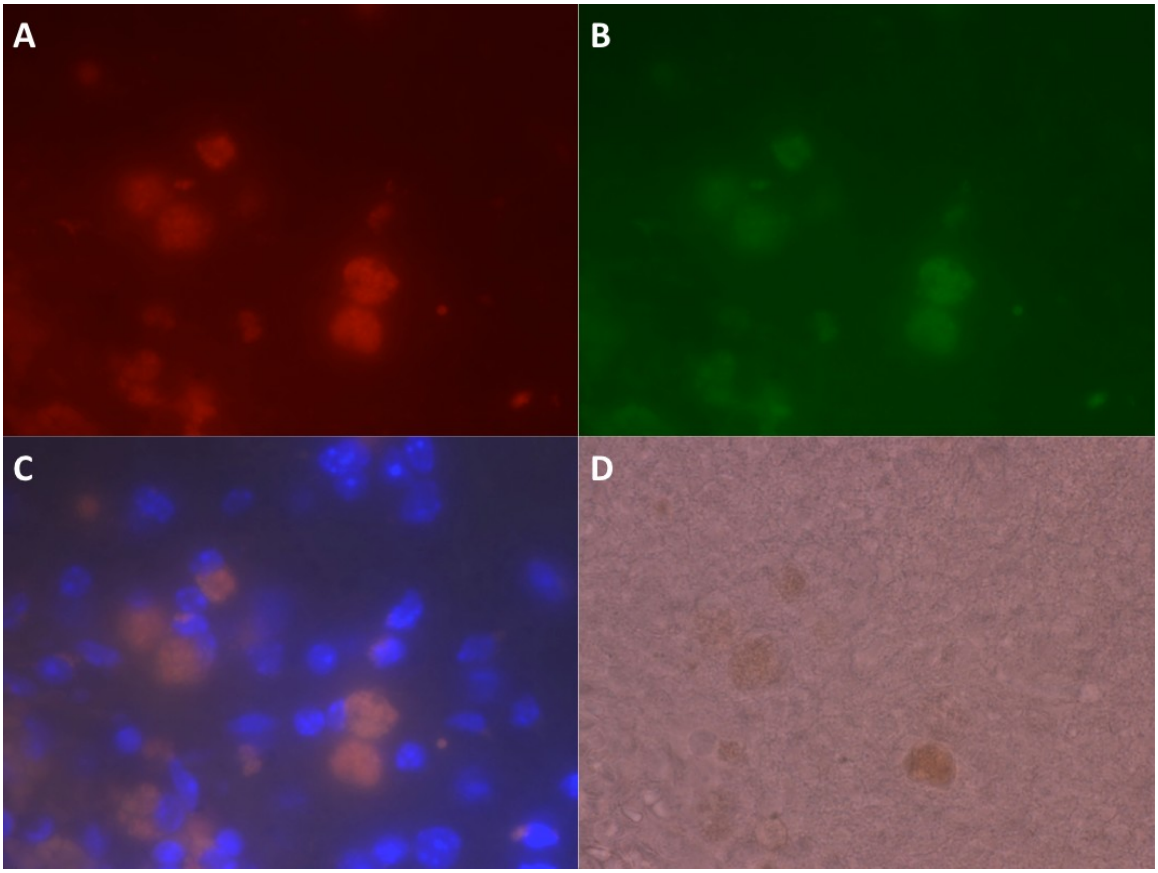

Figure 2.5 Autofluorescent pigmented macrophages. The image of a mouse brain, 26 days after infection, show autofluorescene in both red (A) and green (B) channels in the absence of fluorescent dye, except Dapi. The merged image (C) shows the autofluorescence in orange color, which colocalizes with the brown pigment, observed in phase-contrast (D). These cells are macrophages (see the next figure).

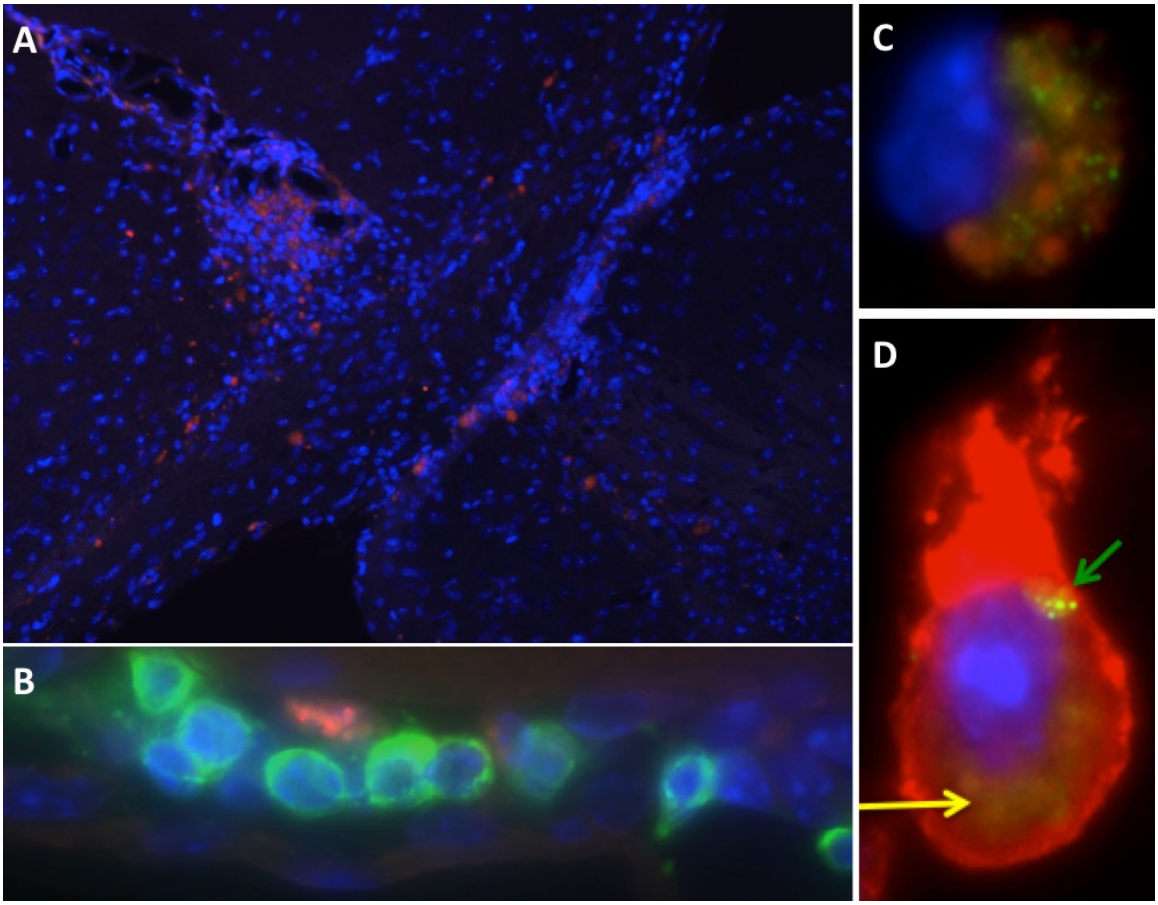

Figure 2.6 The image shows infiltration of the falx cerebri and corpus callosum by autofluorescent macrophages (orange) in the mouse brain, 26 days after TE infection. Autofluorescent macrophages (orange) infiltrate the pia mater (B) together with antibody-producing cells (green). One macrophage also contains SINV proteins (red). Zoom-in image C shows SINV proteins (green) in a cell containing autofluorescent (orange) pigment. The cell (D) with autofluorescence (yellow arrow) is positive for a macrophage surface marker, Iba1 (red), and the viral protein found inside is E1 (green arrow).

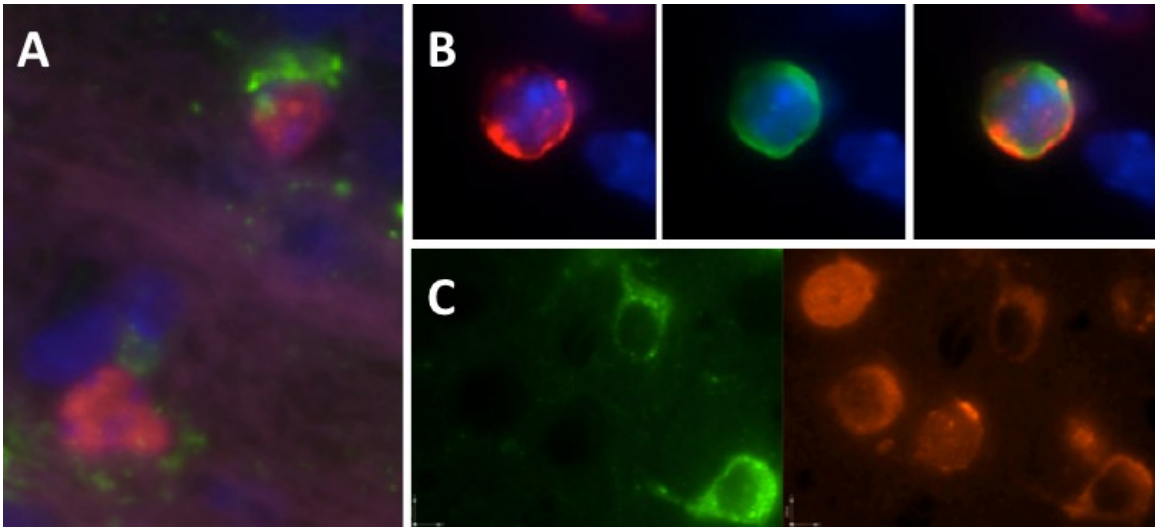

Figure 2.7 The images show cell types in brains 3 days after infection with SINV TE. In white matter tropism, infected cells are mostly oligodendrocytes (A – Olig2 (red) and SV E1E2 (green); B – PLP (red) and SVpolyAg (green)). In gray matter tropism (C), infected cells (SVpolyAg –green) are positive for cytoplasmic NeuN (red), a marker for mature neurons.

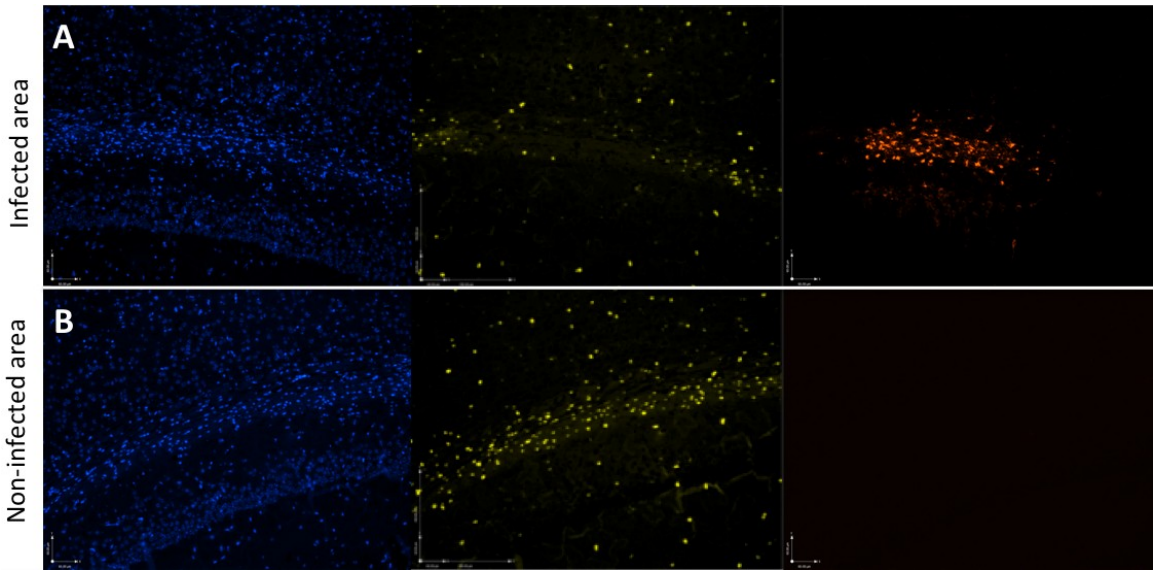

Figure 2.8 In the same mouse brain, 3 days post SINV TE infection, the infected area (A) loses the Olig2 signal (yellow) along the white matter tract, while the non-infected area (B) retains the signal. (red – SINV RNA E1E2, blue – Dapi)

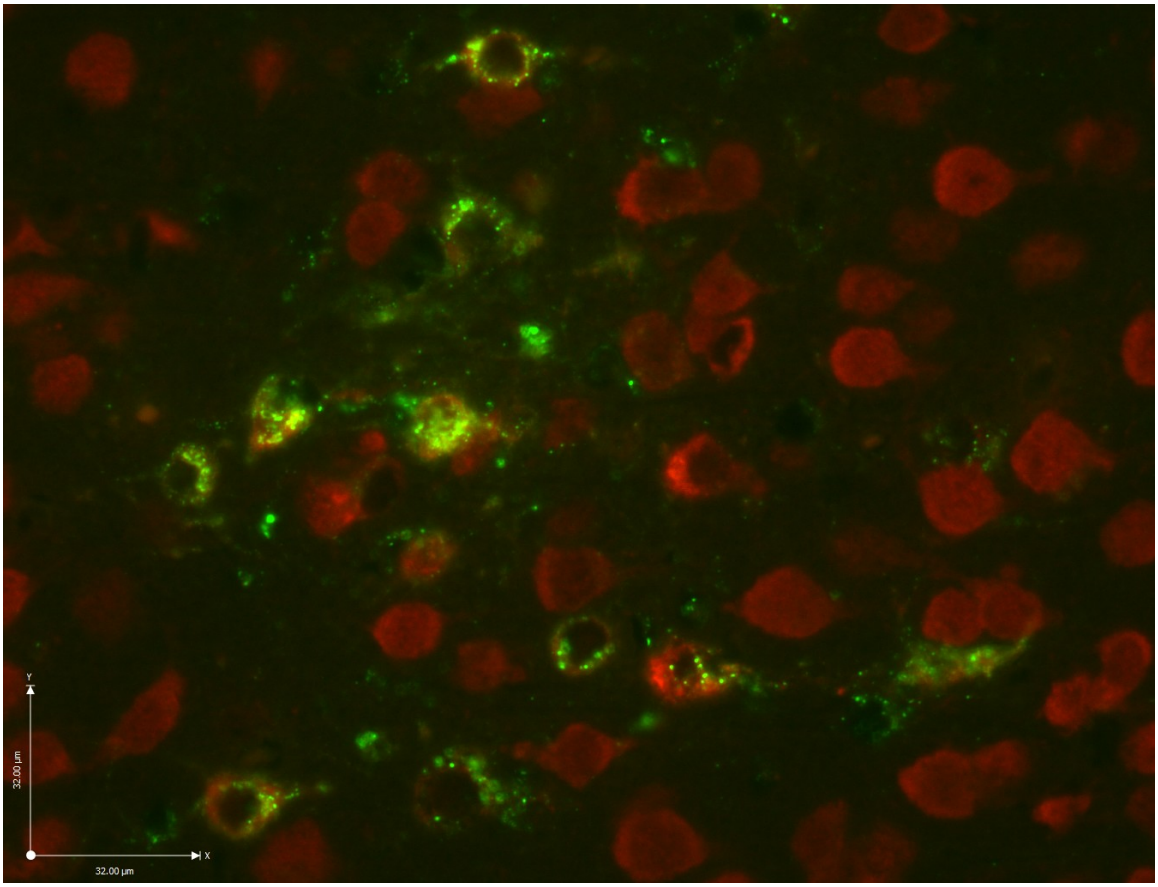

Figure 2.9 In the mouse brain, 3 days post SINV infection, the infected cells (green – E1E2) lose NeuN (red, different monoclonal antibody from Figure 2.7) signal in their nuclei, but have NeuN in the cytoplasm.

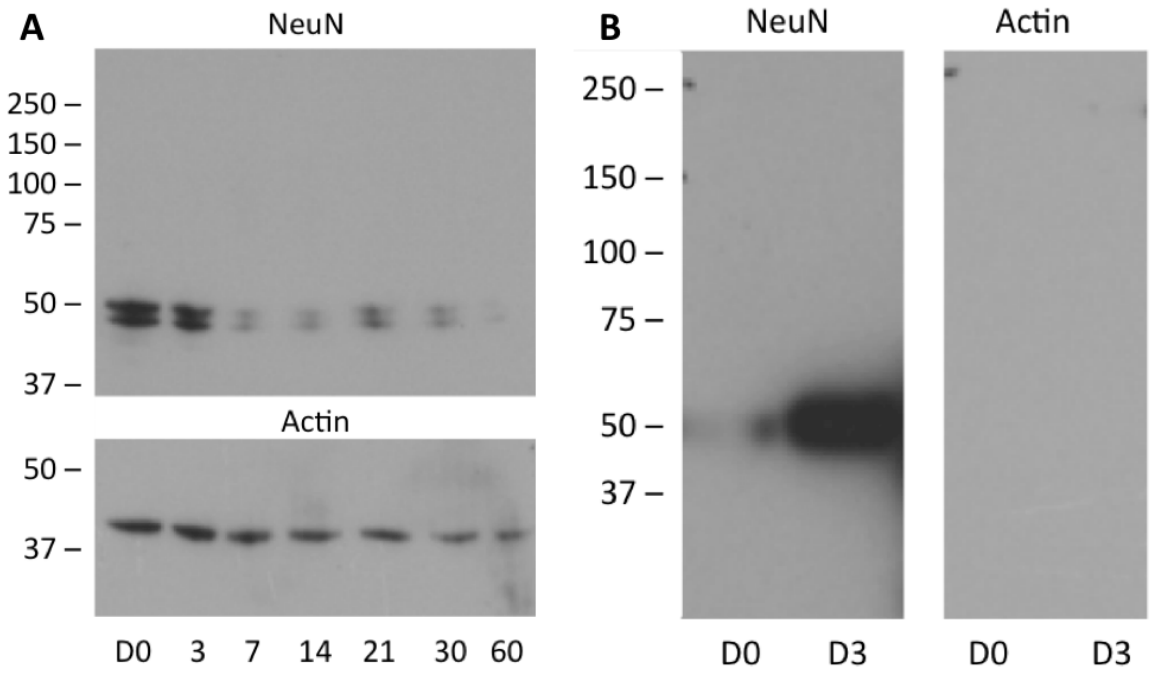

Figure 2.10 Western blot of TE-infected brain homogenates (pooled from 3 mice/time point) during day 0-60 shows the decrease of NeuN from day 7-60 post SINV TE infection (A). Immunoprecipitation with anti-nsP3 (B) co-precipitates NeuN on day 3 after infection (B).

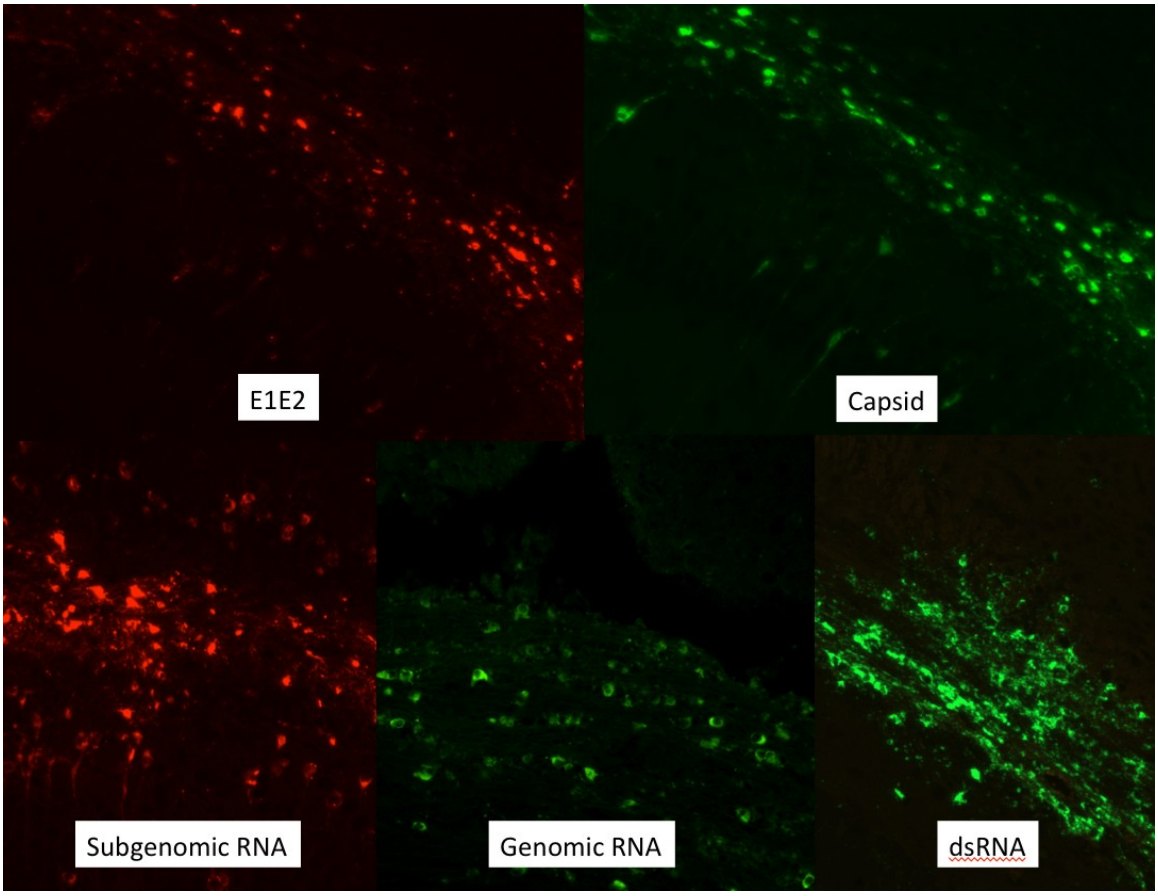

Figure 2.11 All viral components are found in abundance in mouse brains, 3 days post SINV TE infection.

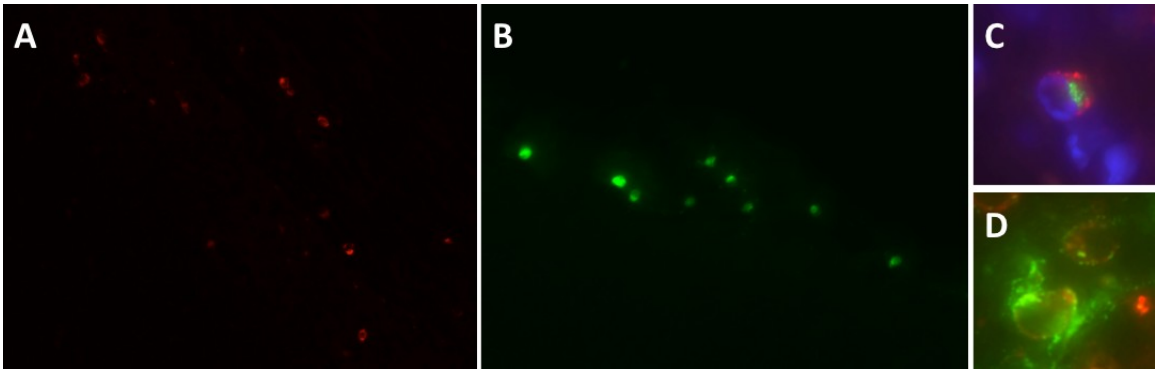

Figure 2.12 On day 7 after SINV TE infection, the main viral components found are subgenomic RNA (A – red) and capsid (B – green), while nsP3 (C – red), envelope (C – green), and dsRNA (D – green) are found infrequently.

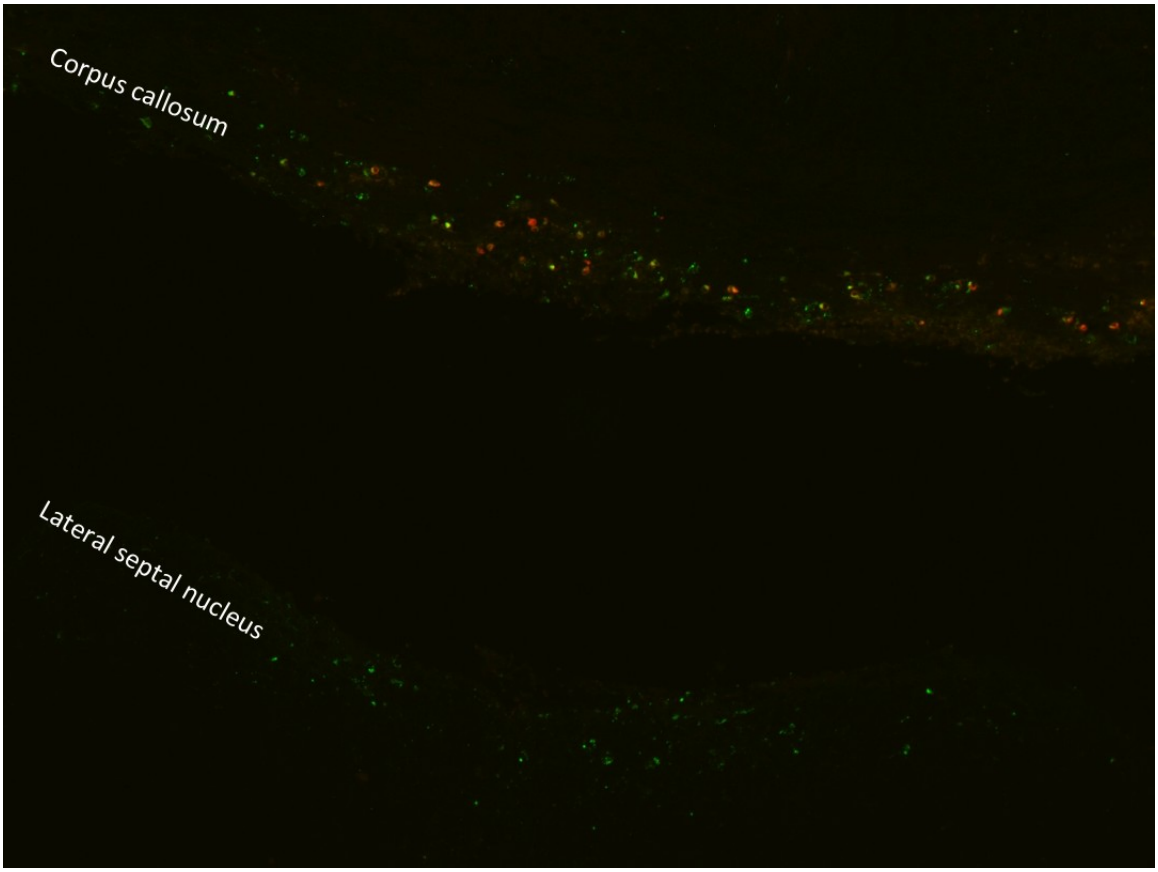

Figure 2.13 On day 7 after SINV TE infection, infected cells along the corpus callosum still have both SINV subgenomic RNA (red) and proteins (green), while only proteins (green) persist in lateral septal nucleus.

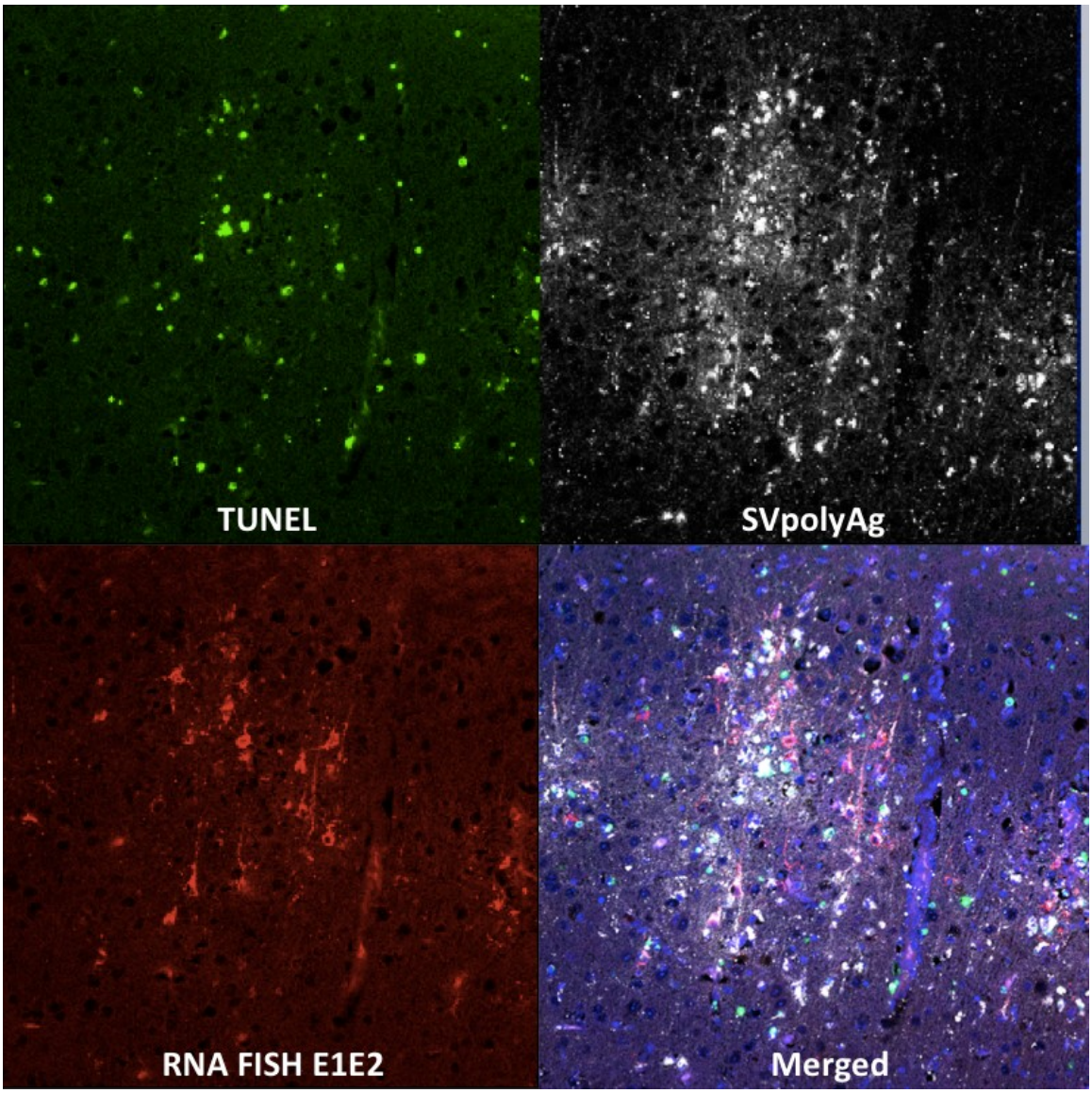

Figure 2.14 The image shows combined TUNEL-TSA (green), RNA FISH E1E2 (red), and IF SVpolyAg (white) of the infected area in the mouse brain, 7 days post SINV TE infection. The merged photo shows that TUNEL (green) is always negative in the infected cells that still have viral RNA (red).

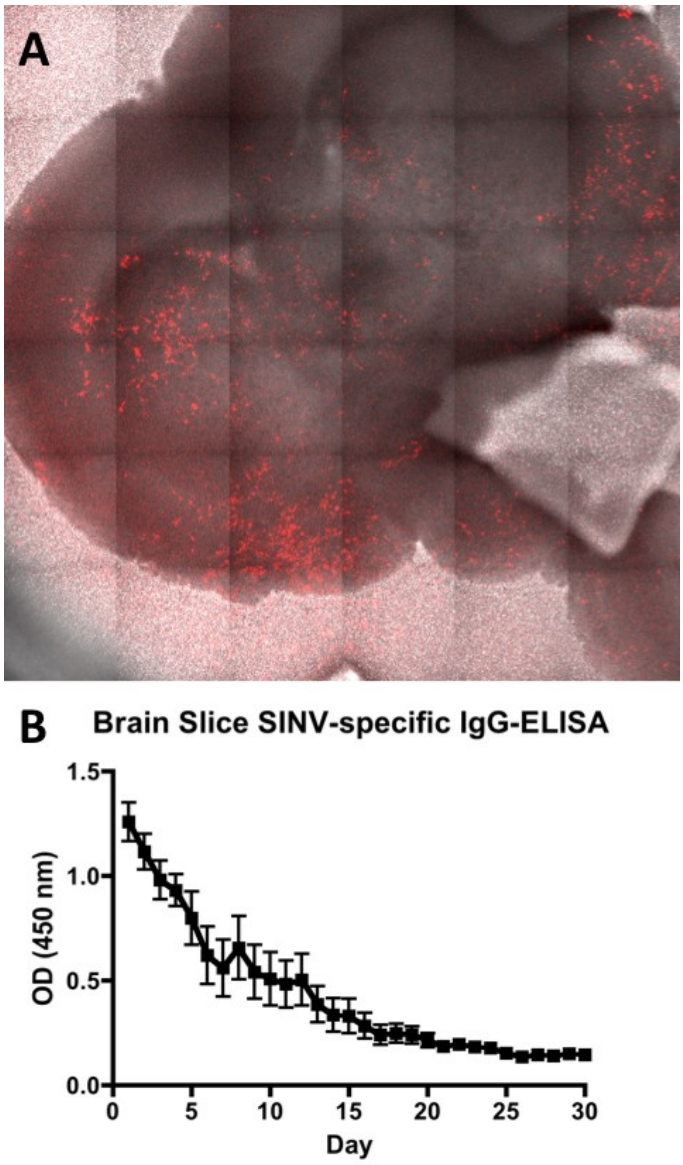

Figure 2.15 The image of 6 by 6 tile scan (A) shows that this brain slice, infected with SINV TOTO E2-mCherry at 1 week *ex vivo* in Transwell insert, still survives and has some infected cells (red) 3 days after *ex vivo* infection. The graph (B) demonstrates the SINV-specific IgG-ELISA from supernatants (1:2 dilution) of mouse brain slice cultures, taken on day 21 post infection with SINV TE. The OD value in each day is the average of supernatants collected from 6 wells (3 brain slices/well, 2 wells/mouse, 3 mice in total).

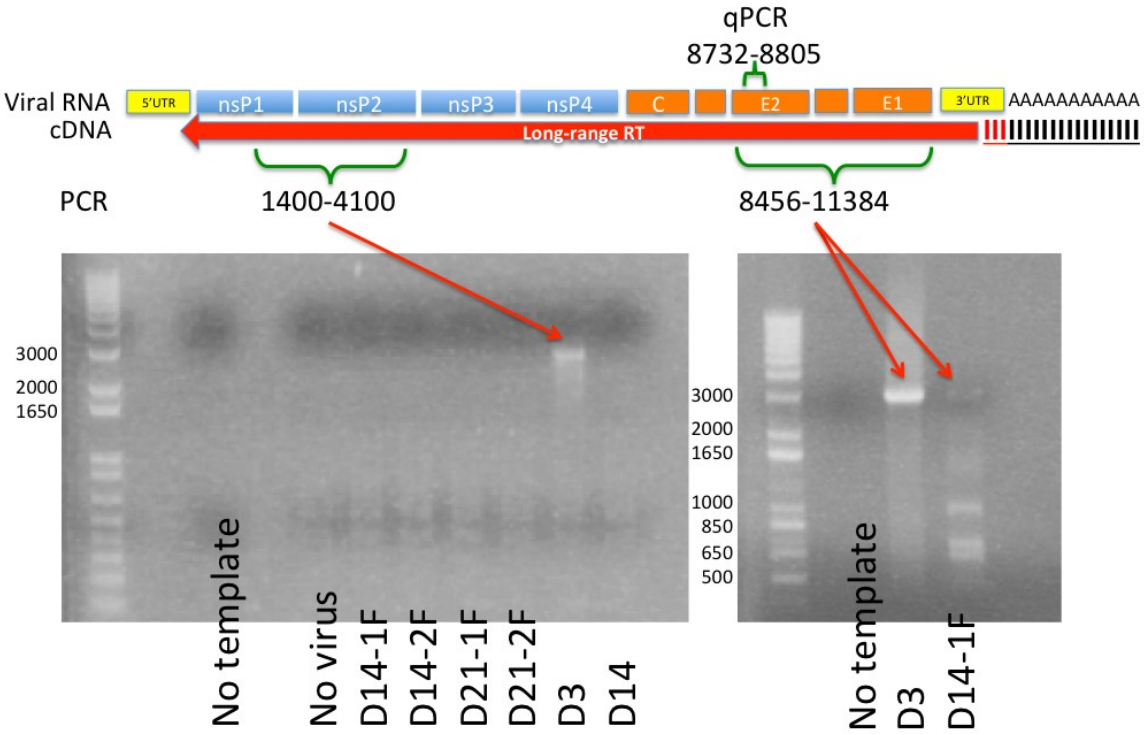

Figure 2.16 Images of agarose gel electrophoresis of long-range RT-PCR products from mouse brain RNA extracts, using GTAAAG-oligo-dT as a primer. Only day 3 is positive for PCR that covers nsP1 and nsP2, which represent genomic RNA (F after the date means RNA is extracted from fresh brains without any freeze-thaw). On the other hand, the subgenomic area (E2 and E1) is still detectable on day 14, but mostly smaller sizes, suggesting large deletions.

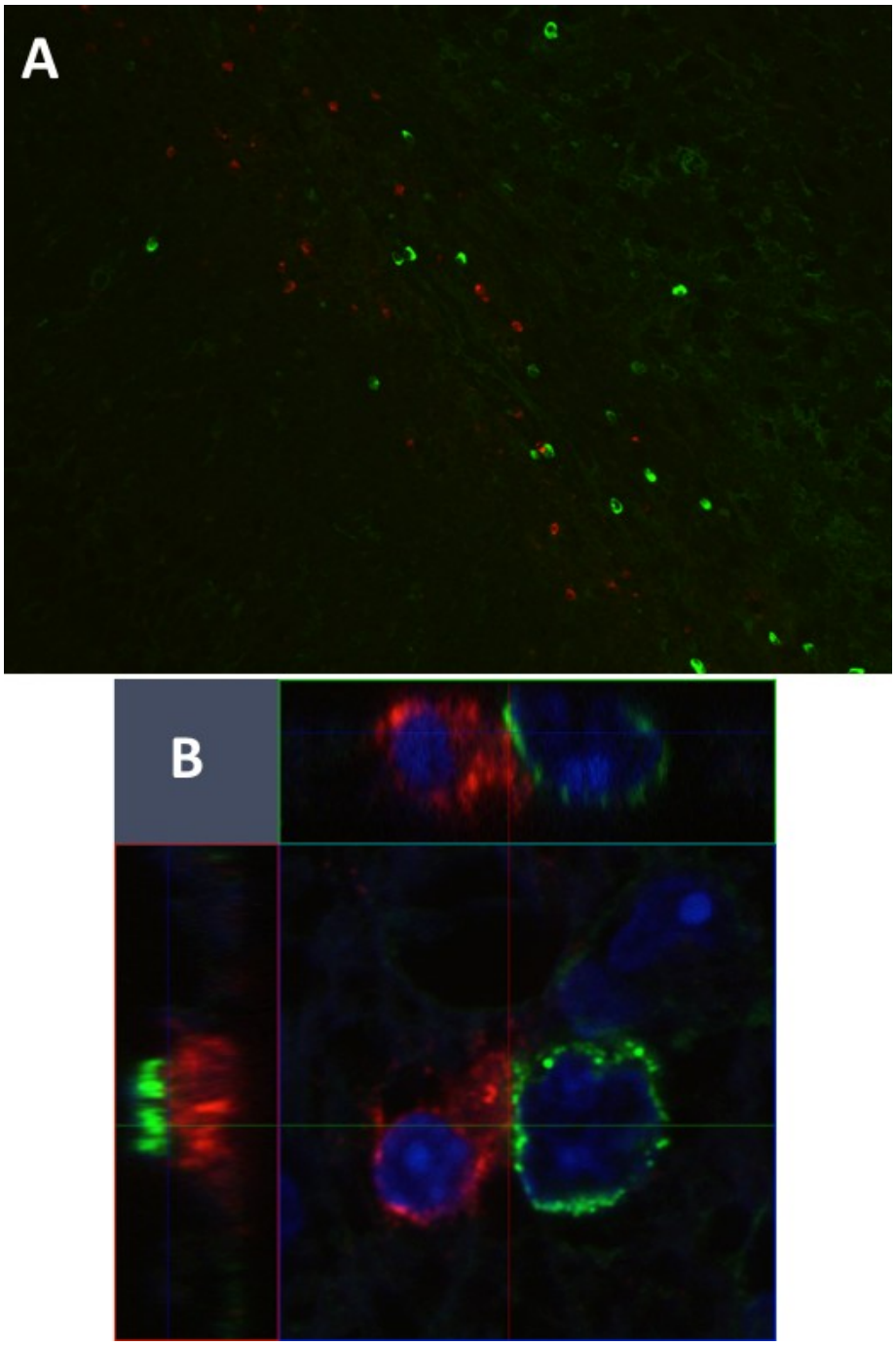

Figure 2.17 The images (A – objective lens 20x, B – 100x, orthogonal view) of the mouse brain, 7 days after SINV TE infection, show that no endogenous immunoglobulin (green) binds to the surface of infected cells (red – SINV subgenomic RNA).

Chapter 3

Antibody-mediated clearance of Sindbis virus from mouse CNS

Introduction:

The key components that clear Sindbis virus from the CNS are antibody and interferon-gamma (IFN-γ) (21). In this chapter, we will focus on antibody-mediated clearance.

In vitro

Without leukocytes or complement, mouse monoclonal anti-SINV E2 IgG of any subclass can inhibit Sindbis viral replication in infected primary cultures of neurons from rat dorsal root ganglia (85, 86). The Fc portion of antibody is not necessary, because the bivalent $F(ab')_2$ retains its antiviral activity. However, the monovalent F(ab) loses this ability, but both bivalency and antiviral properties can be simultaneously restored by cross-linking with a secondary antibody. This underlines the importance of cross-linking of membrane viral E2 glycoprotein on viral clearance (86).

Rat prostatic adenocarcinoma (AT3) cells that overexpresses *bcl-2*, a cellular inhibitor of apoptosis, can survive Sindbis viral infection long enough to study the viral clearance. In this cell line, infected with Sindbis virus, the monoclonal anti-E2 antibody can delay nonstructural protein synthesis and inhibit viral budding. Viral RNA replication increases during very first hours after treatment, but decreases afterward. Antibody treatment also restores host cell protein synthesis, membrane potential, and antiviral activity of IFN-α in late infection (87, 88).

In vivo

Various monoclonal antibodies have been tested for prevention of disease induced by lethal neuroadapted Sindbis virus (NSV) in a mouse encephalitis model. While anti-capsid antibodies have no effect, many anti-E1 and anti-E2 antibodies show protection (given 24 hours before infection) and/or clearance (given 24 hours after infection) (89). Interestingly, neutralization, cell-lysis with complements, and IFN-α/β function (23) are not required for effectiveness. Furthermore, some antibodies that offer protection fail to aid in recovery or clearance of established viral infection (89), suggesting that different mechanisms are involved in these processes.

In severe combined immunodeficiency (SCID) mice, adoptive transfer of anti-SINV E2 antibody can eliminate both infectious virions and viral RNA from persistently infected brains, while sensitized T-cells fail to do so (85). μMT mice lack all classes of antibody, because they do not have mature B-cells due to a defect in the μ-heavy chain. These mice cannot clear Sindbis virus from the brain, but they successfully clear, though delayed, virus from the spinal cord (43) (**Figure 3.1**).

Though IgG is very effective in the adoptive transfer model (85), only SINV-specific IgM-secreting cells infiltrate mouse brains during the clearance of infectious virions (1st week of infection) (51). IgG is produced a few days later and slowly increases during the clearance of viral RNA (2-8 weeks after infection, **Figure 3.2**). Furthermore, athymic nu/nu mice, which produce mainly IgM with little IgG, can clear the infectious virions normally (90). We hypothesize that, *in vivo*, IgM may be sufficient for virion clearance, while IgG may be necessary for viral RNA clearance.

To test our hypotheses, we have compared wild-type C57BL/6 mice (WT) to three types of antibody-deficient mice; activation-induced cytidine deaminase deficient (AID-/-), secretory IgM deficient (sIgM-/-, also known as mu s-/-), and double knockout (DKO; AID-/- sIgM-/-). AID is a key enzyme for class-switch recombination and somatic hypermutation. Thus AID-/- mice can produce and secrete only germline IgM (no IgG, IgA, or IgE) (91). In contrast, sIgM-/- mice lack alternative splicing for secretory IgM, but are still able to produce membranous IgM and switch classes. As a result, sIgM-/- mice can secrete IgG, IgA, and IgE, but not IgM (92). DKO mice cannot secrete any antibodies. Though lacking plasma cells, DKO mice have mature B-cells, which can differentiate into plasmablasts (93).

Materials and Methods:

Mouse strains

All mice were on C57BL/6 background. WT mice were from Jackson Laboratory (#000664). AID+/- and sIgM+/- mice were gifts from Matthew Scharff (Albert Einstein College of Medicine) and Nicole Baumgarth (University of California, Davis), respectively. The heterozygous mice were mated to produce homozygous AID-/- or sIgM-/- mice. Male AID-/- mice were then mated with female sIgM-/- mice to produce double heterozygous mice (AID+/- sIgM+/-), which were subsequently mated with their siblings to produce DKO mice (AID-/- sIgM-/-).

Mouse phenotypes were confirmed by ELISA for serum total IgM, IgG, and IgA. Mouse blood was collected by either facial vein puncture or tail snip under isoflurane anesthesia. Because the AID+/- mothers could vertically transfer IgG to

their pups, serum total IgA ELISA needs to be used instead of IgG for typing before 8 weeks, after which the transferred IgG completely disappeared. The homozygous mice were maintained locally, ready for simultaneous mating in each experiment.

Serum total Ig-ELISA

Each well of the Maxisorp (Nunc) 96-well plate was coated with 1:400 dilution of serum in 50 µl coating buffer at $4^{O}C$ (50 mM $NaHCO_3$ pH 9.6) overnight in plastic wrap. The plate was washed once with 200 µl/well of washing buffer (PBST-2% FBS; PBS, 0.05% Tween20, 2% FBS) and then blocked with 200 µl of blocking buffer (PBST-10% FBS) at $37^{O}C$ for 2 hours.

The plate was washed twice with washing buffer. Each well was then incubated with HRP-conjugated anti-mouse IgM, IgG, or IgA: Southern Biotech) diluted at 1:1000 in 50 µl blocking buffer at room temperature for 1 hour.

The plate was washed 4 times with washing buffer and then incubated with 100 µl/well of TMB substrate at room temperature up to 20 minutes. The reaction was stopped by 25 µl/well of H_2SO_4. The optical density (OD) was read at 450 nm by Multiskan MCC (Thermo Scientific). The level of serum IgM, IgG, and IgA in each mouse group is shown in **Figure 3.3**.

SINV-specific Ig-ELISA is described in Chapter 2: Materials and Methods.

Mouse infection

Each mouse, 4-6 weeks old, was injected with 20 µl of 1000 pfu SINV TE into the left cerebral hemisphere. There were 4 groups of mice; WT, AID-/-, sIgM-/-, and

DKO. Groups of mice were observed for clinical outcomes (see below) or three mice/group/time point/experiment were sacrificed on day 0 (no infection), 3, 5, 7, 10, 14, 21, 30, 45, 60, and 90. Two independent experiments were conducted. Both sexes of mice were used and distributed equally among four groups.

Morbidity-mortality assay

Each mouse was weighed and recorded for clinical score everyday from day 0 (just before intracerebral injection) to day 21. There were 20-30 mice per group. The clinical scores are; 0 – normal; 1 – slightly hunched, abnormal gait and tail position; 2 – very hunched, walking on hind limbs; 3 – sitting on hind limbs, discharge from eyes, ruffled fur on nose; 4 – death. For scoring, the investigators were blinded as to what group each mouse was in.

Collection and handling of specimens

After being euthanized with isoflurane, heart blood was drawn and spun at 6000 rpm $4^{O}C$ for 20 min. The serum/plasma portion was kept at $-20^{O}C$ for ELISA (Chapter 2: Materials and Methods). Intracardiac perfusion with ice-cold PBS was performed. The brain left hemisphere and spinal cord were immediately frozen in liquid nitrogen and stored in the Lysing Matrix D tube (MP Biomedicals) at $-80^{O}C$, waiting for homogenization.

After adding 1ml of ice-cold PBS into the Lysing Matrix D (MP Biomedicals) tube, the specimen was homogenized with FastPrep-24 (MP Biomedicals) at 6 m/sec speed for 40 seconds to make either a 20% brain homogenate or a 10% spinal cord homogenate. The homogenates were centrifuged at 13200 rpm at $4^{O}C$ for 15 minutes. 800

µl of supernatant fluid was collected and stored at -80^{O}C for plaque assay (Chapter 4: Materials and Methods) and ELISA (Chapter 2: Materials and Methods). 1 ml of Qiazol was added to the sediment and re-homogenized with FastPrep-24 (MP Biomedicals) at 6 m/sec speed for 40 seconds. Then the RNeasy Lipid Mini Kit (Qiagen) was used to extract the RNA according to the manufacturer's protocol. The RNA was quantified by Nanodrop and stored at -80^{O}C for RT-qPCR.

Reverse-transcription quantitative real-time polymerase chain reaction (RT-qPCR)

2 µg of each RNA extract was reverse transcribed by the Applied Biosystems 2720 thermocycler (25^{O}C 10 minutes, 37^{O}C 120 minutes, and 85^{O}C 5 seconds) with High Capacity cDNA Reverse Transcription Kit (Themo Scientific) in a 20-µl reaction, using random primers, according to the manufacturer's protocol. qPCR was performed using the Applied Biosystems 7500 Real Time PCR System (50^{O}C 2 minutes, 95^{O}C 10 minutes, and 40 cycles of 95^{O}C 15 seconds – 60^{O}C 1 minute) on 2.5-µl cDNA for SINV E2 (Primers – SV8732F [5'-TGG GAC GAA GCG GAC GAT AA-3', IDT 43567022] and SV8805R [5'-CTG CTC CGC TTT GGT CGT AT-3', IDT 43567023]; TAMRA probe SVE2-8760, Applied Biosystems 5283081), GAPDH (TagMan Rodent GAPDH Control Reagent, VIC probe, Life Technologies 4308313), IFN-γ (exon location 1-2, TAMRA probe, IDT 141107662), and AID (TagMan Gene Expression Assays Mm01184115_m1 Aicda, Applied Biosystems) with TagMan Universal Master Mix (Thermo Scientific) in a 25-µl reaction, according to the manufacturer's protocol. Standards for SINV E2 (TEds plasmid) and GAPDH (TaqMan Rodent GAPDH Control Reagent) were serially diluted 10-fold from 3 X 10^7 to 3 copies. SINV E2 RNA copy number was calculated as absolute number per 10^6 GAPDH RNA copies. IFN-γ and AID

expression were calculated as fold-increase (2^{-ddCT}) using the day 0 samples and GAPDH as controls.

Staining and cell counting of the formalin-fixed paraffin-embedded (FFPE) brains

The brain right hemisphere was sliced into 5 sections, 2 mm thickness each, and fixed in 4% paraformaldehyde in PBS pH 7.2 at 4^{O}C overnight. The fixed brains were then processed as in the previous chapter (Chapter 2: Materials and Methods). IF was used to stain the FFPE brain slices for endogenous IgG, IgM, and SINV (anti-polyNSV). The slices from day 5-10 (during the clearance of infectious virions) were also used for combined TUNEL-TSA, RNA FISH E1&E2 genes, and IF (anti-polyNSV) as described in Chapter 2. The largest slice (usually 3rd one of total 5 slices, the section that contained hippocampus) of each mouse brain was imaged in 4 by 4 tile scan (objective lens 10x, zoom out 0.6, Zeiss LSM780FCS on Axio Observer Z1 inverted microscope). The digital files of the captured images were renamed so that the investigator did not know what group each file belonged to. The number of cells positive for Sindbis viral RNA, TUNEL, endogenous IgG, and IgM was counted manually, while the number for Sindbis viral protein was counted by set threshold in ImageJ software, because it was hard to determine the number of cells for both widely diffused and clumped viral proteins.

Results:

Clinical outcomes are independent of antibody production. All four groups of mice had similar outcomes. Mortality rates were 5-10% (**Figure 3.4A**). Weight loss began on day 3-5, reached maximum at 1 week. The mice then regained weight and recovered the original weight at 2 weeks after infection (**Figure 3.4B**). The median day

of onset of clinical signs was day 5-6 (**Figure 3.4D**), was the worst on day 7-8, and then gradually improved. Recovery of DKO mice was a bit slower during the 3rd week, but this was not statistically significant (**Figure 3.4C**).

Spinal cords do not require antibody for clearance of infectious virions, while brains need only 1 class of antibody. DKO mice were the only group failing to clear infectious virions from brain (**Figure 3.5A)**. DKO mice had higher brain virus titers at the peak (day 3), delayed clearance (day 5-14), and then reactivated (day21 onward). In fact, few DKO mice did reduce infectious virus in brains to be below the detection limit of plaque assay at day 10, 14, 45, and 60. In brains, the sIgM-/- mice had an almost identical pattern of virion clearance to the WT mice, while AID-/- mice had lower peak levels of virus with a short delay in clearance. In spinal cords, all mouse groups could clear infectious virions with only some delay in DKO group (**Figure 3.5B)**.

Antibody is not necessary for the early clearance of viral RNA either from brains or spinal cords. All mouse groups had similar initial viral RNA clearance, as assessed by RT-PCR for the SINV E2 gene, both from brains (**Figure 3.5C**) and spinal cords (**Figure 3.5D**). However, for DKO mice, the decrease in viral RNA stopped after day 30 in brains and day 45 in spinal cords, resulting in higher sustained viral RNA at late time points.

IFN-γ mRNA expression in spinal cords is the same for all groups, but DKO mice have lower early peak expression in brains. Unlike spinal cords, which have a gradual rise in IFN-γ mRNA expression (**Figure 3.6B)**, in brains there is a prominent peak at day 5-7 after infection, except in DKO mice (**Figure 3.6A)**. In DKO mice, the

pattern of IFN-γ mRNA expression in brains and spinal cords were indistinguishable. Except for the absence of the early peak in the brains of DKO mice, the IFN-γ mRNA expression was comparable in all mouse groups, both in brains and spinal cords.

AID mRNA expression in WT mice is higher than in sIgM-/- mice in both brains and spinal cords. The level of expression in brains (**Figure 3.6C**) was 10 times higher than in spinal cords (**Figure 3.6D**). The AID mRNA expression reached a plateau on day 7 and was maintained for 1 month after infection.

Earlier SINV-specific IgG in sIgM-/- mice and higher IgM in AID-/- mice than in WT mice. sIgM-/- mice produced levels of SINV-specific IgG comparable to WT mice in all specimens; sera (**Figure 3.7A**), brains (**Figure 3.7B**), and spinal cords (**Figure 3.10D**). In contrast, AID-/- mice produced much higher levels of SINV-specific IgM than WT mice in all specimens; sera (**Figure 3.7C**), brains (**Figure 3.7C**), and spinal cords (**Figure 3.10C**). However, only in sera, sIgM-/- and AID-/- mice produced earlier SINV-specific IgG and IgM, respectively, than WT mice.

sIgM-/- mice produce different subclasses of SINV-specific IgG from WT mice. Although total levels of SINV-specific IgG were similar, sIgM-/- mice had much higher levels of SINV-specific IgG2a, and lower levels of IgG1 and IgG2b than WT mice in all specimens; sera (**Figure 3.8A-C**), brains (**Figure 3.9A-C**), and spinal cords (**Figure 3.10A-B**). Very little SINV-specific IgG3 is present in either sera (**Figure 3.8D**) or brains (**Figure 3.9D**).

Brain tissue imaging shows the same patterns and comparable numbers of infected cells during the clearance of infectious virions, day 5-10. Distribution

patterns of virus-infected cells are either in white or gray matter (see Chapter 2), independent of mouse group (**Figure 3.11**). The number of cells positive for viral proteins (**Figure 3.12A**) and viral RNA (**Figure 3.12B**) declined over day 5-10 and was comparable between groups. The number of apoptotic cells was highest on day 7 and was comparable between groups (**Figure 3.12C**).

The number of antibody-containing cells in brains is different between mouse groups. Both IgM-and IgG-containing cells infiltrated the infected brain foci and nearby thickened pia mater (**Figure 3.13 and 3.14A**). The number of these cells was quite different between the 4 mouse groups (**Figure 3.14B**). Infiltration of these cells was detected on day 10 for both IgG-positive cells and IgM-positive cells. WT mice had more IgM-positive cells than IgG-positive cells. After day 10,numbers of IgM-positive cells decreased rapidly in WT mice, but AID-/- mice retained large numbers of the IgM-positive cells for much longer. Though sIgM-/- mice had almost no IgM-positive cells, they had the same pattern of IgG-positive cells as WT mice. DKO mice had exclusively IgM-positive cells that fluctuated in number throughout the infection.

Table 3.1 Summary of Sindbis viral clearance in immunoglobulin-deficient mice (NA – not available)

Characteristics compared to WT	AID-/-	sIgM-/-	DKO
Virion clearance	Lower peak, a little slower	Same	Higher peak, slower Rebound only in brains
Viral RNA clearance	Similar	Similar	Similar until D30
IFN-Gamma expression	Similar	Similar	No peak in brain, Similar in spinal cord
Outcomes	Similar	Similar	Similar
IgM	Much higher in all specimens, faster in sera (D3 VS D5), same time in brains and spinal cord (D10)	NA	NA
IgG	NA	Faster in sera (D5 VS D7) and brains/spinal cords (D7 VS D10)	NA

Discussion:

Immunoglobulin-deficiency does not affect clinical outcomes. In neuroadapted Sindbis virus (NSV), a fatal strain for immunocompetent mice, pathology is mediated by the immune response rather than the virus itself, because SCID mice can survive with persistent virus in CNS (94). This immunopathology is mainly caused by T-cells, not antibody (95). On the other hand, Sindbis TE strain rarely causes death in either immune competent or compromised mice. Wild-type and various immunodeficient mice (SCID, IFN-γ-deficient, μMT) can survive TE encephalomyelitis (43). Thus, the milder forms of immunodeficiency used in this study were unlikely to greatly impact outcomes. Nevertheless, DKO mice had some delay in recovery (**Figure 3.4C**). This can probably

be explained by reactivation of the virus (**Figure 3.5A**) and prolonged infiltration of inflammatory cells (**Figure 3.14B**).

Either IgM or IgG alone is sufficient for clearance of infectious virions from brains. Similar to our study, IgM alone is enough to prevent mouse hepatitis virus (MHV) induced chronic demyelination in another study that used AID-/- mice (96). The higher SINV-specific IgM in AID-/- mice and the earlier IgG in sIgM-/- mice might compensate for the lack of another immunoglobulin class. The previously described characteristics of sIgM-/- mice, more IgG2a with less IgG1 and IgG2b (92), were also found in all specimens from our study. Even without antibody, a few DKO mice cleared infectious virions from the brains, though delayed. This suggests that antibody is barely needed for the clearance from the brains. In contrast, spinal cords, which produce much less infectious virions and viral RNA, can clear infectious virions in the absence of antibody. In fact, even SCID mice, which lack most adaptive immunity, can slowly clear the infectious virions almost completely from the spinal cords before reactivation (43). This is analogous to HIV infection, where each anti-retroviral drug has a limited ability to decrease the viral load. Only the combination of multiple drugs can suppress the virus enough to prevent emergence of escape mutants (97). In the same fashion, more aspects of immunity are probably needed for the higher burden of Sindbis virus in brains to suppress and prevent viral reactivation.

How can antibody that is not present in the brain during 1st week help clear the infectious virions? SINV-specific antibody, that is already present in the plasma, might be responsible for the boost of IFN-γ expression in the brains on day 5-7, resulting in the better clearance. In humans, intravenous immunoglobulin (IVIG) can increase IFN-γ in

plasma. Though no activated B or T-cells are observed in peripheral blood mononuclear cells (PBMC), there is an enhancement of Fc-γ receptor 1 (FcγRI) on monocytes (98). Because FcγRI has high affinity for IgG and can bind it in the absence of antigen, monocytes might engage SINV-specific IgG in the plasma before they infiltrate brain parenchyma, where they could help eliminate the virus. On the other hand, FcμR, which has high affinity for IgM (99), might be a major player in AID-/- mice.

Another possibility is that antibody found in plasma during the 1st week might have already reached the brain and helped clear the virus, but the excess amount of viral antigen might render the SINV-specific Ig-ELISA undetectable. Because the adoptive transfer of anti-SINV antibodies can clear infectious virions and viral RNA from SCID mouse brains (85), antibody in circulation must be able to reach the brain parenchyma, where the virus resides.

One major concern is that the DKO mice show higher infectious virions even with the same amount of viral RNA and infected cell count. Because cardiac perfusion with PBS might not completely wash out blood from the brain, virus might become neutralized by a small amount of natural or early SINV-specific antibody in the residual blood *ex vivo* during the homogenization. In agreement with this speculation, AID-/- mice, the only ones that produce SINV-specific antibody in sera as early as day 3, have the lowest peak on day 3 even with the same level of viral RNA as other groups. Another possibility is that the natural antibody in an inevitable bleeding during intracerebral injection might interfere the virus infection from the beginning, leading to the difference in peak amount of infectious virions.

AID gene mRNA expression in both brains and spinal cords of sIgM-/- mice is lower than WT mice, while most immunoglobulin-producing cells in sIgM-/- mouse brains are IgG positive. Thus, class switching in sIgM-/- mice has already happened before the cells infiltrate the CNS. AID-/- mice retain the IgM-positive cells longer than WT mice. These cells stay in CNS longer and contribute to the local IgM production probably due to the inability of systemic IgM to cross blood-brain barrier (BBB). Interestingly, DKO mice cannot secret IgM but still have IgM-producing cells in the brain. Fluctuation in the number of these cells is probably a response to the reactivation of the virus.

In conclusion, immunoglobulin, regardless of its class, helps clear the infectious virions from brains but is not needed in spinal cords. Viral RNA clearance does not need antibody until very late. Antibody also has only subtle effects on clinical outcomes. Though antibody is very powerful in adoptive transfer and *in vitro* models, it reaches the CNS too late to have a major effect on clearance. Instead, antibody may play a more important role in prevention of viral reactivation.

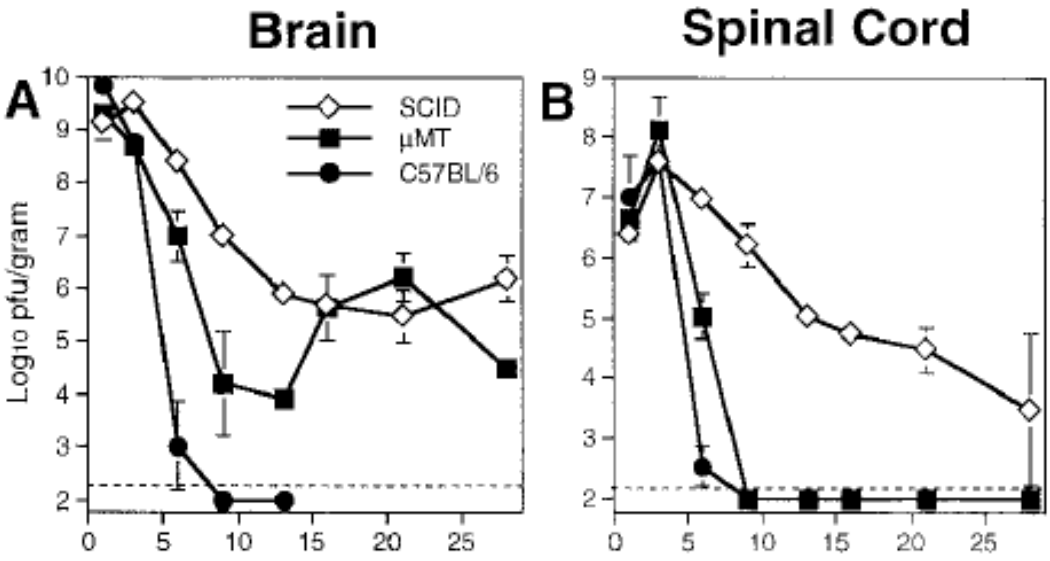

Figure 3.1 Clearance of infectious virions in brains is different from spinal cords, where antibody is not required (complete clearance in µMT mice) (45).

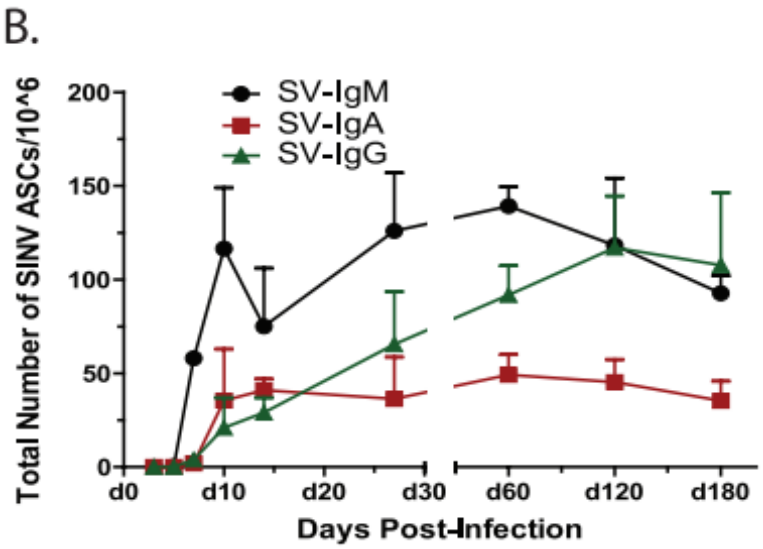

Figure 3.2 The plot shows the number of SINV-specific antibody-secreting cells (ASC) in brain suspensions from TE-infected C57BL/6 mice at various time points. IgG-ASCs infiltrate the brain later than IgM-ASCs (51).

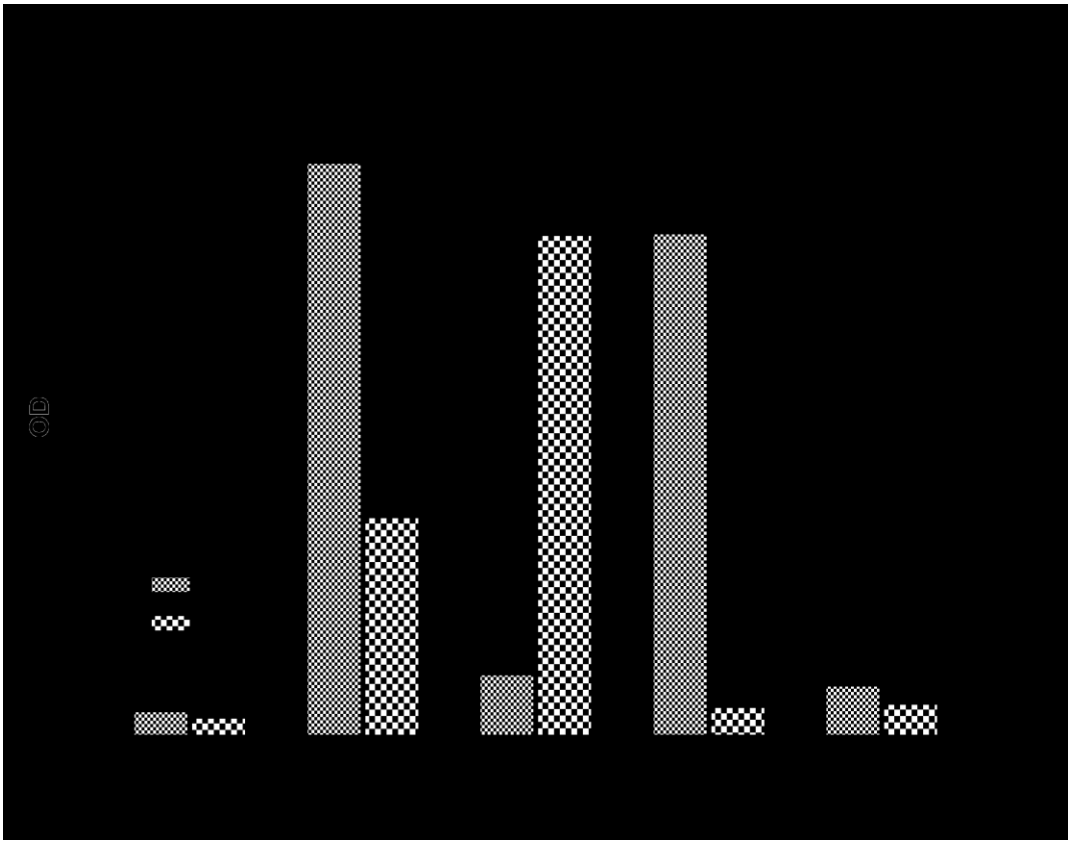

Figure 3.3 This bar chart shows the 450-nm optical density (OD) of total Ig-ELISA for 1:400 diluted sera from different mouse groups. WT mice have both IgG and IgM, while DKO mice have none. AID-/- mice have very high IgM without IgG, and sIgM-/- mice have high IgG without IgM.

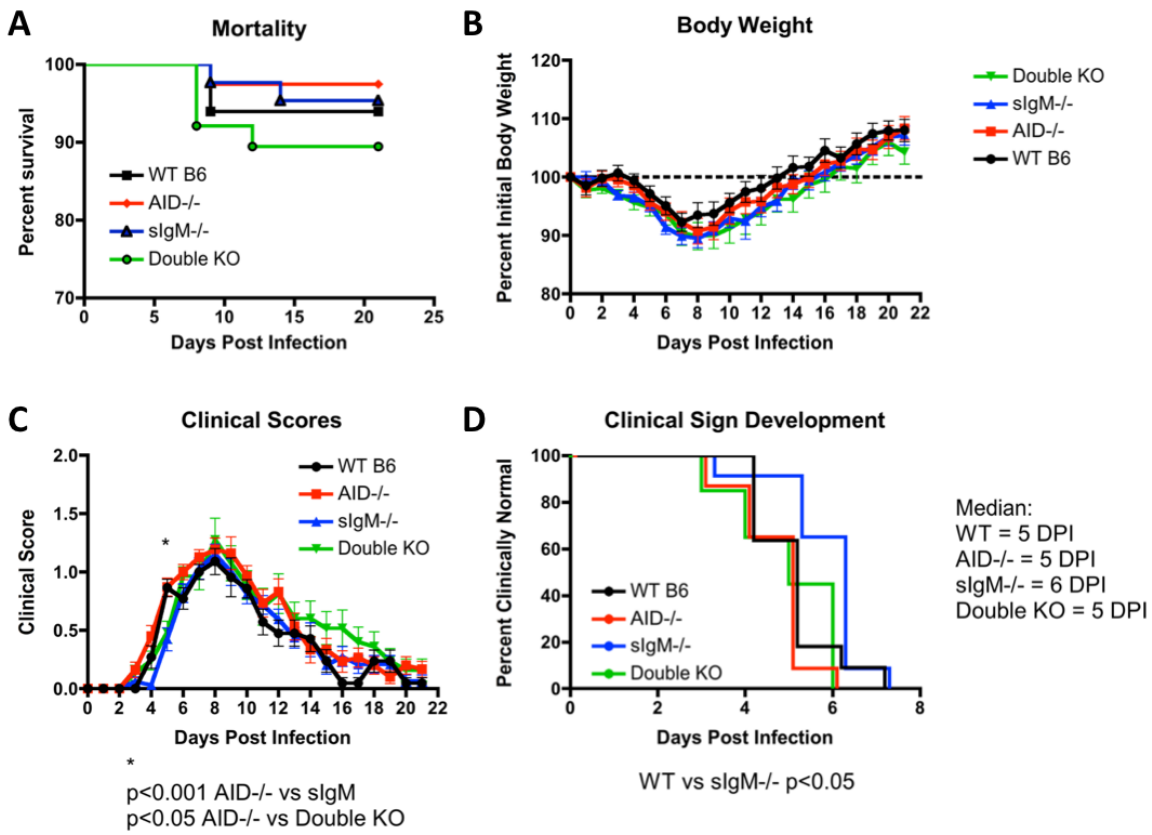

Figure 3.4 Similarity in morbidity/mortality of SINV TE-infected mice from all groups; 4-6-week-old mice were inoculated intracerebrally with 1000 pfu SINV TE; **A** – Survival, **B** – Weight change, **C** – Clinical scores, and **D** – Onset of clinical signs.

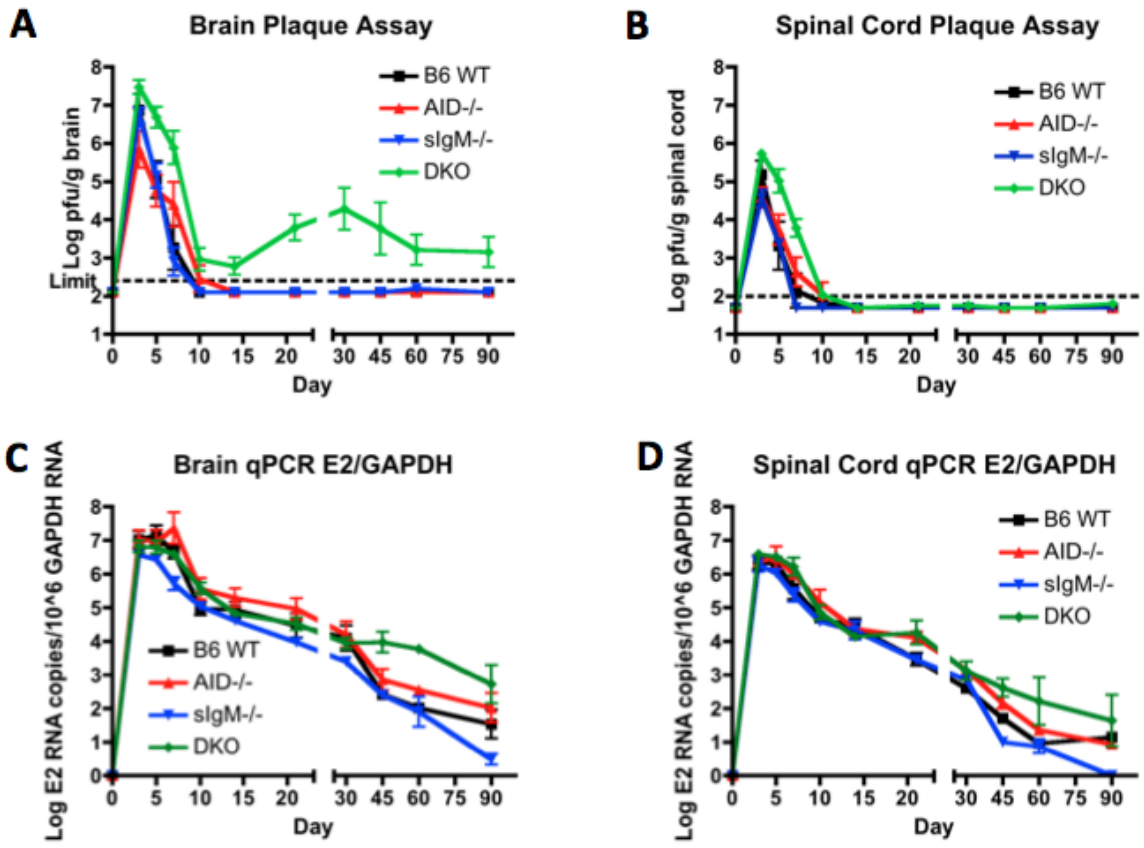

Figure 3.5 Viral clearance. Plaque assay shows the virion clearance patterns for all 4 mouse groups in brains (A) and spinal cords (B). RT-qPCR shows the viral RNA clearance in brains (C) and spinal cords (D).

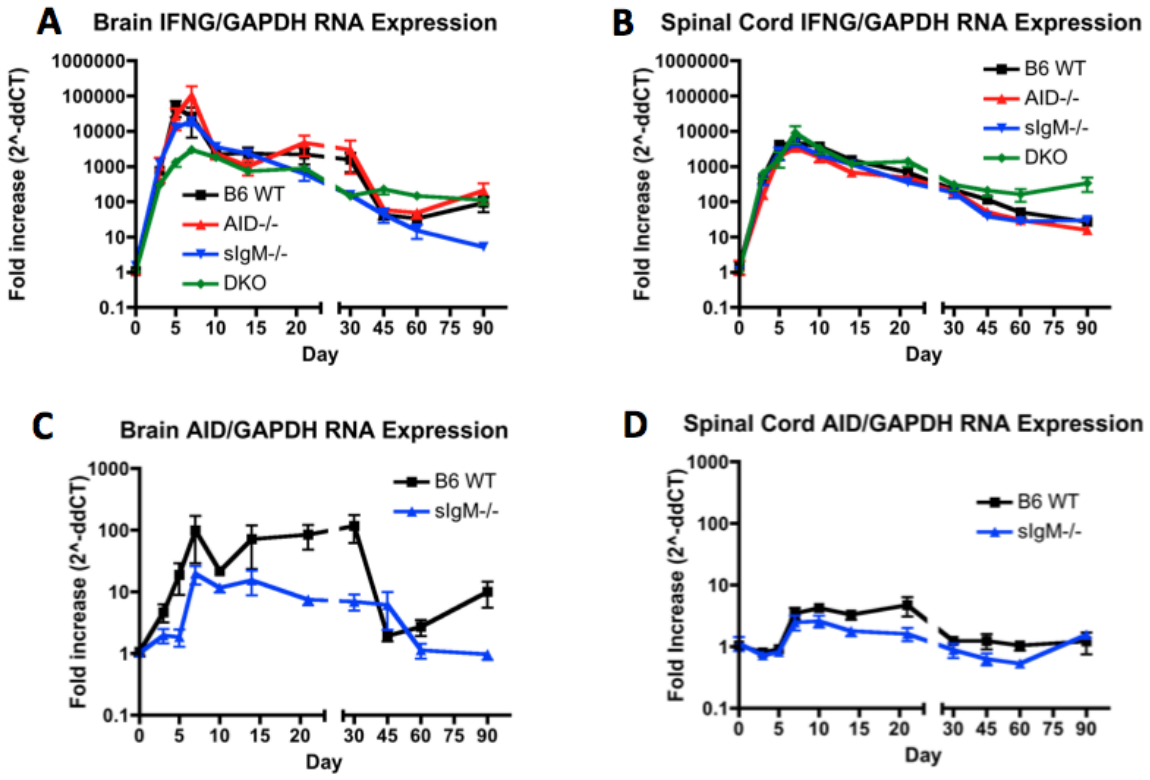

Figure 3.6 IFN-γ and AID mRNA expression. RT-qPCR to determine the change (fold-increase) from before infection (day 0) in IFN-γ mRNA in brains (A) and spinal cords (B) of all mouse groups. Because AID-/- and DKO mice do not express the AID gene, only WT and sIgM-/- were tested for AID mRNA expression in brains (C) and spinal cords (D).

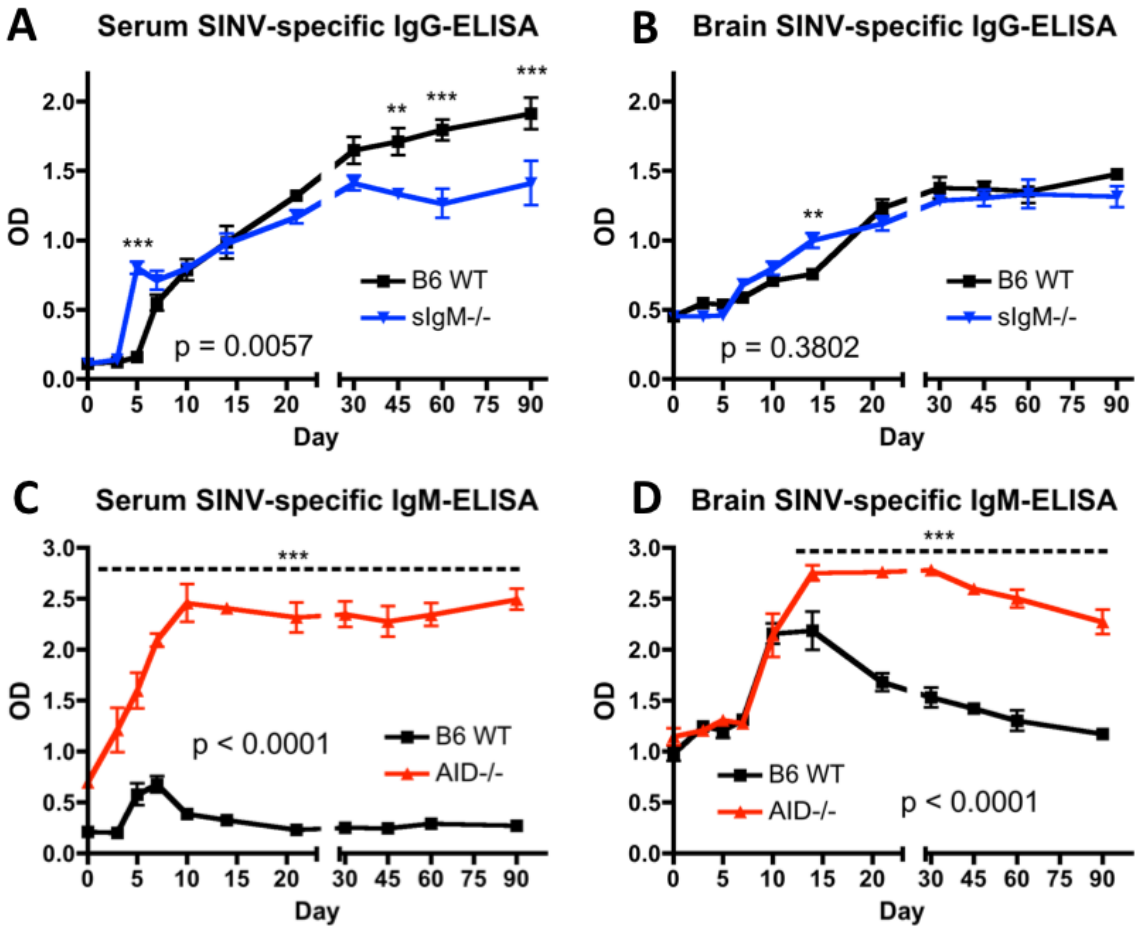

Figure 3.7 Production of SINV-specific antibody. The graphs show optical density (OD) of mouse sera (A and C), 1:100 dilution, and 20% brain homogenates (B and D), 1:8 dilution, both tested for SINV-specific IgG-ELISA (A and B) and IgM-ELISA (C and D). P values represent the significance of difference between mouse groups by 2-way ANOVA. Asterisks show significant difference at particular time points (* $p < 0.05$, ** $p < 0.01$, *** $p < 0.001$)

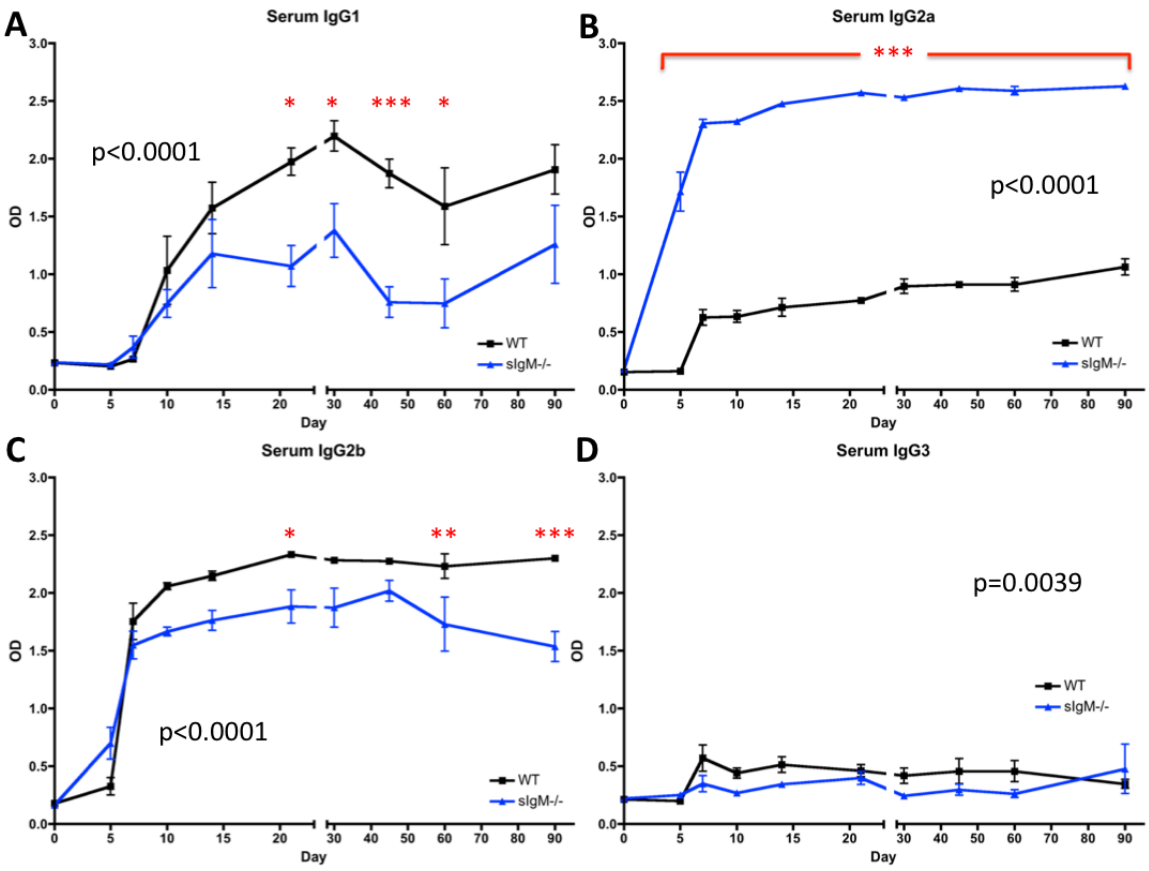

Figure 3.8 The graphs compare the level of each IgG subclass in sera (1:100 dilution) between WT and sIgM-/- mice, detected by SINV-specific Ig-ELISA (A – IgG1, B – IgG2a, C – IgG2b, D – IgG3). P values represent the significance of difference between mouse groups by 2-way ANOVA. Asterisks show significant difference at particular time points (* $p < 0.05$, ** $p < 0.01$, *** $p < 0.001$)

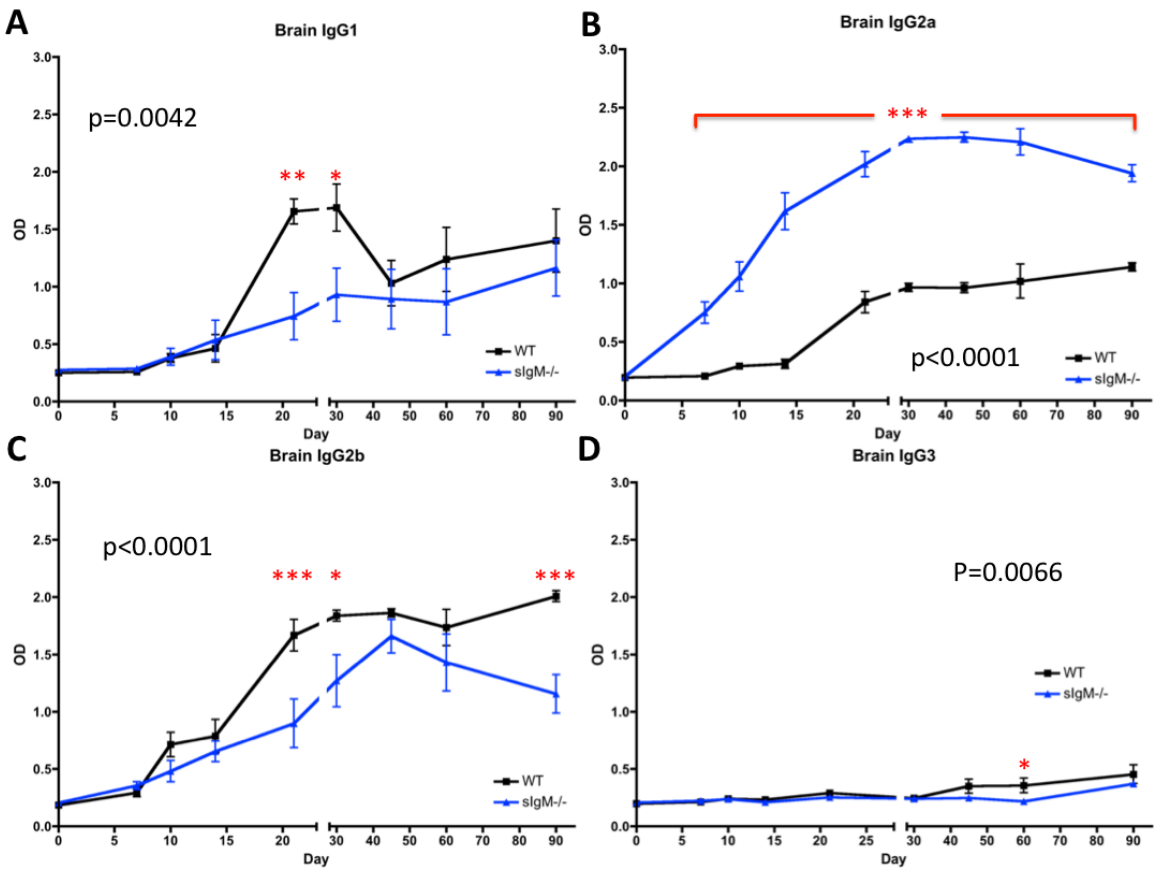

Figure 3.9 The graphs compare the level of each IgG subclass in 20% brain homogenates (1:8 dilution) between WT and sIgM-/- mice, detected by SINV-specific Ig-ELISA (A – IgG1, B – IgG2a, C – IgG2b, D – IgG3). P values represent the significance of difference between mouse groups by 2-way ANOVA. Asterisks show significant difference at particular time points (* $p < 0.05$, ** $p < 0.01$, *** $p < 0.001$)

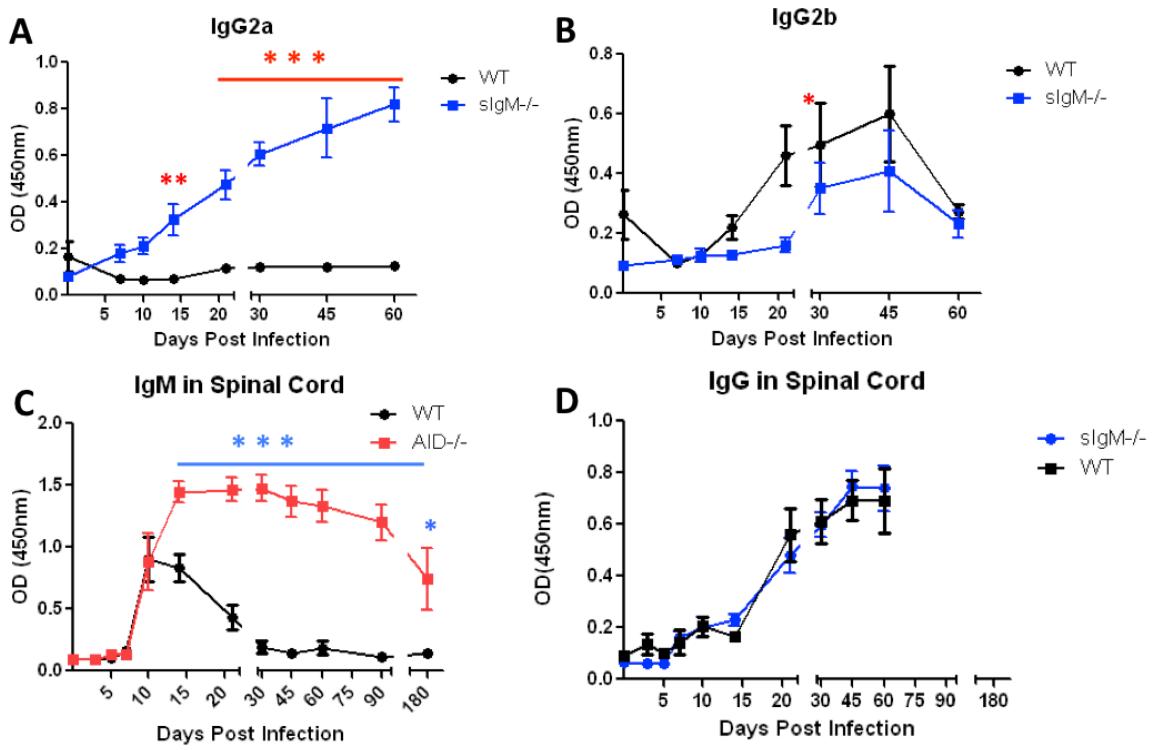

Figure 3.10 The graphs demonstrate the level of SINV-specific antibody in spinal cords by ELISA (A – IgG2a, B – IgG2b, C – IgM, D – IgG). P values represent the significance of difference between mouse groups by 2-way ANOVA. Asterisks show significant difference at particular time points (* $p < 0.05$, ** $p < 0.01$, *** $p < 0.001$)

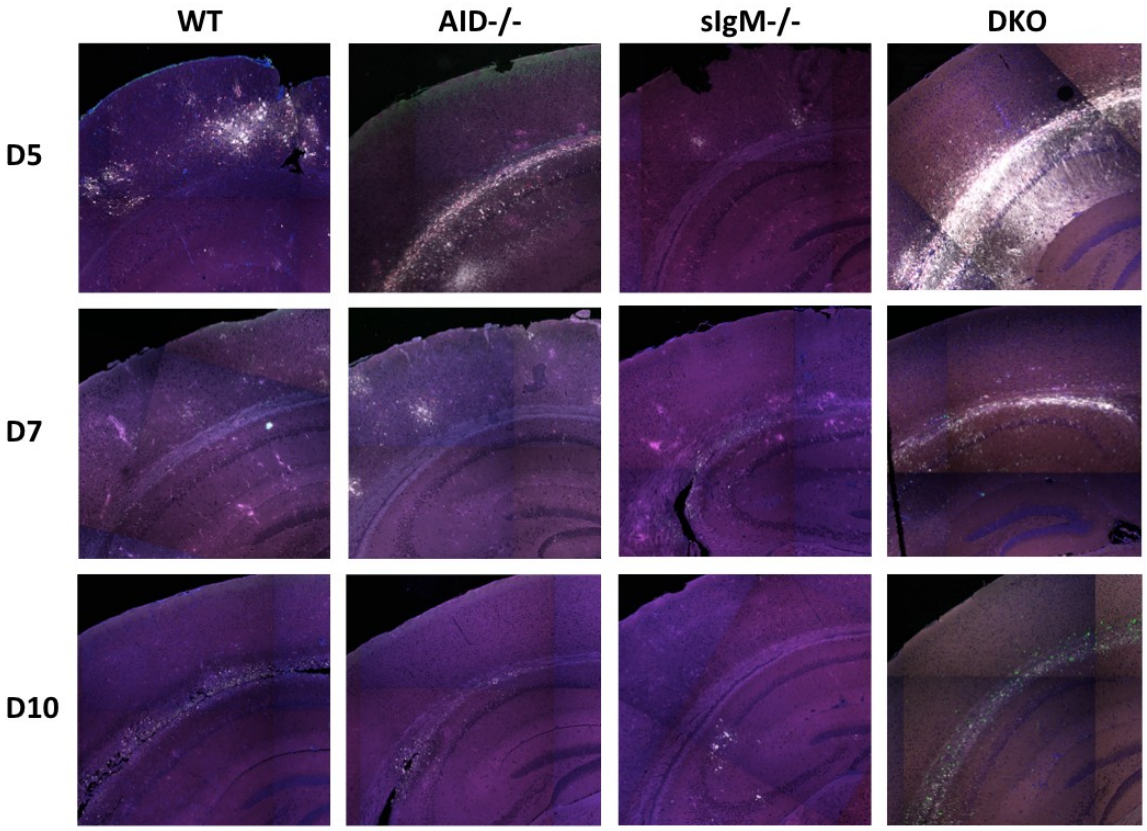

Figure 3.11 Combined TUNEL-TSA (green), RNA FISH E1&E2 genes (red), and IF of SINV proteins (white) on FFPE brain slices of representative 4 mouse groups during day 5-10 shows the distributions of affected cells in cerebral cortex and hippocampus.

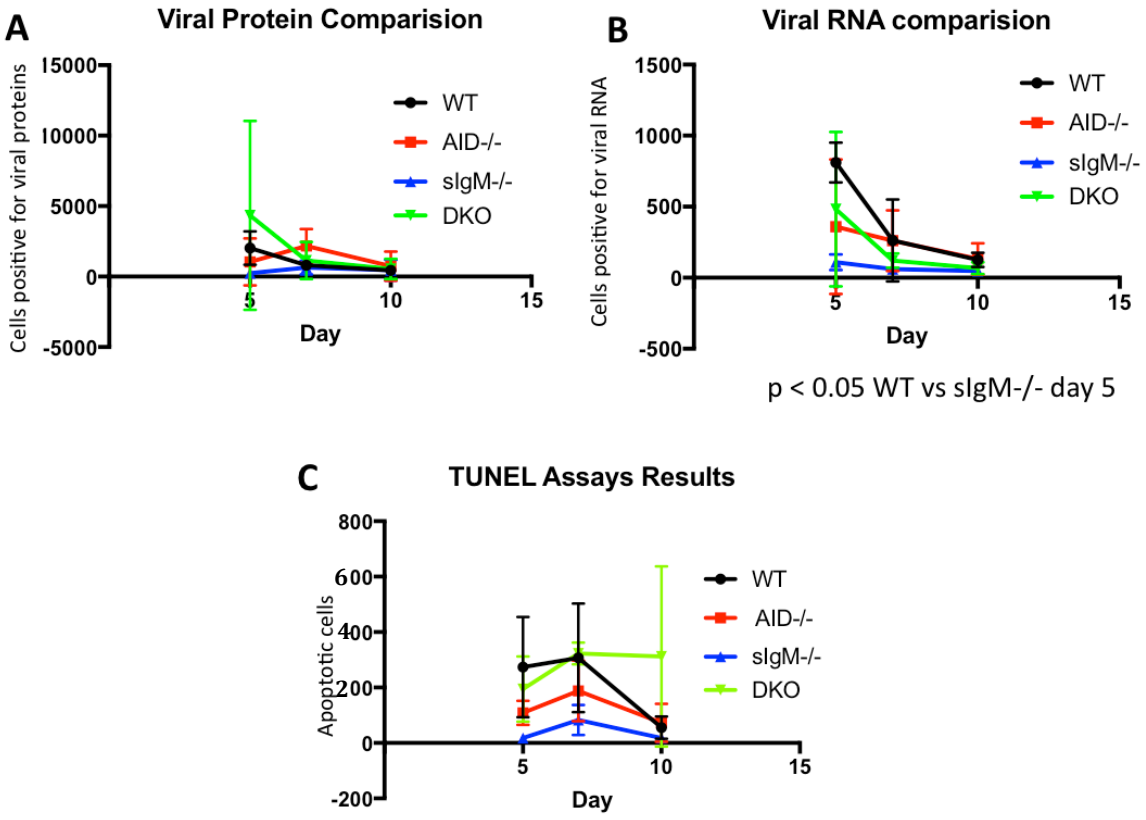

Figure 3.12 The graphs show number of cells positive for viral proteins (A), viral RNA (B), and TUNEL-TSA (C) per slice of right brain hemisphere during the clearance of infectious virions, day 5-10 (3 mice/group/time point).

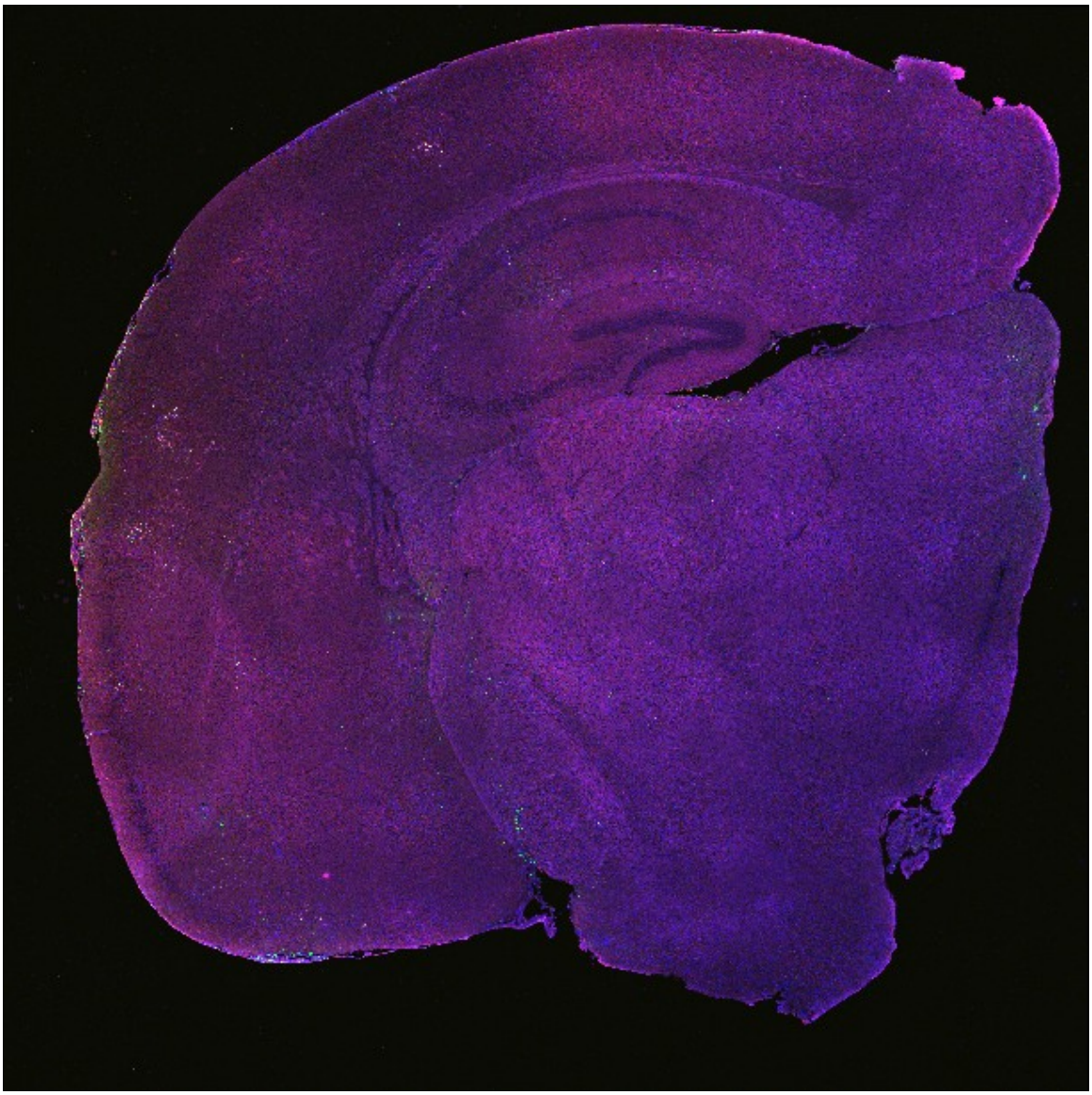

Figure 3.13 The 4 by 4 tile scan image (stitching of 7 by 7 tile scan with 50% overlap) of the right hemisphere of a WT mouse, 10 days post-infection, shows the distribution of cells with viral proteins (white), mouse IgG (red), and IgM (green).

A

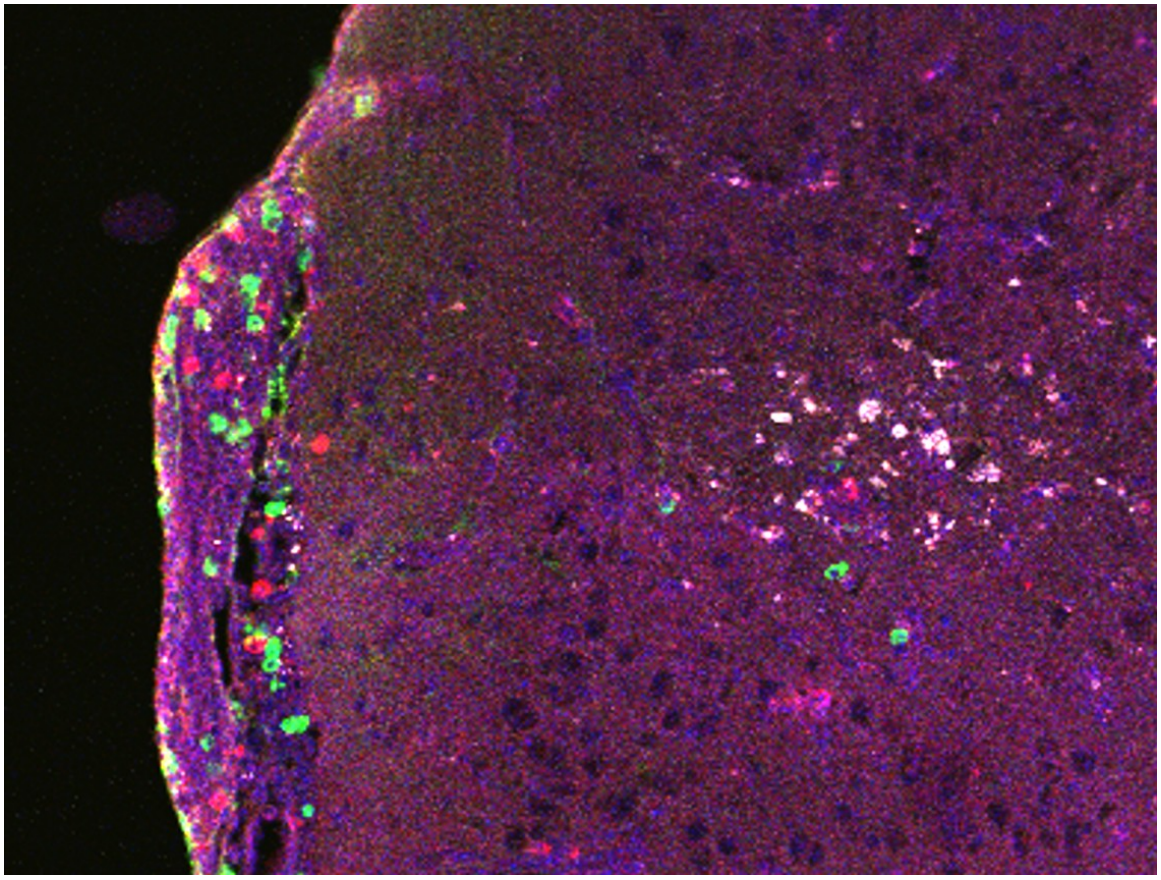

B

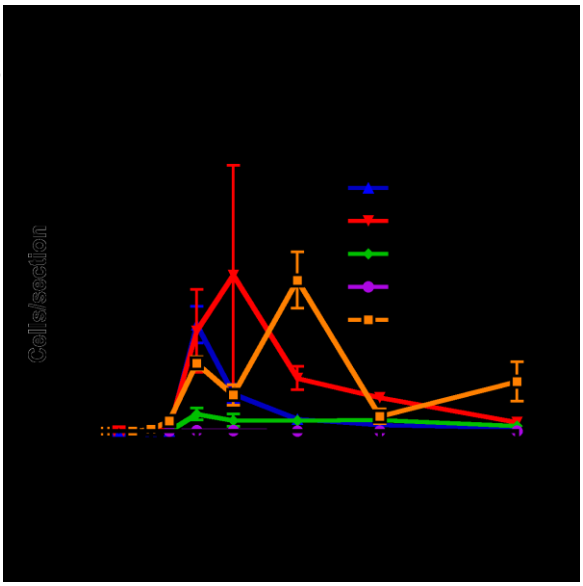

Figure 3.14 A – Higher power examination of figure 3.13 WT mouse brain reveals the Ig-positive cells (IgG – red, IgM – green) infiltrating pia mater and infected brain parenchyma (white). B – Graph of the number of IgM- and IgG-positive cells per slice of right brain hemisphere (3 mice/group/time point).

Chapter 4

Sindbis Virus with Fluorescent RNA Aptamers

Introduction:

The regulation of viral RNA synthesis and degradation in infected cells by cellular and immune factors is poorly understood. To facilitate studies of viral RNA dynamics during infection and immune-mediated clearance, we sought to develop SINV RNA that could be visualized in live cells.

Although techniques for fluorescent tagging and visualization of viral proteins during replication (*e.g.* with green fluorescent protein [GFP]) are well established, visualization of viral RNA has been more challenging. Approaches have included fluorescent antisense probe hybridization and molecular beacons that rely on probe delivery into the cells. In addition to methods for detecting unmodified RNA, RNAs have also been engineered to facilitate detection by inserting repeats that bind GFP-tagged bacteriophage MS2 protein or inserting aptamers that bind a fluorophore (100).

Recently, the Spinach RNA aptamer and its more stable derivative Spinach2 have been inserted into RNA and used in combination with derivatives of the GFP-related conditional fluorophore 4-hydroxybenzidine imidazolinone (HBI) to visualize RNA in live cells (101, 102). The Spinach2 aptamer is a 97 nt RNA stabilized within a tRNA scaffold (103) that can be inserted into an RNA of interest. When the cell-permeable non-toxic conditional fluorophore 3,5-difluoro-4-hydroxybenzylidene imidazolinone (DFHBI), DFHBI-1T, or DFHBI-2T binds the RNA aptamer, it becomes activated with

emission of green fluorescence upon excitation that allows live cell visualization of RNA abundance and localization (101, 104, 105) (**Figure 4.1**). This system has been used to tag and image cellular RNAs (101), but has not previously been applied to viral RNA.

For visualization of SINV RNA, we inserted 1 to 2 Spinach2 aptamers into full-length SINV TE cDNA clones either into the 3'UTR or behind a second subgenomic promoter and recovered viruses that could be used to study the dynamics of viral RNA replication and distribution as well as antibody-mediated clearance in live cells.

Later on, tRNA-Spinach2 had been replaced by the brighter and smaller new RNA-aptamer, Broccoli, in more stable F30 scaffold (106-108) (**Figure 4.1**). We inserted 4 to 28 Broccoli aptamers at the same sites as Spinach2 (see above). Unlike tRNA-Spinach2, F30-Broccoli does not contain any stop codons and therefore can be inserted into the nsP gene for visualization of viral genomic RNA. When Broccoli binds to the fluorophores, it can emit similar fluorescence patterns to Spinach2.

Table 4.1 Maximal excitation/emission wavelength for each aptamer-fluorophore combination (104, 108)

Fluorophores	Spinach2	Broccoli
DFHBI	447/501	447/501
DFHBI-1T	482/502	472/507
DFHBI-2T	500/523	Unknown

Materials and Methods:

***In vitro* signal and specificity of Spinach2-DFHBI.** The pET28c-Spinach2 plasmid that contained Spinach2 within a tRNA scaffold (103) was a gift from Samie

Jaffrey (Weill Cornell Medical College, New York) (102). Spinach2 scaffolded by tRNA was amplified by Taq-polymerase PCR and ligated to the overhung T ends of the PCR II-TOPO vector (Invitrogen). After linearization of the plasmid with BamHI (New England Biolabs), Spinach2 with the tRNA scaffold was *in vitro* transcribed with T7 Maxiscript (Ambion). 4 μg of Spinach2 transcript (1 μM: 3.01 X 10^{13} copies/well) and 4 μg of RNA extracted (RNeasy lipid tissue mini kit, Qiagen) from TE-infected (3 days) and uninfected mouse brains, were incubated in 50 μl of buffer containing 40mM HEPES (Gibco), 100 mM KCl, and 1 mM $MgCl_2$ with or without DFBHI 10 μM for 30 min at 37^{O}C. Fluorescent signal intensity was measured at Ex447/Em501 with a fluorescence plate reader (SpectraMax).

Construction of SINV-Spinach2 (Figure 4.2). Spinach2 within the tRNA scaffold was inserted into the either the TE (24) or TEds (double subgenomic) (109) full length SINV plasmid. The insertion sites were the *Bst*EII restriction site downstream of the second subgenomic promoter or an *Sph*I site in the 3'UTR produced by site-directed mutagenesis. The four constructed SINV plasmids were TEds1xSpinach2 (TEds-1Sp), TEds2xSpinach2 (TEds-2Sp) with 1 or 2 copies of Spinach2 after the second subgenomic promoter; TE-3'UTR1xSpinach2 (TE-1UTRSp) with one copy of Spinach2 in the 3'UTR and TEds1x-3'UTR1xSpinach2 (TEds-1Sp+1UTRSp) with a copy both downstream of the subgenomic promoter and in the 3'UTR.

Construction of SINV-Broccoli (Figure 4.3-4.4). F30-2xdBroccoli, a double dimeric Broccoli (4 copies in total) in F30 scaffold from pET28c plasmid (Addgene 66843) was inserted into *Sph*I and/or *Bst*EII sites (see above). Due to the lack of a stop codon, F30-2xdBroccoli was also inserted into the *Spe*I site of the nsP3 gene. The

constructed plasmids were TEds6xBroccoli (TEds6Br; the ligation resulting in 1½ sets of F30-2xdBroccoli for an unclear reason), TE3'UTR4xBroccoli (TE-UTR4Br), TEds6x-3'UTR4xBroccoli (TEds10Br), TEnsP3-4xBroccoli (TEnsp3-4Br), TEnsP3-8xBroccoli (TEnsP3-8Br), and TEnsP3-4x-ds6x-3'UTR4xBroccoli (TEds14xBr). Furthermore, we made a tandem repeat as described by Jobbagy et al (110). Briefly, *Bam*HI and *Bgl*II restriction sites were added to the 5' and 3' ends of F30-2xdBroccoli, respectively, so that it could be self-ligated by these 2 compatible sites and formed tandem repeats. The strips of *Bst*EII-*Sph*I-*Spe*I restriction sites were also added to both ends of the tandem repeats. The largest contained 3 sets of F30-2xdBroccoli (12 copies). This 12xBroccoli was inserted into each of the 3 restriction sites. Unfortunately, we could not recover the correct insertion of 12xBroccoli at the 3'UTR site. Thus, the maximal number of Broccoli we could produce was 28 copies in TEnsP3-12x-ds12x-3'UTR4xBroccoli (TEds28xBr).

***In vitro* transcription and transfection.** All constructed plasmids were sequenced to confirm the correct insertions and orientations. mRNA of each construct was produced by Sp6 mMessage mMachine (Ambion) after linearization of the plasmid with XhoI (New England Biolabs). 200 µl Opti-MEM (Gibco) with 20 µg of each mRNA was mixed into another 200 µl Opti-MEM containing 40 µl Lipofectamine 2000 (Life Technologies). After adding 3.6 ml Opti-MEM, the total mixture was applied to nearly confluent BHK cells in a T150 flask, washed with phosphate buffered saline (PBS), and incubated at 37^{O}C 5% CO_2 for 4 h with intermittent rocking. The transfection mixture was then replaced by 12 ml of infection medium (see below). At 24 h, the supernatant

fluids were collected and frozen in aliquots at -80 ^{O}C. Titers of the recombinant viruses were determined by plaque assay (see below).

Cell culture, differentiation, and infection (Figure 4.5). BHK cells were cultured at 37^{O}C 5% CO_2 in Dulbecco's Modified Eagle Medium (DMEM, Gibco) with 10% heat-inactivated fetal bovine serum (FBS, Atlanta Biologicals), 1% PenStrep (PS, Gibco), and 2mM glutamine (Gibco). AP7 rat olfactory neurons transformed with a temperature-sensitive SV40 T antigen (111), were either maintained as cycling cells (cAP7) at 33^{O}C 7%CO_2, or were differentiated (dAP7) by adding 1 μg/ml insulin (Sigma), 100 μM ascorbic acid (Sigma), and 20 μM dopamine (Sigma) and culturing at 39^{O}C 5%CO_2 for 7 days. Nearly confluent cells were infected with the recombinant viruses in infection medium at a multiplicity of infection (MOI) of 0.01 to 20.

Live-cell imaging. Cells were grown on glass-bottom 35mm dishes, 24-well plates (Mattek), or 8-well chamber slides (Labtek). Infected cells were imaged after incubation with 20 μM DFHBI or DFHBI-1T (Lucerna) in imaging medium (Fluorobrite [Gibco], 25mM HEPES [Gibco], 5mM $MgSO_4$, 1%FBS) at 37^{O}C for 30 min. For time-lapse imaging, 1% FBS, 1% PS, and 2mM glutamine were also added to the imaging medium. Maximal excitation/emission for DFHBI- and DFHBI-1T-Spinach2 complexes are 447/501 and 482/505, respectively (112). Because of compatibility with the imaging system, most images were obtained using DFBHI-1T. In each imaging session, the laser power and gain were adjusted to minimize autofluorescence from TE (no aptamer) -infected cells. A 488nm laser was used for excitation of Spinach2- or Broccoli-fluorophore complexes in confocal microscopic imaging (Zeiss LSM780CS, Axio Observer Z1, Zen Software). When the signal overlapped with autofluorescence, the

lambda mode was used to capture emission spectrum of each pixel in the image. Because the emission spectra were different, Spinach2 and Broccoli could then be separated from autofluorescence by linear unmixing (Zen Software). Time-lapse experiments were performed in a heated chamber at 24% humidity using the same temperature and CO_2 levels as the culture conditions for each cell type. Images were analyzed with ImageJ Software.

Flow cytometry. Infected and uninfected BHK cells with or without treatment were trypsinized, resuspended in the imaging medium and incubated with or without fluorophores at 37^{O}C for 30 min. Cell suspensions were filtered through 70μm nylon filter (Cell strainer, Falcon). Data were acquired on a BD FACS Canto II flow cytometer in the GFP/FITC channel and analyzed with FlowJo (TreeStar).

Directed viral evolution. BHK cells were infected with dsTE-1Sp+1UTRSp at an MOI of 1 at 4^{o}C for 1 h with rocking every 10 min to allow viral binding but not endocytosis. The cells were then shifted to 37^{O}C for synchronous virus entry. At 6 h, infected cells were sorted in a Beckman Coulter MoFlo Cell Sorter based on brightness in the FITC/GFP channel at 488nm excitation. Single cells were sorted into wells of 96- or 48-well plates pre-seeded with BHK cells in DMEM-1%FBS. After overnight incubation, supernatant fluids were collected and infected cells in each well were trypsinized and incubated with imaging medium for flow cytometry to determine signal intensity. Viruses in supernatant fluids from wells containing cells with the strongest signals were expanded in BHK cells and quantified by plaque assay. The expanded viral clones were retested for fluorescent signal and the brightest clones were chosen for another round of selection by cell sorting.

Virus replication and plaque purification. To assess virus replication, BHK, cAP7, and dAP7 cells were infected in triplicate at an MOI of 5. Supernatant fluids were collected at 3, 6, 9, 12, 18 and 24 h for plaque assay. Plaque assays were performed using nearly confluent BHK cells in 6-well plates incubated with 200 µl of 10-fold serial dilutions of each sample in DMEM+1%FBS for 1 h at 37^{O}C 5%CO_2 with rocking every 10 minutes. The samples were replaced with 1.5ml of agar (0.6% Bactoagar, 1x minimum essential medium (MEM, Gibco), 1%FBS) and returned to the incubator. After 48 h, cells were stained with neutral red (Sigma) in Dulbecco's PBS with calcium and magnesium (DPBS, Lonza) for 2 h at 37^{O}C 5%CO_2 and plaques were counted. For plaque purification the agar over a plaque was aspirated, re-suspended in 100 µl PBS, kept at 4^{O}C overnight and then propagated in BHK cells.

Agarose gel electrophoresis. Viral RNA from infected BHK supernatant fluids following transfection, sorting, and plaque purification, was amplified by RT-PCR. The PCR products were separated by agarose gel electrophoresis, stained with ethidium bromide and captured with Gel Doc (Bio-Rad). Some bands were selected for sequencing.

Treatment of infected cells with antibody. SV127 (209; mouse monoclonal neutralizing IgG3 against SINV E2) (113) from hybridoma supernatant was purified by Melon Gel IgG Purification Kit (Thermo Scientific), quantified by Pierce BCA Protein Assay Kit (Thermo Scientific), and then conjugated with Dylight 594 Antibody Labeling Kit (Thermo Scientific), according to the manufacturer's respective protocols. BHK, cAP7, or dAP7 cells were infected with one of the constructed viruses at an MOI of 5-20. The cells were treated with 1-5 µg/ml of SV127, Dylight594-conjugated SV127 (~5

dyes/IgG molecule), or 500 U/ml of rat IFN-γ at various time points for either imaging or flow cytometry. TrkA antibody (Clone 315104, R&D Systems) at 1μg/ml was used as a control.

In vivo study. TE, TE3'UTR1xSpinach2, TEds1x-3'UTR1xSpinach2, 1a5, 1b6, 1c6 (the brightest three viral clones from second sorting), and all SINV-Broccoli were used for infection of mice. A couple of C57BL/6 mice, 2-3 months old, were intracerebrally injected with 1000 pfu/20 μL of each virus. At day 3, brains were collected and the left anterior quadrant was homogenized with 1 ml PBS in Lysing Matrix A tubes in a FastPrep-24 machine (MP Biomedicals) at 6 m/sec speed for 40 sec to make 10% brain homogenates for plaque assay.

Results:

Spinach2 experiments

The fluorophore does not form fluorescent complexes with non-specific RNAs. To determine specificity of the fluorescent signal, *in vitro* transcribed Spinach2 RNA was analyzed with and without added DFHBI. RNA fluorescence required DFHBI and was concentration-dependent. RNA extracts from SINV-infected and uninfected mouse brains were used to assess nonspecific fluorescence of RNA without Spinach2 in the presence of DFHBI. These controls showed no signal higher than the buffer-only control (**Figure 4.6A**). Flow cytometry was used for analysis of BHK cells infected with TEds-1Sp+1UTRSp with and without exposure to DFHBI (**Figure 4.6B**). The shift of signal from baseline in the GFP/FITC channel occurred only when cells were infected with virus that contained Spinach2 in the presence of DFHBI.

Imaging the Spinach2-fluorophore signal in infected cells. Cells infected with Spinach2 recombinant viruses and incubated with DFHBI showed little signal when viewed in the epifluorescence microscope and prolonged exposure was not possible due to rapid bleaching. Because the signals revived after resting with excess fluorophore in the medium, it was hypothesized that pulse excitation would improve the signal to noise ratio (114). A laser-scanning confocal microscope provides such pulses because the excitation laser hits each tiny point for just few microseconds during each scanning frame, leading to a very short exposure with a very long rest. Multiple repeated scans on the same frame could therefore be averaged to improve the resolution or summed to increase the signal intensity without photobleaching. The signal was sufficient for Z-stack (**Figure 4.7**) and time-lapse imaging.

Effect on fluorescence of the fluorophore and copies of Spinach2. Cells infected with TEds-1Sp+1UTRSp gave the strongest signal both in flow cytometry and microscopic imaging (**Figure 4.8**), followed by TE-1UTRSp and TEds-1Sp. Surprisingly, TEds-2Sp was less bright than either of the viruses with only one copy of Spinach2. The fluorophore DFHBI-1T is more compatible with available laser and filter sets (104) and provided a better signal than DFHBI in our studies (Fig 4B). DFHBI-1T readily enters cells and the intracellular SINV-RNA-Spinach2 signal reached peak intensity within a few minutes after addition (**Figure 4.9**).

Effect of Spinach2 on virus replication. The effect of Spinach2 tagging on virus replication was assessed in generally permissive BHK and cAP7 cells and in more restrictive differentiated dAP7 cells (**Figure 4.10**) (28, 115). Insertion of Spinach2 into the 3'UTR had no effect on replication while insertion after a second subgenomic

promoter generally impaired replication. In particular, replication of TEds-2Sp was reduced 10-20-fold in BHK and cAP7 cells compared to the parent TE virus, although this was not evident in less permissive dAP7 cells.

Directed viral evolution improves the brightness of SINV-Spinach2. To select for the brightest viruses TEds-1Sp+1UTRSp-infected BHK cells were sorted by FACS (**Figure 4.6**) for the 15 brightest cells out of 15,000 events (1:1000). Viruses originating from these bright cells were expanded, quantified, and retested for signal intensity in BHK cells. The 1d11 clone was selected for 2nd-round sorting, because the brightest clone (1c9) did not replicate well. In the 2nd round sort with 1d11-infected BHK cells, propidium iodide exclusion was used to include only single live cells. The 53 brightest cells were sorted from 17 million events (1:300000). The twelve brightest viral clones were expanded, quantified, and retested for signal intensity. Clone 1a5 had a signal 68% brighter than the original TEds1x-3'UTR1xSpinach2 (**Figure 4.8**), without a difference in replication in either BHK or dAP7 cells (**Figure 4.10**). Sequencing from the second subgenomic promoter to 3' end of 1d11 and 1a5 showed point mutations only in the tRNA scaffold (**Figure 4.12**).

Viruses with two Spinach2 copies were unstable. Gel electrophoresis of RT-PCR products of viral RNA extracted from transfection supernatant fluids showed a single band with the correct length in the viruses that had only 1 copy of Spinach2. However, TEds-2Sp had 3 bands consistent with deletion of one copy of tRNA-Spinach2 and TEds-1Sp+1UTRSp and 1a5 (not shown) had 2 bands, the correct length and a shorter one due to a large deletion (341 bases). The deletion included 1 copy of tRNA-Spinach2 (168 bases) and a part of the 3'UTR. Plaque purification could not separate

viruses with full-length RNA from those with the deletion as 2 bands were present in all 8 viral clones purified from TEds-1Sp+1UTRSp (**Figure 4.12**).

SINV-Spinach2 viruses were attenuated *in vivo*. To determine the ability of the Spinach2-tagged viruses to replicate in vivo, we infected two 2-3 month old C57BL/6 mice intracerebrally with 1000 pfu TEds -1Sp+1UTRSp and derivative clones 1a5, 1b6, or 1c6, along with TE (**Figure 4.11**). Brain homogenates collected 3 days after infection were assayed for infectious virus in BHK cells. All mice infected with TE were positive for virus, but no brains from mice infected with clones and only one brain from mice infected with TEds-1Sp+1UTRSp had infectious virus. The virus from this mouse retained its fluorescence after recovery in BHK cells.

Use of SINV-Spinach2 viruses for evaluation of viral RNA dynamics, distribution, and antibody-mediated clearance. Live-cell imaging of BHK cells infected with TEds-1Sp+1UTRSp allowed analysis of the onset of viral RNA replication in individual cells and spread in the culture (**Figure 4.13**). Interestingly, infected cells concentrated viral RNA at the tip of filopodia that contacted adjacent non-infected cells. Viral RNA was subsequently observed in the contacted cell, starting at the contact site followed by spread throughout the cytosol (**Figure 4.13**). Addition of neutralizing anti-SINV E2 antibody to infected BHK cells did not inhibit spread of the virus to adjacent cells and increased the amount of intracellular viral RNA (**Figure 4.14**).

cAP7 cells could also be imaged after infection with TEds-1Sp+1UTRSp and antibody-treatment resulted in clearance of viral RNA (**Figure 4.15**). The anti-SINV E2 (SV127-Dylight594) bound the infected cell membrane more intensely with longer

incubation. With more antibody binding, the less viral RNA (Spinach2 signal) could be found intracellularly.

Spectral imaging can differentiate the overlap between low Spinach2 signal and high autofluorescence in differentiated neuronal cells. SINV replication is restricted in differentiated neuronal cells (**Figure 4.11**) (28, 115) so levels of viral RNA are lower in infected dAP7 cells than BHK and cAP7 cells. With low viral RNA copy number in infected dAP7 cells, the Spinach2 signal intensity from TEds-1Sp+1UTRSp was very close to the autofluorescence associated with differentiated neurons. Spectral imaging showed a 505nm emission peak from Spinach2 and a smooth autofluorescence curve. Linear unmixing revealed the perinuclear autofluorescent granules and the viral RNA accumulated at the tips of dendritic-like processes (**Figure 4.16**). Live-cell imaging of antibody-treated infected dAP7 cells demonstrated an inverse correlation between the amount of antibody bound to the cell surface and amount of viral RNA (**Figure 4.17**).

Broccoli experiments

Once the far superior Broccoli RNA aptamer was available, we replaced Spinach2-labeled SINV with Broccoli-labeled SINV for our experiments.

The signal intensity was correlated with the number of Broccoli copies (Figure 4.18). The F30-2xdBroccoli is much brighter than tRNA-Spinach2. From 4 to 14 copies, the signal intensity increased according to the copy number. However, TEds28Br, which had tandem repeats of F30-2xdBroccoli, did not show a brighter signal than TEds14Br. Because the TEnsP3-4Br and TEnsP3-8Br had Broccoli in genomic RNA only, they were dimmer than those that had Broccoli in subgenomic RNA.

Broccoli signal can survive fixation (Figure 4.19). Unlike Spinach2, fixation with 3.7% paraformaldehyde at room temperature for 10 minutes did not obliterate the Broccoli signal. However, fixation did decrease the signal intensity and also increased autofluorescence. Thus, live-cell imaging gave a better signal to noise ratio than fixed cell imaging.

Broccoli signal was colocalized with SINV RNA FISH (Figure 4.20). Post fixation imaging showed almost identical patterns between RNA FISH and Broccoli signal ($R_{colocalization}$ = 0.9049). In TEds10Br, discrepancy between the 2 signals did rarely occur in a few cells from the whole well (~32000 cells/well) (**Figure 4.21**). Because for TEds10Br Broccoli was inserted into the second subgenomic site, the discrepancy might be the result of differences in efficacy between 1st and 2nd subgenomic promoter of the virus in those particular cells. However, this phenomenon was very rare and should not affect the outcome of experiments.

Broccoli can be used in differentiated neurons. Spinach2 gave very dim signal in dAP7 cells. The spectral imaging (lambda mode) could differentiate the signal from autofluorescence (see above) only in few dAP7 cells, while most of the infected cells did not have enough signal, making it very hard to use in experiments. In contrast, Broccoli was bright enough to be seen in most infected dAP7 cells (**Figure 4.22**), though lambda mode was still needed. The Broccoli signal could also be observed directly through a glass-bottom dish with a brain slice from a mouse, sacrificed on day 3 post intracerebral injection with TEds10Br (**Figure 4.23**). However, a Transwell insert obscured the Broccoli signal; thus, it was not ready for *ex vivo* brain slice culture experiments yet.

Attenuation of SINV with high copy number of Broccoli in differentiated neurons (Figure 4.24). TE3UTR4Br and TEds6Br replicated very well in all types of cells and in mouse brain. On the other hand, TEds10xBr, TEds28Br, and the worst TEds14Br replicated poorly in dAP7 cells and mouse brains, but quite well in BHK and cAP7 cells. TEnsP3-4Br and TEnsP3-8Br replicated well in all types of cells, but inconsistently in mouse brains from very low to very high number of pfu.

SINV genomic viral RNA form vesicle-like arrangement in perinuclear area (Figure 4.25-4.26). Unlike subgenomic Broccoli, genomic Broccoli clearly accumulated close to the nucleus and assumed a circular shape with an inside halo. This halo could contain either viral envelope protein or mitochondrion (**Figure 4.27**). Time-lapse imaging of merged phase contrast-Broccoli (**Figure 4.28**) showed many vesicles surrounded with SINV genomic RNA were gathered around the perinuclear halo (most likely golgi apparatus). Later on, the genomic RNA was accumulated in the halo and formed another vesicle-like arrangement.

Antibody treatment enhanced viral replication and altered the distribution of genomic RNA in BHK cells. The rate of viral replication depended on the multiplicity of infection (MOI) and was increased by anti-E2 [SV127] treatment in BHK cells (Figure 4.29). The genomic RNA distribution was also changed from accumulation at perinuclear area to cell membrane upon antibody treatment (**Figure 4.30**).

Antibody and IFN-γ mediated viral RNA clearance and improved survival in dAP7 cells. In contrast to BHK cells, dAP7 cells could clear the viral RNA during 24-72 hours post infection upon treatments with either anti-E2 [SV127] or IFN-γ. Both

treatments also improved cell survival, especially in combined treated cells (**Figure 4.31)**. However, viral RNA still persisted in a few cells, to which anti-E2 could not bind (**Figure 4.32**). These cells still had intracellular E2 protein, but lacked its expression on the cell membrane (**Figure 4.33**). Flow cytometry on infected dAP7 cells with similar treatments confirmed the live-cell imaging finding (**Figure 4.34**). However, neither antibody nor IFN-γ treatment showed any benefits on BHK cells, while only antibody could mediate virus clearance in cAP7 cells and did not improve survival (**Figure 4.35**).

Discussion:

The successful examples of Spinach labeling are the abundant 5S-ribosomal RNA (10^7 molecules/cell) and CGG-triplet repeat (101, 102). The remarkably lower number of SINV RNA molecules per cell (**Table 4.2**) and low signal intensity of the aptamers become a challenge. Spinach2 can only be used for live-cell imaging of subgenomic RNA in undifferentiated cells. Though not completely covering all the aspects, the brighter Broccoli can be applied to fixed cells, genomic RNA, differentiated cells, and *ex vivo* brain slices (**Table 4.3**).

Table 4.2 The amount of Sindbis viral components in undifferentiated cell lines

SINV components	Molecules/cell	References
Structural proteins	$10^7 – 10^8$	(116)
Subgenomic RNA	5×10^5	
Genomic RNA	1.6×10^5	(117)
dsRNA/minus-stranded RNA	2.7×10^4	(118)

Table 4.3 The applications of SINV-aptamers

SV-aptamer-fluorophore	BHK/cAP7		dAP7		Brain	
	Live	Fixed	Live	Fixed	Live	Fixed
Subgenomic-Spinach2-DFHBI	Poor	No	No	No	No	No
Subgenomic-Spinach2-DFHBI-1T	Fair	No	Poor	No	No	No
Subgenomic-Broccoli-DFHBI-1T	Good	Good	Fair	No	Poor	No
Genomic-Broccoli-DFHBI-1T	Fair	Poor	Poor	No	No	No

More copies of Spinach2 may not always result in the stronger signal. TEds1x-3'UTR1xSpinach2, into which each Spinach2 copy has been inserted separately at 2nd subgenomic promoter and 3'UTR sites, shows the best signal. On the other hand, insertion of 2 Spinach2 copies together as tandem repeats at 2nd subgenomic promoter site in TEds2xSpinach2 gives the dimmest signal. This is at least partially due to its inferior replication in BHK cells. Since tRNA-Spinach2 contains many stop codons in all frames, it is hard to find more sites to accommodate the 3rd copy and beyond.

After 2 cycles of the brightest viral clone sorting by FACS, 1a5 clones remarkably increases the signal intensity from the original one. The clone shows comparable replication in 1-step viral growth curve; thus, the better signal is likely due to the better RNA-folding stability. We cannot find 1a5 a new mutation in Spinach2-tRNA sequence, added to its parental clone, 1d11. Thus, mutations outside Spinach2-tRNA may contribute to the stability too.

Any proteins, RNA aptamers, or promoter sequences that can be coded into viral genome and have their properties quantified by flow cytometry or other types of cell sorting may also get benefits from this "Directed Viral Evolution" as long as the constructed viruses can replicate. For instance, one may insert a fluorescent protein gene

into TEds and use FACS to sort the cells with stronger signal or spectral shift. Each round takes about 1 week, so we can make the virus evolve rapidly until the signal reaches its maximum. Sequencing of the virus will reveal the new desired version of the fluorescence protein. This is similar to the way Broccoli RNA has been discovered (108), except the mutation and the sorting are done in a single step. However, the mutations that limit replication will not be selected. We may also overcome the attenuation in vivo by passage the virus between mouse brains and cell cultures instead of cell cultures only.

Though their signals are improved, TEds1x-3'UTR1xSpinach2 and its mutants are not stable. There are always 2 viral populations with different genome sizes, the correct sequence and the large deletion. The large deletion persists in all viral clones that arise from plaque purification. Thus, the large deletion most likely occurs naturally during the viral replication and cannot be avoided. Homologous recombination and intracellular cleavage of tRNA scaffold might be the causes (107).

F30-2xdBroccoli is much brighter than tRNA-Spinach2. Unlike tRNA, F30 scaffold is not a target of intracellular cleavage (107). However, Broccoli still suffers the similar fates as Spinach2. Too many copies of Broccoli attenuated the viruses *in vivo* and may not improve the signal.

SINV with fluorescent RNA aptamers can be used in many applications, where RT-PCR and FISH techniques are not very useful. In live-cell imaging, we can quantitate the relative amount of viral RNA in each cell/organelle and visualize its distribution. We can see viral RNA clearance, mediated by antibody or interferon, in real time. 3D reconstruction can be done to see colocalization or FRET with viral or host proteins, labeled with fluorescent proteins. For *ex vivo* studies, we may infect mice, making single-

cell suspensions from their infected tissues, and then count or sort aptamer-positive cells with FACS to further study these naturally infected cells outside the bodies.

In this study, we can demonstrate at least two types of vesicle-like genomic RNA arrangement in live cells. The one found earlier is most likely the endosome-derived cytopathic vacuole (CPV) type I, which contains viral replication complex (19). The genomic RNA that surrounds this vacuole might be nascent produced from the replication complex inside. Another one, found later in the perinuclear halo, is probably the trans golgi apparatus-derived CPV type II, which contains envelope proteins and is surrounded by viral nucleocapsid (15). Furthermore, we also find that some of these genomic RNA encircled mitochondria, which haven't been documented before. The mitochondria stop moving after being encased by the viral genomic RNA, which might be the process of mitophagy.

Our study with SINV-aptamer also reveals vast different effects of antibody and IFN-γ treatments on different cell types as shown by both live-cell imaging and flow cytometry (**Table 4.4**). Both replications (**Figure 4.24**) and clearance patterns of viruses in dAP7 cells represent *in vivo* study in mouse brains quite well. Similar to mouse study in Chapter 2, the viral RNA persists in cells that antibody cannot bind, possibly due to lack of envelope proteins on the surface.

Table 4.4 Summary of treatments on different types of cells

Models	IFNG- Ab-	IFNG+ Ab-	IFNG- Ab+	IFNG+ Ab+
BHK	Dead in 18-24h	←→RNA, ←→survival	↑↑RNA, ←→survival	↑↑RNA, ←→survival
cAP7	Dead in 24-48h	←→RNA, ←→survival	↓RNA, ←→survival	↓↓RNA, ←→survival
dAP7	Dead in 48-72h	↓RNA, ↑survival	↓↓RNA, ↑↑survival	↓↓↓RNA, ↑↑↑survival
Mouse brain	Persistence	Partial Clearance	Normal clearance	Normal clearance,
Mouse model	SCID	µMT	IFNG-/-	WT

The production of Sindbis-fluorescent RNA aptamers will be the early step of new approaches toward viral RNA study. With our best clone, we still cannot use it for *ex vivo* brain slice culture. The dim signal that overlapped with autofluorescence is the main problem. This can be partially overcome by separating the different emission spectra between aptamer-fluorophore and autofluorescence with linear unmixing. Low amount of viral RNA is still a challenge. New fluorophores are under development toward emission in red wavelength, where autofluorescence is less problematic (104).

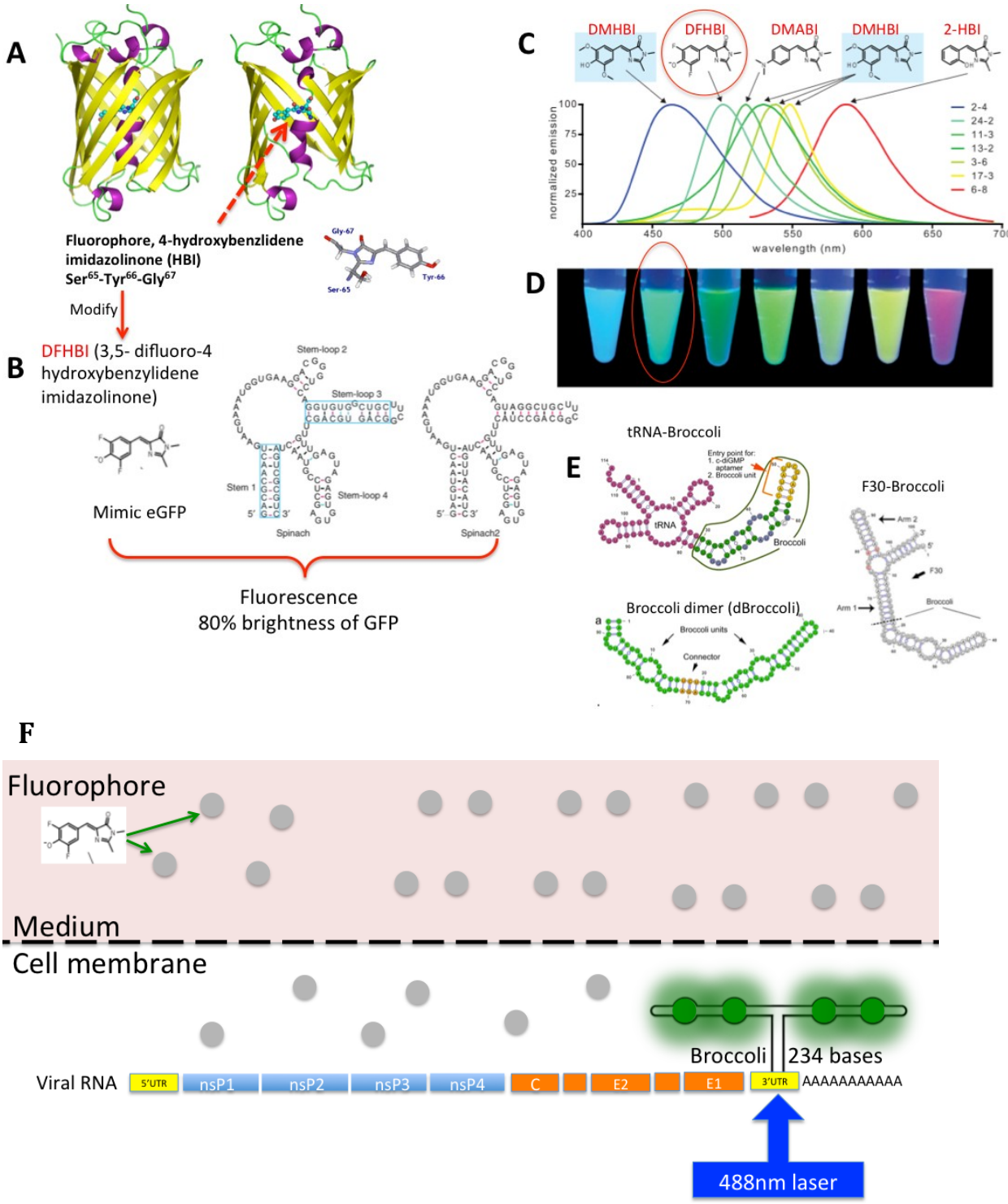
A
Fluorophore, 4-hydroxybenzlidene imidazolinone (HBI)
Ser65-Tyr66-Gly67
Gly-67
Ser-65
Tyr-66
Modify
B
DFHBI (3,5- difluoro-4 hydroxybenzylidene imidazolinone)
Mimic eGFP
Stem-loop 2
Stem-loop 3
Stem-loop 4
Stem 1
Spinach
Spinach2
Fluorescence
80% brightness of GFP
C
DMHBI
DFHBI
DMABI
DMHBI
2-HBI
normalized emission
wavelength (nm)
2-4
24-2
11-3
13-2
3-6
17-3
6-8
D
E
tRNA-Broccoli
Entry point for: 1. c-diGMP aptamer 2. Broccoli unit
tRNA
Broccoli
F30-Broccoli
Arm 2
F30
Arm 1
Broccoli dimer (dBroccoli)
Broccoli units
Connector
F
Fluorophore
Medium
Cell membrane
Broccoli
234 bases
Viral RNA
5'UTR
nsP1
nsP2
nsP3
nsP4
C
E2
E1
3'UTR
AAAAAAAAAA
488nm laser

Figure 4.1 Principle of fluorescent RNA aptamers . Green fluorescent protein (GFP) emits fluorescence upon excitation to its fluorophore core, which is the modified Ser^{65}-Tyr^{66}-Gly^{67}, encased in β-barrel (A). The β-barrel is critical to the signal emission, since it restrains the fluorophore and thus prevents energy lost through the movement of the excited fluorophore. The GFP fluorophore (HBI) can be synthesized and modified to imitate enhanced GFP (eGFP). This modified fluorophore (DFHBI) can permeate into the cells and emit fluorescence upon excitation after binding to the RNA aptamers (B), which act like the β-barrel. Various RNA aptamer-fluorophore combinations give different fluorescence spectra (C and D, red circle – Spinach-DFBHI). Spinach2 has a better folding stability over Spinach due to few point mutations (B). Broccoli was subsequently developed (E). It is smaller and has a better signal than Spinach2. Image E shows a Broccoli monomer in a tRNA scaffold, Broccoli dimer (dBroccoli), and Broccoli monomer in a F30 scaffold. F30 is more stable than tRNA. It has 2 arms – each can accept a set of Broccoli dimer, thus can contain 4 Broccoli at maximum (F30-2xdBroccoli). The example of constructed viral RNA genome, F30-2xdBroccoli insertion at 3'UTR, is shown inside the infected cells (F). The 4 copies of Broccoli RNA aptamers bind the permeable fluorophore, added to the medium, and emit green fluorescence upon blue laser excitation.

A

3'end of original TEds sequence in plasmid (TE lacks the underlined sequence.)

NNNNNNNNNNNNTGNNNATGTAACCNCCNGCTGACCATATCGTGAGCACCCCGCACAAAAATGACCAAGAATTTCAAGCC

GCCATNTCAAAAACATCATGGAGTTGGCTGTTTGCCCTTTTCGGCGGCGCCTCGTCGCTATTAATTATAGGACTTATGAT

TTTTGCTTGCAGCATGATGCTGACTAGCACACGAAGATGACGGGCCCGGTACCGCT**ATCTCTACGGTGGTCCTAAATAGT**

1st E1 stop **2nd subgenomic promoter** Subgenomic start

ACTTCTAGAGATCTGCAGGTCGACGGATCCCCCGAGATTTTCAGGAGCTAAGGAAGCTAAAGGTCACCTGACCGCTACGC

BstEII site 2nd E1 stop

CCCAATGATCCGACCAGCAAAACTCGATGTACTTCCGAGGAACTGATGTGCATAATGCATCAGGCTGGTACATTAGATCC

CCGCTTACCGCGGGCAATATAGCAACACTAAAAACTCGATGTACTTCCGAGGAAGCGCAGTGCATAATGCTGCGCAGTGT

Add A "GCATGC" → SphI site

TGCCACATAACCACTATATTAACCATTTATCTAGCGGACGCCAAAAACTCAATGTATTTCTGAGGAAGCGTGGTGCATAA

TGCCACGCAGCGTCTGCATAACTTTTATTATTTCTTTTATTAATCAACAAAATTTTGTTTTTAACATTTCNAAAAAAAAA

Last base before polyA

NNANAAAAAAAAAAAAAAAAGGGGAATTCCTCGAGGGGAAT

XhoI (linearization site)

B

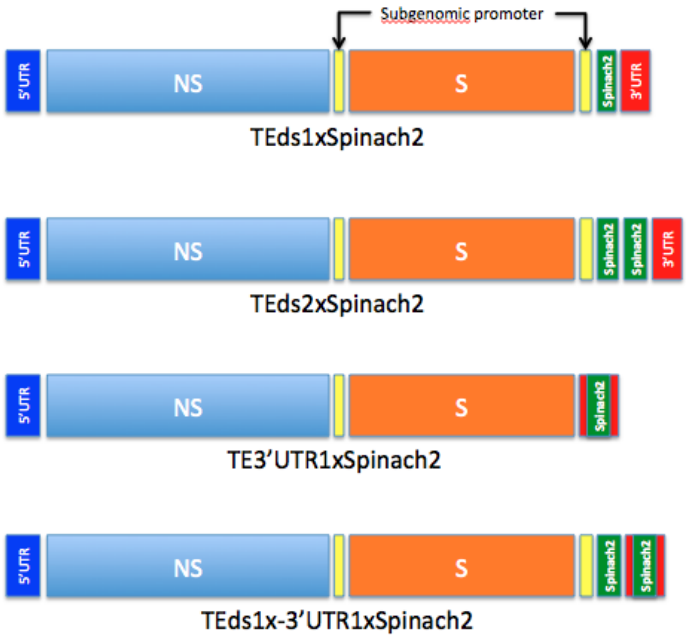

Figure 4.2 Construction of Sindbis virus-Spinach2. The tRNA-Spinach2 sequence was inserted into the plasmids of either TE or TEds (the underlined sequence added to TE) downstream of the 2nd subgenomic promoter (bold characters) at the *Bst*EII site (green characters) and/or 3'UTR at the *Sph*I site created by site-directed mutagenesis (blue characters).

A

UUGCCAUGUGUAUGUGGG**AGACGGUCGGGUCCAUCUGAGACG**

GUCGGGUCCAGAUAUUCGUAUCUGUCGAGUAGAGUGUGGGCU

CAGAUGUCGAGUAGAGUGUGGGCUCCCACAUACUCUGAUGAUC

CAGACGGUCGGGUCCAUCUGAGACGGUCGGGUCCAGAUAUUCG

UAUCUGUCGAGUAGAGUGUGGGCUCAGAUGUCGAGUAGAGUGU

GGGCUGGAUCAUUCAUGGCAA

B

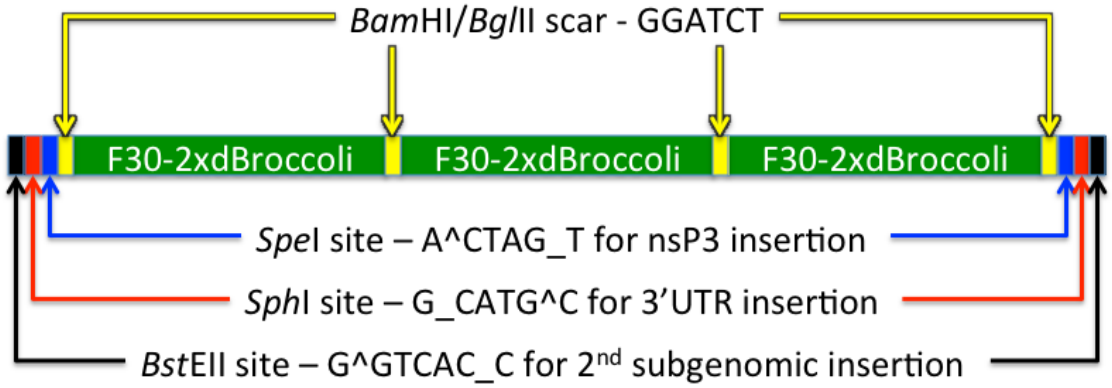

Figure 4.3 F30-2xdBroccoli (A) and construction of tandem repeats. The sequence (A) shows 2 copies of Broccoli dimers (bold green characters) in F30 scaffold (black characters). The tandem repeats (B) consist of 3 sets of F30-2xdBroccoli (12 Broccoli in total), made from self-ligation between the complementary 5' (*Bam*HI – G^GATC_C) and 3' end (*Bgl*II – A^GATC_T). The ligation forms a scar (GGATCT), which can no longer be cut by both *Bam*HI and *Bgl*II. The tandem repeats can be cut and inserted into 3 restriction sites of TEds plasmid in the specific order – nsP3, 3'UTR, and downstream of 2nd subgenomic promoter.

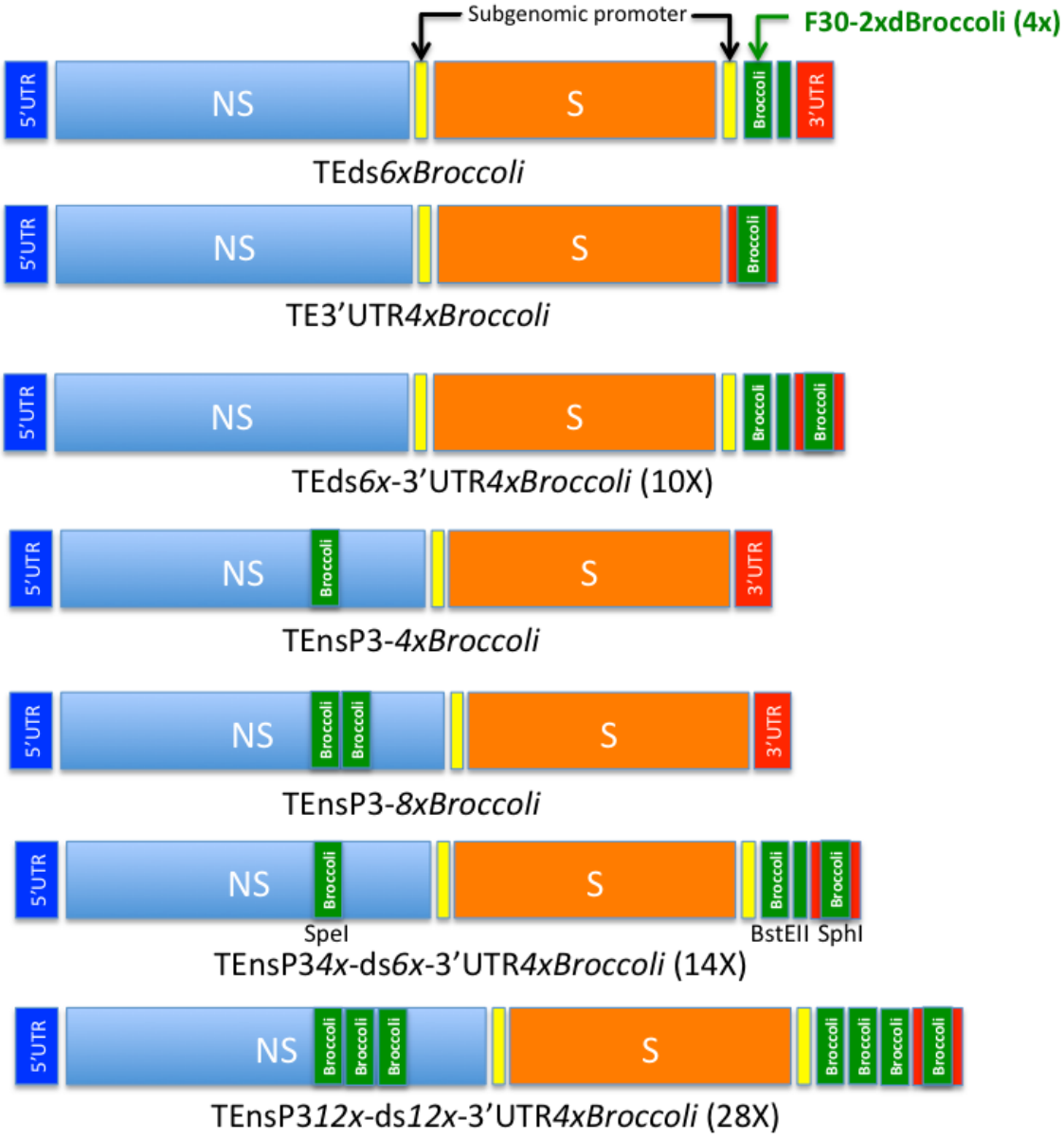

Figure 4.4 Construction of SINV-Broccoli. The F30-2xdBroccoli, 1-3 repeats, has been inserted into 3 restriction sites – *Spe*I in nsP3, *Bst*EII downstream of 2nd subgenomic promoter, and *Sph*I in 3'UTR.

BHK	cAP7	dAP7
Baby hamster kidney	Rat olfactory neuron Immortalized with temperature-sensitive SV40 large T antigen	
$37^{O}C$ 5%CO_2	$33^{O}C$ 7%CO_2	$39^{O}C$ 5%CO_2
Fibroblast	Neuronal progenitor	Mature neuron

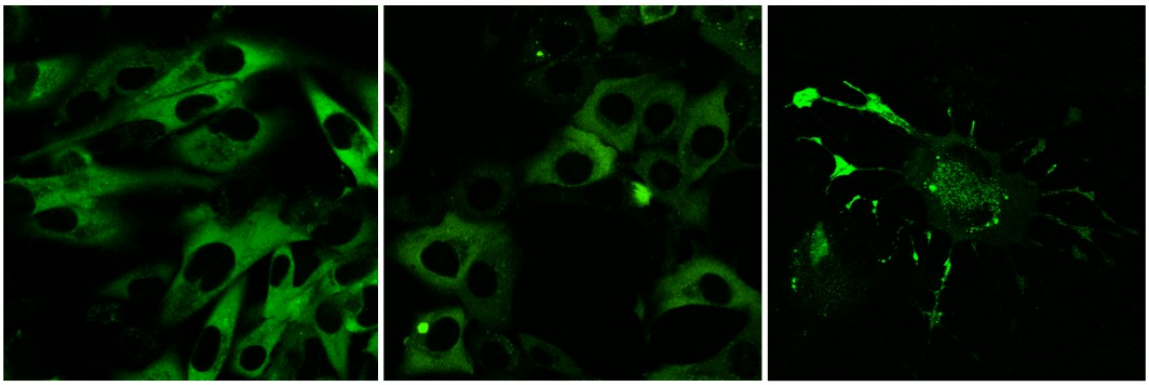

Figure 4.5 Types of cell lines used in this study. The table shows the culture conditions and characteristics of each cell line. The images show green fluorescence from TEds1Sp+1UTRSp-infected cells, MOI of 5, 18-24 hours post infection.

A

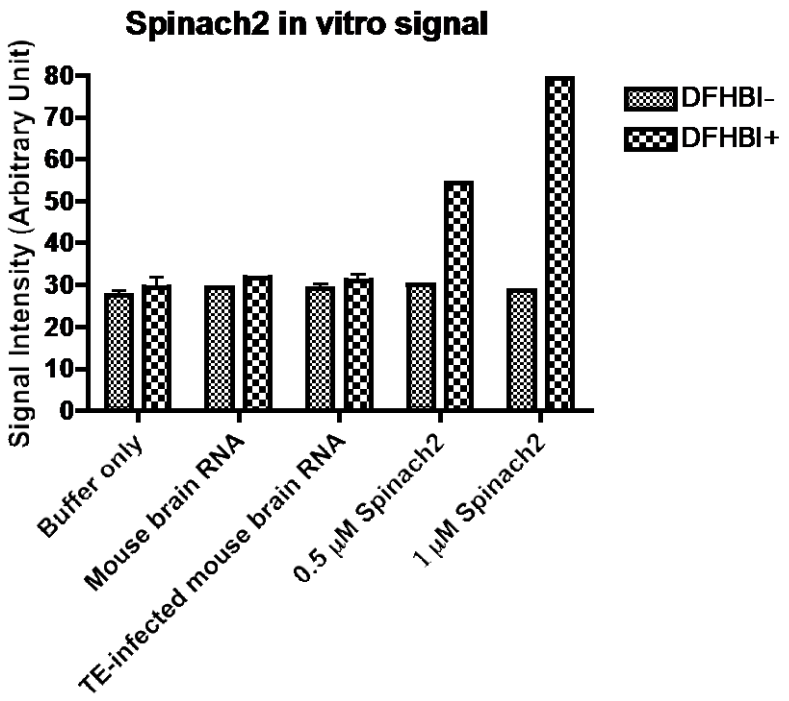
Spinach2 in vitro signal
Signal Intensity (Arbitrary Unit)
80
70
60
50
40
30
20
10
0
DFHBI-
DFHBI+
Buffer only
Mouse brain RNA
TE-infected mouse brain RNA
0.5 μM Spinach2
1 μM Spinach2

B

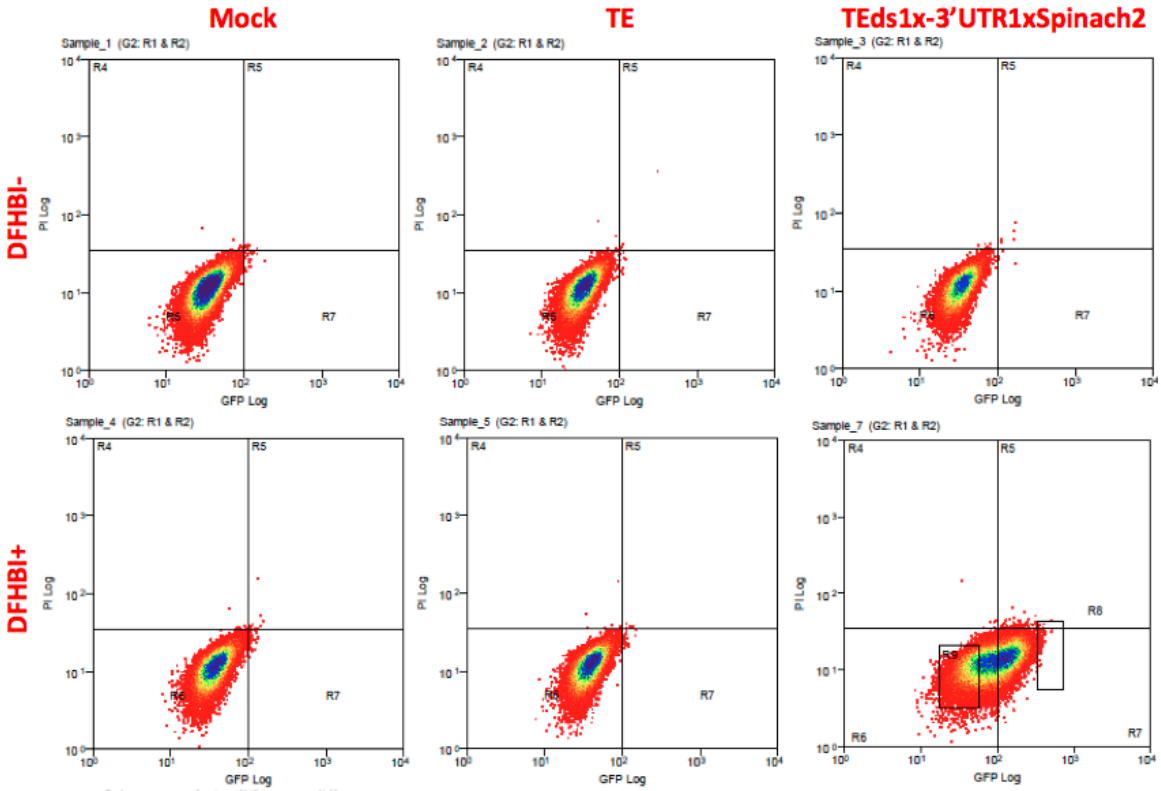
Mock
TE
TEds1x-3'UTR1xSpinach2
DFHBI-
DFHBI+
PI Log
GFP Log
R4
R5
R6
R7
R8
R9

Figure 4.6 Specificity of Spinach2-fluorophore signal. (A) The bar chart showed specific concentration-dependent signal intensity of *in vitro* Spinach2 RNA transcript at 0.5 and 1 μM (4μg/well) in the presence of DFHBI. Non-specific RNA from brain extracts (4μg/well) had the same level of signal as the buffer only control. (B) Analysis of uninfected and TE- or TEds-1Sp+1UTRSp-infected BHK cells (MOI=1, 6 h after infection) by flow cytometry in PI (propidium iodide, Y axis) and GFP (green fluorescent protein, X axis) channels. Only when both the Spinach2 sequence and DFHBI were present (right lower panel) was fluorescence in the GFP channel detected. Cells in the small inset (R8) in the right lower panel were brightest and were sorted to select for viral clones with improved fluorescence.

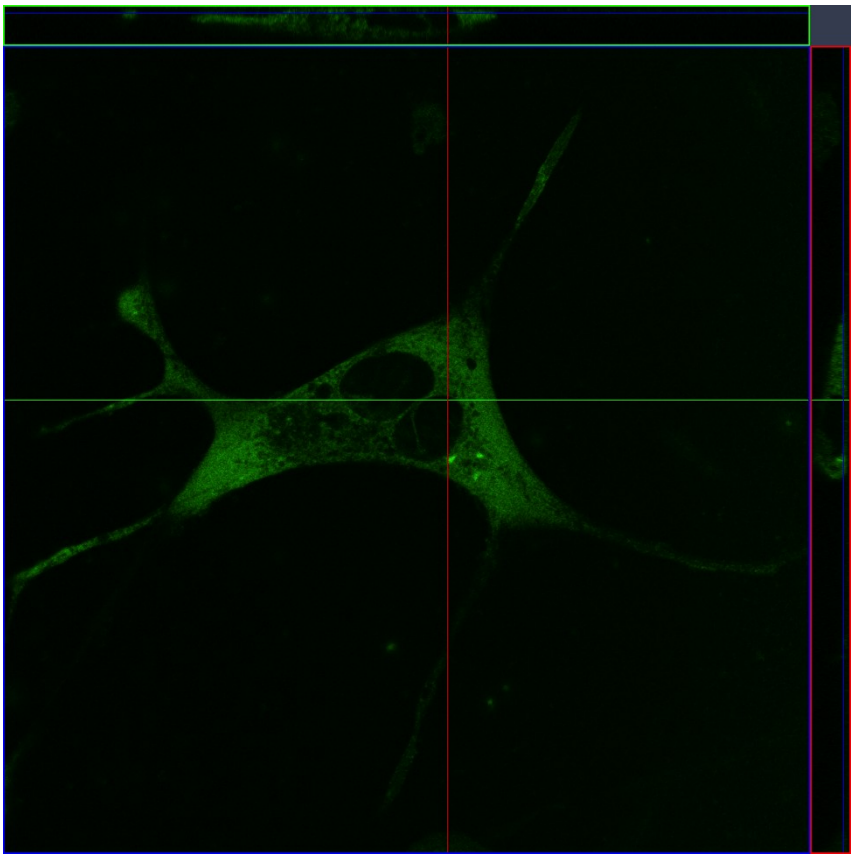

Figure 4.7 Viral RNA distribution. The orthogonal view of live-cell imaging showed the XY and cross-sectional view of viral RNA distribution in the cytosol of TEds1x-3'UTR1xSpinach2-infected BHK cells incubated with DFHBI-1T. (Z-stack imaging, MOI 5, 20 h after infection, objective lens 63x)

A

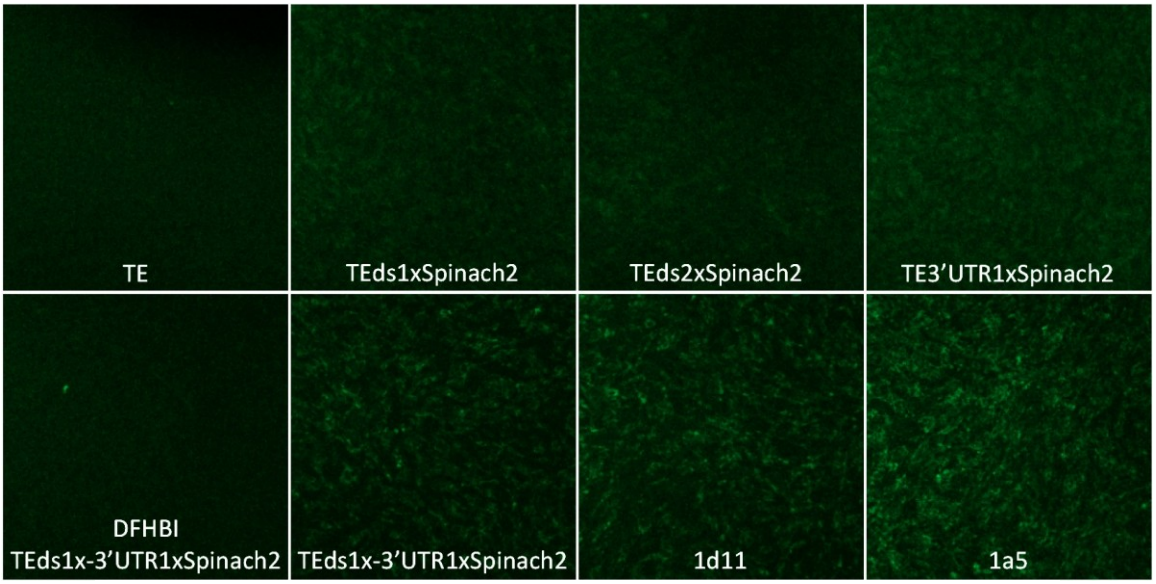
TE
TEds1xSpinach2
TEds2xSpinach2
TE3'UTR1xSpinach2
DFHBI
TEds1x-3'UTR1xSpinach2
TEds1x-3'UTR1xSpinach2
1d11
1a5

B

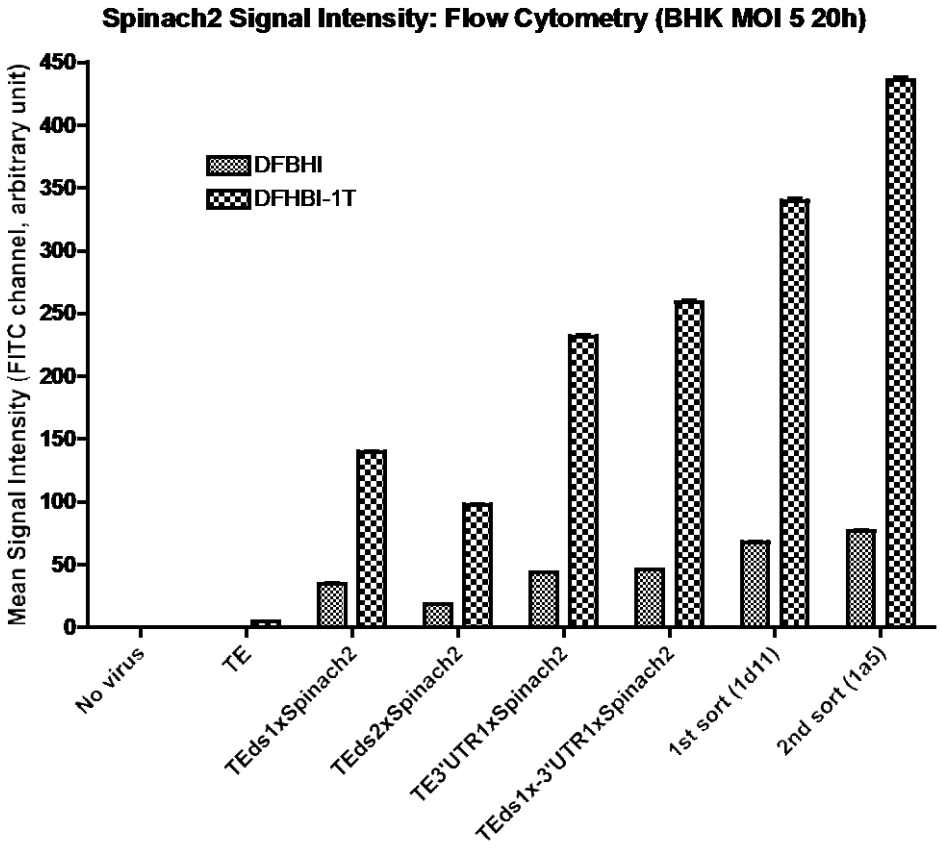
Spinach2 Signal Intensity: Flow Cytometry (BHK MOI 5 20h)
Mean Signal Intensity (FITC channel, arbitrary unit)
450
400
350
300
250
200
150
100
50
0
DFBHI
DFHBI-1T
No virus
TE
TEds1xSpinach2
TEds2xSpinach2
TE3'UTR1xSpinach2
TEds1x-3'UTR1xSpinach2
1st sort (1d11)
2nd sort (1a5)

Figure 4.8 Signal intensity of TE-Spinach2 viruses. Live-cell imaging of infected BHK cells (MOI 5, 20 hours, objective lens 10x) showed relative fluorescence intensity of TEds2xSpinach2< TEds1xSpinach2< TE3'UTR1xSpinach2< TEds1x-3'UTR1xSpinach2. The signal was further improved for viruses selected in the 1st sort (1d11) and 2nd sort (1a5). (A) All images were taken in the presence of DFHBI-1T, except the 1st panel in the lower row where the cells were incubated with DFHBI. DFHBI-1T provided a far brighter signal with excitement from the 488nm laser than DFHBI. (B) Bar chart of mean signal intensity after subtraction of mean fluorescence of uninfected cells (~25,000 cells/infection). The first and the second sorted viral clones improved the signal from TEds1x-3'UTR1xSpinach2 by 31% and 68%, respectively.

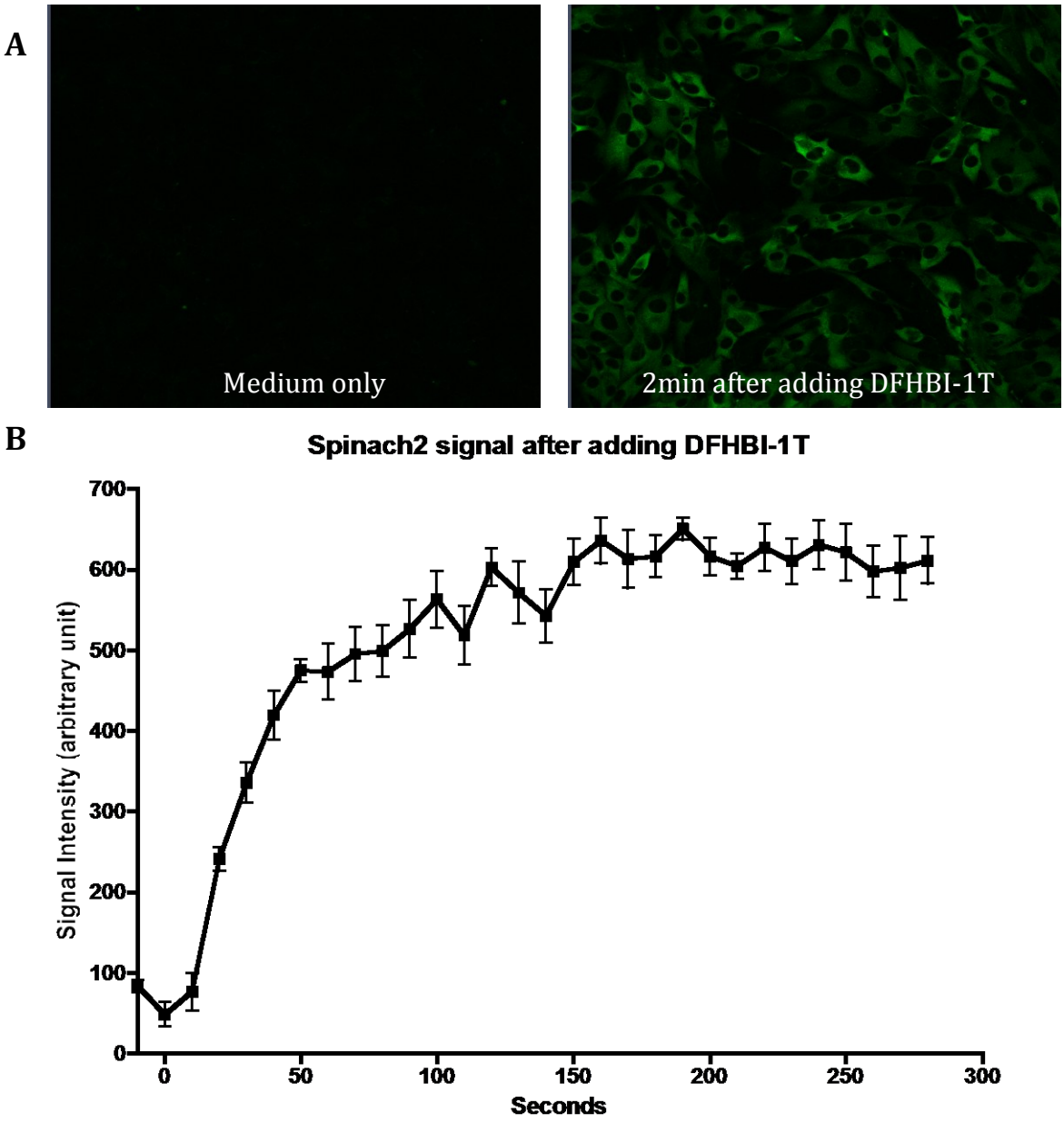

Figure 4.9 Permeability of the fluorophore. These pictures were taken before (left panel) and 2 minutes after (right panel) adding DFHBI-1T into the medium of TEds1x-3'UTR1xSpinach2-infected BHK cells (MOI 5, 20 hours post infection, objective lens 20x). After adding fluorophore at the 2nd frame of time lapse (10 seconds/frame), the signal came up almost immediately and reached its plateau within few minutes.

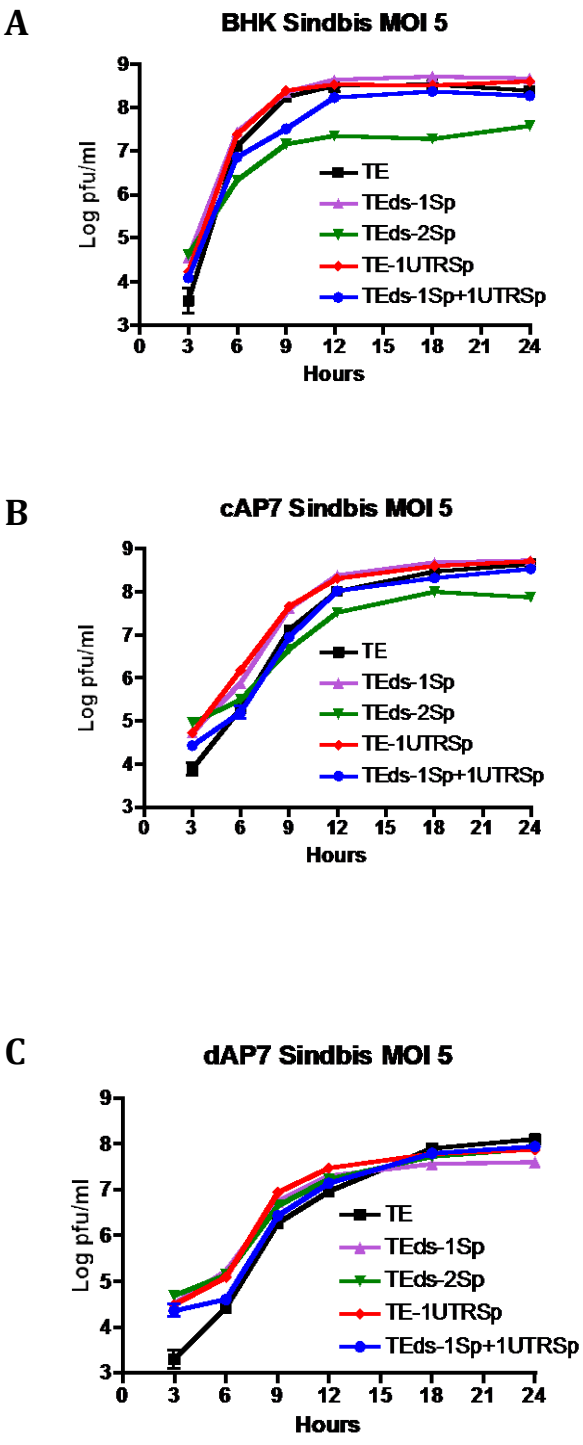

Figure 4.10 One-step viral growth curve. The growth curve showed lower infectious virions in supernatant from TEds2xSpinach2 (green)-infected cells than the others in both BHK and cAP7, but not daP7 cells.

A

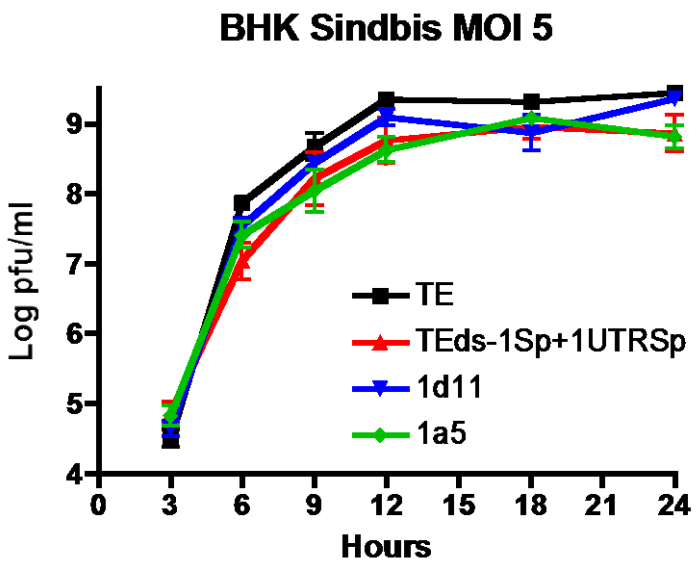
BHK Sindbis MOI 5
Log pfu/ml
Hours
TE
TEds-1Sp+1UTRSp
1d11
1a5

B

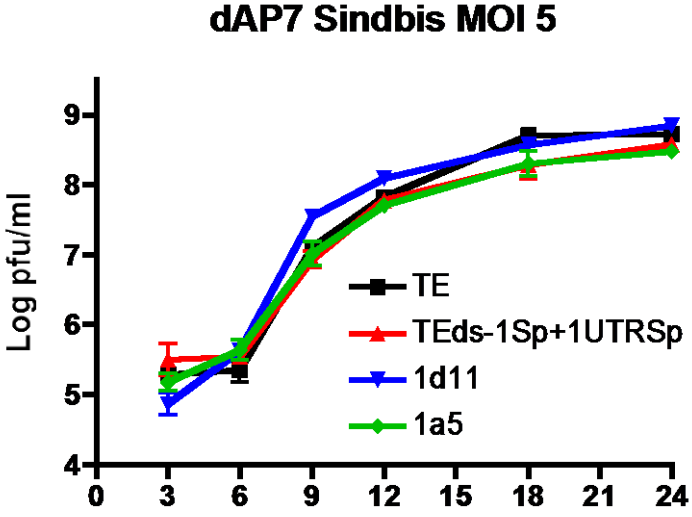
dAP7 Sindbis MOI 5
Log pfu/ml
TE
TEds-1Sp+1UTRSp
1d11
1a5

C

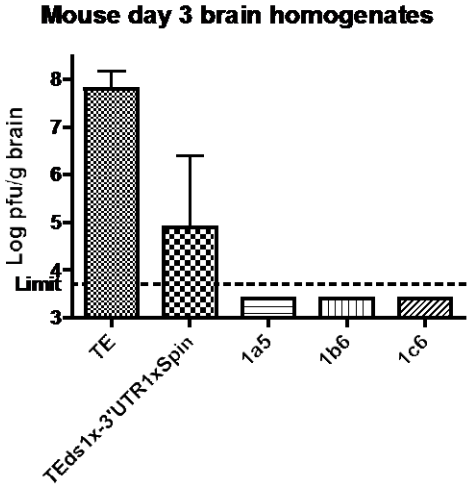
Mouse day 3 brain homogenates
Log pfu/g brain
Limit
TE
TEds1x-3'UTR1xSpin
1a5
1b6
1c6

Figure 4.11 Attenuation of the sorted viral clones occurs *in vivo* not *in vitro*. The brighter 1d11 and 1a5 from 1st and 2nd sorting had the comparable amount of virions in one-step viral growth to their parent, TEds-1Sp+1UTRSp, and the original TE strain in both BHK and dAP7 cells (MOI 5). However, at day 3 (the peak of viral replication in mouse brains), there was no detectable infectious virion from brain homogenate infected with 1a5, 1b6, and 1c6 from the 2nd sorting, while the original TEds-1Sp+1UTRSp exhibited much lower amount than TE.

A

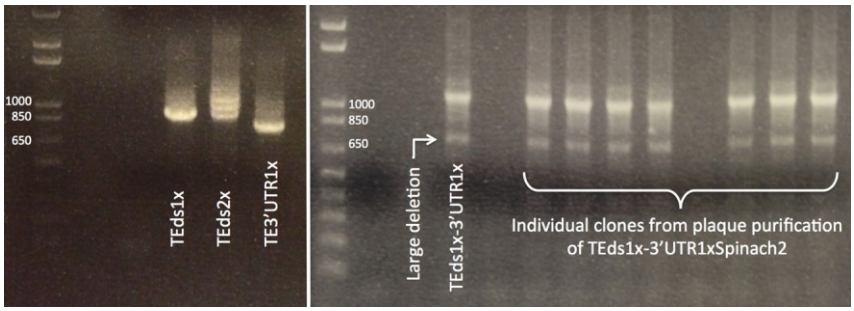

B

Point mutations in TEds1x-3'UTR1xSpinach2 (Underlined sequence is the large deletion, 341 bases.)

ATAGTACTTCTAGAGATCTGCAGGTCGACGGATCCCCCGAGATTTTCAGGAGCTAAGGAAGCTAAAGGTCACCGCCCGGA

TAGCTCAGTCGGTAGAGCAGCGGCCGGATGTAACTGAATGAAATGGTGAAGGACGGGTCCAGTAGGCTGCTTCGGCAGCC

A sub in 1b6

TACTTGTTGAGTAGAGTGTGAGCTCCGTAACTAGTTACATCCGGCCGCGGGTCCAGGGTTCAAGTCCCTGTTCGGGCGCC

A add in 2c9 Del in 1d11, 1a5, 1b6

AGGTCACCTGACCGCTACGCCCCAATGATCCGACCAGCAAAACTCGATGTACTTCCGAGGAACTGATGTGCATAATGCAT

CAGGCTGGTACATTAGATCCCCGCTTACCGCGGGCAATATAGCAACACTAAAAACTCGATGTACTTCCGAGGAAGCGCAG

T sub in 1c9

TGCATAATGCATGCGCCCGGATAGCTCAGTCGGTAGAGCAGCGGCCGGATGTAACTGAATGAAATGGTGAAGGACGGGTC

Del in 2c9

CAGTAGGCTGCTTCGGCAGCCTACTTGTTGAGTAGAGTGTGAGCTCCGTAACTAGTTACATCCGGCCGCGGGTCCAGGGT

TCAAGTCCCTGTTCGGGCGCCAGCATGCGCAGTGTTGCCACATAACCACTATATTAACCATTTATCTAGCGGACGCCAAA

AACTCAATGTATTTCTGAGGAAGCGTGGTGCATAATGCCACGCAGCGTCTGCATAACTTTTATTATTTCTTTTATTAATC

AACAAAATTTTGTTTTTAACATTTC

Figure 4.12 Gel electrophoresis shows unstable viral clones. (A) RT-PCR of RNA extracted from supernatant fluids of transfected or infected BHK cells showed 3 bands in TEds-2Sp PCR product (left panel). The largest band was the correct size, while the smallest band was the same size as TEds-1Sp. The TEds-1Sp+1UTRSp PCR product had 2 bands (right panel). The larger was the correct size, while the smaller had a large deletion. All clones from the plaque purification had RNAs the same deletion. (B) Sequences from the RNA extracts of the viruses in the supernatant fluids of BHK cells infected with TEds-1Sp+1UTRSp or its sorted clones, starting from 2nd subgenomic start to the last base before poly-A showed various point mutations in the sorted viruses (1st sorting – 1c9, 1d11, 2c9; 2nd sorting – 1a5, 1b6). The sequence deleted from the smaller band shown in the gel electrophoresis is underlined. (Green characters – restriction sites, bold characters – tRNA scaffolds, red characters – Spinach2)

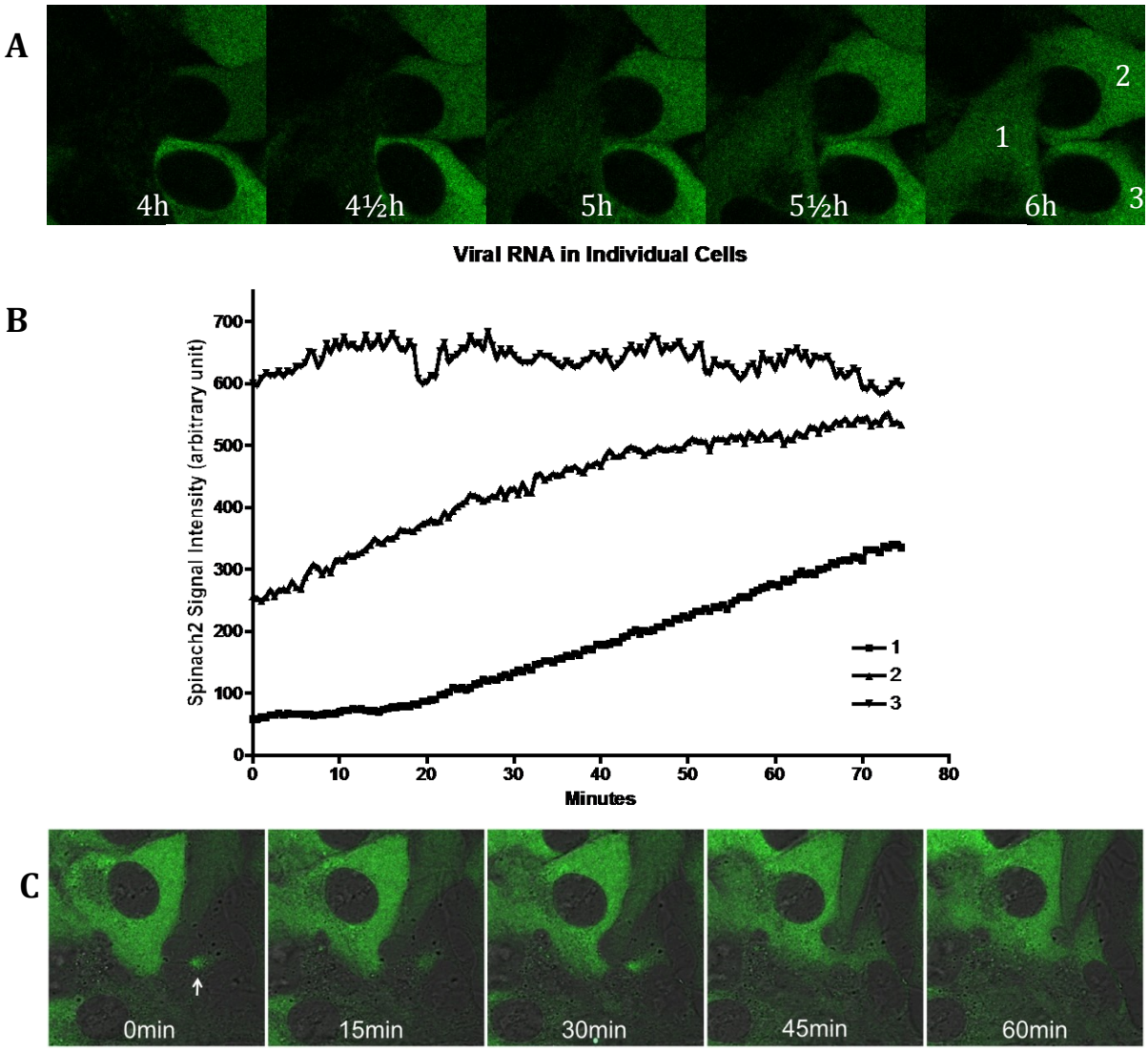

Figure 4.13 Viral RNA dynamics and cell-to-cell viral transmission. The time course of viral RNA replication differed from cell to cell. Spinach2 signals from 3 cells (A) were plotted against time. In the same time frame, viral replication had just begun, been in the middle, and reached the plateau in cell number 1, 2, and 3, respectively. Viral RNA was concentrated at the filopodial tip (white arrow) of an infected BHK cell at 4h (B). The tip adheres to the adjacent uninfected cell. The viral RNA was first detected in and then spread away from the adhesion site. (Time lapse imaging from 4 h after infection, MOI 20, objective lens 63x, 30 seconds/frame)

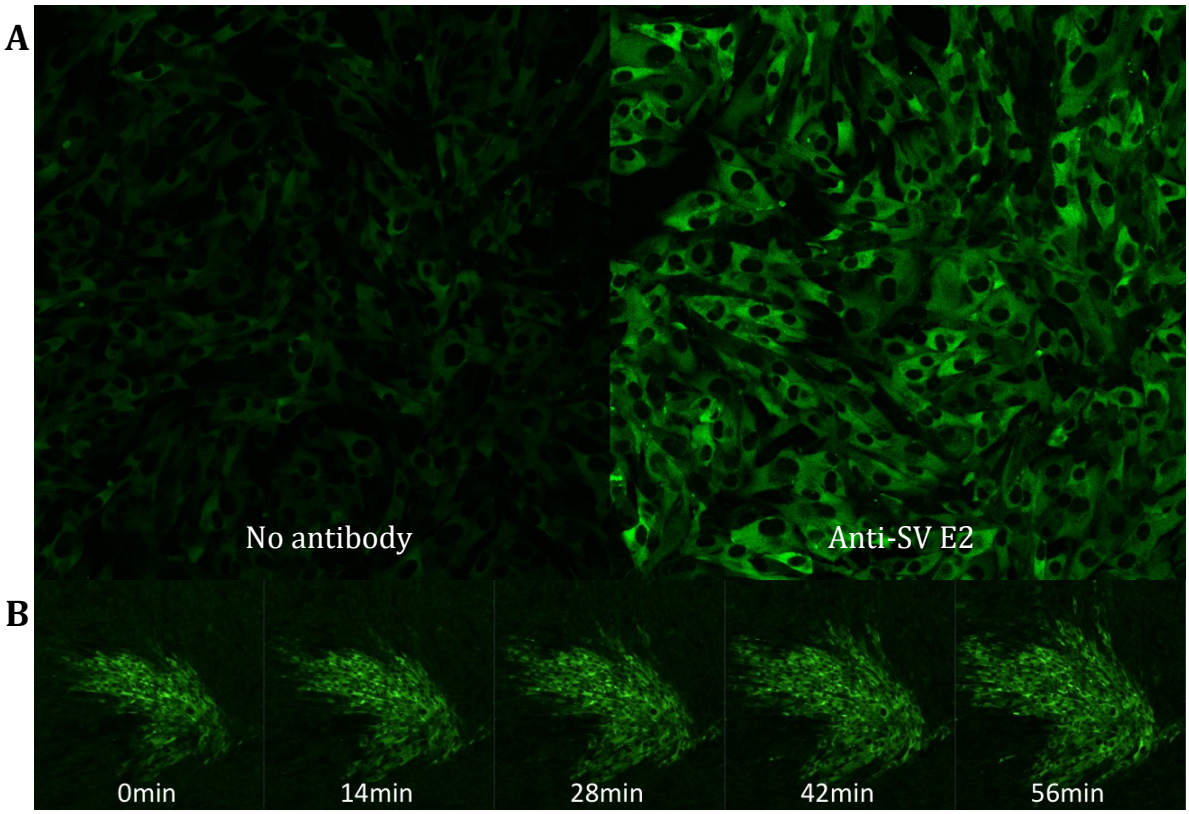

Figure 4.14 Anti-E2 antibody increases intracellular viral RNA and fails to inhibit cell-to-cell transmission in BHK cells. At 6 h after infection of BHK cells (TEds-1Sp+1UTRSp, MOI 5), more spinach2 signal was observed when treated (A, right panel) with anti-SV E2 (clone SV127, 1μg/ml) at 2 h after infection than untreated (A, left panel). When cells were infected at a low MOI (0.01), antibody failed to inhibit spread of virus to the adjacent cells as shown in time-lapse imaging (B) started at 24 h after infection. (objective lens 20x)

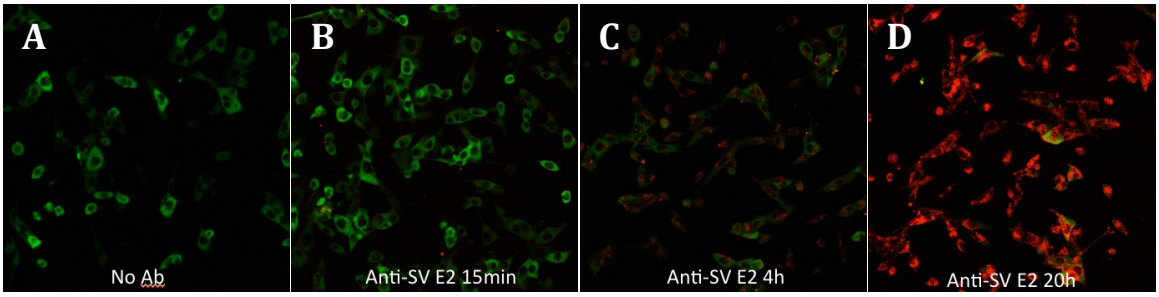

Figure 4.15 Anti-E2 antibody clears intracellular viral RNA in undifferentiated neuronal cells. RNA in cAP7 cells infected with TEds-1Sp+1UTRSp (MOI=5) was imaged 20h after infection (green). Treatment with Dylight594-conjugated anti-SINV E2 (red) at 1μg/ml decreased viral RNA within 4 h after treatment (16-20 hours post infection) (C). The effect of antibody on viral RNA was greater when treated 2 h after infection (D). (objective lens 20x)

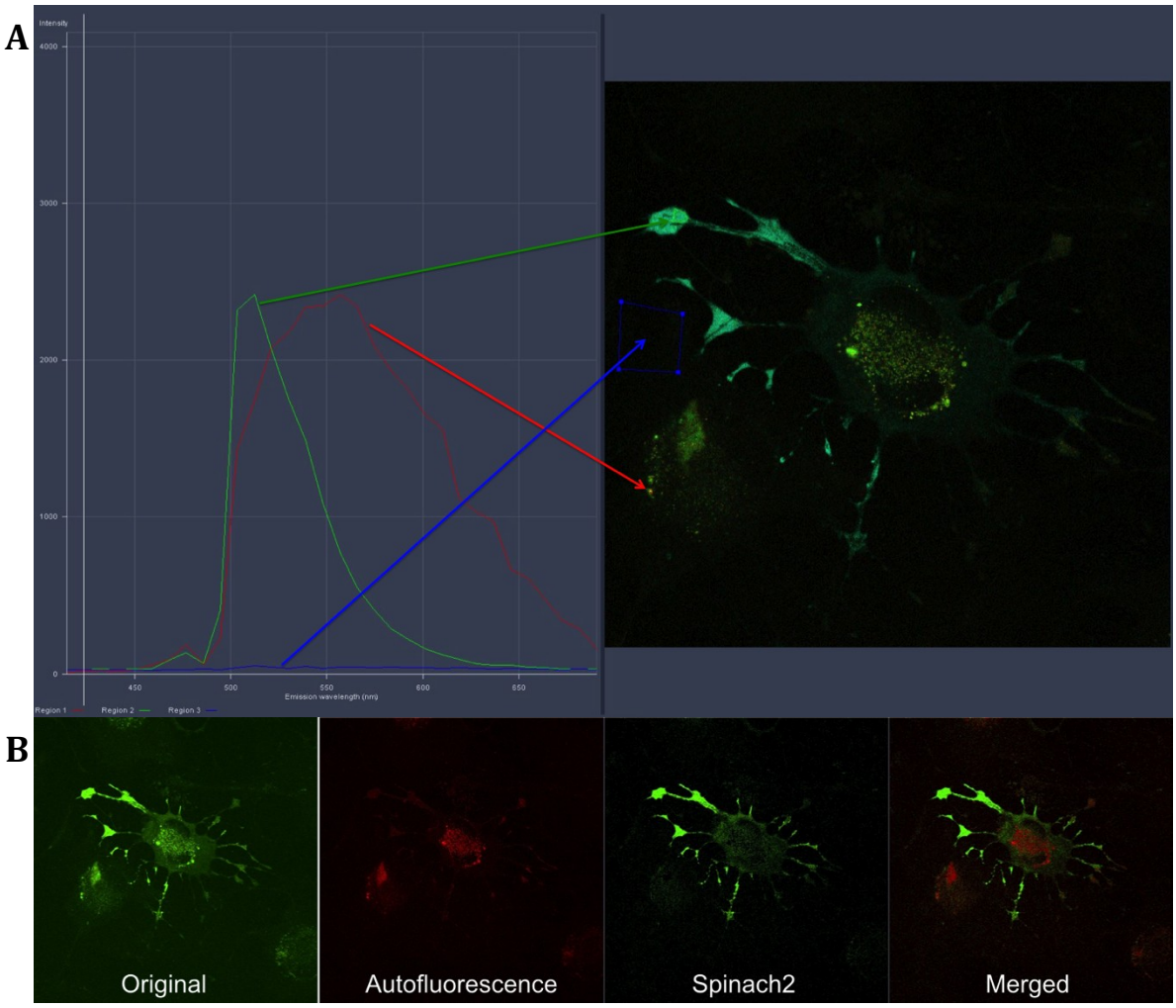

Figure 4.16 Spectral imaging can differentiate dim Spinach2 signal from high autofluorescence in differentiated neuronal cells. In dAP7 cells, dim Spinach2 signal overlapped with high autofluorescence in the usual channel mode (B, 1st panel). The lambda mode (A), which recorded the emission spectra, showed the difference between Spinach2 signal (green), autofluorescence (yellow), and background (blue). Linear unmixing (B, 2nd to 4th panels) separated the signal into 2 channels, Spinach2 represented by green color and autofluorescence represented by red color. Viral RNA was prominent in the dendritic-like process, while autofluorescence was mainly found in perinuclear granules.

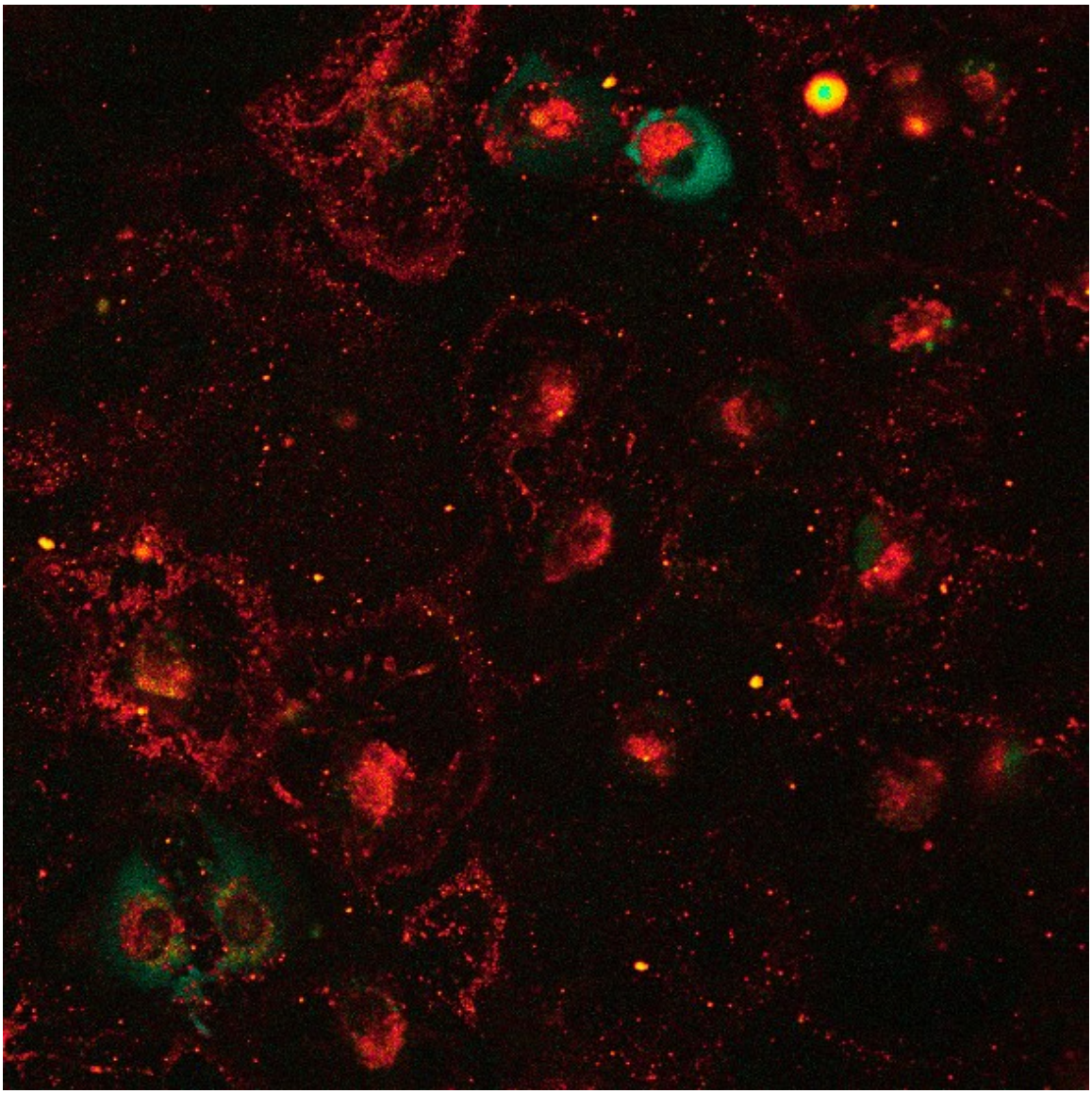

Figure 4.17 Antibody-mediated viral RNA clearance in dAP7 cells is associated with antibody binding to the cell membrane. dAP7 cells infected with TEds-1Sp+1UTRSp, MOI 5, were treated with 1μg/ml of Dylight594-conjugated anti-SV E2 (clone SV127) at 2 hours post infection. This picture (20 hours post infection, objective lens 63x, lambda mode) showed the amount of viral RNA (Spinach2 in green) was reversely correlated with the amount of the antibody (red) that bound to the cell membrane.

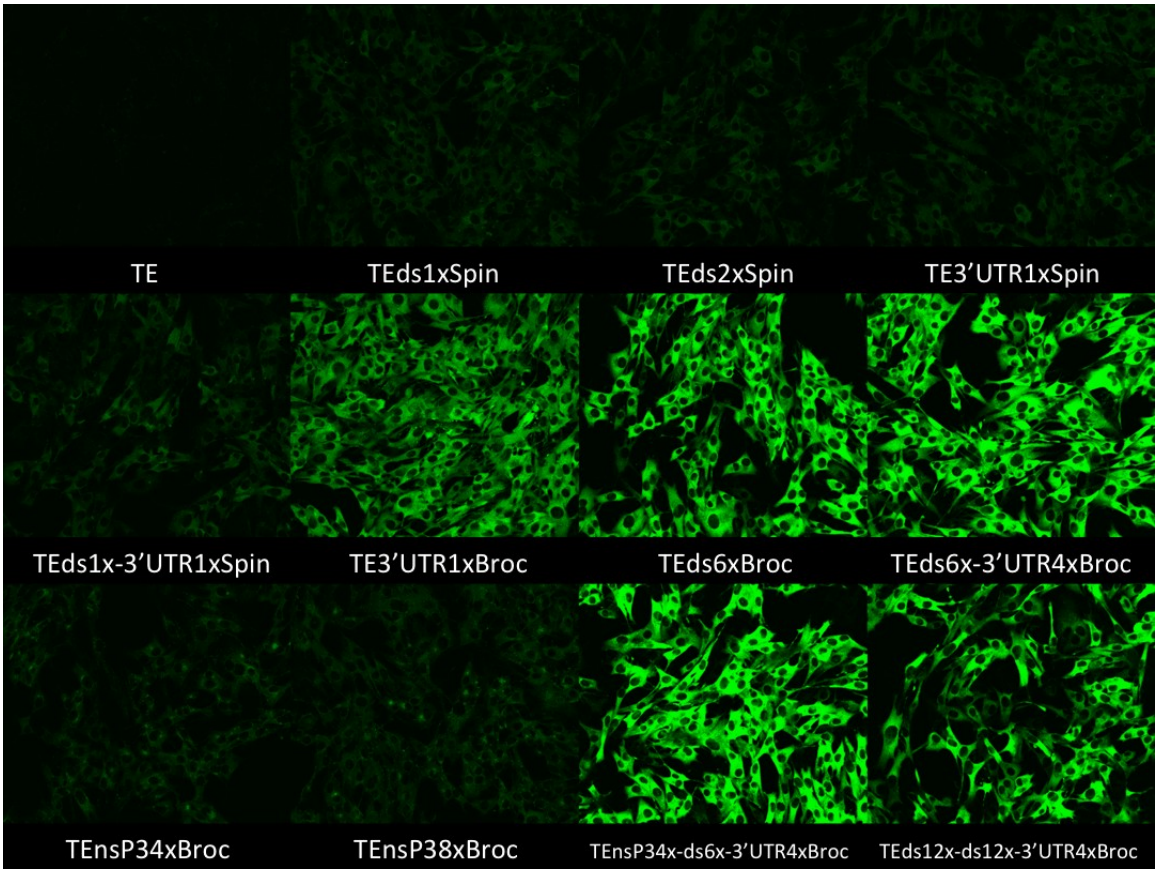

Figure 4.18 Signal intensities of all constructed viruses. The live-cell images (objective lens 20x) compare signal intensities of all viral constructs after adding DFHBI-1T to the infected BHK cells (MOI = 5, 6 hours post infection).

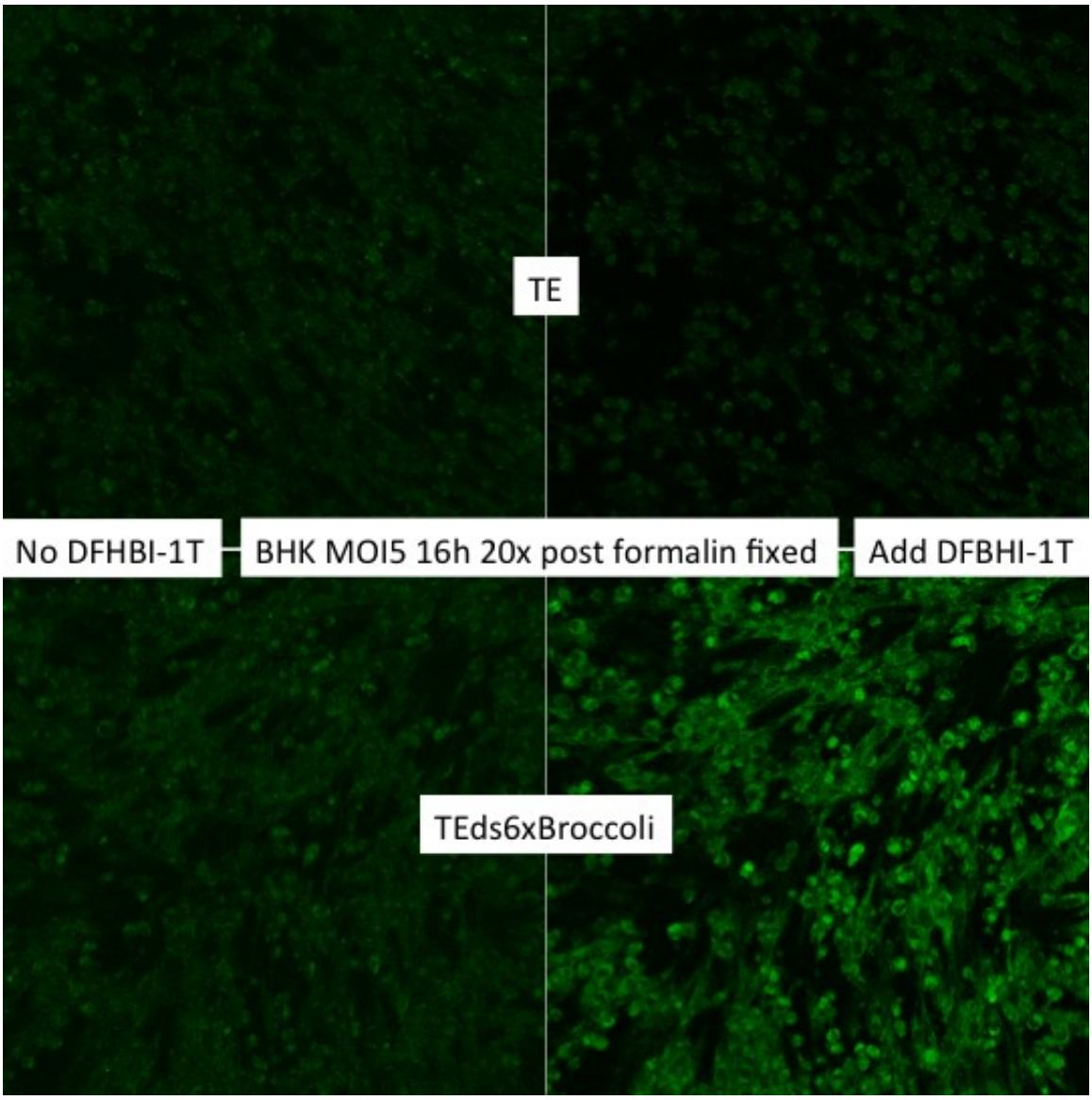

Figure 4.19 The effect of formaldehyde fixation on Broccoli signal. The images (objective lens 20x) show infected BHK cells (MOI = 5), fixed with 3.7% formaldehyde at 16 hours post infection. After adding DFHBI-1T, there is still Broccoli signal in the cells, infected with TEds6Br.

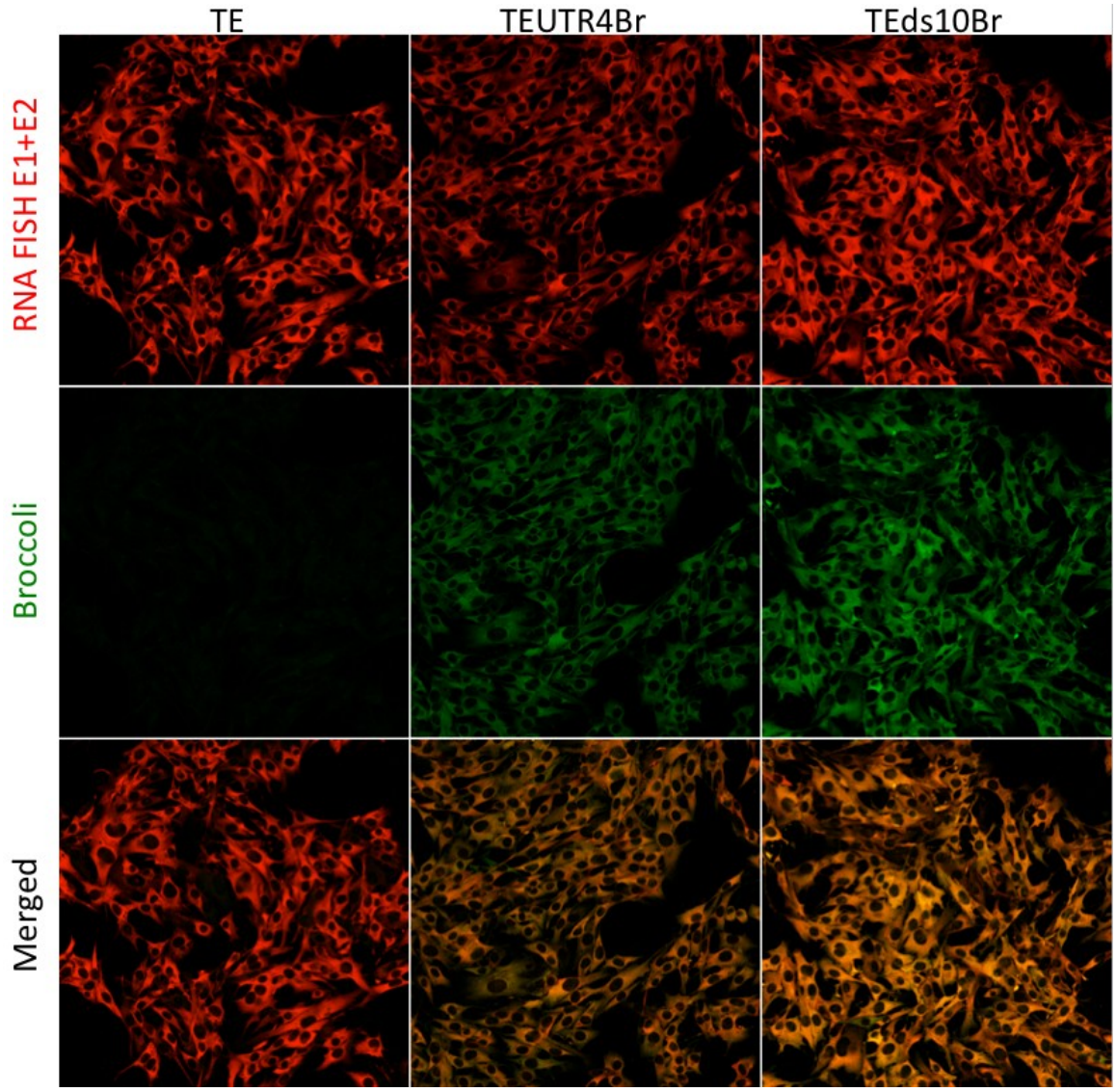

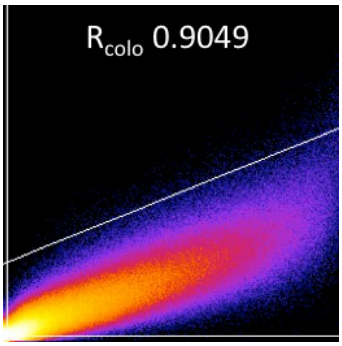

Figure 4.20 Colocalization between SINV RNA FISH and Broccoli. The images (objective lens 20x) show infected BHK cells (MOI = 5), fixed with 3.7% formaldehyde in PBS at 6 hours post infection. After adding DFHBI-1T, RNA FISH E1+E2 (red) colocalizes well with Broccoli-DFHBI-1T (green) signal in both TEUTR4Br and TEds10Br. The scatter plot (X – red, Y – green) shows strong colocalization ($R_{colocalization}$ = 0.9049).

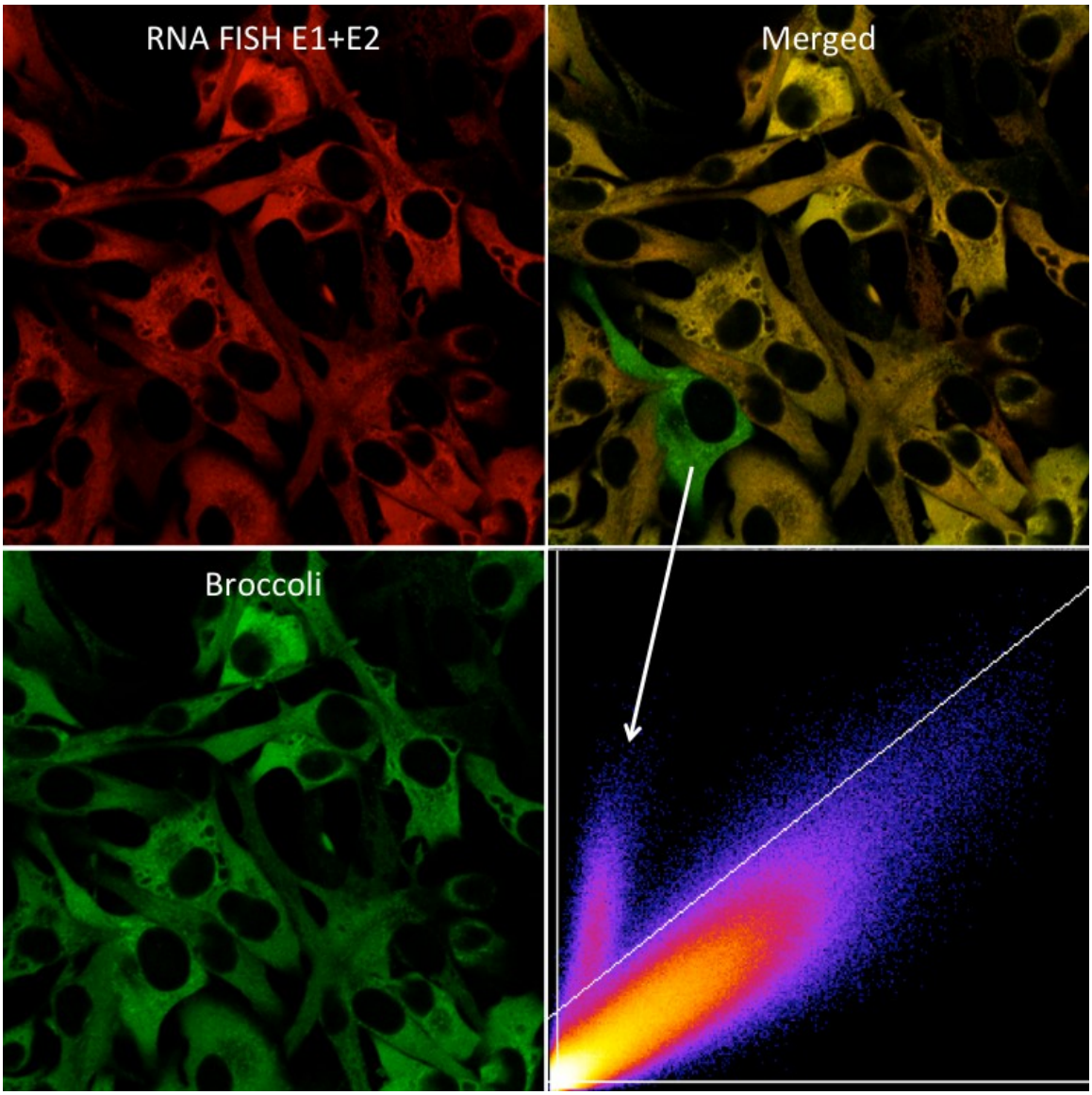

Figure 4.21 Rare discrepancy between RNA FISH and Broccoli. The images (objective lens 63x) show TEds10Br-infected BHK cells (MOI = 5), fixed with 3.7% formaldehyde in PBS at 6 hours post infection. Though very rarely, some cells may have discrepancy between FISH and Broccoli signal (white arrow), resulting in a separated cluster in the scatter plot (X – red, Y – green).

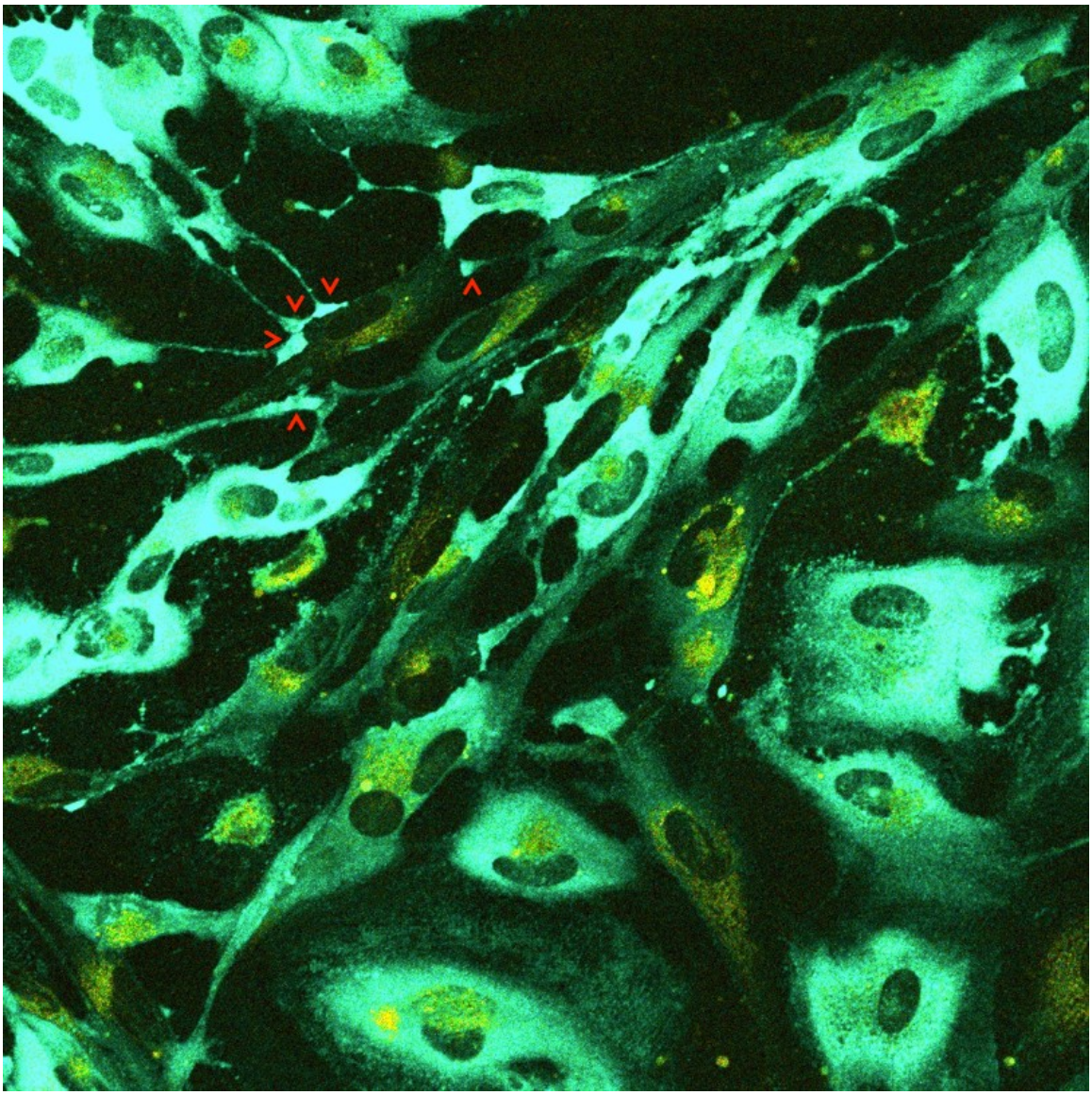

Figure 4.22 Accumulation of viral RNA in foot processes. Live-cell imaging (objective lens 20x) has been taken in lambda mode (spectral imaging). TEds10Br-infected dAP7 cells (MOI = 20, 24 hours post infection) accumulate viral RNA (green – Broccoli-DFHBI-1T) at their filopodial tips (red arrow heads), which adhere to the uninfected cell (only yellow – autofluorescence).

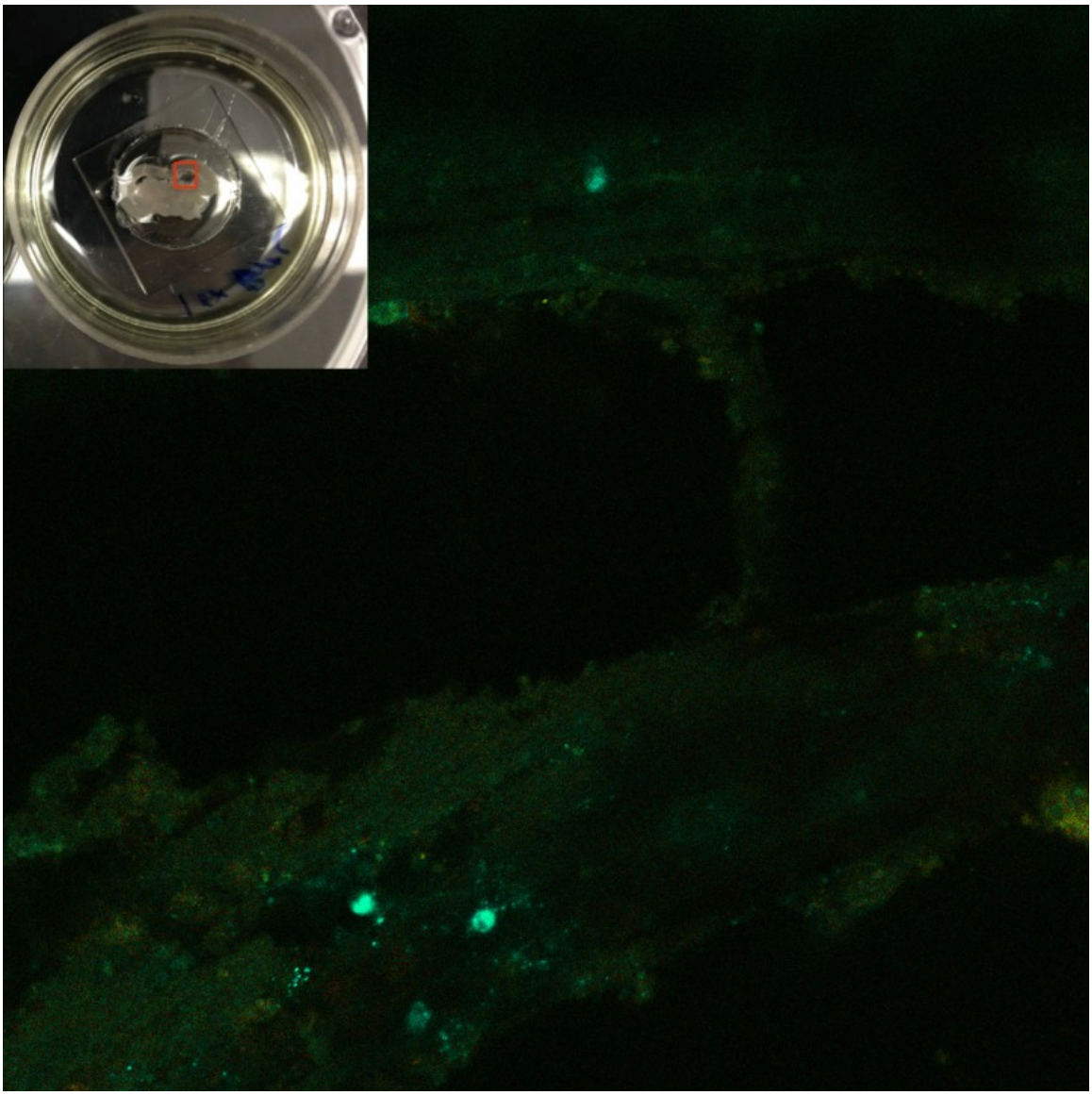

Figure 4.23 Live-cell imaging in the infected mouse brain slice. The small inlet shows the TEds10Br-infected mouse brain 250-µm slice (3 days post infection) on glass-bottom of a 35-mm dish in imaging medium (DFHBI-1T). Live-cell imaging of the red square area on the brain slice (objective lens 20x, lambda mode) shows Broccoli-DFHBI-1T signal (green) in some cells along corpus callosum.

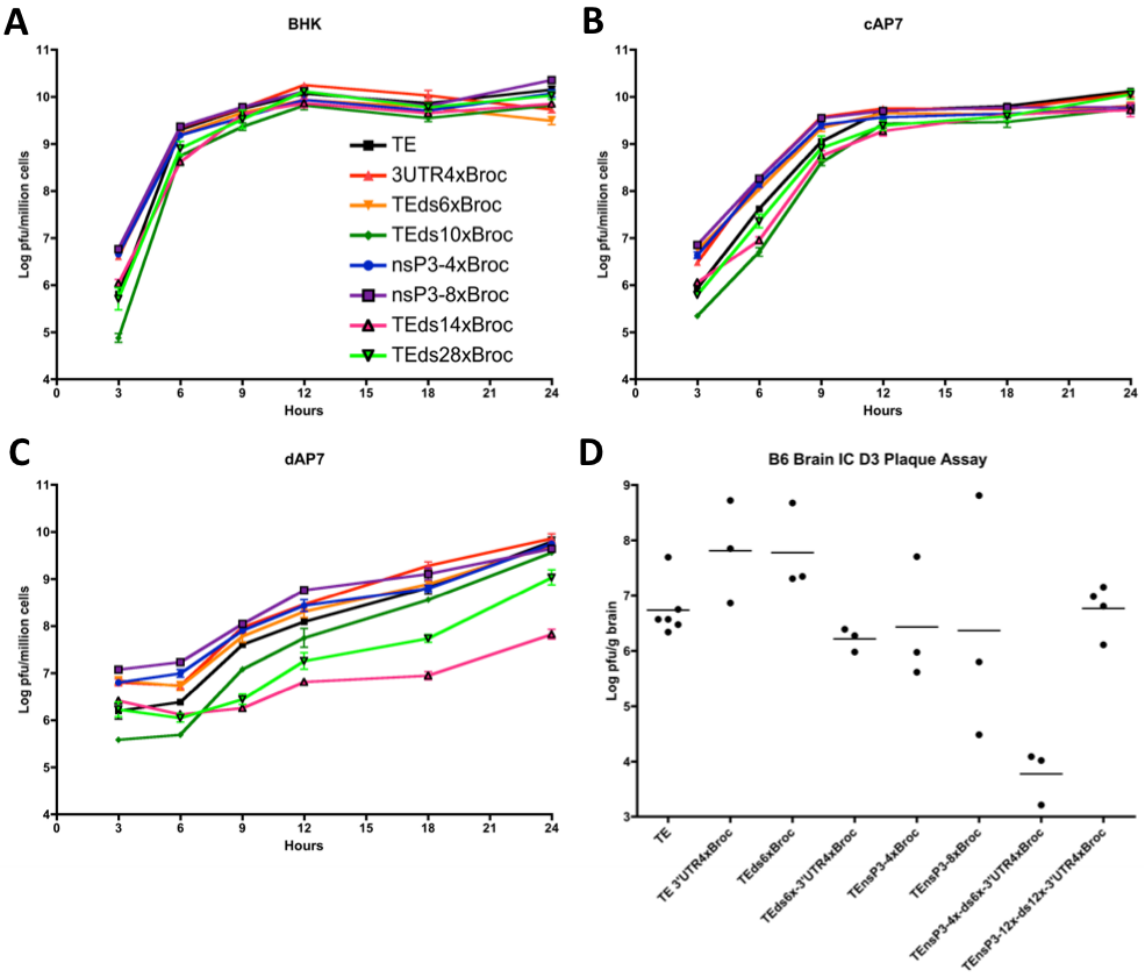

Figure 4.24 One-step growth curve of SINV-Broccoli. The graphs show the amount of infectious virus in the supernatant fluids from BHK (A), cAP7 (B), or dAP7 (C) cells infected with various SINV-Broccoli recombinant viruses (3 replicates per virus per time point). (D) Amount of infectious virus in brain homogenates from mice at day 3 post infection with various SINV-Broccoli recombinant viruses (3-6 mice per virus)

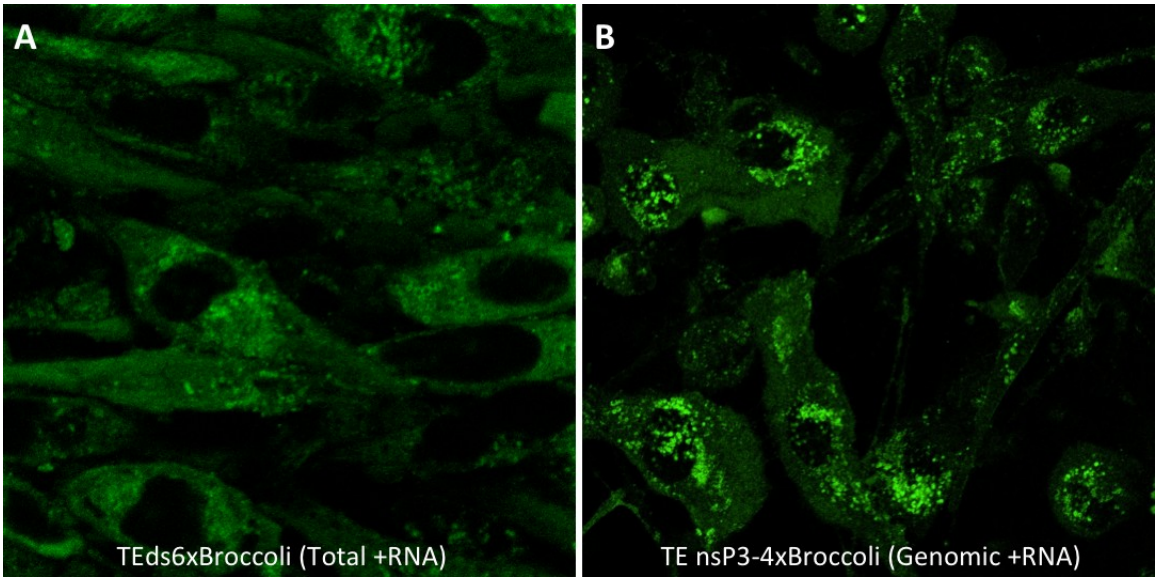

Figure 4.25 The distribution of SINV genomic and subgenomic RNA. Live-cell imaging (objective lens 63x) of infected BHK cells (MOI = 5, 16 hours post infection) shows more diffused distribution of viral RNA (green – Broccoli-DFHBI-1T) of TEds6Br (A), of which both genomic and subgenomic viral RNA are labeled with Broccoli. On the other hand, only genomic RNA is labeled with Broccoli in TEnsP3-4Br infection (B). SINV genomic RNA is accumulated in perinuclear area.

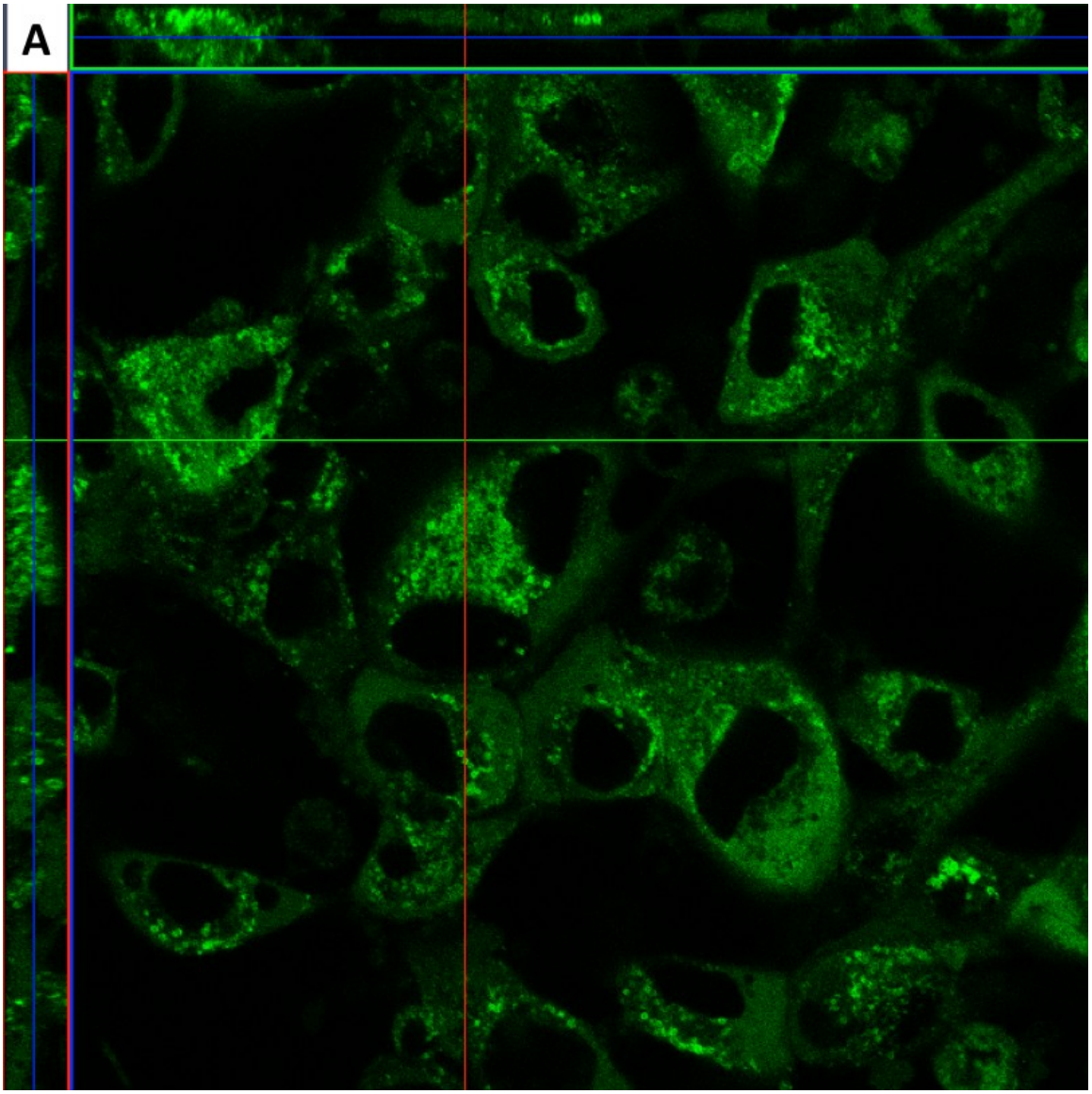

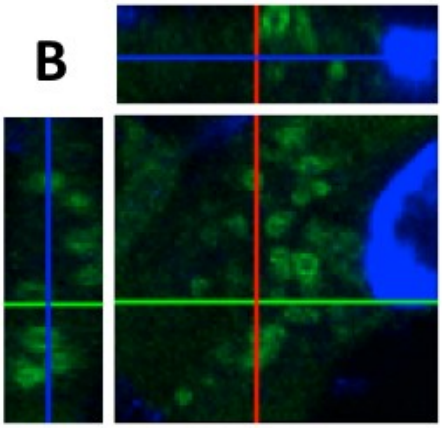

Figure 4.26 Vesicle-like arrangement of Sindbis viral genomic RNA. Live-cell imaging of TEds14Br-infected BHK cells (MOI = 5, 20 hours post infection) shows perinuclear vesicle-like arrangement of viral RNA (green – Broccoli-DFHBI-1T) in orthogonal view (A and B – zoom in).

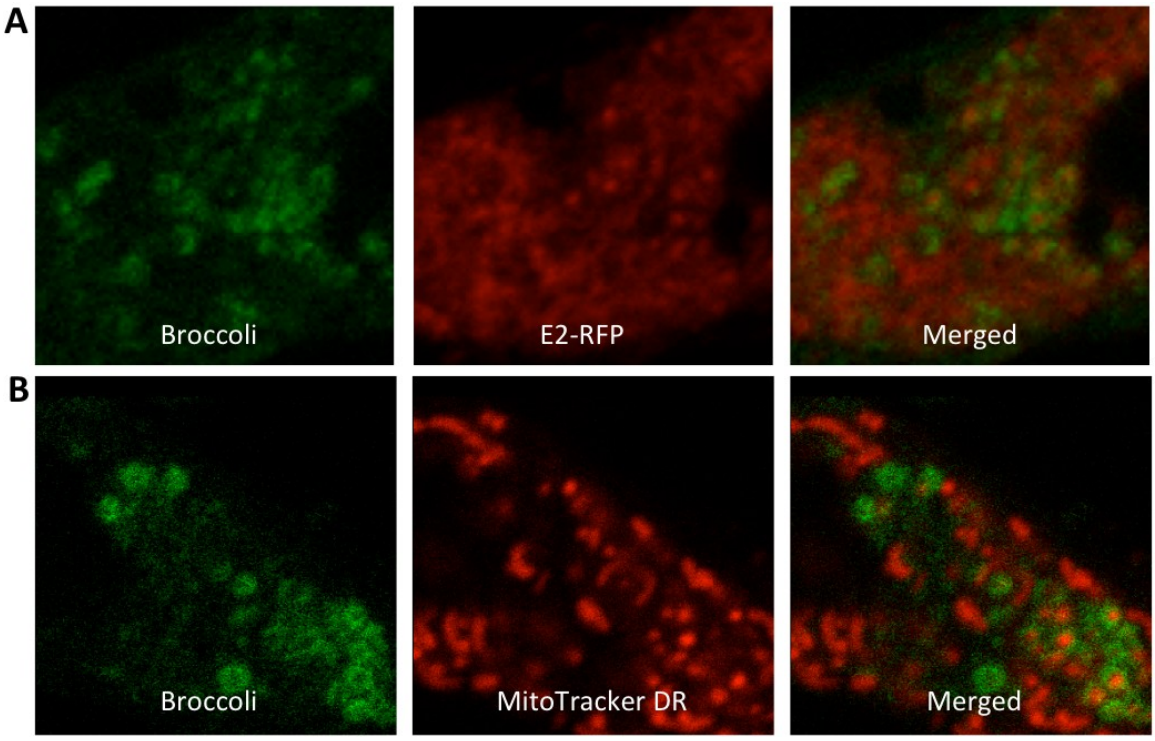

Figure 4.27 Genomic RNA-associated structures. Live-cell imaging (objective lens 63x) of TEds14Br-infected BHK cells (MOI = 5, 20 hours) shows the association between SINV genomic RNA, in vesicle-like arrangement, and SINV E2 protein (A) or mitochondria (B). A – Cells had been co-infected with the same amount of SINV TOTO E2-mCherry (a gift from Richard Kuhn, Purdue Institute for Inflammation, Immunology and Infectious Disease). B – Cells had been pre-labeled with MitoTracker DR 1 hour before infection.

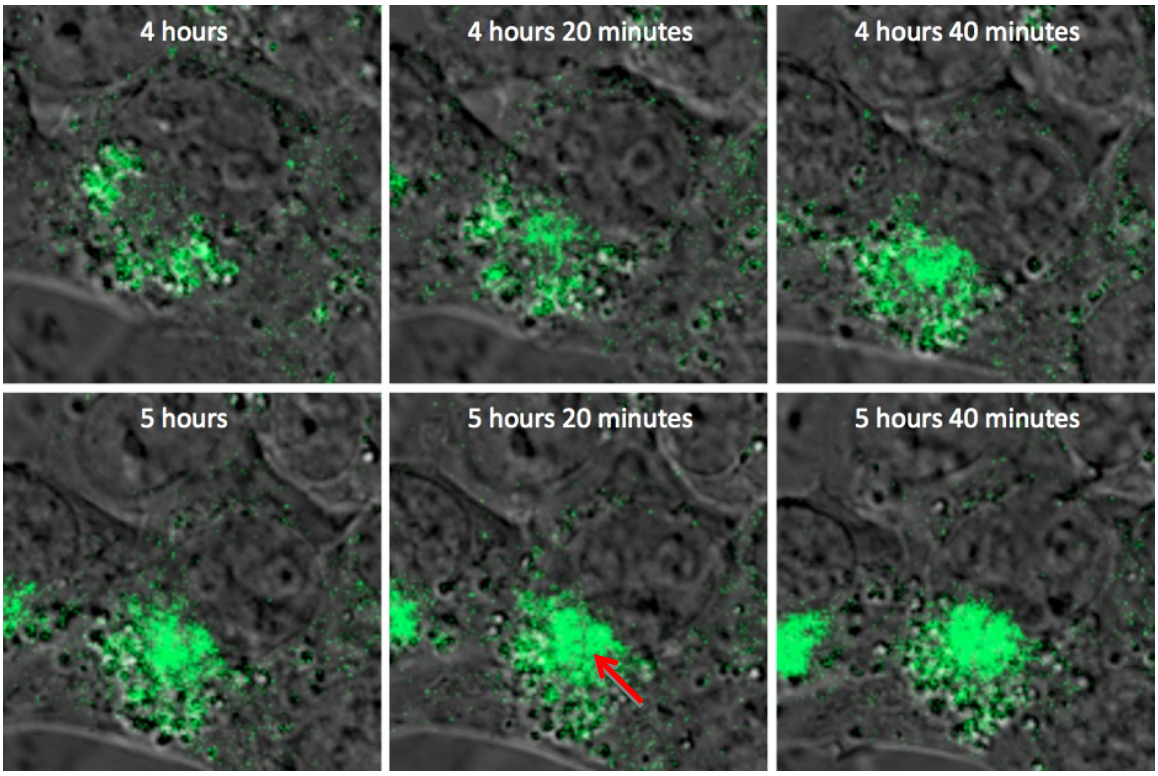

Figure 4.28 Accumulation of SINV genomic RNA at the perinuclear halo. Time-lapse live-cell imaging (objective lens 63x) of TEnsP3-8Br-infected BHK cells (MOI = 20, 4-6 hours post infection) shows genomic RNA-associated vesicles/vacuoles (green) surrounding the perinuclear halo (most likely the Golgi apparatus). Then the new genomic RNA is increasingly accumulated and formed vesicle-like arrangement (red arrow) in the perinuclear halo.

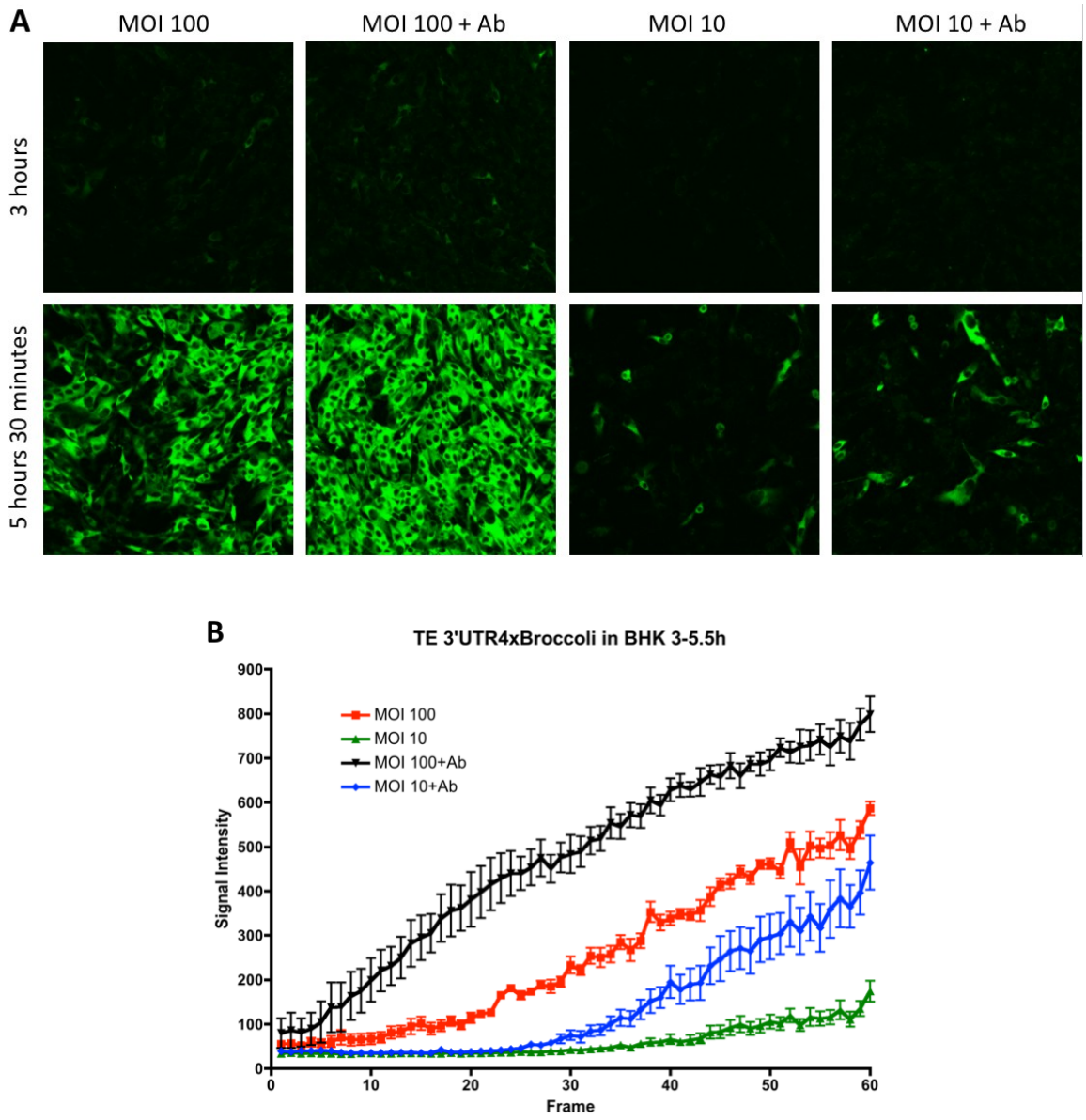

Figure 4.29 SINV RNA replication enhanced by higher MOI and antibody treatment. Time-lapse live-cell imaging (A, objective lens 20x) of TEUTR4Br-infected BHK cells (3-5.5 hours post infection) shows the effects of MOI (10 VS 100) and anti-E2 [SV127] antibody treatment (5 μg/ml at 2 hours post infection) on the replication rate of viral RNA (green). The graph (B) shows the average signal intensity of the 5 brightest cells from each group (1 frame = 150 seconds).

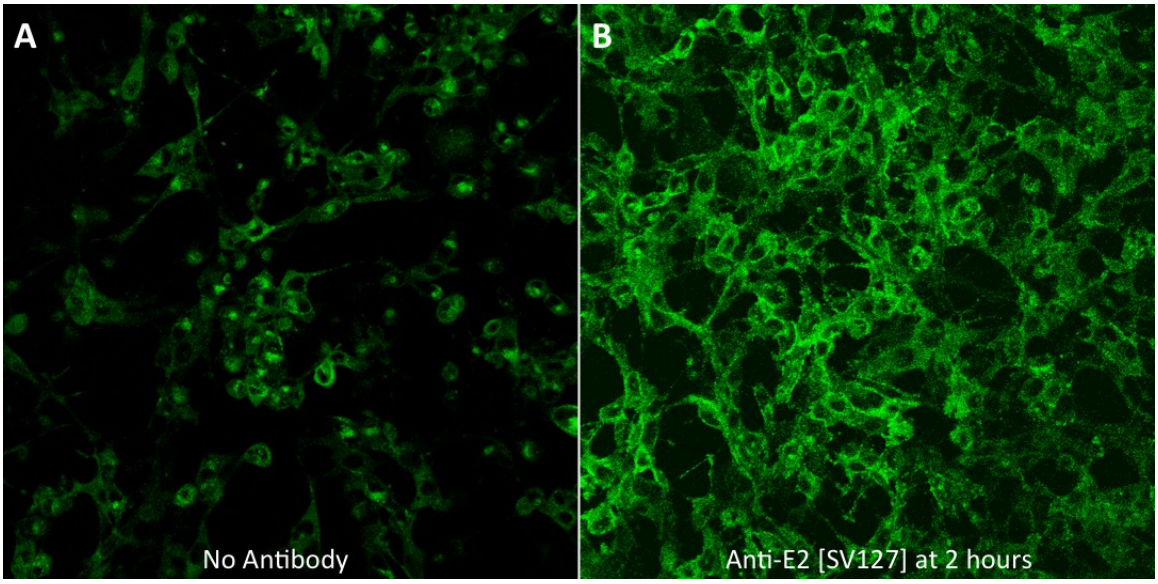

Figure 4.30 Effect of antibody on viral RNA distribution. Live-cells imaging (objective lens 20x) compares the effect of antibody treatment (B) to no treatment (A) in TEnsP3-4Br-infected BHK cells (MOI = 20, 12 hours post infection). Without antibody treatment (A), the viral genomic RNA (green) is mainly accumulated around perinuclear area. In contrast, the RNA is accumulated at the membrane of antibody-treated cells (B).

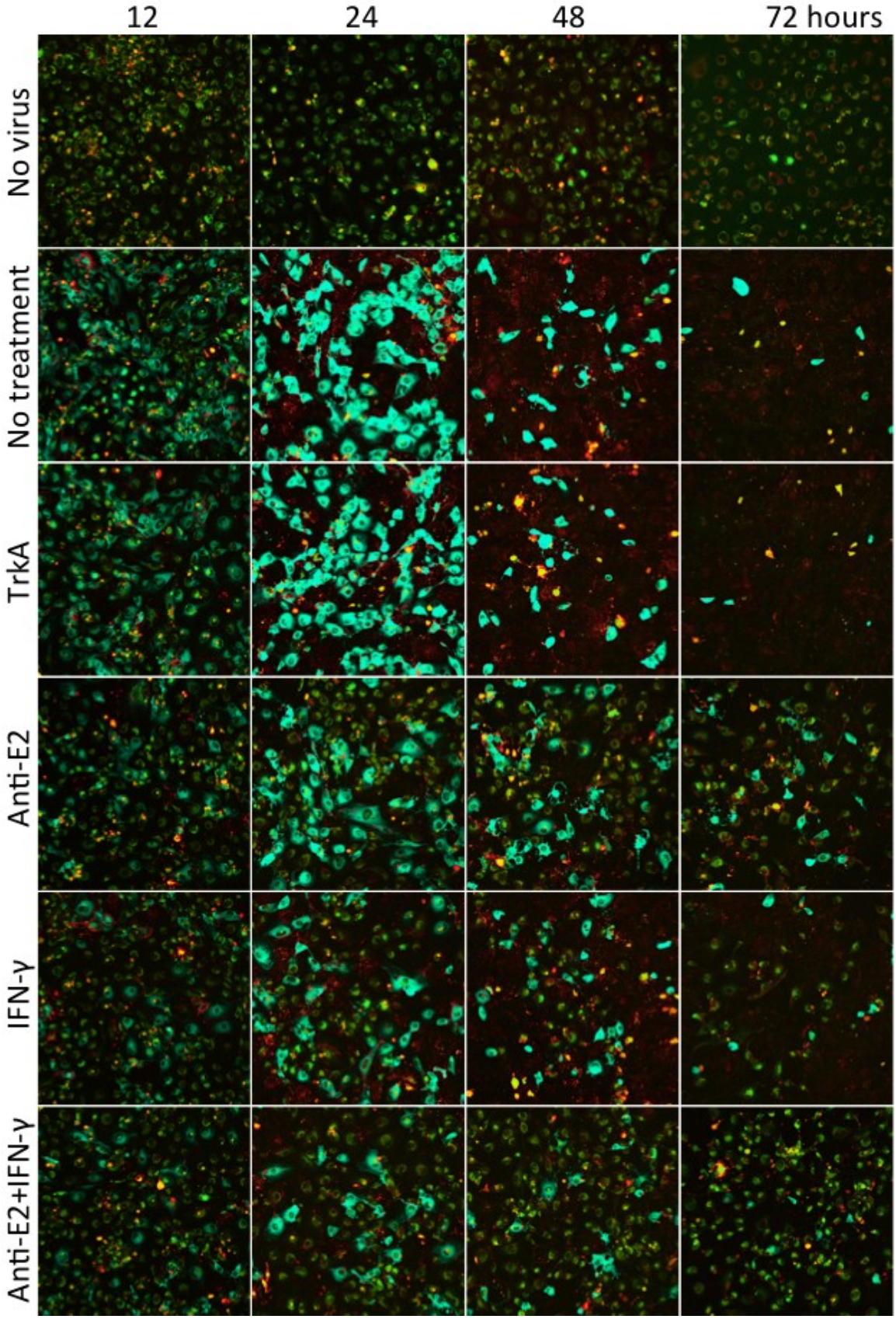
12
24
48
72 hours
No virus
No treatment
TrkA
Anti-E2
IFN-γ
Anti-E2+IFN-γ

Figure 4.31 Antibody- and IFN-γ-mediated SINV RNA clearance. Live-cell imaging (objective lens 20x, lambda mode) shows the effects of antibody and IFN-γ on viral RNA clearance in TEUTR4Br-infected dAP7 cells (MOI = 20) from 12 to 72 hours post infection (yellow – autofluorescence, green – Broccoli-DFHBI-1T, red – propidium iodide (dead cells)) . All treatments were applied at 2 hours post infection (TrkA control Ab 5 μg/ml, Anti-E2 [SV127] 5 μg/ml, rat IFN-γ 500 u/ml). The viral RNA begins to decrease at 24 hours. At 72 hours, viral RNA is mostly cleared, especially in the combined antibody-IFN-γ treatment. In contrast, most of the cells are dead and detached from the plate in no treatment and control antibody (TrkA) treatment groups.

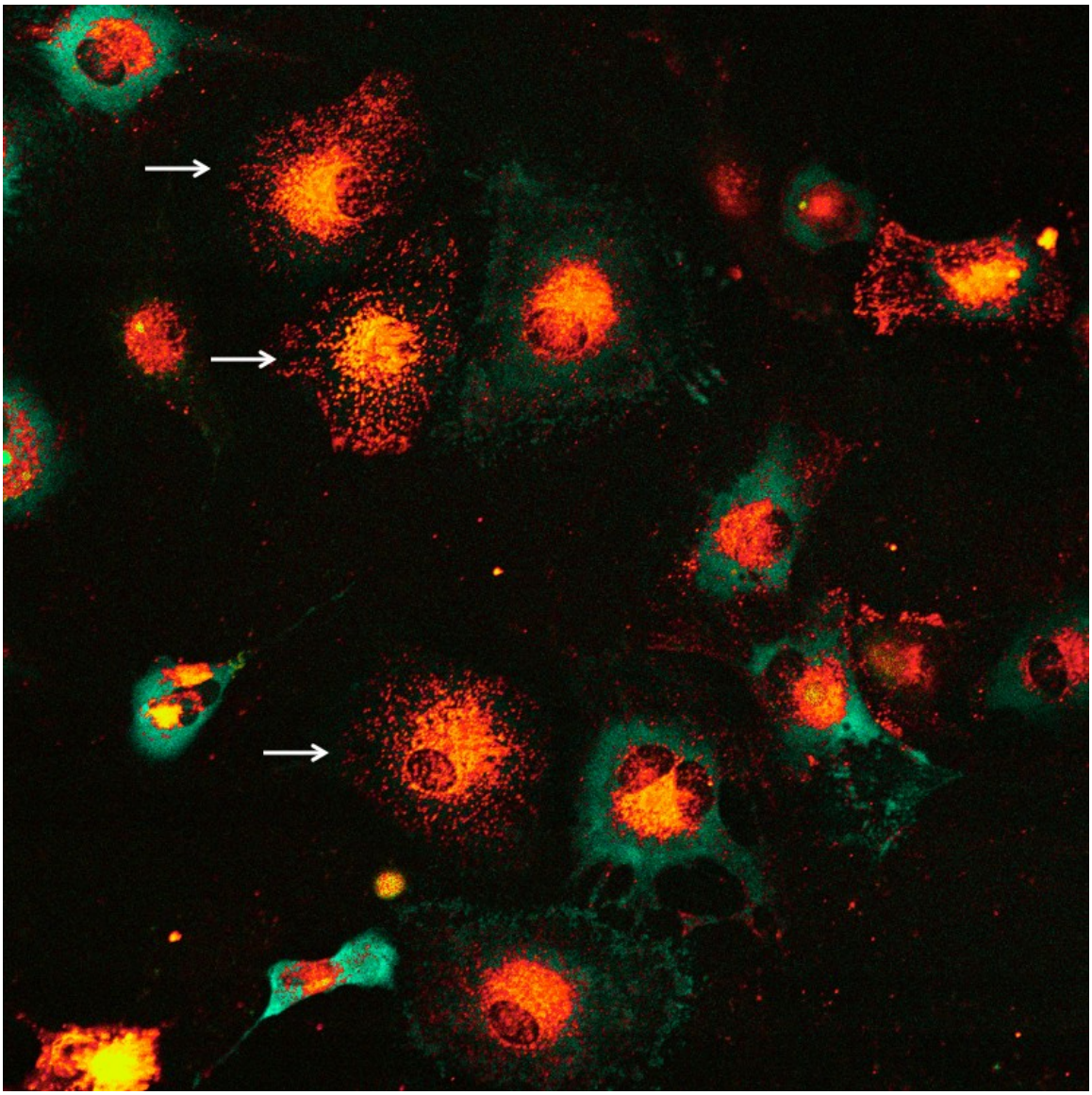

Figure 4.32 Inverse correlation between the amount of intracellular viral RNA and antibody on the cell membrane. Live-cell imaging (objective lens 20x, lambda mode) shows the amount of viral RNA (green) in TEUTR4Br-infected dAP7 (MOI = 20, 24 hours post infection), treated with 1 μg/ml of SV127-Dylight594 at 2 hours post infection. The cells that have antibody (red) bound to their membranes (white arrows) can clear the viral RNA, while the cells that lack antibody on their membrane cannot.

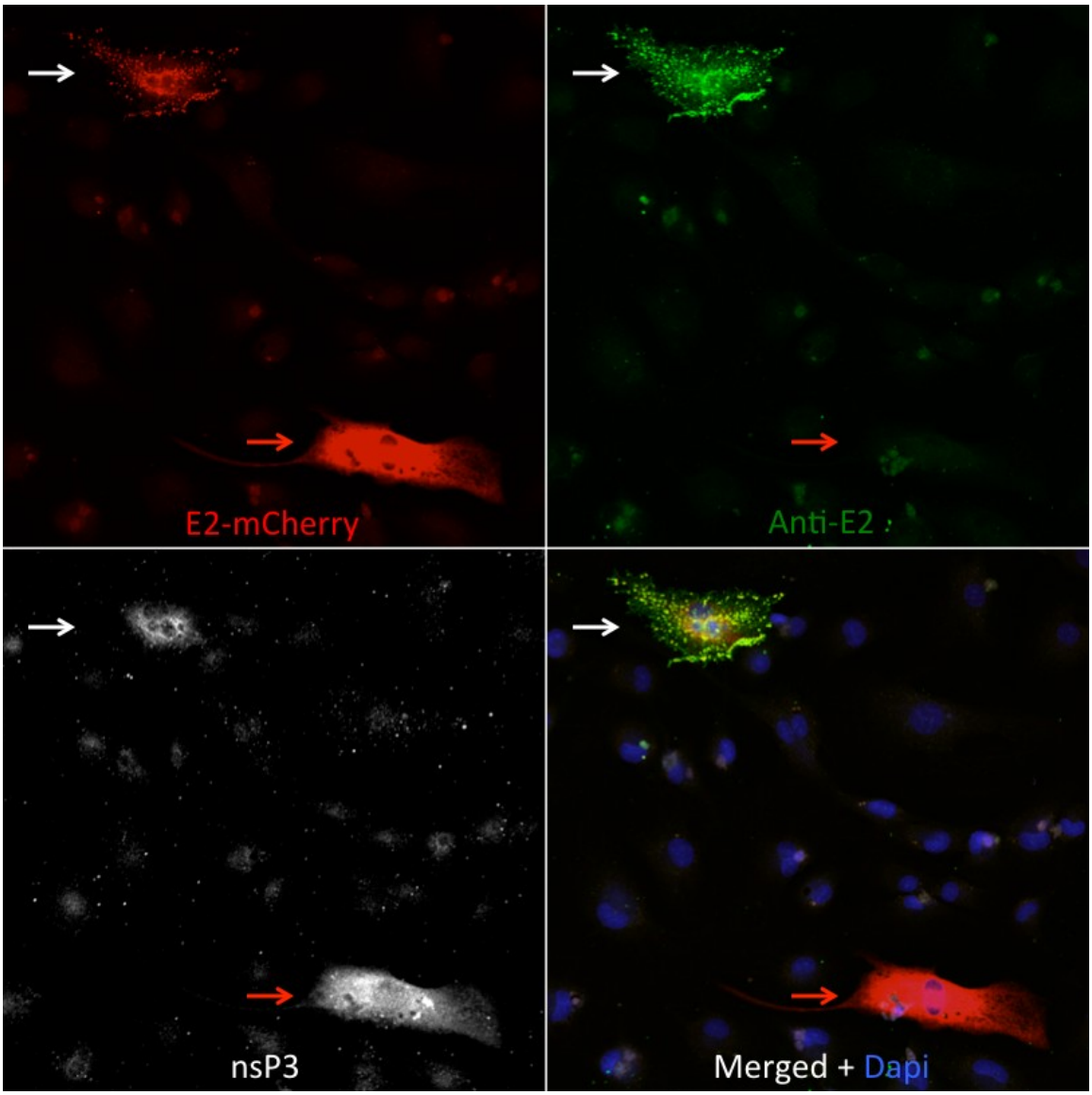

Figure 4.33 Lack of envelope protein on the surface of some SINV-infected cells. dAP7 cells infected with SINV TOTO E2-mCherry (MOI = 20), followed by anti-E2 [SV127, 5 μg/ml] treatment at 2 hours post infection, were fixed with 3.7% formaldehyde at 24 hours. Being stained with anti-mouse IgG (green), E2 protein (red) appears on the membrane of the cell that antibody (green) can bind (white arrows). In contrast, antibody cannot bind another cell that has only intracellular E2 (red arrows).

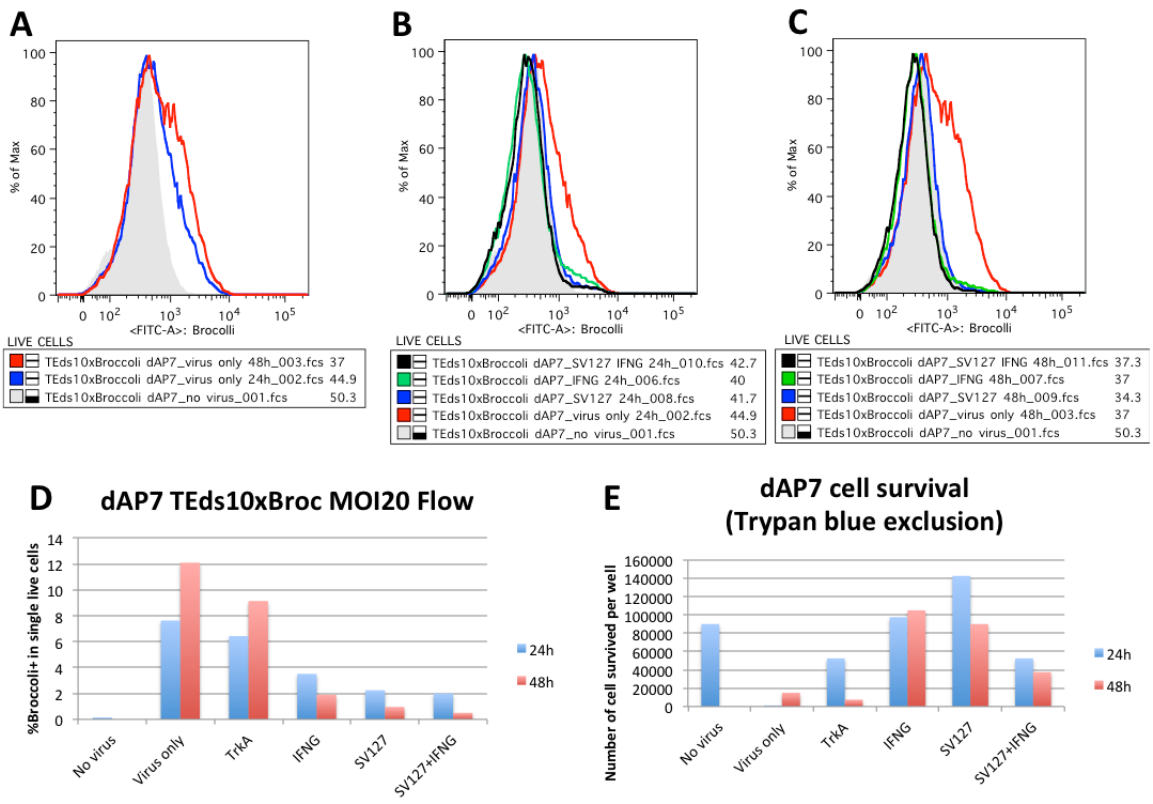

Figure 4.34 The effects of antibody and IFN-γ on viral clearance and cell survival in dAP7 cells. The flow cytometry histograms show the Broccoli-DFHBI-1T signal in dAP7 cells, infected with TEds10Br (MOI = 20). A – the signal intensity of infected cells at 24 (blue) and 48 (red) hours after infection still overlaps with autofluorescence (gray). The numbers of Broccoli+ cells at 24 hours (B) and 48 hours (C) after treatment with or without antibody and IFN-γ at 2 hours post infection are summarized as a bar chart (D), showing that both antibody and IFN-γ can mediated viral RNA clearance. E – a bar chart shows the effect of treatments on cell survival. Both SV127 and IFN-γ improve survival in dAP7 cells.

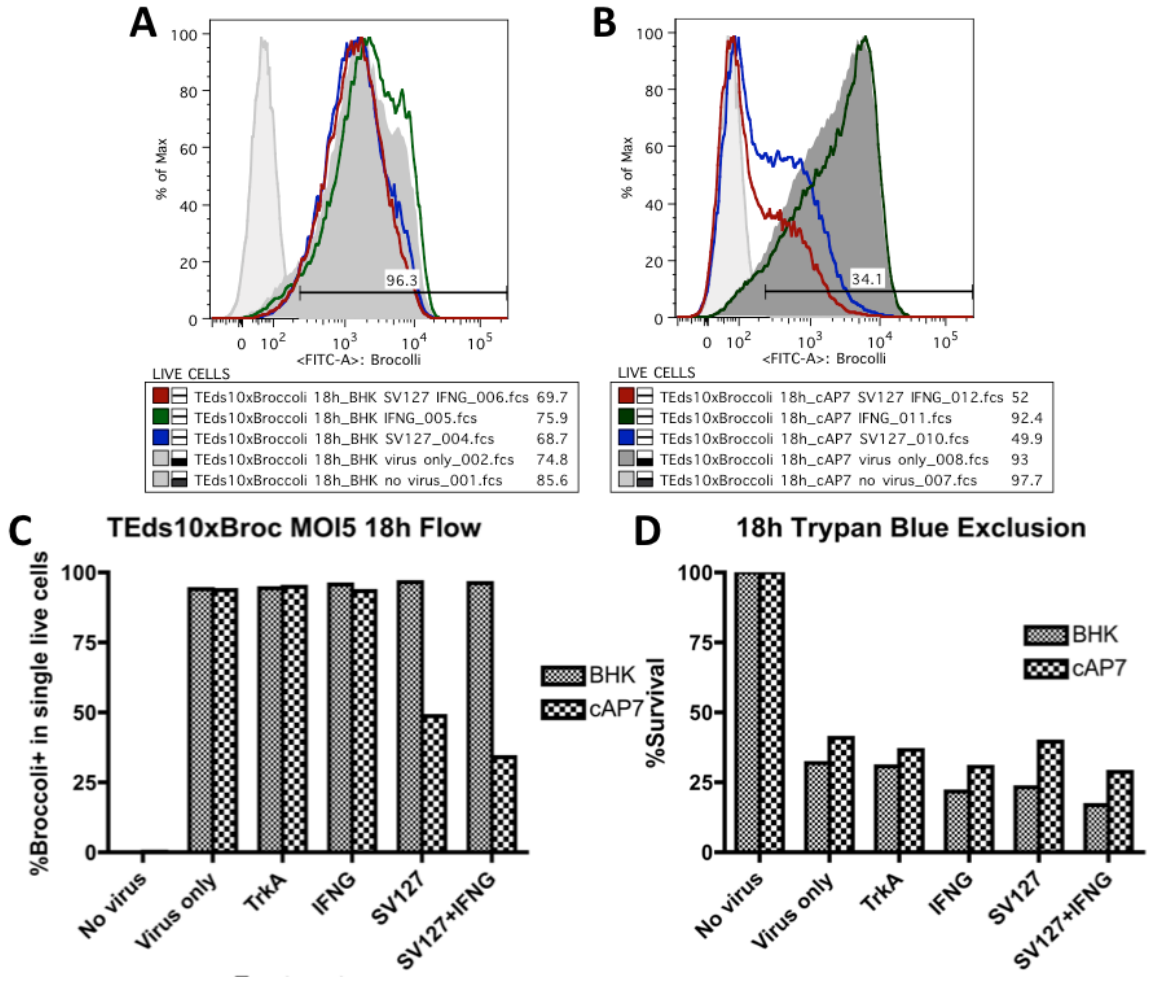

Figure 4.35 The effects of antibody and IFN-γ on viral clearance and cell survival in BHK and cAP7 cells. The flow cytometry histograms show the Broccoli-DFHBI-1T signal in cells, infected with TEds10Br (MOI = 20). The numbers of Broccoli+ cells in BHK (A) and cAP7 (B) cells after treatment with or without antibody and IFN-γ at 2 hours post infection are summarized as a bar chart (C). D – a bar chart shows the effect of treatments on cell survival. None of the treatments improve survival in both cells, while only antibody treatment can clear viral RNA in cAP7 cells, but not in BHK cells.

Chapter 5

General Discussion

Despite growing evidence, the persistence of typical RNA viruses is not well-known to physicians, scientists, or even virologists. So far, most studies mention the persistence just from RT-PCR of a small specific viral gene fragment. Our study aimed to find more complete answers to this enigma.

Significance of routes of infection

Intracerebral inoculation is probably not an appropriate route of infection for experiments, because it is not natural and can cause 2 distribution patterns, which are opposite to each other (**Chapter 2**). However, it did allow us to determine that there is no specific set of cells for viral persistence. SINV will persist in oligodendrocytes, if the infection begins in the white matter. On the other hand, SINV will persist in neurons, if the infection begins in the gray matter. Studies of SINV encephalitis usually assume that infection and clearance mainly occur in neurons. These previous studies used intracerebral inoculation and need to take into consideration the possibility of infection in oligodendrocytes.

There is no obvious difference in virus persistence between white and gray matter tropisms, detected by plaque assay, SINV RT-qPCR, and anti-SINV ELISA. However, in assessment of morbidity and mortality, this can be a confounding factor, but it is impossible to know the distribution pattern in a mouse without examining the brain.

Therefore, intranasal inoculation, which always affects gray matter, may provide more consistent results.

Naturally, SINV is transmitted by mosquito bites, so subcutaneous inoculation is probably the most relevant, but entry into the CNS may not occur reliably. SINV-specific antibody is found in plasma 2-4 days before it is found in the brain (**Chapter 3**), despite the fact that the primary site of infection is the brain after intracerebral inoculation. Hosts may have the best outcome after subcutaneous inoculation, which takes multiple steps before the virus can reach CNS (**Figure 1.4**). In IFN-α/β receptor-deficient mice (A129) infected with low virulent SINV (TOTO 1101), weanling mice died 2 days later after subcutaneous inoculation than after intracerebral inoculation, and adult mice survived subcutaneous, but not intracerebral inoculation (**Figure 5.1**) (23). Thus, study results likely depend on route of infection.

Intracerebral inoculation may resemble rabies virus infection, which hides itself from the immune response until it reaches the CNS (119), while intranasal inoculation may resemble influenza virus encephalitis, in which the infection originates from the nasal mucosa (120).

Longer detection of Sindbis viral proteins than viral RNA

Viral proteins were found in more cells than viral RNA after the clearance of infectious virus. Viral proteins were also found in apoptotic cells and in the phagosomes of macrophages. During optimization of the brain slice culture, it became apparent that during prolonged culture of a 300-µm-brain slice, most of the cells die, resulting in only about 5 ng of RNA per slice, compared to 100 ng in a fresh brain slice. However,

antibody staining can still detect a lot of viral proteins in a degraded brain slice. Furthermore, in SINV-Broccoli-infected BHK cells, we observed a rapid loss of Broccoli signal just before propidium iodide entered the cells. This means that the viral RNA is degraded or loses its secondary structure even before the cell loses integrity of its plasma membrane.

Persistence mechanisms of SINV

Both SINV viral RNA and proteins can be detected with RNA FISH and IF, respectively, for at least 1 month after infection, when IFN-γ and SINV-specific antibody levels are high. This is similar to subacute sclerosing panencephalitis (SSPE), a disease in which measles virus (MV) is propagated in the the brain in the presence of very high levels of anti-measles antibody in the brain (63, 121).

How can SINV evade antibody-mediated clearance? The most straightforward answer would be selection of escape mutants. However, in adoptive antibody transfer model, the reactivated virus recovered from SCID mice after the antibody level dropped can still be neutralized by the original antibody (66). This makes escape mutants as a mechanism less likely, but still possible, because we cannot exclude the reversion of mutants into WT.

The timing of antibody production or treatment might also be important. In SINV-Broccoli-infected dAP7 cells, anti-E2 antibody treatment is effective for viral RNA clearance when applied 2-4 hours after infection, but not at 12 hours (data not shown). SINV induced host translation shut-off (44) might cause the failure of clearance with late antibody treatment. However, in other models, antibody treatment can successfully clear

the virus when applied even later; 24 hours for AT3-*bcl-2* cells (87, 88), 2 days for dorsal root ganglion neurons (85), 7 days for SCID mouse brains (66, 85). The differences in viral strains, multiplicity of infection (MOI), cell types, and the presence of other aspects of the immune response are possibly responsible for the different results. In dAP7 cells, even treating with antibody as early as 2 hours post infection, SINV RNA can still persist in some cells (**Figure 4.31**).

The evidence from FISH/IF shows that antibody is not detected on the surface of infected cells even at the time points (day 10 onward) when we can detected SINV-specific antibody in brain homogenates by ELISA. By incubating SINV-infected BHK cells with a diluted brain homogenate, we can detect antibody heavily bound to the cell surface with immunofluorescence. Thus, SINV-specific antibody is definitely present in brains and capable of binding infected cells in vitro, but cannot bind the surface of persistently infected cells in mouse brains. In dAP7 cells infected with either SINV-Broccoli or SINV-Spinach2, antibody treatment clears viral RNA in all cells, except the ones that antibody cannot bind to.

After clearance of infectious virus (D7-10), immunofluorescence shows that persistently infected cells in brains either do not express SINV E2 protein on the cell membrane or do not express it at all. The total loss of SINV E2 expression can be explained by the results from long-range PCR, which shows large deletions in the E2 gene by day 14 after infection. A few cells in the brain still have SINV E2 protein intracellularly, but not on the surface. dAP7 cells to which anti-E2 antibody cannot bind also have SINV E2 protein intracellularly, but not on the surface. Mutations in some

regions of E2 can inhibit transportation of E2 to plasma membrane, even though E2 production is comparable to that of WT (**Figure 5.2**) (122).

How can SINV evade IFN-γ clearance? In SINV-Broccoli-infected dAP7 cells, IFN-γ treatment is effective for viral RNA clearance applied at 2-4 hours after infection, but not at 12 hours (data not shown). SINV induced host translation shut-off (44) might cause the failure of clearance with late IFN-γ treatment. However, in other models, IFN-γ treatment can successfully clear or reduce the virus when applied even later; 24 hours for both dCSM14.1 cells (29, 48) and dorsal root ganglion neurons (48). For dNSC34 cells, IFN-γ treatment at 2-5 hours shows clear benefit, while treatment at 24 hours results in only marginal improvement (12). In previous study, dAP7 cells treated with IFN-γ at 24 hours still cleared the virus with excellent survival (48). Our study with SINV-Broccoli fails to replicate these results even when IFN-γ treatment was applied at 12 hours. Different virus strains and MOIs (=1 in previous study) might be the reason.

dAP7 cells are very resistant to SINV replication and inefficiently infected (28). By Poisson distribution, MOI of 5 should get more than 99% cells infected, if 1 virion is enough to infect 1 cell. However, unlike BHK cells, MOI of 5 is not enough to infect most of the dAP7 cells even in the unattenuated SINV-Broccoli clones (TEUTR4Br and TEds6Br) that give higher titer of infectious virus than SINV TE both *in vitro* and *in vivo*. At an MOI of 20, which we used for our study, more than 90% of dAP7 cells are infected at 12 and 24 hours. The most attenuated clone, TEds14Br, infects less than 1% of dAP7 cells even at an MOI of 20. This indicates that 1 virion might not be enough for some dAP7 cells. Thus, the results of previous studies that used a less virulent SINV and low

MOI must be interpreted carefully, because most of these differentiated neuronal cells may not be infected.

In BHK cells infected with SINV-Broccoli, it is clear that viral replication is faster with a higher MOI. This might possibly be true for dAP7 cells, where high MOI is needed for virus to replicate fast enough to shut down dAP7 innate cellular response. Unfortunately, the poor Broccoli signal and slow viral replication in dAP7 cells make it hard to repeat the experiment in dAP7 cells. The same explanation might also apply to why SINV persists in a few dAP7 cells even when IFN-γ treatment is as early as 2 hours post infection. There will be a small percentage of cells that are infected by more virions than average, which might lead to viral replication that is fast enough to suppress the cellular response to IFN-γ. On the other hand, it might be simply that some cells may express lower levels of IFN-γ receptors or have a defect in this signaling pathway (e.g. STAT). Using FACS, it is possible to separate the high Broccoli signal in persistently infected cells from the low Broccoli signal in cells that successfully clear the virus. Then comparisons (by e.g. microarray, reverse phase protein microarray, Western blot, etc.) between these 2 groups of cells can be done to provide some clues on what determines the fate of these cells.

The nature of persistent SINV RNA

Persistent SINV RNA is mainly incomplete subgenomic RNA. Some of this persistent subgenomic RNA still has a poly-A tail, but has lost the E2 gene by deletion. The lack of the E2 gene makes it unlikely to spread to new cells. The large deletion in the E2 gene, detected by long-range RT-PCR with an oligo-dT primer, contradicts the

detection of a lot of E2 gene at the same time points by RNA FISH E2 gene and RT-qPCR that targets a short sequence within E2 gene. This means both RNA FISH and RT-qPCR detect the E2 gene in the viral RNA fragments that lack a poly-A tail. Cellular RNases might cause the fragmentation of viral RNA.

The large deletions are about 2000 nucleotides, about half size of the subgenomic RNA. The size of the remaining subgenomic RNA is similar to the SINV 20S defective interfering particle (DI) RNA (123). Though the sequence itself might be able to replicate, the lack of intact genomic RNA for translation of the replicase proteins makes it unlikely to replicate. Alphavirus DI RNAs are usually generated *in vitro* with few *in vivo* reports. For example, an avirulent strain (A7) of Semliki Forest virus (SFV) can form DI RNAs in mouse brains on day 4 after peritoneal inoculation (124).

These SINV RNAs with large deletions of E2 gene might still produce capsid protein, because RNA-FISH-positive cells frequently lack E2 proteins, but always have capsid proteins inside. However, our set of primers covers E3-E2-6K-E1, but not capsid. Thus, we cannot exclude the possibility that there might be multiple deletions in the same RNA.

Interestingly, in a model of mouse chronic inflammatory myopathy, coxsackievirus RNA persists in muscle at 1 month after infection in the form of dsRNA (**Figure 5.3**). Moreover, the persistent RNA is an intact complete genome without mutation (125). Because our study focuses on the viral RNA persistence during the 2nd phase of clearance (gradual decrease in viral RNA), the unexplored nature of persistent viral RNA in the 3rd phase (sustained low level viral RNA) might still be dsRNA.

The fact that SINV viral RNA during clearance has so many forms (genomic, subgenomic, minus, dsRNA, deletion/defective, fragments, etc.) poses a challenge for the definition of viral RNA clearance. The degradation ranges from a single cleavage, which is probably enough to make viral RNA lose function, to complete degradation of viral RNA. The former is likely to be much faster than the latter. Our RT-qPCR covers only 74 nucleotides in the E2 gene (8732-8805). If we expand the size of the region covered by RT-PCR, the results of RNA clearance by different immunoglobulin-deficient mice in Chapter 3 may not be the same.

Synergism and redundancy of antibody and IFN-γ-mediated SINV clearance

In previous *in vitro* studies, responses of infected cells to anti-E2 antibody are quite similar to IFN-γ. Both treatments increase viral replication early on before restoration of host functions and later suppression of the replication (29, 88). Our study in SINV-Broccoli-infected dAP7 also shows similarity between the 2 treatments. Both are effective at 2 hours after infection, but not at 12 hours. Both show the same time frame of clearance, though antibody is better in both viral RNA clearance and survival improvement than IFN-γ. Combined treatments do not speed up the clearance, but increase the number of cells that respond. This suggests that both treatments might partially share the same pathway responsible for clearance and survival. For instance, both treatments are known to potentiate the type-I IFN response (87, 126-128)

The study of SINV-Broccoli supports the mouse model results. Both IFN-γ and antibody are effective and synergistic. In brains, where infectious virus titer is very high, antibody is better than IFN-γ. In spinal cords, where infectious virus titer is quite low,

both treatments are equal. If the virus is attenuated (e.g. TEds10Br), then antibody might not be needed even in brains.

Viral clearance in DKO mice (no secreted antibody) in our study is similar to μMT mice (no B-cell) in previous studies (43, 45). However, a direct comparison between DKO and μMT mice would be interesting, because B-cells themselves might contribute to the viral clearance by functions in addition to secreting antibody. The role of the adaptive immune response in viral clearance from mouse CNS is summarized in **Table 5.1**.

Table 5.1 Summary of mouse models used in SINV clearance studies (SC – spinal cord, P – persistent, C – clear, NA – not available)

Mice	T-cell	IFN-γ	B-cell	IgM	IgG	Brains	SC
SCID (43, 45, 85)	-	+	-	-	-	P	P
Athymic nude (90, 129)	-	+	+	+	-	C	NA
μMT (43, 45)	+	+	-	-	-	P	C
IFN-γ-/- (43, 47)	+	-	+	+	+	C	C
μMT IFN-γ-/- (43)	+	-	-	-	-	P	P
AID-/-	+	+	+	+	-	C	C
sIgM-/-	+	+	+	-	+	C	C
AID-/- sIgM-/-	+	+	+	-	-	P	C

Problem with mouse models

The mice from the 4 antibody-knockout mouse groups are clearly different in weight. The heaviest mice are sIgM-/-, followed by WT, DKO, and AID-/- mice, respectively. Previously, we had done the same morbidity-mortality experiments (as in Chapter 3) to compare the outcomes of 24 WT mice versus 24 AID-/- mice and then also 24 WT mice versus 31 sIgM-/- mice, where AID-/- had the worst and sIgM had the best outcomes. The differences were quite remarkable. However, when we finished breeding the DKO (AID-/- sIgM-/-) mice and repeated another 2 independent experiments (Chapter 3) with all 4 groups of mice (WT, AID-/-, sIgM-/-, DKO), the differences were gone.

All AID-/- and sIgM-/- mice from the 1st round of experiments were the F2-3 generations of AID+/- mice from Albert Einstein College of Medicine and sIgM+/- mice from University of California, Davis, while WT C57BL/6 mice were from Jackson Laboratory. There have been studies that have shown that mice with the same genetic background but from different facilities/vendors have different gene expressions and microbiomes (130), which result in differential susceptibility to some pathogens, e.g. *Plasmodium yoelii* (131) and *Burkholderia thailandensis* (132). The latter example reveals the amazing role of microbiome. *E. coli* O21:H^{+} found in C57BL/6 mice from University of California, Berkeley, but not from Jackson Laboratory, can translocate from the intestine to colonize adipose tissues and activate the inflammasome, resulting in the release of IGF-1 which prevents muscle wasting induced by *B. thailandensis* (132). When we conducted the 1st experiment, our mice might not have adjusted their microbiome to the new environment, resulting in the different outcomes.

Even with the same genetics, mice can still have largely different microbiomes. It would be surprising if immuno-deficient mice did not have microbiome different from wild type mice. Indeed, AID-/- mice, which lack IgA in guts, have 100-fold expansion of anaerobes in the small intestine (21). The intestinal epithelium up-regulates interferon and suppresses GATA4-related functions, leading to fat malabsorption and low fat deposit (133). This might explain why AID-/- mice have the lowest body weight. Antibiotic treatment or IgA restoration, which decreases these bacteria, can reverse lymphoid hyperplasia and germinal center enlargement, typical phenotypes found in AID-/- mice (134, 135). DKO mice suffered the same fate (133). This complicates the interpretation of the results of most experiments involving immuno-deficient animals where the effect may be caused by the deficiency per se or by specific microbiome-induced immune response.

Regarding effects of the microbiome on immune responses and outcomes after experimental infection, which approach would be the best to understand the function of immune-related gene that is deficient in the knockout mice? We have to choose between germ-free, artificial colonization of specific pathogen free flora (130), shared microbiome (e.g. co-housing), or signature microbiome. As for the signature microbiome that would be specific to each type of immuno-deficient mice, we do not yet know how many generations it takes to reach equilibrium, if the environment remains unchanged.

For example, in AID-/- mice, the transition would begin with the 1st generation of homozygous AID-/- mice, of which microbiome is transferred from their immunocompetent heterozygous AID+/- parents. These AID-/- pups are also surrounded by their competent siblings (AID+/+ or AID+/-). Furthermore, though the AID-/- pups

cannot produce IgG or IgA by themselves, they acquire IgA through milk and IgG through placenta. It is very unlikely that these first-generation AID-/- mice will reach their own signature microbiome early on. These mice will then pass their microbiome to their next generation. Therefore, the mice in our 1st morbidity-mortality experiment might still be in the transitional phase of microbiome changing, while the mice in 2nd and 3rd experiments, a year after the 1st, had probably acquired their signature microbiome, resulting in a difference in the results. Due to the mouse housing cost, most investigators probably conduct the experiments as soon as there are enough mice. This might be problematic if the microbiome does affect the experiment.

In conclusion, SINV RNA and proteins persist long after clearance of infectious virus from the mouse CNS. SINV E2 gene deletion helps the virus evade antibody-mediated clearance. As a result, antibody may not be necessary for the 2nd-phase of viral RNA clearance from the mouse CNS, even though antibody is very effective *in vitro* and in adoptive transfer models. In the presence of T-cells and IFN-γ, the main advantage of having antibody in SINV encephalomyelitis is the suppression of viral reactivation, not the clearance of viral RNA. Our study emphasizes the flexibility and reserve power of the immune system. A deficiency in one aspect can be replaced with another, and all aspects are needed only when the burden of infection is very high.

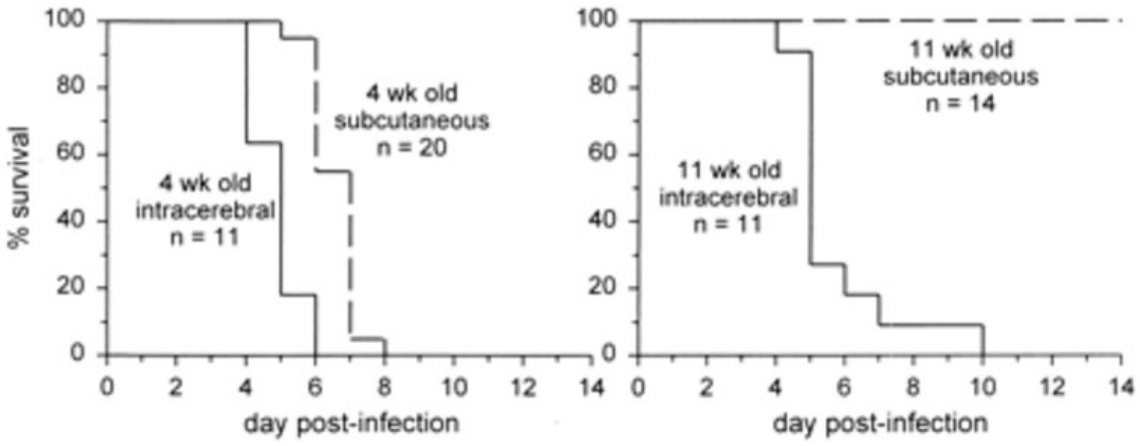

Figure 5.1 Survival rate of A129 mice infected with SINV TOTO 1101 (low virulent) in different age groups and inoculum sites (23).

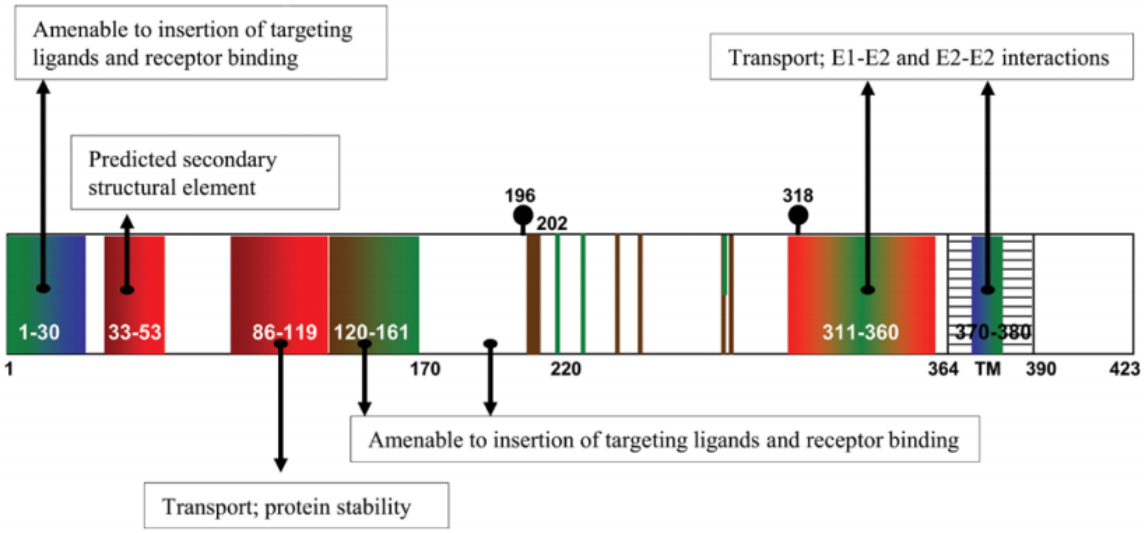

Figure 5.2 Functional regions of Sindbis virus E2 protein, characterized from insertional transposon mutagenesis of E2 gene. Each color represents plaque size of mutant viruses. Blue – large (wild-type-like), green – medium, brown – small, red – lethal (122).

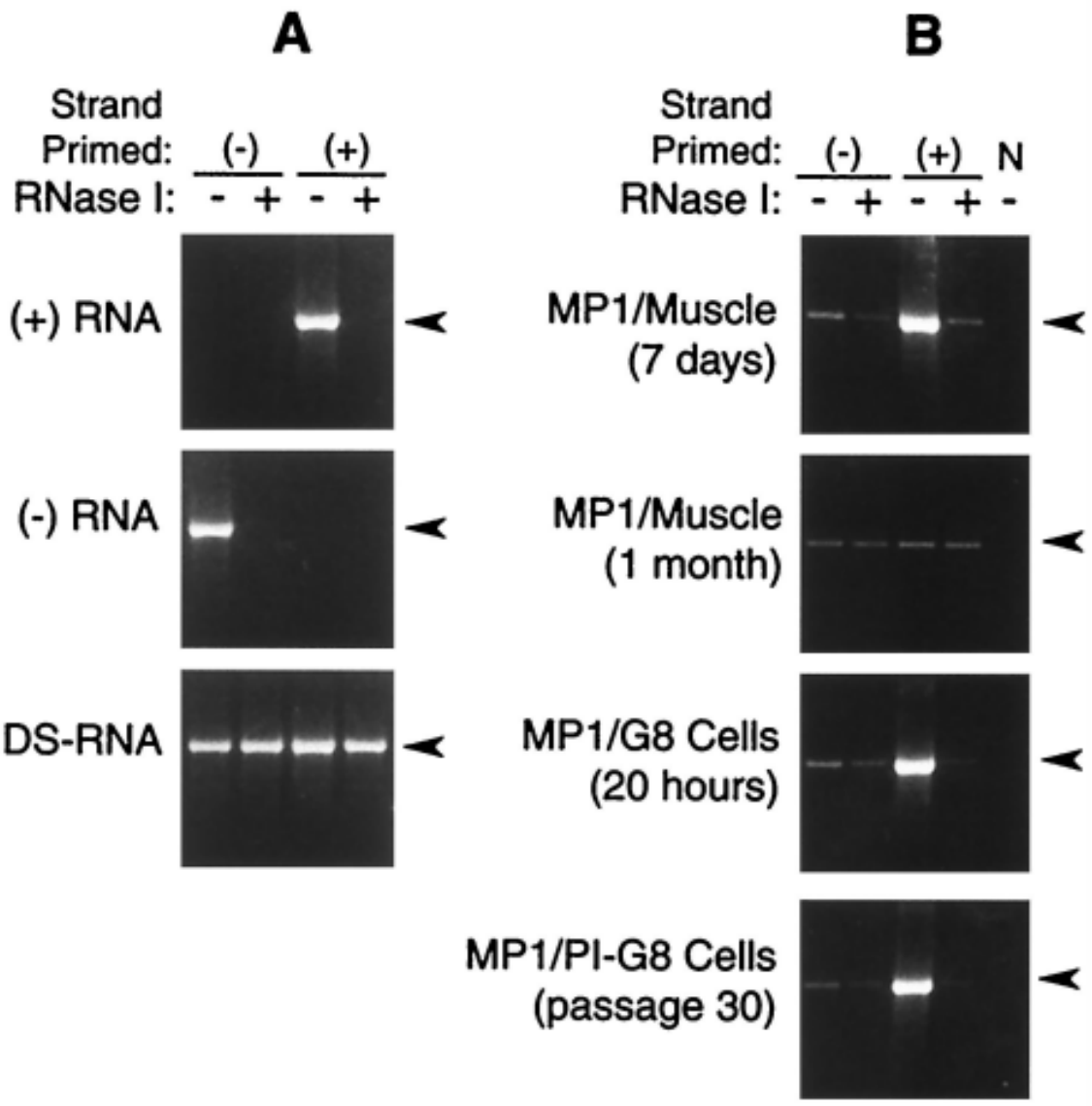

Figure 5.3 A – Control viral RNAs (+, -, double stranded) were generated by *in vitro* transcription and amplified by strand-specific (+ or -) RT-PCR with or without RNase I digestion of single-stranded RNA. B – Coxsackievirus (MP1) infection in mouse muscle or myoblast (G8) at different time points. (N – No primer control, PI – persistent infected) (125)

References

1. Taylor RM, Hurlbut HS, Work TH, Kingston JR, Frothingham TE. Sindbis virus: a newly recognized arthropodtransmitted virus. The American journal of tropical medicine and hygiene. 1955 Sep;4(5):844-62. PubMed PMID: 13259009.

2. Shope RE. The discovery of arbovirus diseases. Annals of the New York Academy of Sciences. 1994 Dec 15;740:138-45. PubMed PMID: 7840445.

3. Niklasson B, Espmark A, LeDuc JW, Gargan TP, Ennis WA, Tesh RB, et al. Association of a Sindbis-like virus with Ockelbo disease in Sweden. The American journal of tropical medicine and hygiene. 1984 Nov;33(6):1212-7. PubMed PMID: 6150655.

4. Espmark A, Niklasson B. Ockelbo disease in Sweden: epidemiological, clinical, and virological data from the 1982 outbreak. The American journal of tropical medicine and hygiene. 1984 Nov;33(6):1203-11. PubMed PMID: 6150654.

5. Griffin D. Alphaviruses. In: Knipe D, Howley P, editors. Fields Virology: Lippincott Williams & Wilkins; 2007. p. 1024-67.

6. Gerardin P, Couderc T, Bintner M, Tournebize P, Renouil M, Lemant J, et al. Chikungunya virus-associated encephalitis: A cohort study on La Reunion Island, 2005-2009. Neurology. 2016 Jan 5;86(1):94-102. PubMed PMID: 26609145.

7. Nelson J, Waggoner JJ, Sahoo MK, Grant PM, Pinsky BA. Encephalitis caused by Chikungunya virus in a traveler from the Kingdom of Tonga. Journal of clinical microbiology. 2014 Sep;52(9):3459-61. PubMed PMID: 24958800. Pubmed Central PMCID: 4313184.

8. Adouchief S, Smura T, Sane J, Vapalahti O, Kurkela S. Sindbis virus as a human pathogen-epidemiology, clinical picture and pathogenesis. Reviews in medical virology. 2016 Jul;26(4):221-41. PubMed PMID: 26990827.

9. Rose PP, Hanna SL, Spiridigliozzi A, Wannissorn N, Beiting DP, Ross SR, et al. Natural resistance-associated macrophage protein is a cellular receptor for sindbis virus in both insect and mammalian hosts. Cell host & microbe. 2011 Aug 18;10(2):97-104. PubMed PMID: 21843867. Pubmed Central PMCID: 3164510.

10. Shirako Y, Strauss JH. Regulation of Sindbis virus RNA replication: uncleaved P123 and nsP4 function in minus-strand RNA synthesis, whereas cleaved products from P123 are required for efficient plus-strand RNA synthesis. Journal of virology. 1994 Mar;68(3):1874-85. PubMed PMID: 8107248. Pubmed Central PMCID: 236650.

11. Strauss JH, Strauss EG. The alphaviruses: gene expression, replication, and evolution. Microbiological reviews. 1994 Sep;58(3):491-562. PubMed PMID: 7968923. Pubmed Central PMCID: 372977.

12. Snyder JE, Kulcsar KA, Schultz KL, Riley CP, Neary JT, Marr S, et al. Functional characterization of the alphavirus TF protein. Journal of virology. 2013 Aug;87(15):8511-23. PubMed PMID: 23720714. Pubmed Central PMCID: 3719798.

13. Grimley PM, Berezesky IK, Friedman RM. Cytoplasmic structures associated with an arbovirus infection: loci of viral ribonucleic acid synthesis. Journal of virology. 1968 Nov;2(11):1326-38. PubMed PMID: 5750316. Pubmed Central PMCID: 375472.

14. Lombard Y, Poindron P, Porte A. [Origin and formation of different types of vacuoles induced by the multiplication of the alphavirus Sindbis virus in various cell

systems]. Canadian journal of microbiology. 1979 Dec;25(12):1452-9. PubMed PMID: 534962. Origine et formation de differents types de vacuoles induites par la multiplication d'alphavirus Sindbis dans divers systemes cellulaires.

15. Soonsawad P, Xing L, Milla E, Espinoza JM, Kawano M, Marko M, et al. Structural evidence of glycoprotein assembly in cellular membrane compartments prior to Alphavirus budding. Journal of virology. 2010 Nov;84(21):11145-51. PubMed PMID: 20739526. Pubmed Central PMCID: 2953181.

16. Froshauer S, Kartenbeck J, Helenius A. Alphavirus RNA replicase is located on the cytoplasmic surface of endosomes and lysosomes. The Journal of cell biology. 1988 Dec;107(6 Pt 1):2075-86. PubMed PMID: 2904446. Pubmed Central PMCID: 2115628.

17. Romero-Brey I, Bartenschlager R. Membranous replication factories induced by plus-strand RNA viruses. Viruses. 2014 Jul;6(7):2826-57. PubMed PMID: 25054883. Pubmed Central PMCID: 4113795.

18. Spuul P, Balistreri G, Kaariainen L, Ahola T. Phosphatidylinositol 3-kinase-, actin-, and microtubule-dependent transport of Semliki Forest Virus replication complexes from the plasma membrane to modified lysosomes. Journal of virology. 2010 Aug;84(15):7543-57. PubMed PMID: 20484502. Pubmed Central PMCID: 2897599.

19. Thaa B, Biasiotto R, Eng K, Neuvonen M, Gotte B, Rheinemann L, et al. Differential Phosphatidylinositol-3-Kinase-Akt-mTOR Activation by Semliki Forest and Chikungunya Viruses Is Dependent on nsP3 and Connected to Replication

Complex Internalization. Journal of virology. 2015 Nov;89(22):11420-37. PubMed PMID: 26339054. Pubmed Central PMCID: 4645633.

20. Frolova EI, Gorchakov R, Pereboeva L, Atasheva S, Frolov I. Functional Sindbis virus replicative complexes are formed at the plasma membrane. Journal of virology. 2010 Nov;84(22):11679-95. PubMed PMID: 20826696. Pubmed Central PMCID: 2977861.

21. Griffin DE, Metcalf T. Clearance of virus infection from the CNS. Current opinion in virology. 2011 Sep;1(3):216-21. PubMed PMID: 21927638. Pubmed Central PMCID: 3171972.

22. Cook SH, Griffin DE. Luciferase imaging of a neurotropic viral infection in intact animals. Journal of virology. 2003 May;77(9):5333-8. PubMed PMID: 12692235. Pubmed Central PMCID: 153972.

23. Byrnes AP, Durbin JE, Griffin DE. Control of Sindbis virus infection by antibody in interferon-deficient mice. Journal of virology. 2000 Apr;74(8):3905-8. PubMed PMID: 10729167. Pubmed Central PMCID: 111901.

24. Lustig S, Jackson AC, Hahn CS, Griffin DE, Strauss EG, Strauss JH. Molecular basis of Sindbis virus neurovirulence in mice. Journal of virology. 1988 Jul;62(7):2329-36. PubMed PMID: 2836615. Pubmed Central PMCID: 253389.

25. Tucker PC, Strauss EG, Kuhn RJ, Strauss JH, Griffin DE. Viral determinants of age-dependent virulence of Sindbis virus for mice. Journal of virology. 1993 Aug;67(8):4605-10. PubMed PMID: 8392602. Pubmed Central PMCID: 237845.

26. Thach DC, Kimura T, Griffin DE. Differences between C57BL/6 and BALB/cBy mice in mortality and virus replication after intranasal infection with neuroadapted

Sindbis virus. Journal of virology. 2000 Jul;74(13):6156-61. PubMed PMID: 10846099. Pubmed Central PMCID: 112114.

27. Griffin DE, Levine B, Tyor WR, Tucker PC, Hardwick JM. Age-dependent susceptibility to fatal encephalitis: alphavirus infection of neurons. Archives of virology Supplementum. 1994;9:31-9. PubMed PMID: 8032263.

28. Schultz KL, Vernon PS, Griffin DE. Differentiation of neurons restricts Arbovirus replication and increases expression of the alpha isoform of IRF-7. Journal of virology. 2015 Jan;89(1):48-60. PubMed PMID: 25320290. Pubmed Central PMCID: 4301127.

29. Burdeinick-Kerr R, Griffin DE. Gamma interferon-dependent, noncytolytic clearance of sindbis virus infection from neurons in vitro. Journal of virology. 2005 May;79(9):5374-85. PubMed PMID: 15827152. Pubmed Central PMCID: 1082728.

30. Labrada L, Liang XH, Zheng W, Johnston C, Levine B. Age-dependent resistance to lethal alphavirus encephalitis in mice: analysis of gene expression in the central nervous system and identification of a novel interferon-inducible protective gene, mouse ISG12. Journal of virology. 2002 Nov;76(22):11688-703. PubMed PMID: 12388728. Pubmed Central PMCID: 136759.

31. Kulcsar KA, Baxter VK, Abraham R, Nelson A, Griffin DE. Distinct Immune Responses in Resistant and Susceptible Strains of Mice during Neurovirulent Alphavirus Encephalomyelitis. Journal of virology. 2015 Aug;89(16):8280-91. PubMed PMID: 26041298. Pubmed Central PMCID: 4524229.

32. Thach DC, Kleeberger SR, Tucker PC, Griffin DE. Genetic control of neuroadapted sindbis virus replication in female mice maps to chromosome 2 and

associates with paralysis and mortality. Journal of virology. 2001 Sep;75(18):8674-80. PubMed PMID: 11507212. Pubmed Central PMCID: 115112.

33. Griffin DE, Johnson RT. Role of the immune response in recovery from Sindbis virus encephalitis in mice. Journal of immunology. 1977 Mar;118(3):1070-5. PubMed PMID: 845432.

34. Savarin C, Bergmann CC. Neuroimmunology of central nervous system viral infections: the cells, molecules and mechanisms involved. Current opinion in pharmacology. 2008 Aug;8(4):472-9. PubMed PMID: 18562249. Pubmed Central PMCID: 2613975.

35. Esen N, Blakely PK, Rainey-Barger EK, Irani DN. Complexity of the microglial activation pathways that drive innate host responses during lethal alphavirus encephalitis in mice. ASN neuro. 2012;4(4):207-21. PubMed PMID: 22471445. Pubmed Central PMCID: 3342594.

36. Neighbours LM, Long K, Whitmore AC, Heise MT. Myd88-dependent toll-like receptor 7 signaling mediates protection from severe Ross River virus-induced disease in mice. Journal of virology. 2012 Oct;86(19):10675-85. PubMed PMID: 22837203. Pubmed Central PMCID: 3457316.

37. Wollish AC, Ferris MT, Blevins LK, Loo YM, Gale M, Jr., Heise MT. An attenuating mutation in a neurovirulent Sindbis virus strain interacts with the IPS-1 signaling pathway in vivo. Virology. 2013 Jan 20;435(2):269-80. PubMed PMID: 23084425. Pubmed Central PMCID: 3534923.

38. Ryman KD, White LJ, Johnston RE, Klimstra WB. Effects of PKR/RNase L-dependent and alternative antiviral pathways on alphavirus replication and pathogenesis. Viral immunology. 2002;15(1):53-76. PubMed PMID: 11952147.

39. Giannakopoulos NV, Arutyunova E, Lai C, Lenschow DJ, Haas AL, Virgin HW. ISG15 Arg151 and the ISG15-conjugating enzyme UbE1L are important for innate immune control of Sindbis virus. Journal of virology. 2009 Feb;83(4):1602-10. PubMed PMID: 19073728. Pubmed Central PMCID: 2643764.

40. Lenschow DJ, Lai C, Frias-Staheli N, Giannakopoulos NV, Lutz A, Wolff T, et al. IFN-stimulated gene 15 functions as a critical antiviral molecule against influenza, herpes, and Sindbis viruses. Proceedings of the National Academy of Sciences of the United States of America. 2007 Jan 23;104(4):1371-6. PubMed PMID: 17227866. Pubmed Central PMCID: 1783119.

41. Kozaki T, Takahama M, Misawa T, Matsuura Y, Akira S, Saitoh T. Role of zinc-finger anti-viral protein in host defense against Sindbis virus. International immunology. 2015 Jul;27(7):357-64. PubMed PMID: 25758257. Pubmed Central PMCID: 4565983.

42. Ryman KD, Klimstra WB, Nguyen KB, Biron CA, Johnston RE. Alpha/beta interferon protects adult mice from fatal Sindbis virus infection and is an important determinant of cell and tissue tropism. Journal of virology. 2000 Apr;74(7):3366-78. PubMed PMID: 10708454. Pubmed Central PMCID: 111838.

43. Burdeinick-Kerr R, Wind J, Griffin DE. Synergistic roles of antibody and interferon in noncytolytic clearance of Sindbis virus from different regions of the

central nervous system. Journal of virology. 2007 Jun;81(11):5628-36. PubMed PMID: 17376910. Pubmed Central PMCID: 1900320.

44. Yin J, Gardner CL, Burke CW, Ryman KD, Klimstra WB. Similarities and differences in antagonism of neuron alpha/beta interferon responses by Venezuelan equine encephalitis and Sindbis alphaviruses. Journal of virology. 2009 Oct;83(19):10036-47. PubMed PMID: 19641001. Pubmed Central PMCID: 2748036.

45. Binder GK, Griffin DE. Interferon-gamma-mediated site-specific clearance of alphavirus from CNS neurons. Science. 2001 Jul 13;293(5528):303-6. PubMed PMID: 11452126.

46. Kulcsar KA, Baxter VK, Greene IP, Griffin DE. Interleukin 10 modulation of pathogenic Th17 cells during fatal alphavirus encephalomyelitis. Proceedings of the National Academy of Sciences of the United States of America. 2014 Nov 11;111(45):16053-8. PubMed PMID: 25362048. Pubmed Central PMCID: 4234572.

47. Griffin DE, Baxter VK. Interferon gamma modulation of disease manifestation and the local antibody response to alphavirus encephalomyelitis. The Journal of general virology. 2016 Sep 22. PubMed PMID: 27667782.

48. Burdeinick-Kerr R, Govindarajan D, Griffin DE. Noncytolytic clearance of sindbis virus infection from neurons by gamma interferon is dependent on Jak/STAT signaling. Journal of virology. 2009 Apr;83(8):3429-35. PubMed PMID: 19176616. Pubmed Central PMCID: 2663278.

49. Tschen SI, Stohlman SA, Ramakrishna C, Hinton DR, Atkinson RD, Bergmann CC. CNS viral infection diverts homing of antibody-secreting cells from lymphoid

organs to the CNS. European journal of immunology. 2006 Mar;36(3):603-12. PubMed PMID: 16437540.

50. Metcalf TU, Baxter VK, Nilaratanakul V, Griffin DE. Recruitment and retention of B cells in the central nervous system in response to alphavirus encephalomyelitis. Journal of virology. 2013 Mar;87(5):2420-9. PubMed PMID: 23255791. Pubmed Central PMCID: 3571404.

51. Metcalf TU, Griffin DE. Alphavirus-induced encephalomyelitis: antibody-secreting cells and viral clearance from the nervous system. Journal of virology. 2011 Nov;85(21):11490-501. PubMed PMID: 21865385. Pubmed Central PMCID: 3194963.

52. Matthews AE, Weiss SR, Shlomchik MJ, Hannum LG, Gombold JL, Paterson Y. Antibody is required for clearance of infectious murine hepatitis virus A59 from the central nervous system, but not the liver. Journal of immunology. 2001 Nov 1;167(9):5254-63. PubMed PMID: 11673540.

53. Kundig TM, Hengartner H, Zinkernagel RM. T cell-dependent IFN-gamma exerts an antiviral effect in the central nervous system but not in peripheral solid organs. Journal of immunology. 1993 Mar 15;150(6):2316-21. PubMed PMID: 8450214.

54. Grebely J, Prins M, Hellard M, Cox AL, Osburn WO, Lauer G, et al. Hepatitis C virus clearance, reinfection, and persistence, with insights from studies of injecting drug users: towards a vaccine. The Lancet infectious diseases. 2012 May;12(5):408-14. PubMed PMID: 22541630. Pubmed Central PMCID: 3608418. Epub 2012/05/01. eng.

55. Zhou X, Ramachandran S, Mann M, Popkin DL. Role of lymphocytic choriomeningitis virus (LCMV) in understanding viral immunology: past, present and future. Viruses. 2012 Nov;4(11):2650-69. PubMed PMID: 23202498. Pubmed Central PMCID: 3509666. Epub 2012/12/04. eng.

56. Chan PK, Lim PL, Liu EY, Cheung JL, Leung DT, Sung JJ. Antibody avidity maturation during severe acute respiratory syndrome-associated coronavirus infection. The Journal of infectious diseases. 2005 Jul 1;192(1):166-9. PubMed PMID: 15942907. Epub 2005/06/09. eng.

57. Murray K, Walker C, Herrington E, Lewis JA, McCormick J, Beasley DW, et al. Persistent infection with West Nile virus years after initial infection. The Journal of infectious diseases. 2010 Jan 1;201(1):2-4. PubMed PMID: 19961306. Pubmed Central PMCID: 2791189. Epub 2009/12/08. eng.

58. Putcharoen O, Krajiw S, Nilaratanakul V, Rojnuckarin P, Bhattarakosol P, Nisalak A, editors. Presence of dengue virus genome in the bone marrow of asymptomatic adults in a dengue-hyperendemic country: implication for complicated dengue pathogenesis. 17th European Congress of Clinical Microbiology and Infectious Diseases; 2007; Munich, Germany.

59. Nilaratanakul V, Thaivanich S, Songcharoen K, Arunyingmongkol K, Plongla R, Sriprapun M, et al., editors. Detection of dengue virus in lymphoid tissues of persons with remote dengue infections. 20th European Congress of Clinical Microbiology and Infectious Diseases; 2010 April 10-13; Vienna, Austria.

60. Plongla R, Songcharoen K, Arunyingmongkol K, Tantiwongse K, Kulwichit W, editors. Presence of dengue virus genome in kidney tissue of adults without recent

dengue infection: another piece of evidence of in vivo persistence of the virus. 22nd European Congress of Clinical Microbiology and Infectious Diseases; 2012 March 31-April 3; London, United Kingdom.

61. Perret C, Chanthavanich P, Pengsaa K, Limkittikul K, Hutajaroen P, Bunn JE, et al. Dengue infection during pregnancy and transplacental antibody transfer in Thai mothers. The Journal of infection. 2005 Nov;51(4):287-93. PubMed PMID: 16291281. Epub 2005/11/18. eng.

62. Chantler JK, Ford DK, Tingle AJ. Persistent rubella infection and rubella-associated arthritis. Lancet. 1982 Jun 12;1(8285):1323-5. PubMed PMID: 6123637. Epub 1982/06/12. eng.

63. Griffin DE, Lin WH, Pan CH. Measles virus, immune control, and persistence. FEMS microbiology reviews. 2012 May;36(3):649-62. PubMed PMID: 22316382. Pubmed Central PMCID: 3319515.

64. Lin WH, Kouyos RD, Adams RJ, Grenfell BT, Griffin DE. Prolonged persistence of measles virus RNA is characteristic of primary infection dynamics. Proceedings of the National Academy of Sciences of the United States of America. 2012 Sep 11;109(37):14989-94. PubMed PMID: 22872860. Pubmed Central PMCID: 3443140.

65. Feuer R, Ruller CM, An N, Tabor-Godwin JM, Rhoades RE, Maciejewski S, et al. Viral persistence and chronic immunopathology in the adult central nervous system following Coxsackievirus infection during the neonatal period. Journal of virology. 2009 Sep;83(18):9356-69. PubMed PMID: 19570873. Pubmed Central PMCID: 2738251.

66. Levine B, Griffin DE. Persistence of viral RNA in mouse brains after recovery from acute alphavirus encephalitis. Journal of virology. 1992 Nov;66(11):6429-35. PubMed PMID: 1383564. Pubmed Central PMCID: 240135.

67. Kim H, Kim E, Park M, Lee E, Namkoong K. Organotypic hippocampal slice culture from the adult mouse brain: a versatile tool for translational neuropsychopharmacology. Progress in neuro-psychopharmacology & biological psychiatry. 2013 Mar 5;41:36-43. PubMed PMID: 23159795.

68. Park E, Griffin DE. Interaction of Sindbis virus non-structural protein 3 with poly(ADP-ribose) polymerase 1 in neuronal cells. The Journal of general virology. 2009 Sep;90(Pt 9):2073-80. PubMed PMID: 19515826. Pubmed Central PMCID: 2887572.

69. Park E, Griffin DE. The nsP3 macro domain is important for Sindbis virus replication in neurons and neurovirulence in mice. Virology. 2009 Jun 5;388(2):305-14. PubMed PMID: 19395054. Pubmed Central PMCID: 2683903.

70. Badea A, Ali-Sharief AA, Johnson GA. Morphometric analysis of the C57BL/6J mouse brain. NeuroImage. 2007 Sep 1;37(3):683-93. PubMed PMID: 17627846. Pubmed Central PMCID: 2176152.

71. McCarthy DP, Richards MH, Miller SD. Mouse models of multiple sclerosis: experimental autoimmune encephalomyelitis and Theiler's virus-induced demyelinating disease. Methods in molecular biology. 2012;900:381-401. PubMed PMID: 22933080. Pubmed Central PMCID: 3583382.

72. Setinek U, Wondrusch E, Jellinger K, Steuer A, Drlicek M, Grisold W, et al. Cytomegalovirus infection of the brain in AIDS: a clinicopathological study. Acta neuropathologica. 1995;90(5):511-5. PubMed PMID: 8560985.

73. Benner B, Martorell AJ, Mahadevan P, Najm FJ, Tesar PJ, Freundt EC. Depletion of Olig2 in oligodendrocyte progenitor cells infected by Theiler's murine encephalomyelitis virus. Journal of neurovirology. 2016 Jun;22(3):336-48. PubMed PMID: 26631080.

74. Evangelidou M, Karamita M, Vamvakas SS, Szymkowski DE, Probert L. Altered expression of oligodendrocyte and neuronal marker genes predicts the clinical onset of autoimmune encephalomyelitis and indicates the effectiveness of multiple sclerosis-directed therapeutics. J Immunol. 2014 May 1;192(9):4122-33. PubMed PMID: 24683189.

75. Dredge BK, Jensen KB. NeuN/Rbfox3 nuclear and cytoplasmic isoforms differentially regulate alternative splicing and nonsense-mediated decay of Rbfox2. PloS one. 2011;6(6):e21585. PubMed PMID: 21747913. Pubmed Central PMCID: 3126832.

76. Van Nassauw L, Wu M, De Jonge F, Adriaensen D, Timmermans JP. Cytoplasmic, but not nuclear, expression of the neuronal nuclei (NeuN) antibody is an exclusive feature of Dogiel type II neurons in the guinea-pig gastrointestinal tract. Histochemistry and cell biology. 2005 Nov;124(5):369-77. PubMed PMID: 16049694.

77. Unal-Cevik I, Kilinc M, Gursoy-Ozdemir Y, Gurer G, Dalkara T. Loss of NeuN immunoreactivity after cerebral ischemia does not indicate neuronal cell loss: a

cautionary note. Brain research. 2004 Jul 23;1015(1-2):169-74. PubMed PMID: 15223381.

78. Lee DR, Helps SC, Gibbins IL, Nilsson M, Sims NR. Losses of NG2 and NeuN immunoreactivity but not astrocytic markers during early reperfusion following severe focal cerebral ischemia. Brain research. 2003 Nov 7;989(2):221-30. PubMed PMID: 14556944.

79. Hahn YK, Masvekar RR, Xu R, Hauser KF, Knapp PE. Chronic HIV-1 Tat and HIV reduce Rbfox3/NeuN: evidence for sex-related effects. Current HIV research. 2015;13(1):10-20. PubMed PMID: 25760045. Pubmed Central PMCID: 4665621.

80. Lucas CH, Calvez M, Babu R, Brown A. Altered subcellular localization of the NeuN/Rbfox3 RNA splicing factor in HIV-associated neurocognitive disorders (HAND). Neuroscience letters. 2014 Jan 13;558:97-102. PubMed PMID: 24215932. Pubmed Central PMCID: 3880598.

81. Sokoloski KJ, Dickson AM, Chaskey EL, Garneau NL, Wilusz CJ, Wilusz J. Sindbis virus usurps the cellular HuR protein to stabilize its transcripts and promote productive infections in mammalian and mosquito cells. Cell host & microbe. 2010 Aug 19;8(2):196-207. PubMed PMID: 20709296. Pubmed Central PMCID: 2929003.

82. Dickson AM, Anderson JR, Barnhart MD, Sokoloski KJ, Oko L, Opyrchal M, et al. Dephosphorylation of HuR protein during alphavirus infection is associated with HuR relocalization to the cytoplasm. The Journal of biological chemistry. 2012 Oct 19;287(43):36229-38. PubMed PMID: 22915590. Pubmed Central PMCID: 3476290.

83. Kim HH, Abdelmohsen K, Lal A, Pullmann R, Jr., Yang X, Galban S, et al. Nuclear HuR accumulation through phosphorylation by Cdk1. Genes & development.

2008 Jul 1;22(13):1804-15. PubMed PMID: 18593881. Pubmed Central PMCID: 2492667.

84. Lind D, Franken S, Kappler J, Jankowski J, Schilling K. Characterization of the neuronal marker NeuN as a multiply phosphorylated antigen with discrete subcellular localization. Journal of neuroscience research. 2005 Feb 1;79(3):295-302. PubMed PMID: 15605376.

85. Levine B, Hardwick JM, Trapp BD, Crawford TO, Bollinger RC, Griffin DE. Antibody-mediated clearance of alphavirus infection from neurons. Science. 1991 Nov 8;254(5033):856-60. PubMed PMID: 1658936.

86. Ubol S, Levine B, Lee SH, Greenspan NS, Griffin DE. Roles of immunoglobulin valency and the heavy-chain constant domain in antibody-mediated downregulation of Sindbis virus replication in persistently infected neurons. Journal of virology. 1995 Mar;69(3):1990-3. PubMed PMID: 7853547. Pubmed Central PMCID: 188823.

87. Despres P, Griffin JW, Griffin DE. Antiviral activity of alpha interferon in Sindbis virus-infected cells is restored by anti-E2 monoclonal antibody treatment. Journal of virology. 1995 Nov;69(11):7345-8. PubMed PMID: 7474167. Pubmed Central PMCID: 189667.

88. Despres P, Griffin JW, Griffin DE. Effects of anti-E2 monoclonal antibody on sindbis virus replication in AT3 cells expressing bcl-2. Journal of virology. 1995 Nov;69(11):7006-14. PubMed PMID: 7474120. Pubmed Central PMCID: 189620.

89. Stanley J, Cooper SJ, Griffin DE. Monoclonal antibody cure and prophylaxis of lethal Sindbis virus encephalitis in mice. Journal of virology. 1986 Apr;58(1):107-15. PubMed PMID: 2419592. Pubmed Central PMCID: 252882.

90. Tyor WR, Moench TR, Griffin DE. Characterization of the local and systemic B cell response of normal and athymic nude mice with Sindbis virus encephalitis. Journal of neuroimmunology. 1989 Oct;24(3):207-15. PubMed PMID: 2553771.

91. Muramatsu M, Kinoshita K, Fagarasan S, Yamada S, Shinkai Y, Honjo T. Class switch recombination and hypermutation require activation-induced cytidine deaminase (AID), a potential RNA editing enzyme. Cell. 2000 Sep 1;102(5):553-63. PubMed PMID: 11007474.

92. Boes M, Esau C, Fischer MB, Schmidt T, Carroll M, Chen J. Enhanced B-1 cell development, but impaired IgG antibody responses in mice deficient in secreted IgM. J Immunol. 1998 May 15;160(10):4776-87. PubMed PMID: 9590224.

93. Kumazaki K, Tirosh B, Maehr R, Boes M, Honjo T, Ploegh HL. AID-/-mus-/- mice are agammaglobulinemic and fail to maintain B220-CD138+ plasma cells. J Immunol. 2007 Feb 15;178(4):2192-203. PubMed PMID: 17277124.

94. Wesselingh SL, Levine B, Fox RJ, Choi S, Griffin DE. Intracerebral cytokine mRNA expression during fatal and nonfatal alphavirus encephalitis suggests a predominant type 2 T cell response. J Immunol. 1994 Feb 1;152(3):1289-97. PubMed PMID: 8301132.

95. Rowell JF, Griffin DE. Contribution of T cells to mortality in neurovirulent Sindbis virus encephalomyelitis. Journal of neuroimmunology. 2002 Jun;127(1-2):106-14. PubMed PMID: 12044981.

96. Gil-Cruz C, Perez-Shibayama C, Firner S, Waisman A, Bechmann I, Thiel V, et al. T helper cell- and CD40-dependent germline IgM prevents chronic virus-induced demyelinating disease. Proceedings of the National Academy of Sciences of the

United States of America. 2012 Jan 24;109(4):1233-8. PubMed PMID: 22232667. Pubmed Central PMCID: 3268283.

97. Laskey SB, Siliciano RF. A mechanistic theory to explain the efficacy of antiretroviral therapy. Nature reviews Microbiology. 2014 Nov;12(11):772-80. PubMed PMID: 25263222.

98. Ling ZD, Yeoh E, Webb BT, Farrell K, Doucette J, Matheson DS. Intravenous immunoglobulin induces interferon-gamma and interleukin-6 in vivo. Journal of clinical immunology. 1993 Sep;13(5):302-9. PubMed PMID: 8245176.

99. Kubagawa Y, Honjo K, Kang DW, Kubagawa H. Monoclonal antibodies specific for human IgM Fc receptor inhibit ligand-binding activity. Monoclonal antibodies in immunodiagnosis and immunotherapy. 2014 Dec;33(6):393-400. PubMed PMID: 25545208. Pubmed Central PMCID: 4278172.

100. Filonov GS, Jaffrey S. Visualizing RNA dynamics in the cell. Methods in enzymology. 2016;572.

101. Paige JS, Wu KY, Jaffrey SR. RNA mimics of green fluorescent protein. Science. 2011 Jul 29;333(6042):642-6. PubMed PMID: 21798953. Pubmed Central PMCID: 3314379. Epub 2011/07/30. eng.

102. Strack RL, Disney MD, Jaffrey SR. A superfolding Spinach2 reveals the dynamic nature of trinucleotide repeat-containing RNA. Nature methods. 2013 Dec;10(12):1219-24. PubMed PMID: 24162923. Pubmed Central PMCID: 3852148.

103. Ponchon L, Dardel F. Recombinant RNA technology: the tRNA scaffold. Nature methods. 2007 Jul;4(7):571-6. PubMed PMID: 17558412.

104. Song W, Strack RL, Svensen N, Jaffrey SR. Plug-and-play fluorophores extend the spectral properties of Spinach. Journal of the American Chemical Society. 2014 Jan 29;136(4):1198-201. PubMed PMID: 24393009. Pubmed Central PMCID: 3929357.

105. Strack RL, Jaffrey SR. Live-cell imaging of mammalian RNAs with Spinach2. Methods in enzymology. 2015;550:129-46. PubMed PMID: 25605384. Pubmed Central PMCID: 4382203.

106. Filonov GS, Jaffrey SR. RNA Imaging with Dimeric Broccoli in Live Bacterial and Mammalian Cells. Current protocols in chemical biology. 2016;8(1):1-28. PubMed PMID: 26995352. Pubmed Central PMCID: 4829638.

107. Filonov GS, Kam CW, Song W, Jaffrey SR. In-gel imaging of RNA processing using broccoli reveals optimal aptamer expression strategies. Chemistry & biology. 2015 May 21;22(5):649-60. PubMed PMID: 26000751. Pubmed Central PMCID: 4441765.

108. Filonov GS, Moon JD, Svensen N, Jaffrey SR. Broccoli: rapid selection of an RNA mimic of green fluorescent protein by fluorescence-based selection and directed evolution. Journal of the American Chemical Society. 2014 Nov 19;136(46):16299-308. PubMed PMID: 25337688. Pubmed Central PMCID: 4244833.

109. Levine B, Goldman JE, Jiang HH, Griffin DE, Hardwick JM. Bc1-2 protects mice against fatal alphavirus encephalitis. Proceedings of the National Academy of Sciences of the United States of America. 1996 May 14;93(10):4810-5. PubMed PMID: 8643485. Pubmed Central PMCID: 39361.

110. Jobbagy Z, Ward JL, Toan SV, Leung GP, Tse CM. One-step unidirectional cloning of tandem repeats of DNA fragments: an application for fusion protein production. Analytical biochemistry. 2002 Apr 1;303(1):104-7. PubMed PMID: 11906158.

111. Murrell JR, Hunter DD. An olfactory sensory neuron line, odora, properly targets olfactory proteins and responds to odorants. The Journal of neuroscience : the official journal of the Society for Neuroscience. 1999 Oct 1;19(19):8260-70. PubMed PMID: 10493727.

112. Walker CL, Lukyanov KA, Yampolsky IV, Mishin AS, Bommarius AS, Duraj-Thatte AM, et al. Fluorescence imaging using synthetic GFP chromophores. Current opinion in chemical biology. 2015 Aug;27:64-74. PubMed PMID: 26117808.

113. Stanley J, Cooper SJ, Griffin DE. Alphavirus neurovirulence: monoclonal antibodies discriminating wild-type from neuroadapted Sindbis virus. Journal of virology. 1985 Oct;56(1):110-9. PubMed PMID: 2411947. Pubmed Central PMCID: 252488.

114. Han KY, Leslie BJ, Fei J, Zhang J, Ha T. Understanding the photophysics of the spinach-DFHBI RNA aptamer-fluorogen complex to improve live-cell RNA imaging. Journal of the American Chemical Society. 2013 Dec 18;135(50):19033-8. PubMed PMID: 24286188. Pubmed Central PMCID: 3908778.

115. Vernon PS, Griffin DE. Characterization of an in vitro model of alphavirus infection of immature and mature neurons. Journal of virology. 2005 Mar;79(6):3438-47. PubMed PMID: 15731238. Pubmed Central PMCID: 1075694.

116. Hahn CS, Hahn YS, Braciale TJ, Rice CM. Infectious Sindbis virus transient expression vectors for studying antigen processing and presentation. Proceedings of the National Academy of Sciences of the United States of America. 1992 Apr 1;89(7):2679-83. PubMed PMID: 1372987. Pubmed Central PMCID: 48725.

117. Wang YF, Sawicki SG, Sawicki DL. Sindbis virus nsP1 functions in negative-strand RNA synthesis. Journal of virology. 1991 Feb;65(2):985-8. PubMed PMID: 1824787. Pubmed Central PMCID: 239844.

118. Mai J, Sawicki SG, Sawicki DL. Fate of minus-strand templates and replication complexes produced by a p23-cleavage-defective mutant of Sindbis virus. Journal of virology. 2009 Sep;83(17):8553-64. PubMed PMID: 19515769. Pubmed Central PMCID: 2738138.

119. Schnell MJ, McGettigan JP, Wirblich C, Papaneri A. The cell biology of rabies virus: using stealth to reach the brain. Nature reviews Microbiology. 2010 Jan;8(1):51-61. PubMed PMID: 19946287.

120. van Riel D, Leijten LM, Verdijk RM, GeurtsvanKessel C, van der Vries E, van Rossum AM, et al. Evidence for influenza virus CNS invasion along the olfactory route in an immunocompromised infant. The Journal of infectious diseases. 2014 Aug 1;210(3):419-23. PubMed PMID: 24550441.

121. Oldstone MB. Modeling subacute sclerosing panencephalitis in a transgenic mouse system: uncoding pathogenesis of disease and illuminating components of immune control. Current topics in microbiology and immunology. 2009;330:31-54. PubMed PMID: 19203103.

122. Navaratnarajah CK, Kuhn RJ. Functional characterization of the Sindbis virus E2 glycoprotein by transposon linker-insertion mutagenesis. Virology. 2007 Jun 20;363(1):134-47. PubMed PMID: 17306321. Pubmed Central PMCID: 1959473.

123. Weiss B, Goran D, Cancedda R, Schlesinger S. Defective interfering passages of Sindbis virus: nature of the intracellular defective viral RNA. Journal of virology. 1974 Nov;14(5):1189-98. PubMed PMID: 4473568. Pubmed Central PMCID: 355635.

124. Woodward CG, Smith H. Production of defective interfering virus in the brains of mice by an avirulent, in contrast with a virulent, strain of Semliki forest virus. British journal of experimental pathology. 1975 Aug;56(4):363-72. PubMed PMID: 1174462. Pubmed Central PMCID: 2072764.

125. Tam PE, Messner RP. Molecular mechanisms of coxsackievirus persistence in chronic inflammatory myopathy: viral RNA persists through formation of a double-stranded complex without associated genomic mutations or evolution. Journal of virology. 1999 Dec;73(12):10113-21. PubMed PMID: 10559326. Pubmed Central PMCID: 113063.

126. Palmer P, Charley B, Rombaut B, Daeron M, Lebon P. Antibody-dependent induction of type I interferons by poliovirus in human mononuclear blood cells requires the type II fcgamma receptor (CD32). Virology. 2000 Dec 5;278(1):86-94. PubMed PMID: 11112484.

127. Levy DE, Lew DJ, Decker T, Kessler DS, Darnell JE, Jr. Synergistic interaction between interferon-alpha and interferon-gamma through induced synthesis of one subunit of the transcription factor ISGF3. The EMBO journal. 1990 Apr;9(4):1105-11. PubMed PMID: 2108862. Pubmed Central PMCID: 551785.

128. Sainz B, Jr., LaMarca HL, Garry RF, Morris CA. Synergistic inhibition of human cytomegalovirus replication by interferon-alpha/beta and interferon-gamma. Virology journal. 2005;2:14. PubMed PMID: 15727684. Pubmed Central PMCID: 554982.

129. Hirsch RL, Griffin DE. The pathogenesis of Sindbis virus infection in athymic nude mice. J Immunol. 1979 Sep;123(3):1215-8. PubMed PMID: 469246.

130. Laukens D, Brinkman BM, Raes J, De Vos M, Vandenabeele P. Heterogeneity of the gut microbiome in mice: guidelines for optimizing experimental design. FEMS microbiology reviews. 2016 Jan;40(1):117-32. PubMed PMID: 26323480. Pubmed Central PMCID: 4703068.

131. Stough JM, Dearth SP, Denny JE, LeCleir GR, Schmidt NW, Campagna SR, et al. Functional Characteristics of the Gut Microbiome in C57BL/6 Mice Differentially Susceptible to Plasmodium yoelii. Frontiers in microbiology. 2016;7:1520. PubMed PMID: 27729904.

132. Schieber AM, Lee YM, Chang MW, Leblanc M, Collins B, Downes M, et al. Disease tolerance mediated by microbiome E. coli involves inflammasome and IGF-1 signaling. Science. 2015 Oct 30;350(6260):558-63. PubMed PMID: 26516283. Pubmed Central PMCID: 4732872.

133. Shulzhenko N, Morgun A, Hsiao W, Battle M, Yao M, Gavrilova O, et al. Crosstalk between B lymphocytes, microbiota and the intestinal epithelium governs immunity versus metabolism in the gut. Nature medicine. 2011 Dec;17(12):1585-93. PubMed PMID: 22101768. Pubmed Central PMCID: 3902046.

134. Fagarasan S, Muramatsu M, Suzuki K, Nagaoka H, Hiai H, Honjo T. Critical roles of activation-induced cytidine deaminase in the homeostasis of gut flora. Science. 2002 Nov 15;298(5597):1424-7. PubMed PMID: 12434060.

135. Suzuki K, Meek B, Doi Y, Muramatsu M, Chiba T, Honjo T, et al. Aberrant expansion of segmented filamentous bacteria in IgA-deficient gut. Proceedings of the National Academy of Sciences of the United States of America. 2004 Feb 17;101(7):1981-6. PubMed PMID: 14766966. Pubmed Central PMCID: 357038.

CURRICULUM VITAE FOR Ph.D. CANDIDATES

The Johns Hopkins University School of Medicine

Voraphoj Nilaratanakul Oct 17th, 2016

Educational History

Ph.D. expected 2016		Program in Cellular and Molecular Medicine Johns Hopkins University School of Medicine Mentors: Diane E. Griffin, M.D.-Ph.D.
M.S.	2010	Medicine Chulalongkorn University, Thailand
Diploma	2010	Thai subspecialty board of Infectious Diseases
Diploma	2008	Thai board of Internal Medicine
M.D.	2002	Doctor of Medicine Chulalongkorn University, Thailand

Professional Experience

Research rotation 2012		Laboratory of Zaver M. Bhujwalla Johns Hopkins University School of Medicine
	2012	Laboratory of Diane E. Griffin Johns Hopkins University School of Public health

	2011	Laboratory of Lewis Romer
		Johns Hopkins University School of Medicine
Electives	2009	Laboratory of Sharone Green
		Center of Infectious Diseases and Vaccine Research,
		University of Massachusetts
	2009	Laboratory of Daniel Kuritzkes
		Partners AIDS Research Center, Harvard University
	2009	Laboratory of Laura White
		Carolina Vaccine Institute,
		University of North Carolina, Chapel Hill
Clinical training	2010-2011	Infectious disease faculty
		King Chulalongkorn Memorial Hospital, Thailand
	2008-2010	Infectious disease fellow
		King Chulalongkorn Memorial Hospital, Thailand
	2005-2008	Internal Medicine resident
		King Chulalongkorn Memorial Hospital, Thailand
	2003-2005	General physician, Namon Hospital, Thailand
	2002-2003	Intern, Kalasin Hospital, Thailand

Scholarship

Anandamahidol Foundation Scholarship in Medicine (awarded 2010) for tuition, fees, insurance, and stipend support, 2011-2016

Academic honors

2010	Representative young scientists of the Association of Southeast Asian Nations (ASEAN) to participate in the 60th Meeting of Nobel Laureates	
2010	Top scorer	National infectious disease board exam, Thailand
2008	First prize	Faculty of Medicine's Annual Residents' Research Competition, Chulalongkorn University, Thailand
2008	2nd runner-up	Royal College of Physicians of Thailand's Annual Residents' Research Competition
2007	Top scorer	Written national internal medicine board exam, Thailand
2002	1st class honor	Faculty of Medicine, Chulalongkorn University, Thailand
2000	Top scorers	Surgery, Anesthesiology, Radiology, Psychology
1999	Top scorers	Medicine, Otolaryngology, Forensic Medicine
1998	Top scorers	Anatomy, Physiology, Pathology, Clinical Pathology, Microbiology, Psychology, Preventive and Social Medicine
1997	Top scorer	Biochemistry
1996	Top scorer	Statistics

Publications

1. Fumin Chang, Christopher A. Lemmon, **Voraphoj Nilaratanakul**, Varda Rotter, and Lewis Romer. Endothelial Matrix Assembly during Capillary Morphogenesis: Insights from Chimeric TagRFP-Fibronectin Matrix. *Journal of Histochemistry & Cytochemistry* 2014; 62(11): 774–790.

2. Talibah U. Metcalf, Victoria K. Baxter, **Voraphoj Nilaratanakul**, Diane E. Griffin. Recruitment and Retention of B Cells in the Central Nervous System in Response to Alphavirus Encephalomyelitis. *Journal of Virology* 2012; 87(5): 2420-2429.
3. Chusana Suankratay, Ekkachai Thiansukhon, **Voraphoj Nilaratanakul**, Chaturong Putaporntip, Somchai Jongwutiwes. Disseminated infection caused by novel species of *Microsporidium*, Thailand. *Emerging Infectious Diseases* 2012; 18(2): 302-4.
4. *Weekitt Kittisupamongkol, ***Voraphoj Nilaratanakul**, Wanla Kulwichit. Near-fatal bleeding, senna, and the opposite of lettuce. *Lancet* 2008; 371: 784. ***These authors contributed equally**.

Manuscripts

Submitted to Journal of Virology on October 6th, 2016

Voraphoj Nilaratanakul, Debra Hauer, Diane E. Griffin. Development of Sindbis virus with encoded fluorescent RNA aptamer Spinach2 for imaging of replication and immune-mediated changes in intracellular viral RNA.

In preparation

1. **Voraphoj Nilaratanakul**, Debra Hauer, Talibah U. Metcalf, Diane E. Griffin. Sindbis viral persistence in mouse CNS.
2. **Voraphoj Nilaratanakul**, Angela Chen, Oanh Tran, Victoria K. Baxter, Kirsten Kulcsar, Elizabeth Troisi, Jane Xie, Diane E. Griffin. Sindbis viral RNA clearance from CNS of immunoglobulin-deficient mice.

3. **Voraphoj Nilaratanakul**, Debra Hauer, Diane E. Griffin. Live-cell imaging of Sindbis viral RNA replication and immune-mediated clearance using Sindbis virus with fluorescent Broccoli RNA aptamer.

Poster Presentations

1. **Voraphoj Nilaratanakul**, Kirsten Kulcsar, Diane E. Griffin. Comparison of IgM versus IgG antibody-mediated clearance of Sindbis virus from neurons in activation-induced cytidine deaminase (AID) and soluble IgM (sIgM) knockout mice. 18th International Conference on Emerging Infectious Diseases (EID), US – Japan Viral Diseases Panel Meeting. Bethesda, Maryland, USA. January 13-14, 2016.
2. **Voraphoj Nilaratanakul**, Balaji Krishnamachary, Mayur Gadiya, Zaver M. Bhujwalla. Fluorescent Timer: Revealing hypoxia duration and interval in breast cancer cells. SKCCC (Sidney Kimmel Comprehensive Cancer Center) Fellow Research Day 2012. Baltimore, Maryland, USA. May 15, 2012.
3. **Voraphoj Nilaratanakul**, Fumin Chang, Lewis Romer. MT1-MMP expression modulation of tubulogenesis and matrix remodeling by HUVEC on fibroblast-derived fibronectin matrices. 13th Annual ACCM (Anesthesilogy and Critical Care Medicine) Research Day. Baltimore, Maryland, USA, Dec 7, 2011.
4. **Voraphoj Nilaratanakul**, Soraya Thaivanich, Kuakul Songcharoen, Kesinee Arunyingmongkol, Rongpong Plongla, Methee Sriprapun, Wanla Kulwichit. Detection of dengue virus in lymphoid tissues of persons with remote dengue infections. 20th European Congress of Clinical Microbiology and Infectious Diseases. Vienna, Austria. April 10-13, 2010.

5. **Voraphoj Nilaratanakul**, Ubolrat Rirerm, Tanittha Chatsuwan, Wanla Kulwichit. Using digital tinctorial properties to rapidly distinguish *Pseudomonas aeruginosa* from other Gram- negative bacteria in bacteraemic patients. 19th European Congress of Clinical Microbiology and Infectious Diseases. Helsinki, Finland. May 16-19, 2009.
6. **Voraphoj Nilaratanakul**, Ubolrat Rirerm, Tanittha Chatsuwan, Wanla Kulwichit. Differentiating *Pseudomonas aeruginosa* from common enteric bacteria by digital tinctorial properties. 18th European Congress of Clinical Microbiology and Infectious Diseases. Barcelona, Spain. April 19-22, 2008.